CR 73320

AVAILABLE TO THE PUBLIC

VOUGHT AERONAUTICS DIVISION
LTV AEROSPACE CORPORATION
P O BOX 5907 · DALLAS TEXAS 75222

Report No. 2-55400/9R-2565
7 February 1969

RESEARCH REPORT

JET-FLAP ROTOR

PRELIMINARY APPLICATION STUDY

VOLUME II ANALYSIS REPORT

Prepared Under Contract No. NAS 2-4244 by
Vought Aeronautics Division
LTV Aerospace Corporation
for
Ames Research Center, National Aeronautics
and Space Administration
and
U. S. Army Aeronautical Research Laboratory
Moffett Field, California

VOUGHT AERONAUTICS DIVISION
LTV AEROSPACE CORPORATION
P.O. BOX 5907 · DALLAS, TEXAS 75222

TABLE OF CONTENTS

TABLE OF CONTENTS (CONTINUED)

TABLE OF CONTENTS (CONTINUED)

TABLE OF CONTENTS (CONTINUED)

LIST OF TABLES (Concluded)

1.0 INTRODUCTION AND SUMMARY

This volume, Volume II, contains all the substantiating data of the Preliminary Application Study of the Jet-Flap Rotor conducted by Vought Aeronautics Division of LTV Aerospace Corporation under contract to NASA Ames Research Center and to the U. S. Army Aeronautical Research Laboratory, Moffett Field, California. A summary of the work is reported in Volume I. Volumes I and II complement each other.

The purpose of the Preliminary Application Study was to investigate basic performance of helicopters equipped with jet-flap rotors and to compare that performance with that of shaft-driven helicopters. The mission was not defined by the Statement of Work. Rather the contractor was to conduct a mission analysis in which high speed and heavy lift missions of all types were to be surveyed and typical missions in each area selected as base points. One of the primary goals of the study was to determine the mission best suited to utilize the jet-flap rotor's capabilities and potentials. Additionally the study was to identify other areas of research required to enhance the use of the jet-flap rotor concept.

The study was conducted in two phases. The first phase utilized the Dorand DH 2011 39-foot test rotor as a base for performance calculation. Only cold cycle jet-flap pure helicopters were included in the phase of the study with best realistic estimates of performance parameters. The second phase consisted of a sensitivity study in which the effect of variation of some of the key parameters on the designs was determined. Other studies in the second phase included brief studies of thrust compounding, DH2011 test planning, and jet-flap stopped/stowed rotor flying qualities.

In this volume data are presented by technical descipline including the mission analysis, aerodynamics, propulsion, weights, structural and design. Also included are descriptions of the computer programs used in the study.

As reported in the Summary Volume, on the basis of cost and performance alone no decided advantage of the jet-flap configured helicopter could be shown over shaft-driven helicopters in missions which the shaft-driven helicopters perform well. Some intangible factors such as smooth flight characteristics at high speeds which could contribute to an improvement of the jet-flap maintainability could not be accounted for in a performance study such as this. They could have an important effect on the desirability of the pure jet-flap helicopter and should be further studied.

In more severe missions such as those requiring higher disc loadings, and in particular, the stoppable rotor application, the jet-flap rotor or a variation of it, appears highly competitive.

2.0 MISSION ANALYSIS

2.1 INTRODUCTION

The objective of the subject contract was to define applications for the jet-flap helicopter concept based on the coincidence of the strongest points in jet-flap technology expressed in performance, economics, and the practical evolution of military and civil helicopter needs. Prior to any evaluation of the relative merits of the jet-flap helicopter versus conventional shaft-driven vehicles, it was necessary to perform a mission analysis as a basis for defining point design vehicles. Reference 1 which was submitted previously established mission requirements for helicopters in the 1975-1985 time frame. The requirements as specified in Reference 1 were developed as a result of a survey of projected needs for high-speed and heavy-lift helicopter operations. Design points thus established were used for the first iteration in the comparative evaluations. During the course of the overall study, the original mission requirements defined in Reference 1 were re-appraised and updated to bring them more into line with helicopter state-of-the-art capabilities. Paragraph 2.0 serves a twofold purpose: (1) to summarize and update the earlier report and (2) to indicate potential helicopter applications which make use of a shaft-driven vehicle with jet-flap augmentation, as well as a stopped/stowed rotor jet-flap concept.

2.2 POINT DESIGN RECOMMENDATION BASED ON PRELIMINARY STUDY

In the course of the preliminary requirements study reported earlier, an extensive volume and variety of military and commercial planning

literature was reviewed. Other major sources of information and data were military specifications and previously completed LTVAC studies. The latter studies examined in depth the mission requirements for future attack and transport air vehicles.

Since the need for the high-speed and heavy-lift helicopter characteristics may be coincident or independent in occurrence, the same established mission function, e.g., Army transport, may be considered from two different perspectives. The final design point recommendations, therefore, resulted from defining the consensus of what the typical helicopter of 1975-1985 having high-speed or heavy-lift capabilities might encompass.

The following design point was recommended for the initial evaluation of the high-speed helicopter:

- Payload - 4,000 pounds
- Radius of Action - 200 nmi
- Desired Maximum Speed of 250 kt
- Desired Cruise Speed of 200 kt

No loiter or extensive midmission hover is required beyond a normal 5 minutes at origin and 10 minutes at midpoint. The midmission environment condition is 95°F and 6,000 feet. This specification is based on the Army's requirement for the Utility Tactical Transport (UTT). The cabin configuration must be suitable for a variety of uses and is to have two doors, one on each side with each door having a width of at least 4 feet. No ferry range is prescribed.

The following design point was recommended for the initial evaluation of the heavy-lift helicopter:

- Payload - Radius Combinations
- Prime: 50 tons at 50 nmi
- Extended: 35 tons at 100 nmi
- Desired Maximum Speed of 175 kt
- Desired Cruise Speed of 150 kt (both with cabin fuselage)

The cabin configuration internal cross section was prescribed as no less than 12 feet by 12 feet. (This cabin may be designed such that it can be separated from the vehicle, permitting the hauling of externally slung loads.) The cabin would have a rear door and ramp of the same indicated cross section. The midmission environment condition was specified as 95°F at 6,000 feet.

2.3 DISCUSSION OF PRELIMINARY ANALYSIS

Table 2-1 summarizes the major performance and configurations expected to be associated with future high-speed and heavy-lift helicopter missions. The major design points covered include payload, radius of action (or equivalent radius), speeds, cabin configuration, environment conditions, and ferry considerations.

2.3.1 High Speed Missions

The missions taken to be most demanding for high speed operational capability in the 1975-1985 time frame include: light tactical transport for the Army and Marine Corps; escort and weapon delivery for the same

TABLE 2-1 SURVEY OF FUTURE HELICOPTER MISSIONS FOR HIGH SPEED AND HEAVY LIFT

CONFIGURATION	MISSIONS	PAYLOAD	RADIUS OF ACTION	SPEED	CABIN CONFIGURATION	ALTITUDES TEMPERATURE	FERRY
HIGH SPEED	Military Transport	≥ 2,500 lb	150 nmi	200 kt	Rear or Side Doors	Midmission Land and TO at 95°F 6,000 ft	Not Important Cause Moved In C5 Overseas
	Escort and Weapon Delivery	≥ 4,000 lb	200 nmi	250 kt	Wide Side Doors	Not Important W/O Midmission Landing	
	Surveillance and Reconnaissance	≤ 2,000 lb	200 nmi	250 kt	Side Doors		
	Civil.	–	–	–	At least 6 ft Wide Fuselage. Side Doors	–	
	Recommended	4,000 lb	200 nmi	Vmax ≥ 250 kt Vcr ≥ 200 kt	2 Side Doors Fuselage ≥ 6 ft Wide	Midmission Operations at 95°F 6,000 ft	–
HEAVY LIFT	Aircraft Recovery	≥ 30 ton	≥ 100 nmi	≥ 100 kt Aver ≤ 50 kt	External	Midmissions at 95°F and 6,000 ft	Minimum 2,000 nmi Desired 3,500 nmi
	Army-Marine TO&E Logistic	≤ 50 ton	Aver 50 nmi	Vmax ≥ 175 kt Vcr ≥ 150 kt	Cross Section 12 ft x 12 ft Length 54 ft to 77 ft		
	Army-Marine Unit Movement	≤ 30 ton	≥ 100 nmi	Vmax ≥ 175 kt Vcr ≥ 150 kt	Length ≥ 75 ft		
	Navy-Marine Intership and Ship-to-Shore	≤ 20 ton	≥ 50 nmi	–	–		
	Civil	≥ 40 ton	100 nmi	–	Length ≥ 75 ft		
	Recommended	Prime: 50 ton Extended: 35 ton	Prime. 50 nmi Extended: 100 nmi	Vmax ≥ 175 kt Vcr ≥ 150 kt	12 ft x 12 ft X 75 ft		

organizations; surveillance, reconnaissance, and rescue; and the general civil application.

Although Table 2-I shows payload requirements ranging from less than 2,000 pounds to 4,000 pounds, it was recommended that the point design payload be 4,000 pounds. This is because the helicopter is becoming a weapon-carrying vehicle, as indicated by design trends for new systems such as the AH-1G Cobra and AAFSS, and it is also applicable to a multiplicity of uses.

The recommended design point radius of action was 200 nmi. This radius provides for the escort/weapon capability with the full 4,000-pound payload. Additional loiter and/or station time required for the surveillance and reconnaissance function can be obtained by trading off payload for loiter and station-time fuel, since about 2,000 pounds less payload is visualized for the intelligence and information-gathering function.

The consensus of the survey concerning speed requirements was that cruise speed for the point design vehicles be no less than 200 knots with a designed maximum speed of 250 knots.

There was no clear mandate for the rear-loading configuration in high-speed helicopter design. Several large side doors, preferably on opposite sides and having a sizable width (at least 4 feet is desirable) to accommodate rescue stretchers, etc., are desirable. Cabin size is one of the few design points for which commercial applications have a notable input for the high-speed vehicle. A 4,000-pound payload capability will accommodate about 20 passengers. In order to avoid excessive fuselage length, it was recommended that the fuselage be wide enough for an aisle

and three seats abreast; therefore, a width of no less than 9 feet was recommended.

The lack of midmission landing requirement for the escort/weapon and surveillance and reconnaissance missions reduces somewhat the importance of altitude and temperature as design parameters. It is expected that environment constraints at origin (takeoff) can be alleviated by rolling and short takeoff techniques in most cases. Environment conditions at midmission for the transport function when performed in potential limited war areas do, however, justify a requirement that midmission landing and takeoff be accomplished at 95°F at 6,000 feet.

By the 1975 time period, the C5 type aircraft will be a major element in the military overseas deployment and logistic support system. Smaller tactical helicopters, such as the type under discussion, can easily be made transportable in this aircraft; therefore, the design of the smaller craft need not be affected by ferry range requirements.

2.3.2 Heavy Lift Missions

The future needs for heavy lifting capability in helicopters appear to be pinned to five mission areas: downed military aircraft recovery, Army TO&E logistics, Army unit movement, Navy and Marine intership shuttle and ship-to-shore movement, and the civilian short-haul passenger operations.

In order that the full potential application for the heavy-lift helicopter be exercised, it was recommended that the prime point design payload be 50 tons with an extended radius payload of 35 tons. This prime payload will provide the capability for lifting all items of military significance. The 35-ton capacity is more compatible with present trends in military assault operations and commercial passenger movement.

[illegible] Army, it was estimated that [illegible] for a heavy-lift helicopter in military operations will vary between 50 nmi and 100 nmi, depending on payload requirements. Therefore, it was recommended that the design radius for the prime payload be 50 nmi and that an extended radius of operation be defined as 100 nmi.

The value of speed is closely tied to mission economics but is often subjected to factors resulting from the operational environment; e.g., need for speed to survive or to acquire a target or to achieve the element of surprise. If one considers the heavy-lift helicopter for missions on which the cargo is or could be carried in an enclosed compartment, then the speed capability should logically be at least as good as that of contemporary systems performing these missions. In this case a maximum speed of 175 knots was specified as desirable with a cruise capability of at least 150 knots.

If one considers the external cargo situation, then current experience would indicate the capability cruise speeds seldom exceed 100 knots, with the majority of missions conducted at speeds under 50 knots.

Because aviation economics summarily dictates that the cost is highest when aerodynamic drag is greatest and since the majority of missions could be accomplished with cargo carried internally, it was recommended that the design maximum speed be at least 175 knots with a 150-knot cruise capability for an enclosed fuselage.

Review of the military and commercial applications for a heavy-lift helicopter of the payload, radius, and speed capabilities thus far prescribed resulted in the conclusion that the internal cabin configuration should be at least 12 feet by 12 feet in cross section with a length of 75 feet.

It is assumed that seven-a react seating is possible in the 12-foot by 12-foot cross section plus a drive-in ramp in order to accommodate military operations.

A review of domestic and overseas ferry routes indicated that the minimum acceptable ferry capability for the heavy-lift helicopter is 2,600 nmi. A more desirable capability would be 3,300 nmi. Since special cabin fuel tanks are expected to be acceptable, and since adequate payload capability is also expected to be available, no ferry-range requirement was spelled out for the heavy-lift vehicle.

2.4 UPDATED MISSIONS

2.4.1 Updated High-Speed Helicopter Mission

In the optimization studies of the preliminary high-speed helicopter point design, the payload/speed/radius combination of 4,000 lb/200 kt/200 nmi recommended by the mission study summarized above, together with the drag of the vehicle, resulted in a divergent fuel required/fuel available situation. In an effort to resolve this discrepancy, the preliminary point design requirements were reviewed. It was the conclusion of the study group that an equally valid mission was one of 150-nmi radius with a more dense cargo compartment to accommodate both passengers and cargo. Thus, the point design was reduced, and a more dense cargo compartment was designed, resulting in a cleaner fuselage and lower drag.

The refined typical high-speed helicopter mission defined for comparing a jet-flap rotor helicopter with a shaft-driven helicopter is:

- Payload - 4,000 lb
- Radius of Action - 150 nmi
- Desired Cruise Speed - 200 knots
- Cargo Compartment - Minimum cross section
- Midmission Hover - 10 minutes

2.4.2 Updated Heavy-Lift Helicopter Mission

Initial studies of the jet-flap helicopter required to meet the typical missions recommended in the preliminary study indicated that installed shaft horsepower on the order of 150,000 was required. The shaft-driven 50-ton heavy-lift vehicle required approximately 46,000 hp. The study group is of the opinion that these power requirements represent a step beyond what should be considered for the base point. The 50-ton shaft-driven design is illustrated in Figure 2-1. The preliminary design requirements were reviewed and were updated in order to conduct the parametric study around a power requirement which is more realistic for the 1975-1980 time period.

The following point design was recommended:

- Payload - 40,000 lb
- Radius of Action - 10 nmi
- Speed - 40 knots
- Midmission Hover - 2 minutes
- Cargo Compartment - Crane-type vehicle—hence, cargo compartment size not a factor in design study

It is believed that this mission is representative of that required of the next generation crane-type helicopter designs. It includes most cases

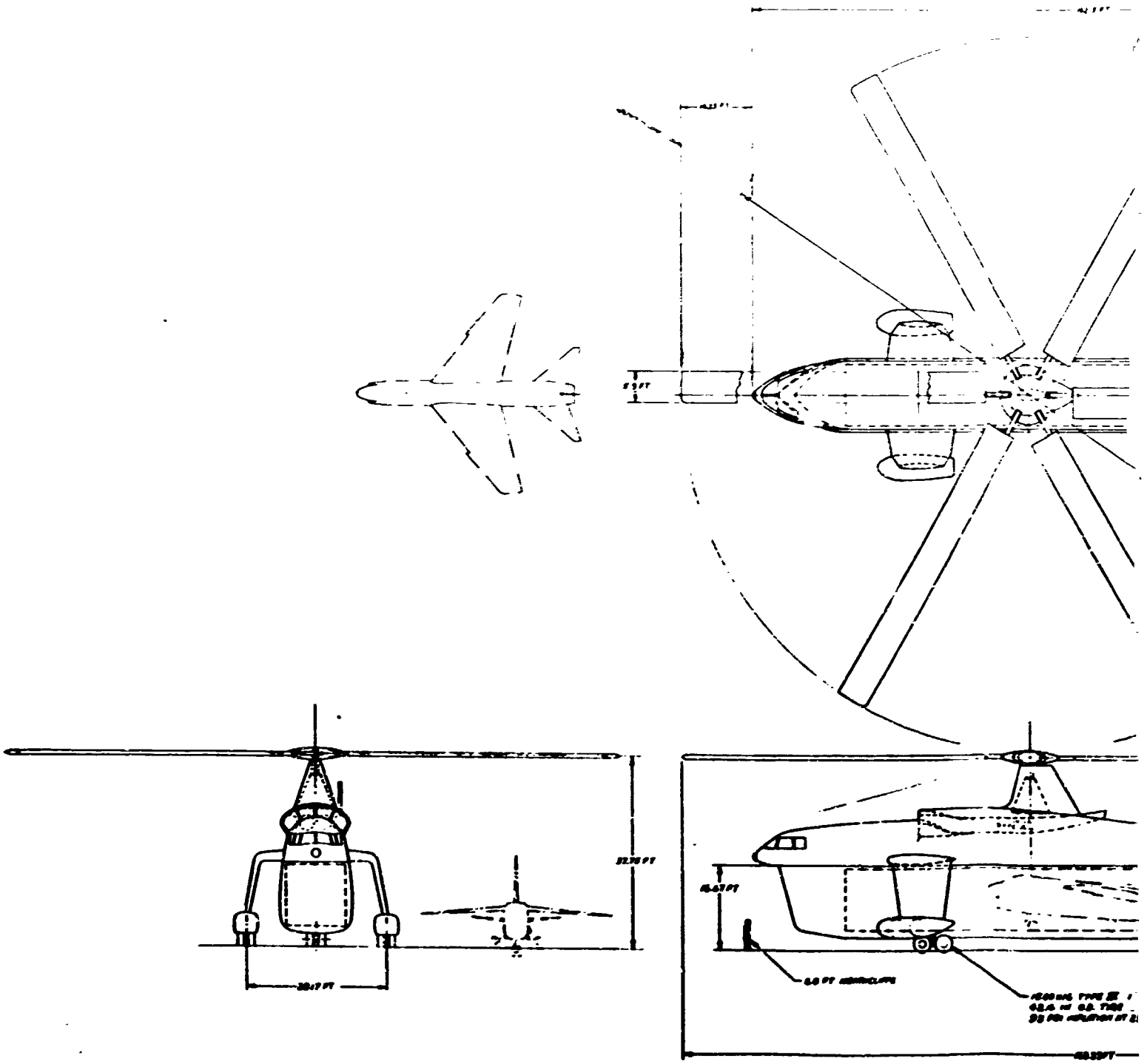

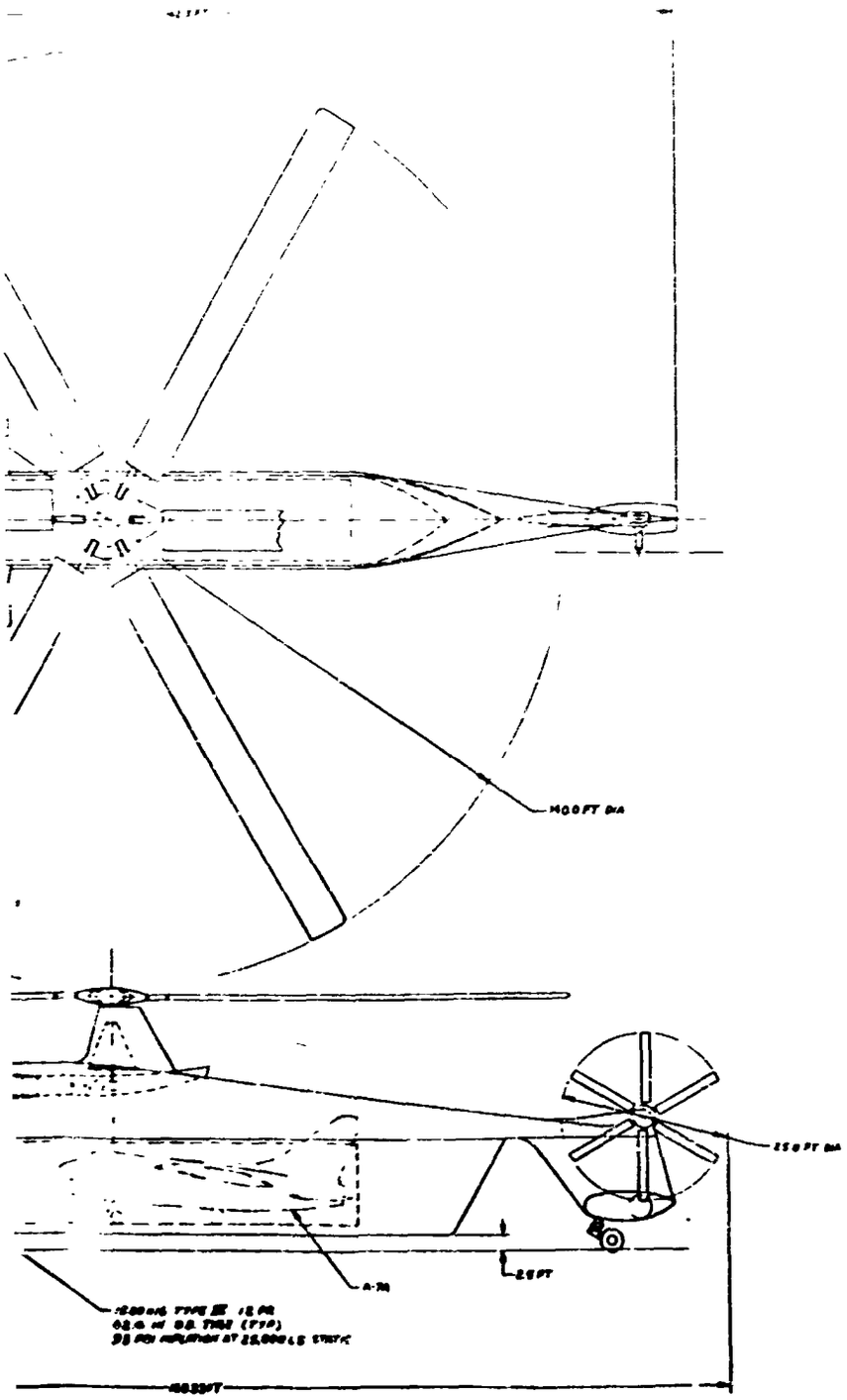

NOTES

1. PAYLOAD 30 TONS
2. GROSS WT 231,000 LB
3. RATED HP 41,600
4. ROTOR SOLIDITY 0.16
5. CARGO COMPARTMENT 120 FT x 12 0 FT x 7.5 0 FT

Figure 2-1

		GENERAL ARRANGEMENT - HLH 30 TON CAPACITY, SHAFT DRIVEN ROTOR
		69370 LI2-HLH-010

2-11-B

where a crane-type vehicle would be used, such as retrieval of downed aircraft, unloading on ships where port facilities are inadequate, movement of heavy equipment across areas impassible by surface means (rivers, swamp, and marsh land), etc.

2.5 ADDITIONAL JET-FLAP CONCEPT APPLICATIONS

Studies to date concerning the jet-flap concept have been primarily concerned with comparing the pure jet-flap vehicle with the shaft-driven vehicle. In most cases these comparisons have been made in the regime where the conventional (shaft-driven) vehicle is already extremely efficient. Thus, in an effort to define areas (missions) where the jet-flap concept may prove to be most applicable and to satisfy the terms of the NASA contract, additional applications were briefly explored to the extent that time would permit. Two particular areas which appear promising include shaft-driven vehicles with jet-flap augmentation and a stopped/stowed rotor jet-flap concept. This paragraph identifies missions for which these two concepts would be applicable.

2.5.1 Astronaut/Space Capsule Recovery

With the advent of the Apollo moon mission, payloads on the order of 14,000 to 15,000 pounds (capsule weight including water shipped aboard for ballast) will be required to be recovered in the open ocean. In the future the recovery of even heavier space capsules will be required. Present day operations require this recovery to be made by surface means, particularly in the case of a space capsule, because of range (5 to 100 mmi)

and payload requirement combinations. Because of the jet-flap concept's lifting capability (estimated to be 2 to 2-1/2 times that of the conventional helicopter), it appears that a shaft-driven vehicle with jet-flap augmentation could perform this mission most effectively. Under normal conditions, "splash-down" area and time are known. The vehicle used in the conventional mode could be in the area hovering and preparing for capsule pickup. After "splash down" and during hookup with the capsule, all helicopter operations would be in the conventional mode. This period would last up to 30 minutes or longer. Thus, a more economical use of the vehicle is realized in that fuel requirements are greatly reduced over that of the pure jet-flap vehicle. After hookup, the helicopter converts to the jet-flap mode for pickup, climb, and acceleration to cruise speed. Depending upon conditions after obtaining cruise speed, reconversion to conventional flight mode may or may not be accomplished. However, location of the surface vehicle is not as critical, and recovery of the capsule and its return to a more friendly environment is accomplished in a much shorter time period than presently achievable.

For the case of an aborted Apollo mission where "splash down" location and time are unknown, a stopped/stowed rotor jet-flap vehicle appears feasible. In this mission, time becomes important in that recovery of personnel is paramount. Here a better match of power is available between forward speed and the power required for hover with the jet-flap concept.

2.5.2 Combat Aircrew Rescue

If this mission is to be accomplished by helicopter type vehicles, it appears that the stopped/stowed rotor jet-flap concept would be very practical. As in the aborted Apollo mission, time, and therefore speed, are important in addition to the hovering capabilities during actual pickup. Again a much better match of power requirements for hover and forward speed is available.

2.5.3 Downed Aircraft Retrieval and Large Equipment Movement

Since it is never possible to know in advance the location of a downed aircraft or when large equipment is to be moved, it is not always possible to have present a lifting vehicle in the required location. Thus, a shaft-driven, jet-flap augmented vehicle appears ideal for this mission. The helicopter might be located some distance away from the downed aircraft or equipment. It could be operated in the conventional mode from its base to the location of the item to be moved. After hookup with the item, the helicopter would convert to the jet-flap mode for pickup, climb, and acceleration to cruise speed. Reconversion to conventional helicopter flight would be accomplished as required.

2.5.4 Radar Surveillance Station

The Giravions-Dorand Co. has investigated an application of the jet-flap rotor as a stationary hovering radar surveillance platform. This concept is described in Volume I.

2.5.5 Other Applications

Additional applications which could most effectively utilize the shaft-driven, jet-flap augmented vehicle and/or stopped/stowed rotor concept include:

- Marine over-the-beach (vertical envelopment) - shaft-driven, jet-flap augmented concept
- Navy Intra-Task Force Resupply - shaft-driven, jet-flap augmented concept
- Army/Navy/Air Force high priority cargo delivery (utility mission) - stopped/stowed rotor jet-flap concept.

3.0 AERODYNAMICS

The results of the parametric study are presented in Volume I. Presented in this section are additional aerodynamics data which substantiate the results presented in Volume I. Also included are discussion of some additional aerodynamics studies. Descriptions of the computer programs used in the performance analysis are contained in the Appendix to this Volume.

3.1 HIGH-SPEED HELICOPTER PARAMETRIC STUDY

The design mission for both the high-speed shaft-driven and jet-flapped helicopters is detailed below:

Payload = 4,000 lb

Radius of action = 150 nmi

Cruise speed = 200 kt or NRP speed

Power requirement = T/W = 1.0 K at 6,000 ft, 95°F

Hover time:

At origin = 5 min

At mid-mission = 10 min

Warm-up allowance = 5 min at NRP

Reserve = 10% initial fuel

3.1.1 Shaft-Driven Helicopter Optimization

3.1.1.1 Range of Parameters

Table 3-1 presents the range of variables for the high-speed shaft-driven helicopter parametric study. A rotor tipspeed, V_T = 640 ft/sec, was selected to: (1) achieve a maximum rotor tip Mach number, M_{TIP} = .95, at the desired maximum dash speed, V_{max} = 250 kt; and (2) maintain sufficient

rpm to limit coning angle. The number of blades was set at two. The combination of these parameters yields rotor lift coefficients of reasonable value which bracket a $\bar{C}_L = .8$.

TABLE 3-1 HIGH-SPEED SHAFT-DRIVEN HELICOPTER - RANGE OF PARAMETERS

Gross Weight, lb	12,000, 14,000, 16,000
Rotor Diameter, ft	55, 65, 75
Solidity	.08, .10, .12
Tipspeed, ft/sec	640
No. of blades	2

3.1.1.2 **Engine Sizes**

Engine size was based on the requirement in hover for an out-of-ground-effect rotor thrust/gross weight ratio, T/W = 1.0 K, at 6,000 feet, 95°F. It should be recognized that this requirement results in a rather oversize engine for the design mission hover condition at sea level, 59°F. However, the desired high speed in cruise, V = 200 knots, justifies this engine size. Table 3-2 presents the rated engine sizes for the 27 parametric points. Included in the thrust requirement of the vehicle in hover is the vertical drag imposed by the fuselage interaction with the rotor downwash. As a first-order check on the sensitivity of power-required to diameter, let ideal conditions apply in hover. Momentum theory then predicts that hover power required is inversely proportional to diameter for constant thrust. Thus the rapid increase in power with reduction in diameter is [illegible]ified.

TABLE 3-2 RATED HORSEPOWER, HIGH-SPEED SHAFT-DRIVEN HELICOPTER

V_T = 640 FPS

T/W = 1.0K at 6000 ft, 95°F

GROSS WEIGHT Lb	DIAMETER Ft	DISC LOADING Lb/Ft^2	SOLIDITY	$SHP_{RATED\ T.O.}$ Hp
12,000	55	5.06	.08	2,090
			.10	2,145
			.12	2,205
	65	3.61	.08	1,870
			.10	1,960
			.12	2,050
	75	2.72	.08	1,775
			.10	1,900
			.12	2,025
14,000	55	5.9	.08	2,565
			.10	2.620
			.12	2,670
	65	4.22	.08	2,265
			.10	2,345
			.12	2,435
	75	3.17	.08	2,105
			.10	2,225
			.12	2,350

TABLE 3-2 RATED HORSEPOWER, HIGH-SPEED SHAFT-DRIVEN HELICOPTER (CONCLUDED)

GROSS WEIGHT Lb	DIAMETER Ft	DISC LOADING Lb/Ft^2	SOLIDITY	SHP_{RATED} Hp
16,000	55	6.74	.08	3,090
			.10	3,140
			.12	3,190
	65	4.82	.08	2,680
			.10	2,760
			.12	2,845
	75	3.62	.08	2,465
			.10	2,580
			.12	2,700

3.1.1.3 **Fuel Required**

Fuel required to perform the design mission is presented in Figures 3-1, 3-2, and 3-3, versus takeoff gross weight for the three rotor diameters and three solidities noted in Paragraph 3.1.1.1. The calculation of fuel required for the 27 points is accomplished by the LTVAC Mission Performance Program detailed in Appendix A. The substantially greater fuel requirement of the 55-foot diameter configuration, particularly at high gross weights, is attributed to several factors. First, there is a significant rise in power required at high speeds for a heavily loaded rotor due to compressibility and retreating blade stall. This condition, coupled with the larger engine size for hover with the 55-foot rotor results in relatively high fuel consumption. At the higher gross weights, power required in cruise is of such magnitude to allow the larger diameter configuration to achieve

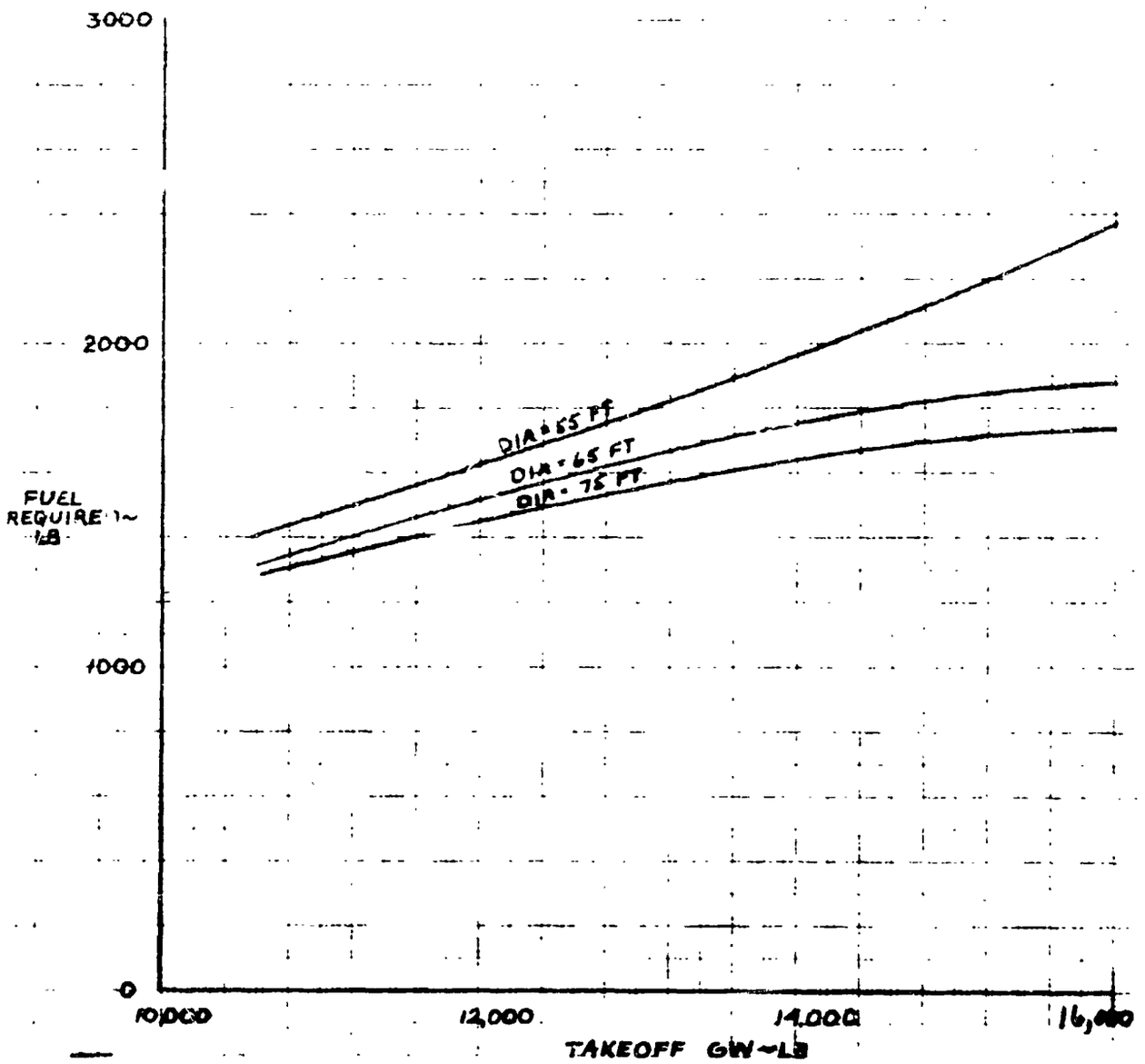

Figure 3-1 Fuel Vs Takeoff GW HSH Shaft-Driven σ = .08

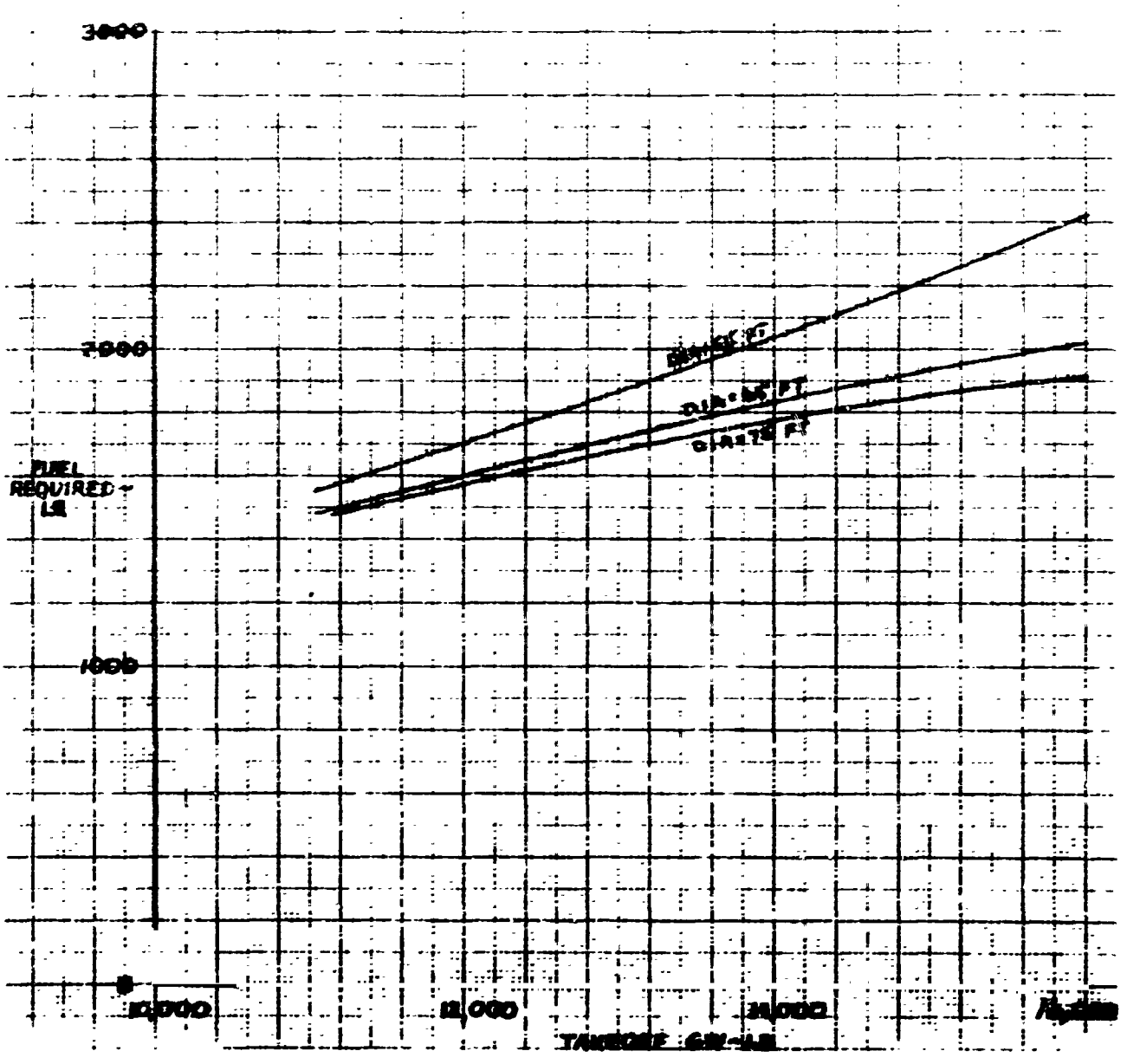

Figure 3-2 Fuel Required Vs Takeoff GW Shaft-Driven σ = .10

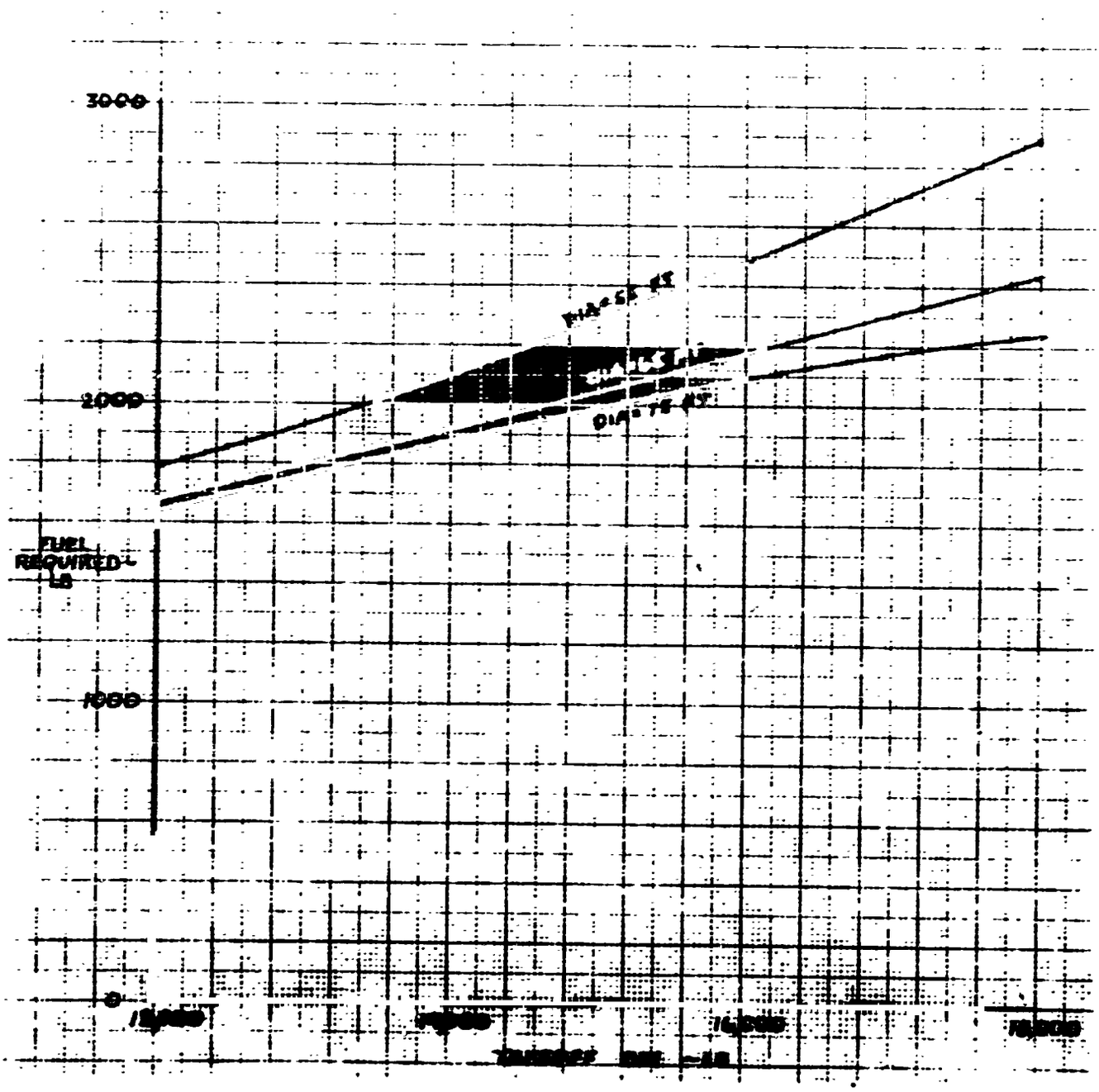

Figure 3-3 Fuel Required Vs Takeoff GW HSH Shaft-Driven σ = .12

the 200-knot cruise speed at reduced power levels. However, the 55-foot diameter rotor configuration, even with larger size engines, is speed-limited at normal rated power slightly below the desired cruise speed.

3.1.1.4 Fuel Available

The fuel available for various gross weights, rotor diameter, and solidities is presented in Figures 3-4, 3-5, and 3-6 for the high-speed shaft-driven helicopter.

3.1.1.5 Point Design Selection

Procedures. Having obtained the fuel required for the 27 configurations and the fuel available, the intersection of these data plotted versus gross weight determines a set of gross weights capable of performing the mission radius. The mission is performed at the desired cruise speed of 200 knots or HRP speed, whichever is less. Figure 3-7 is a plot of these gross weight intersections versus diameter. It is noted that the diameter for minimum gross weight (D = 67 ft) is constant for the three solidities and is well above the boundary for 200 knot cruise speed. Leading to the optimum gross weight, Figure 3-8 presents the minimum gross weights versus solidity for a diameter of 67 feet. This curve indicates that the optimum solidity for minimum gross weight has not been reached. However, to satisfy kinetic energy needed for transition to autorotation, minimum blade mass and, thus, solidity must be limited. Furthermore, blade centrifugal force determines coning angle at constant lift; a reduction in mass and, thus, centrifugal force increases the coning angle. In this case the coning angle is limited to 2.5 degrees which limits solidity to .0785 and gross weight to 14,870 pounds.

Performance. Presented in Table 3-3 is a summary of the optimized high-speed shaft-driven helicopter.

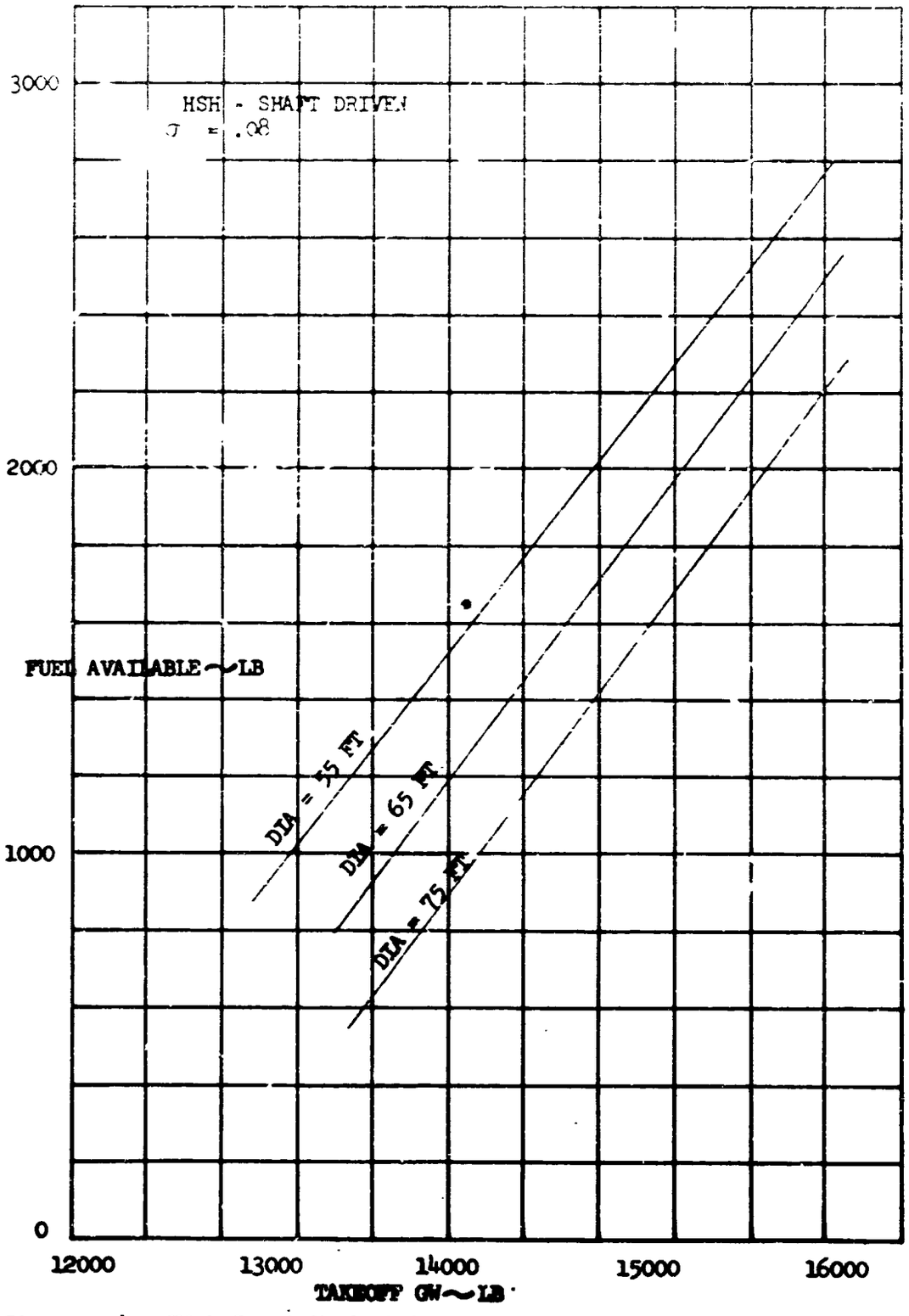

Figure 3-4 High-Speed Shaft-Driven Fuel Available Vs Rotor Diameter and Gross Weight

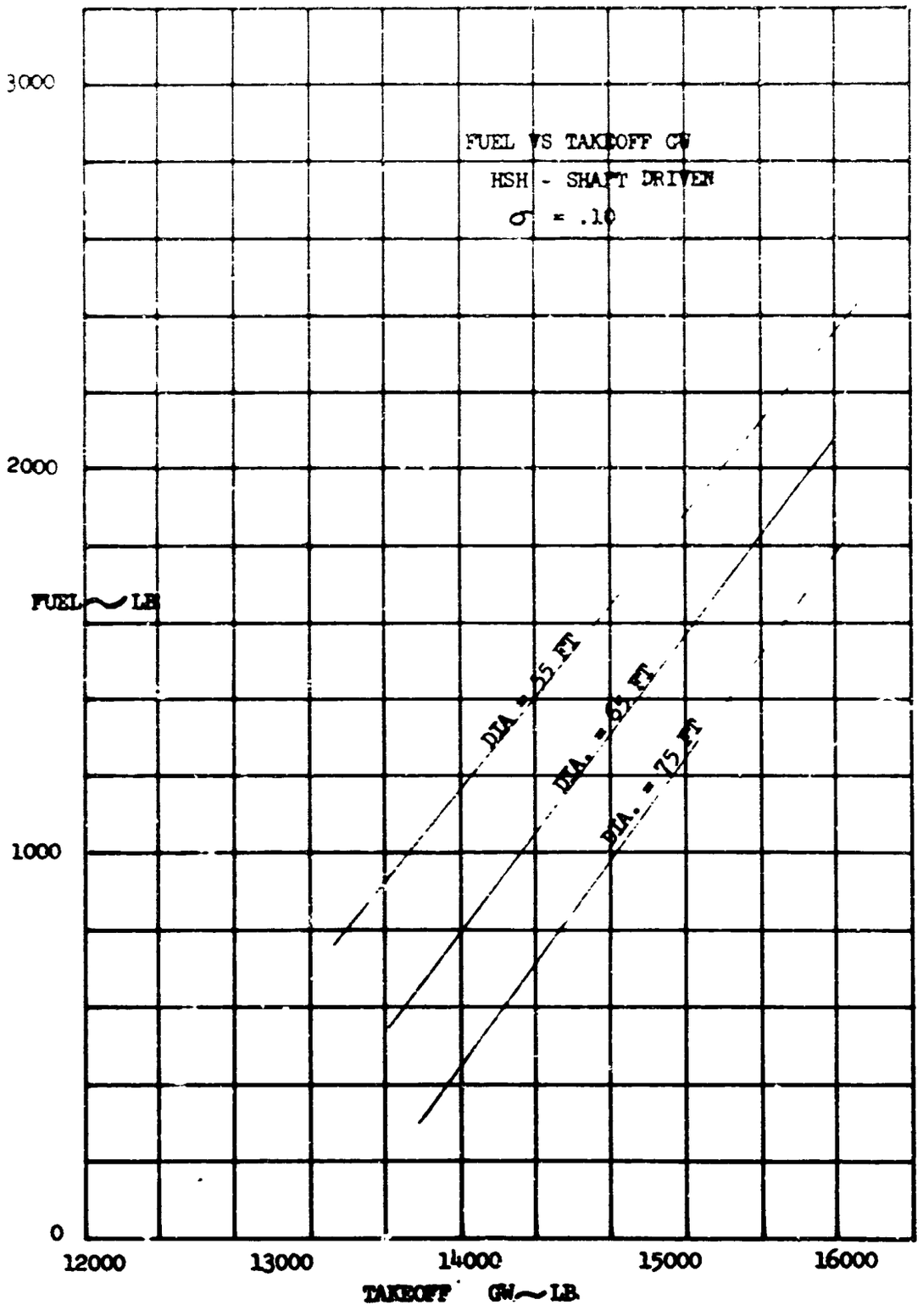

Figure 3-5 High-Speed Shaft-Driven Fuel Available Vs Rotor Diameter and Gross Weight

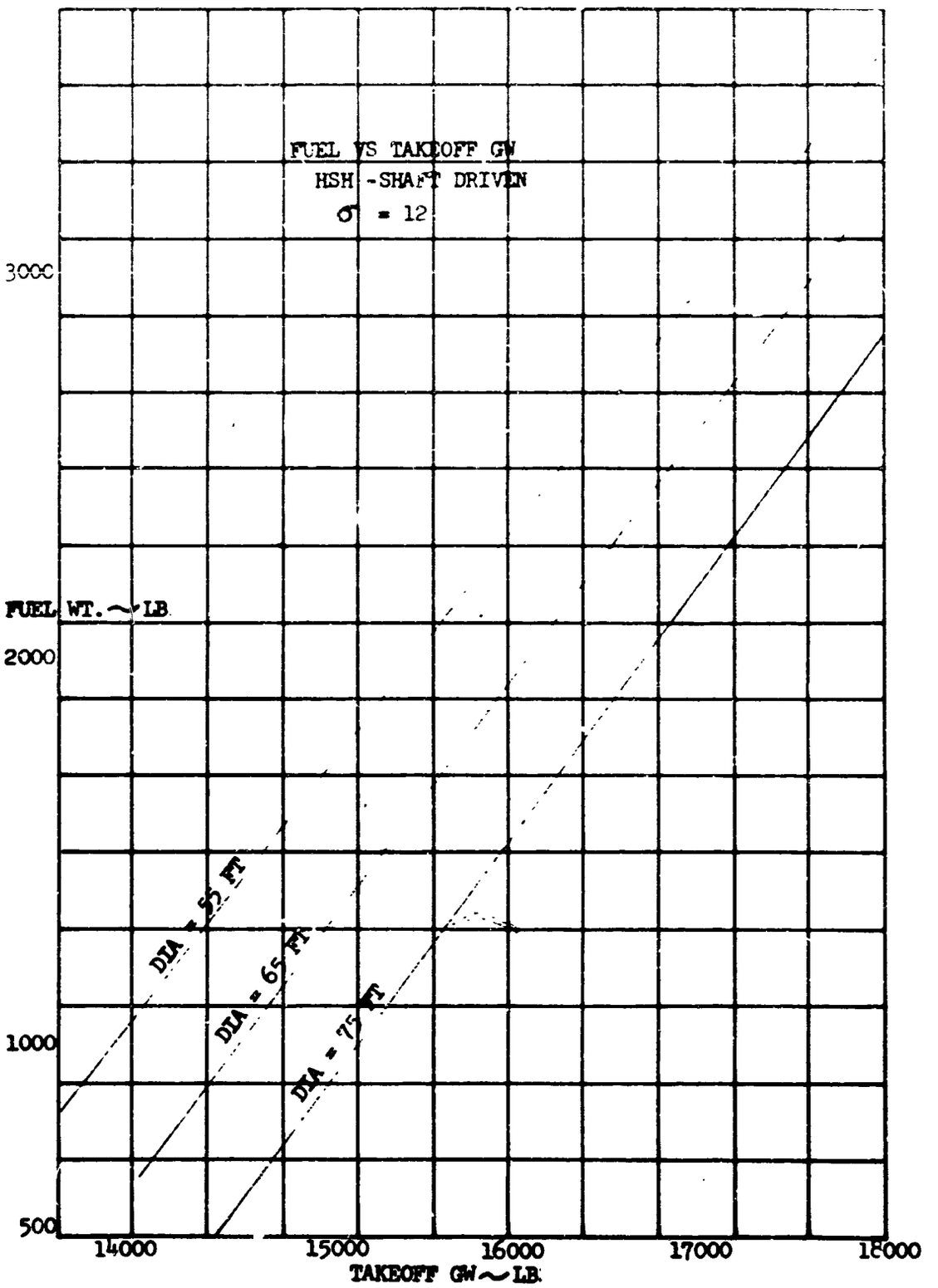

Figure 3-6 High-Speed Shaft-Driven Fuel Available Vs Rotor Diameter and Gross Weight

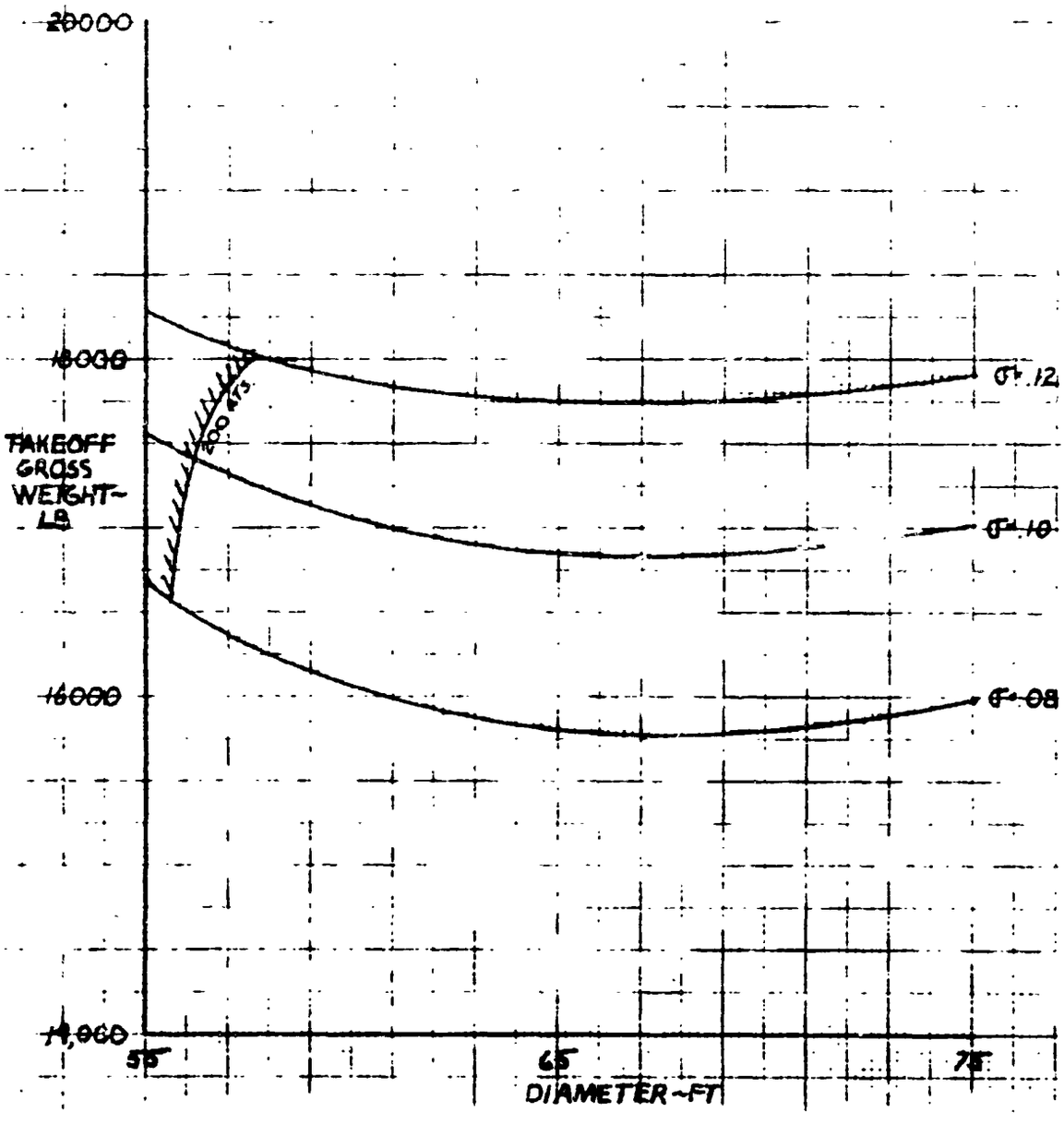

Figure 3-7 Takeoff Gross Weight Vs Diameter HSH-Shaft Driven

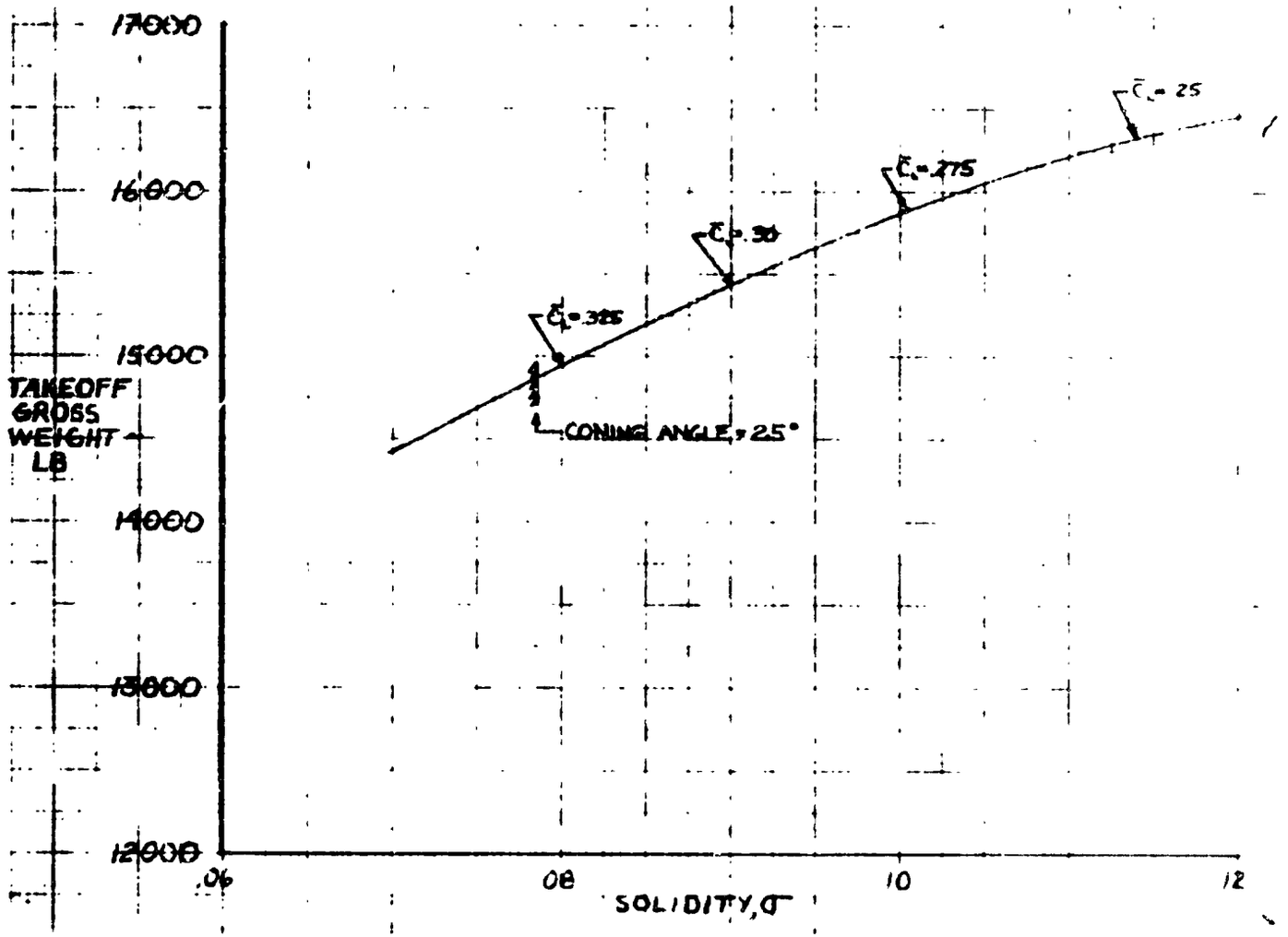

Figure 3-8 Takeoff Gross Weight Vs Solidity HSH-Shaft-Driven Dia = 67 Ft

The power and fuel requirements for the optimum shaft-driven configuration were checked by an independent means. The rated horsepower, based on hover, and the ESHP for a flight speed of 200 Knots was determined using Reference 1. A comparison is shown below:

	POINT DESIGN	CR-114
Rated horsepower, hp	2,395	2,370
ESHP at V = 200 Kt, hp	1,877	2,205
Fuel, lb	1,760	1,836

TABLE 3-3 HIGH-SPEED SHAFT-DRIVEN HELICOPTER

Gross weight, lb	14,870
Rotor diameter, ft	67
Solidity	.0785
No. of blades	2
Rotor tipspeed, ft/sec	640
Rated horsepower, hp	2,395
Fuel, lb	1,760
Payload, lb	4,000
OWE, lb	9,110

3.1.2 Jet-Flap Helicopter Optimization

3.1.2.1 Range of Parameters

Presented in Table 3-4 is the range of parameters for the high-speed jet-flapped helicopter study.

The range of these parameters was selected to yield average rotor lift coefficients consistent with results from the Ames First Series Wind Tunnel Test of the Dorand rotor.

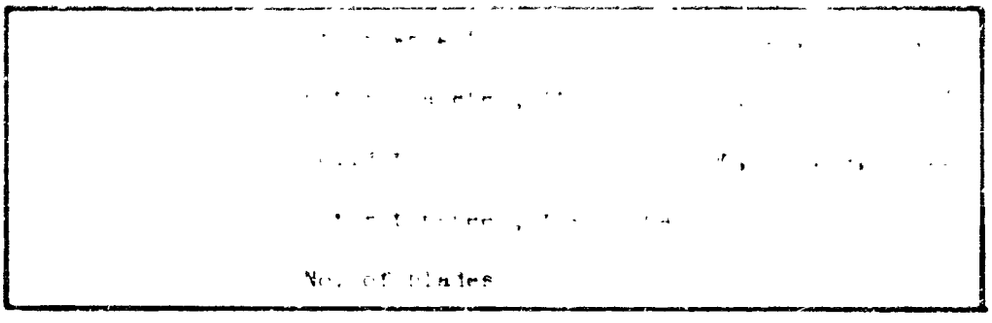

3.1.2.2 Engine Sizes

Presented in Figure 3-9 is the equivalent shaft horsepower at the rotor exhaust nozzle (see Section 4.0) used in sizing the engines. The power requirement, as for the shaft-drive helicopter, is based on a hover thrust/weight ratio, T/W = 1.0 K, at 6,000 ft, 95°F. As explained in Section 4.0 there exists a relationship between required blade duct flow area and available rotor shaft horsepower. Thus, for specific rotor diameters and number of blades, the minimum solidity is limited by the minimum blade chord required to accommodate the duct flow. This limit is shown in Figure 3-9. A side study proved that, for this range of solidity, the minimum gross weight vehicle capable of meeting the mission increased as solidity increased. Thus, by using the solidity defined by the duct area limit for each diameter, the lowest permissible optimum gross weight was obtained. Table 3-5 defines this solidity and the accompanying rated engine horsepower for the three gross weights and three diameters.

3.1.2.3 Fuel Required

Presented in Figure 3-10 is the fuel required to perform the design mission versus gross weight for diameters of 55 ft, 65 ft, and 75 ft.

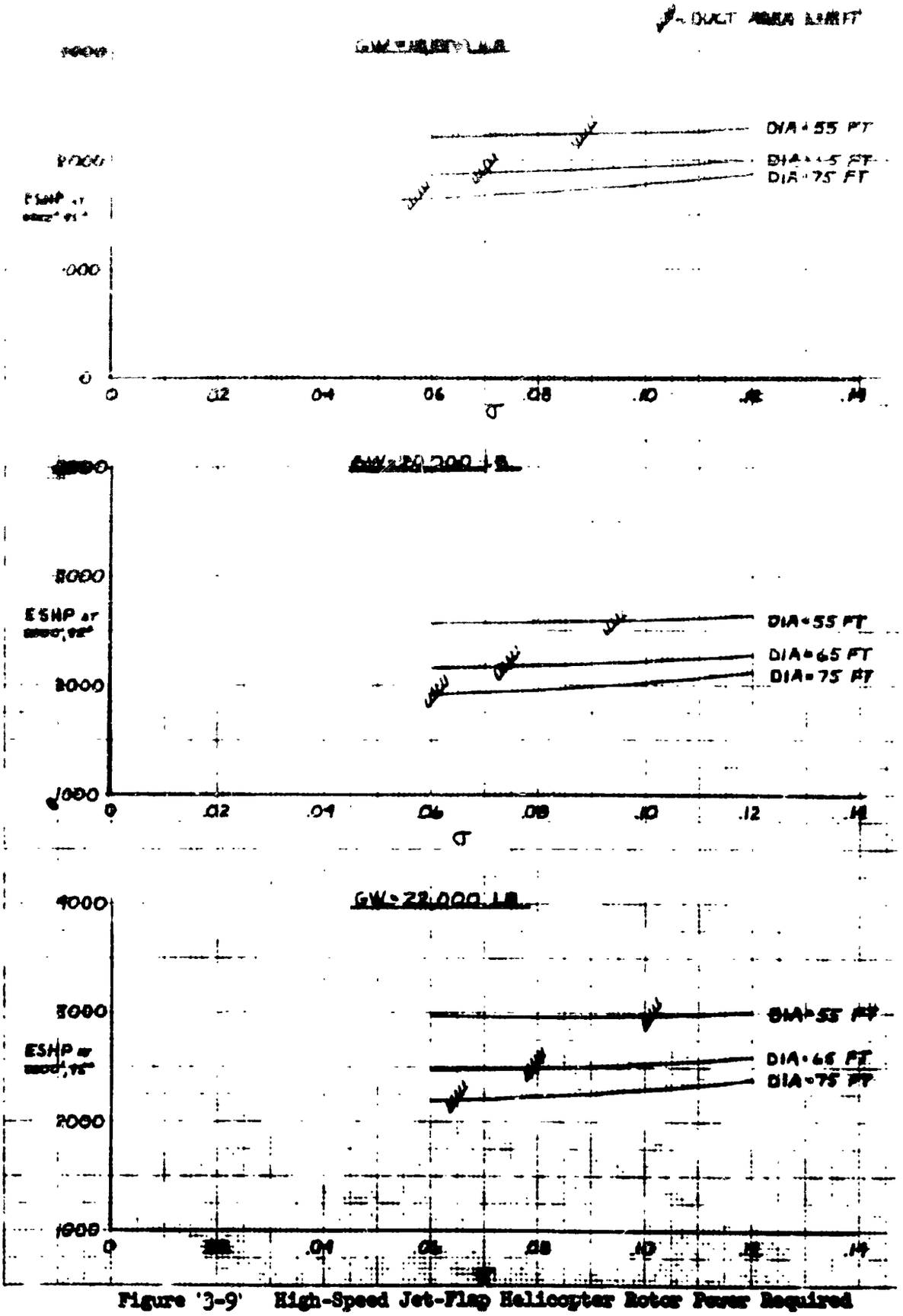

Figure '3-9' High-Speed Jet-Flap Helicopter Rotor Power Required

FUEL REQUIRED VS GW
HSH JET-FLAP
RANGE NM
V_{cr} = 200 KT

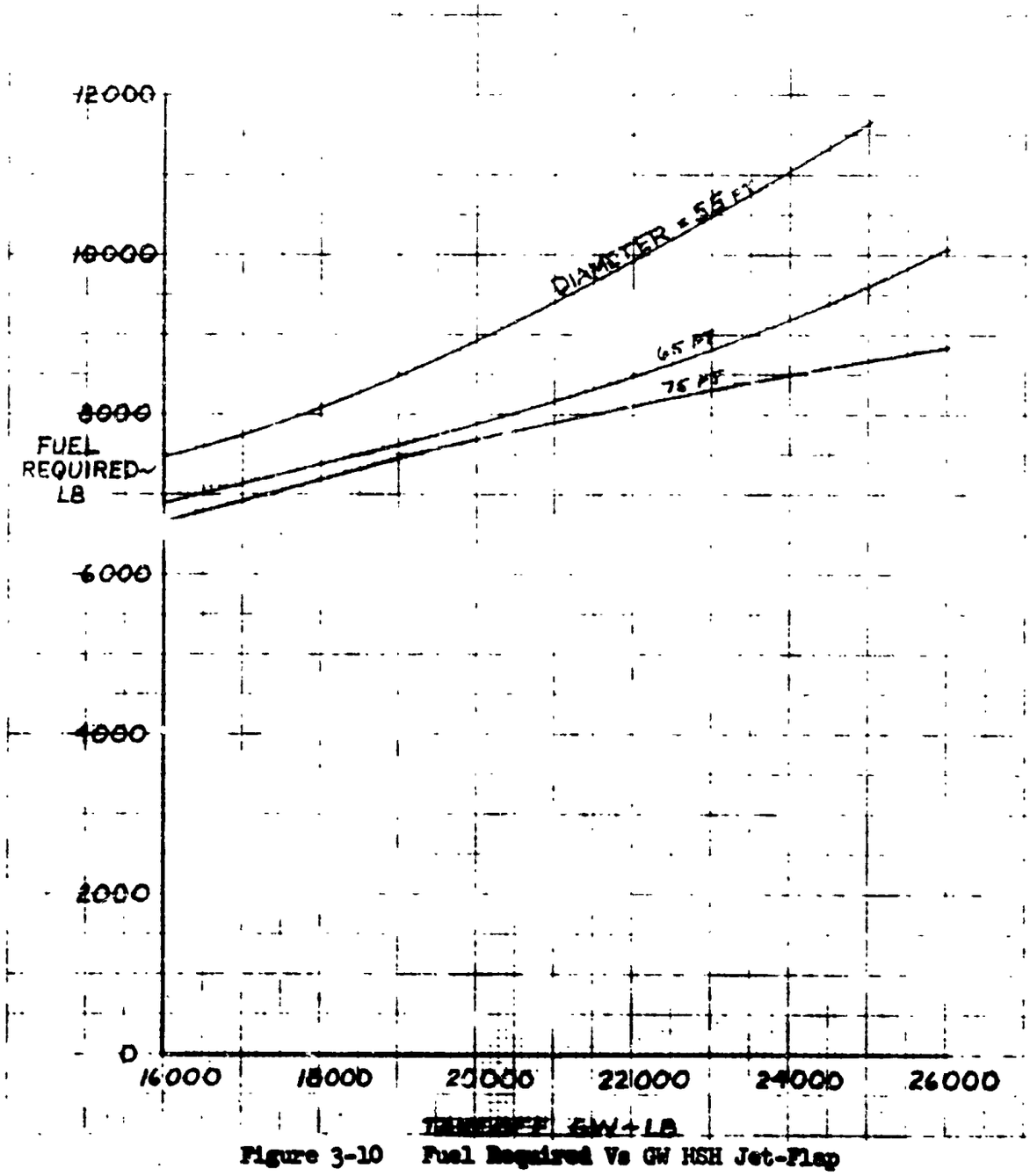

Figure 3-10 Fuel Required Vs GW HSH Jet-Flap

Due to the solidity limitation imposed by duct flow requirements, as explained in Paragraph 3.1.2.2, each combination of diameter and gross weight in Figure 3-10 corresponds to a specific solidity.

3.1.2.4 Fuel Available

Fuel available versus rotor diameter and gross weight is presented for the jet-flap HSH in Figure 3-11.

TABLE 3-5 RATED HORSEPOWER, HIGH-SPEED JET-FLAP HELICOPTER

V_T = 640 ft/sec

T/W = 1.0 K at 6,000 ft 95°

GW LB	DIA FT	DL LB/FT^2	σ	$SHP_{RATED\ T/O}$
18,000	55	7.58	.0892	12,860
	65	5.44	.070	10,300
	75	4.08	.0575	9,550
20,000	55	8.42	.0945	14,950
	65	6.04	.0745	12,650
	75	4.54	.0615	11,200
22,000	55	9.27	.102	17,350
	65	6.63	.0795	14,500
	75	4.99	.065	12,750

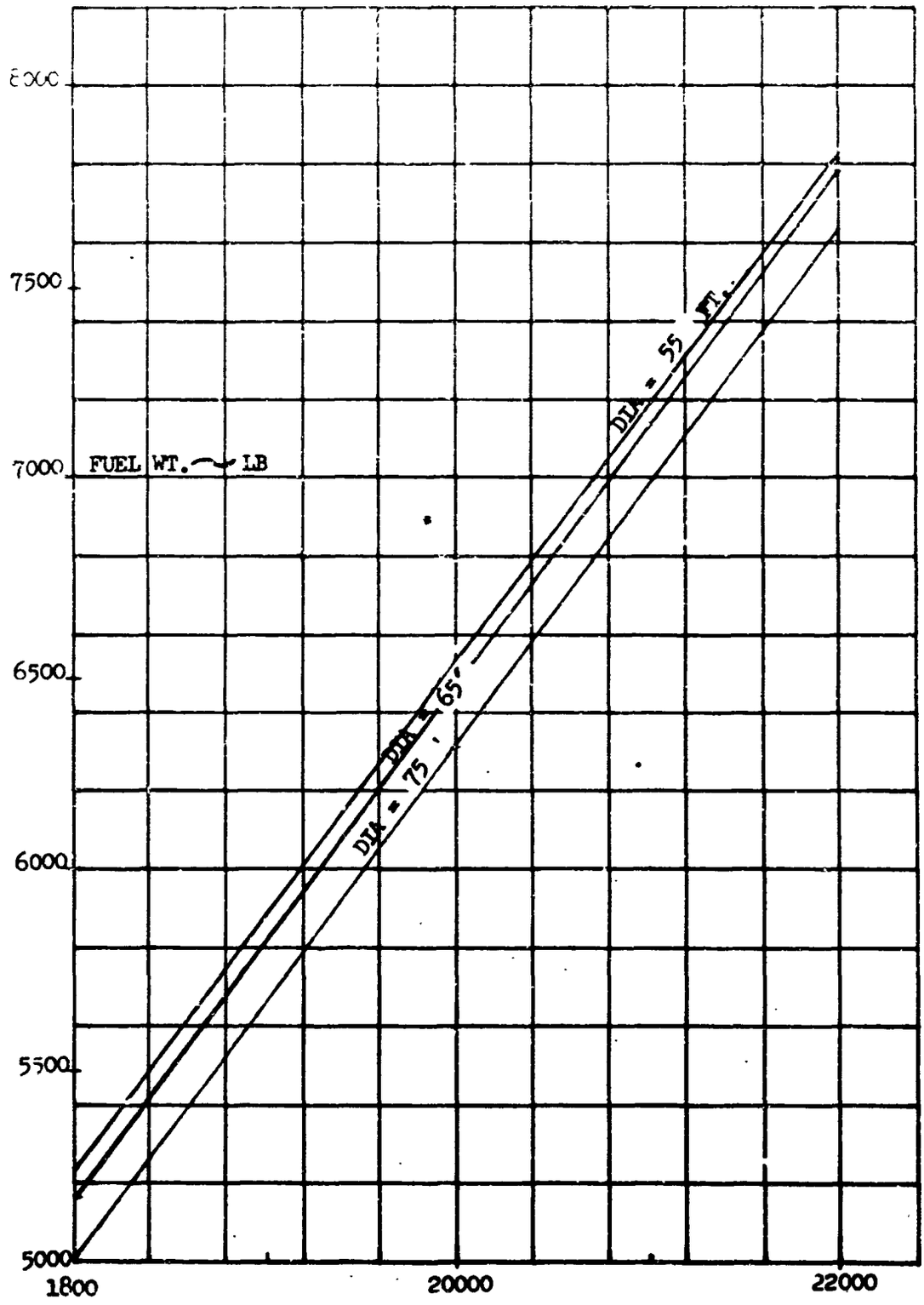

Figure 3-13 High-Speed Jet-Flap Fuel Available Vs Rotor Diameter and Gross Weight

3.1.2.5 Point Design Selection

Of the configurations shown in Table 3-5, those capable of meeting the mission requirements are shown in Figure 3-12 versus diameter. Initially, several radii-of-action were investigated. It is observed that the diameter for minimum gross weight is approximately 72 feet for each radius-of-action. Vehicle gross weight is 22,980 lb for the design mission radius of 150 nm. Constructed from the data of Table 3-5, Figure 3-13 defines the design solidity, σ = .0735, at the optimum gross weight.

Presented in Table 3-6 is a summary of the optimized high-speed jet-flapped helicopter.

TABLE 3-6 HIGH-SPEED JET-FLAPPED HELICOPTER

Gross weight, lb	22,980
Rotor diameter, ft	72.2
Solidity	0.0735
No. of blades	2
Rotor tipspeed, ft/sec	640
Rated horsepower, hp	14,040
Fuel, lb	8,345
Payload, lb	4,000
OWE, lb	10,635

To demonstrate validity of the results, an independent check was performed using the data extrapolated from the Dorand First Series Ames Wind Tunnel Tests. Results compare favorably as shown below.

	Point Design	Ames Test
Rated horsepower, hp	14,040	12,820
ESHP at V = 200 kt, hp	2,527	2,440
Fuel, lb	8,345	7,800

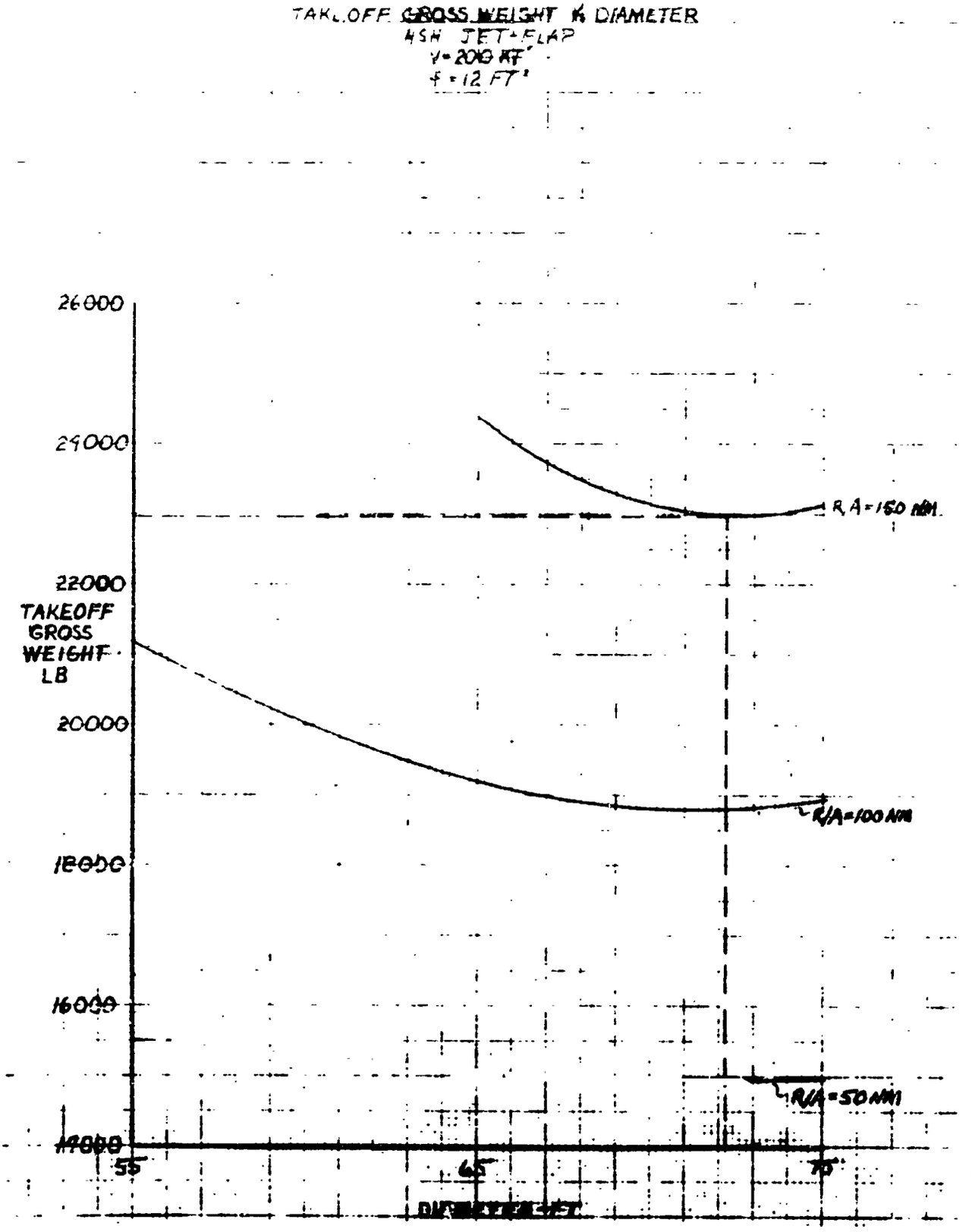

Figure 3-12 Takeoff Gross Weight Vs Diameter HSH-Jet-Flap

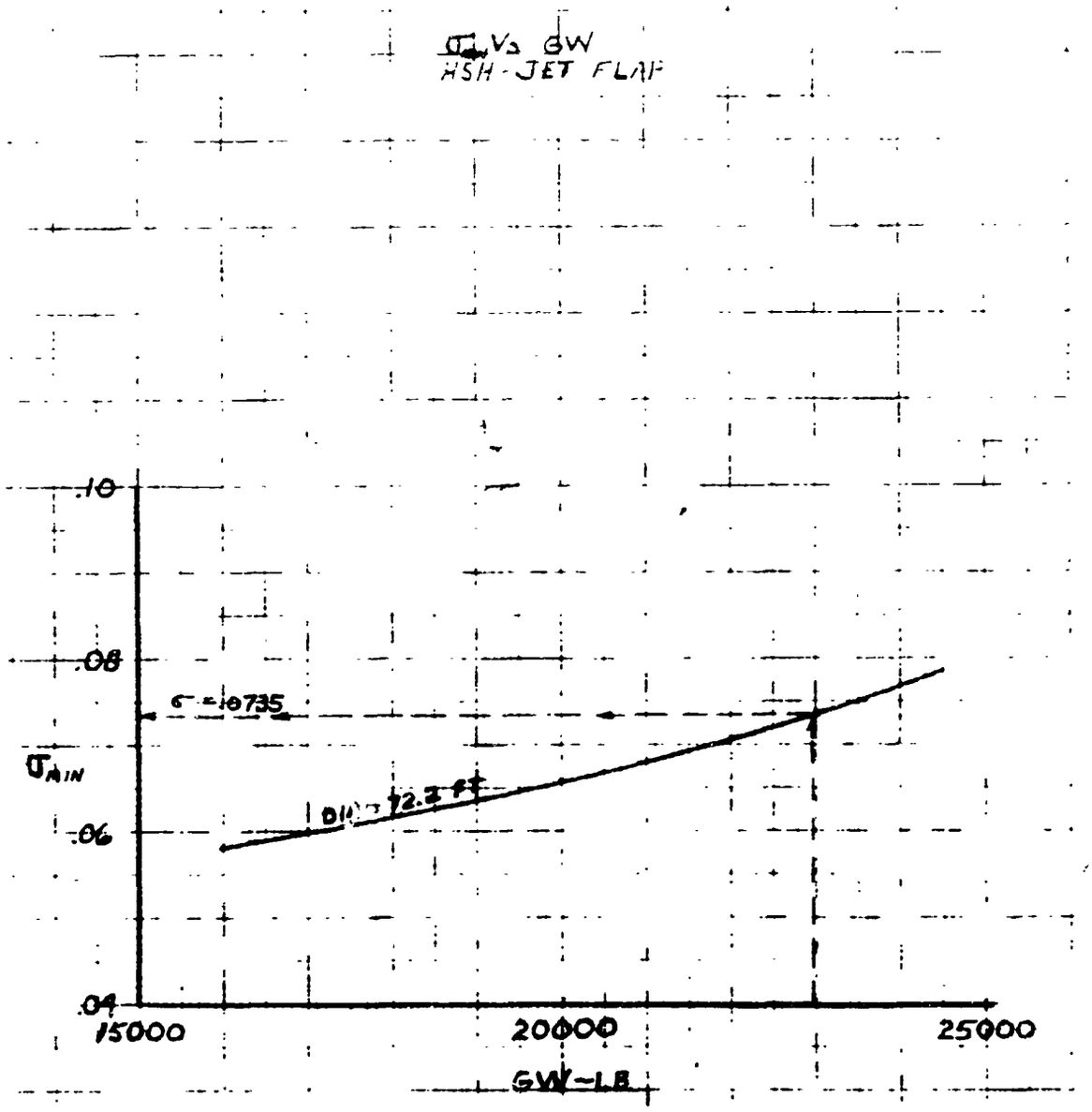

Figure 3-13 σ min Vs GW HSH-Jet Flap

F Deflection for Trim. Figure 3-14 defines the maximum trailing edge flap deflection for trim versus velocity for the high-speed jet-flapped helicopter. The angles were calculated using the LTV Rotor Performance Program No. 2 for a fixed-blade pitch at the 70% radius of $\theta_{.7}=4°$. The effect of c.g. location was investigated by assuming a range of c.g. positions defined by:

Location of c.g. = y/h

where y = distance of c.g. ahead of shaft

h = height of hub above c.g.

Since the lateral cyclic deflection is negligible, the flap deflections shown are the maximum and occur at azimuth positions of 90° and 270°. The deflections are the sum of the collective and longitudinal cyclic deflections as shown in Figure 3-15. In order to evaluate the maximum required deflections versus airspeed, it is necessary to consider both the advancing and retreating blades shown in Figure 3-14. As the speed increases and the disparity in relative "q" over the advancing and retreating blades increases, a greater contribution in terms of flap deflection is required of the retreating blade than of the advancing blade. Thus, there exists for each c.g. position a speed at which the 270° azimuth-position requires the more downward flap deflection. Such a curve is significant in assessing control available, control required, and possible limitation on c.g. range, trim speed, and maneuver load factor. Note, for example, that the limit trim speed for a design flap deflection of 50° down is 95 knots for Y/H = 0, and 170 knots for Y/H = .05. For Y/H = .1, trim with 50° flap is feasible only between 150 and 200 knots.

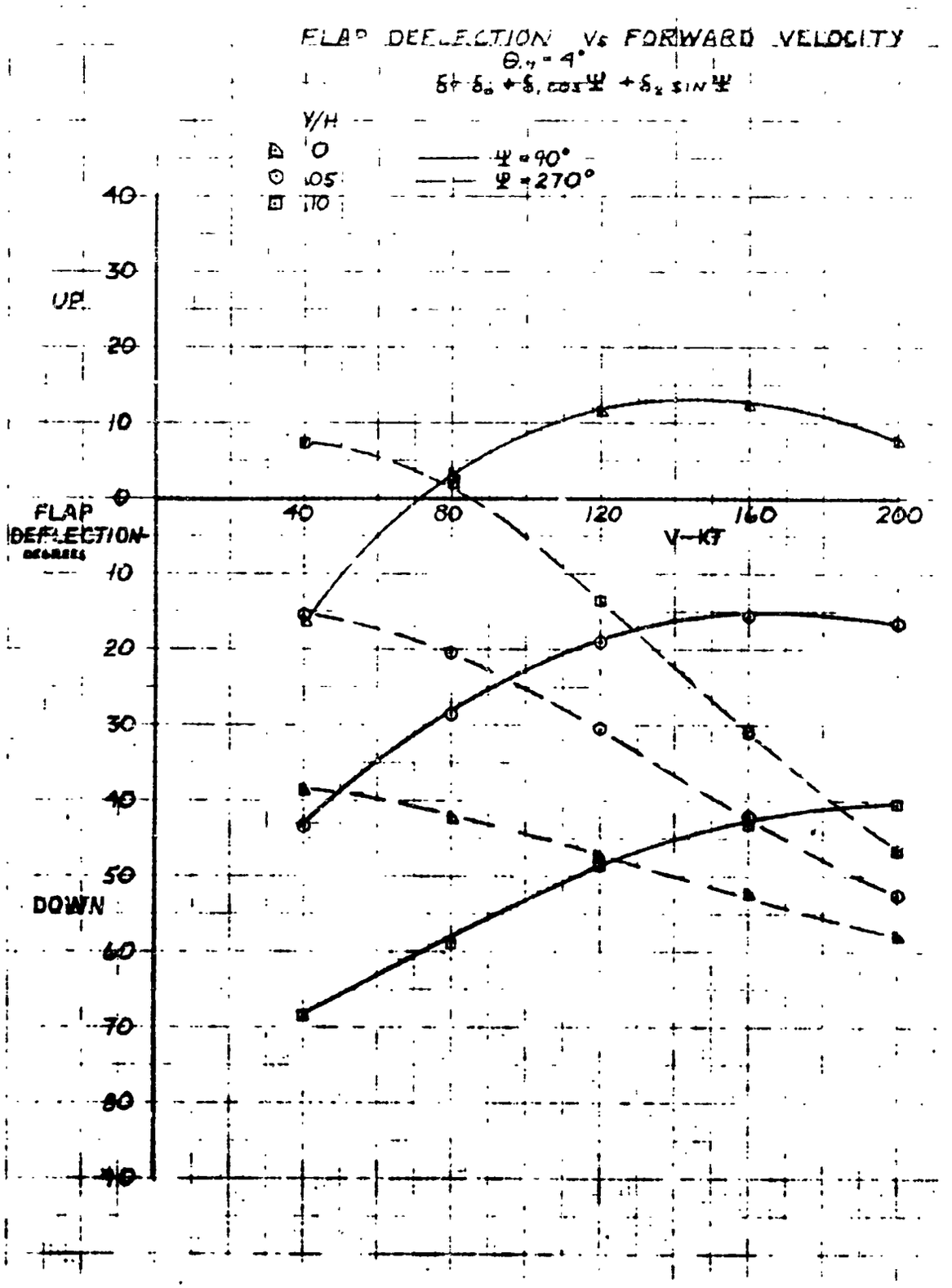

Figure 3-14 Flap Deflection Vs Forward Velocity

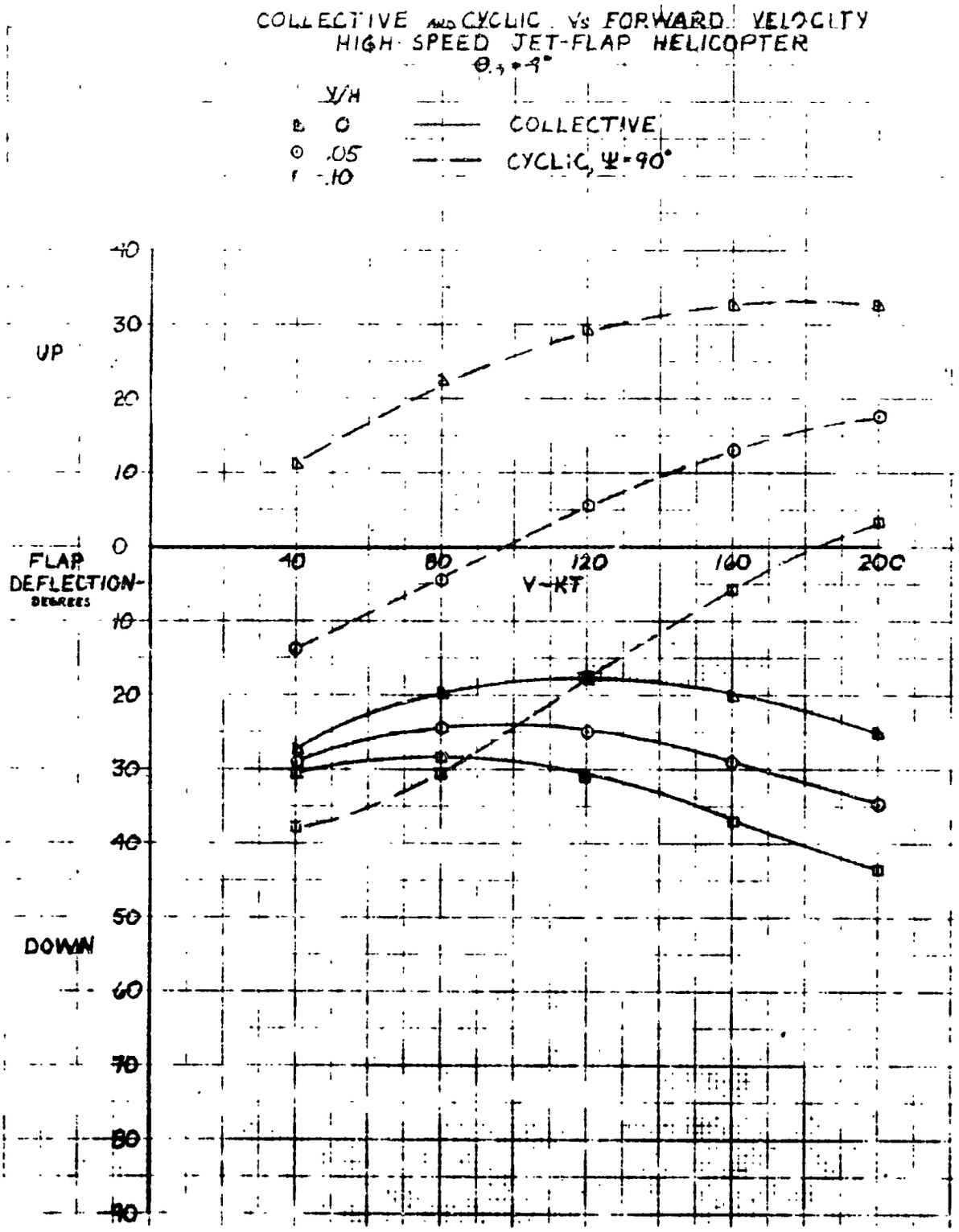

Figure 3-15 Collective and Cyclic Vs Forward Velocity High-Speed Jet-Flap Helicopter

3.1.3 Comparison - Shaft-Driven and Jet-Flap Concepts

Figures 3-16 and 3-17 present a comparison of the performance of the high-speed shaft-driven and jet-flap designs. Figure 3-16 shows mission time and payload-carrying capability versus radius of action. Mission time and payload-carrying capability versus cruise speed for the design radius of action is given in Figure 3-17. Pertinent physical characteristics of the two designs are summarized in Tables 3-3 and 3-6. The greater weight of the jet-flap vehicle is due to the power required to complete the design mission. This results in a higher fuel requirement for the jet-flap, approximately a 4.74 to 1 ratio compared to the shaft-driven vehicle, and thus the greater gross weight by 8,110 pounds.

Figure 3-17 gives the results of speed variation for the two vehicles for the design mission. It is noted that, if the cruise speed requirement is reduced from 200 knots to 160 knots and 150 knots for the jet-flap and shaft-driven vehicles respectively, approximately optimum cruise speeds, the jet-flap is capable of carrying about 1,000 pounds more payload than the shaft-driven vehicle over the design radius of action. However, the fuel requirement is again greater for the jet-flap design by a ratio of about 5.5 to 1.

3.1.4 Engine Selection

3.1.4.1 Hot/Warm Cycle

A limited parametric study was conducted to assist in determining the hot-warm cycle engine selection for the sensitivity study. In this study, the most optimistic (100% thrust recovery and 5% static duct pressure loss), intermediate (90% T.R. and 15% D.L.), and pessimistic (80% T.R. and 25% D.L.) cases were run through the HSH mission routine with high, intermediate, and

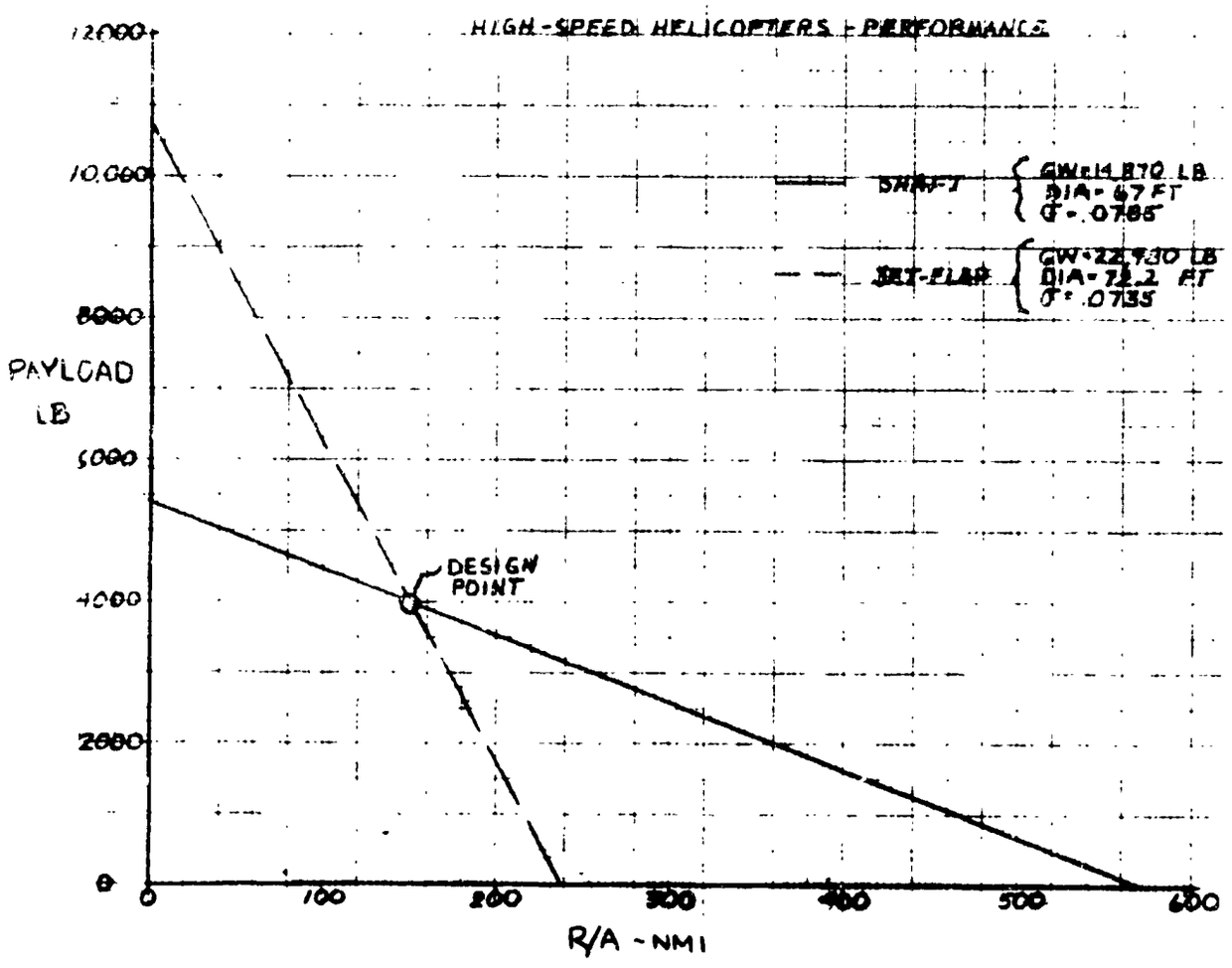

Figure 3-16 High-Speed Helicopters-Performance

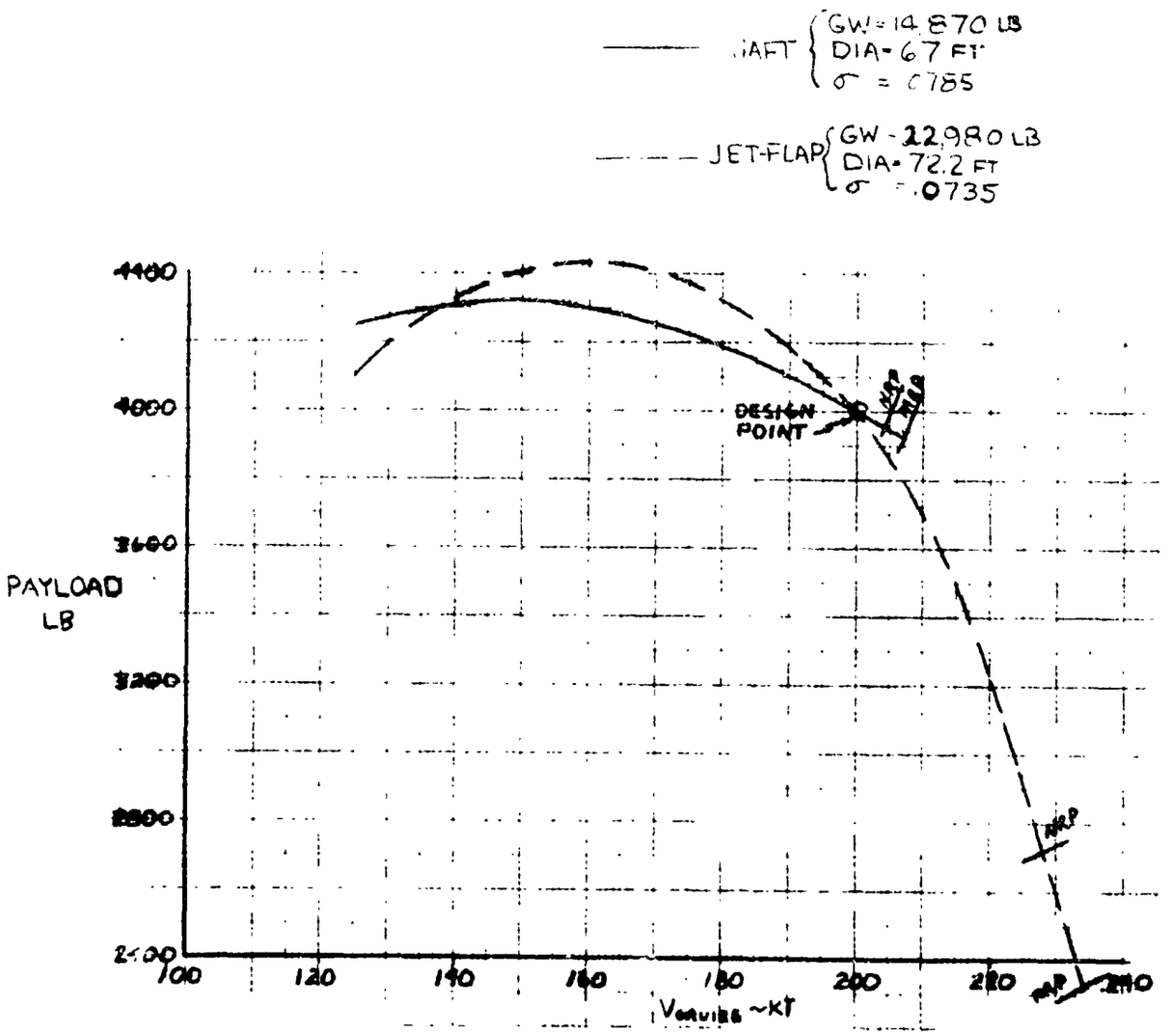

Figure 3-17 High-Speed Helicopters-Performance Payload Vs Cruise Speed

low engine pressure ratios (engines 4, 5, and 6). The solidity for each parametric configuration was based on the duct flow requirements of each engine for a rotor diameter of 72.2 ft.

Figures 3-18, 3-19, and 3-20 present fuel available and required for the three engines of the parametric study. To determine the effect of disc loading, a similar study was conducted for the intermediate propulsion case (90% T.R. and 15% D.L.) at diameters of 55 and 65 feet. Figures 3-21, and 3-22 present fuel available and required.

3.1.4.2 Cold Cycle

A similar study was conducted to select the optimum pressure ratio for the cold cycle high-speed helicopter. Figure 3-23 shows the fuel required and available for pressure ratios of 2.0, 3.0, and 4.2.

3.1.5 High Speed Compound

The high-speed helicopter modified with an auxiliary thrust was evaluated. Configurations were sized for three cases using auxiliary cruise thrust, i.e. (1) a turbojet exhaust, (2) a turbotip fan, and (3) a turboprop. The engine size for each parametric point is based on the jet-flap hover requirement only. An auxiliary engine was included to drive the turboprop design. The following basic high-speed parameters were fixed:

Engine	= No. 1 (PR = 4.05)
Thrust recovery	= 90%
Duct loss	= 15%
Equiv. flat plate area	= 12 FT^2
Duct area ratio	= .5
Rotor Diameter	= 72.2 Ft.

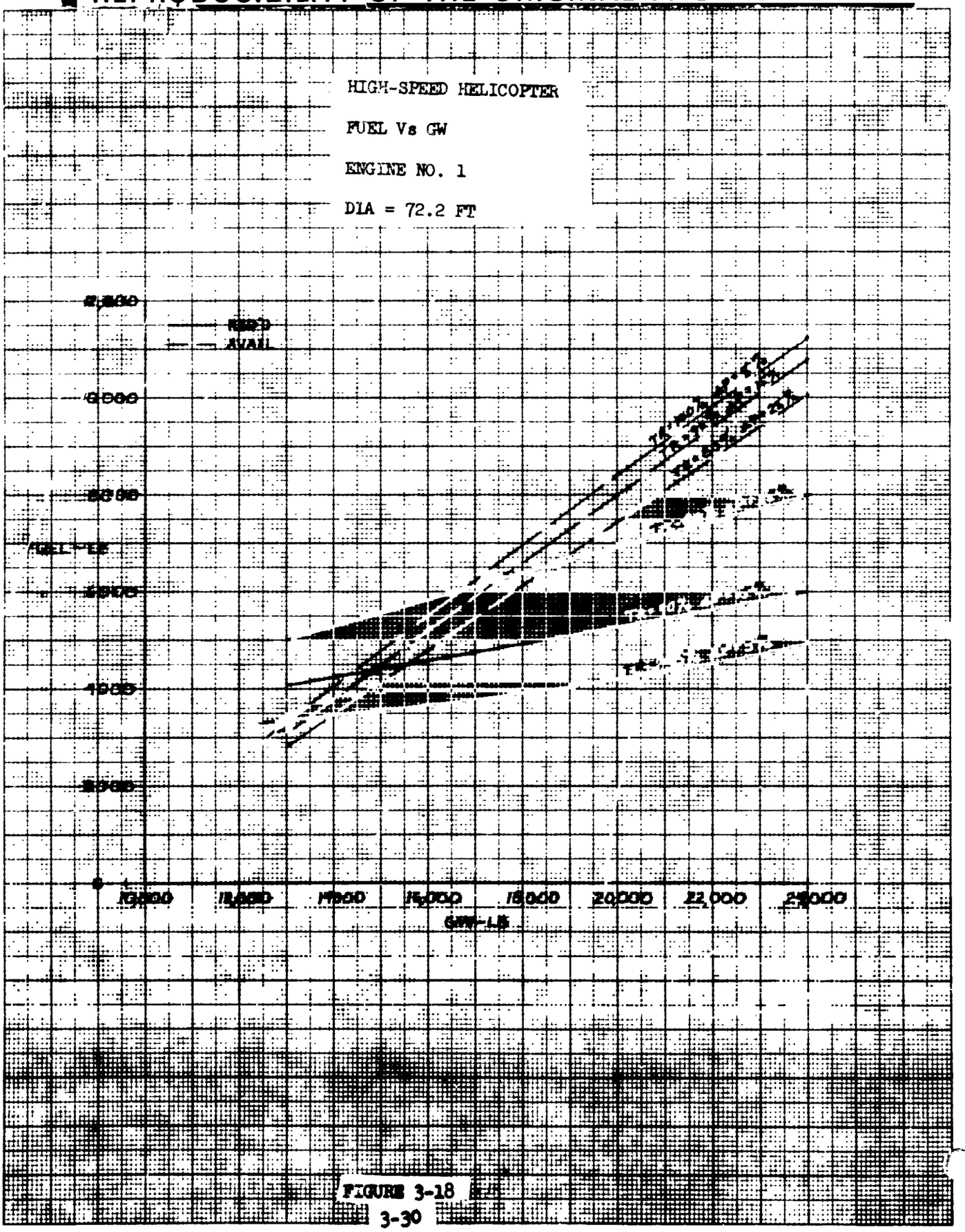

FIGURE 3-18

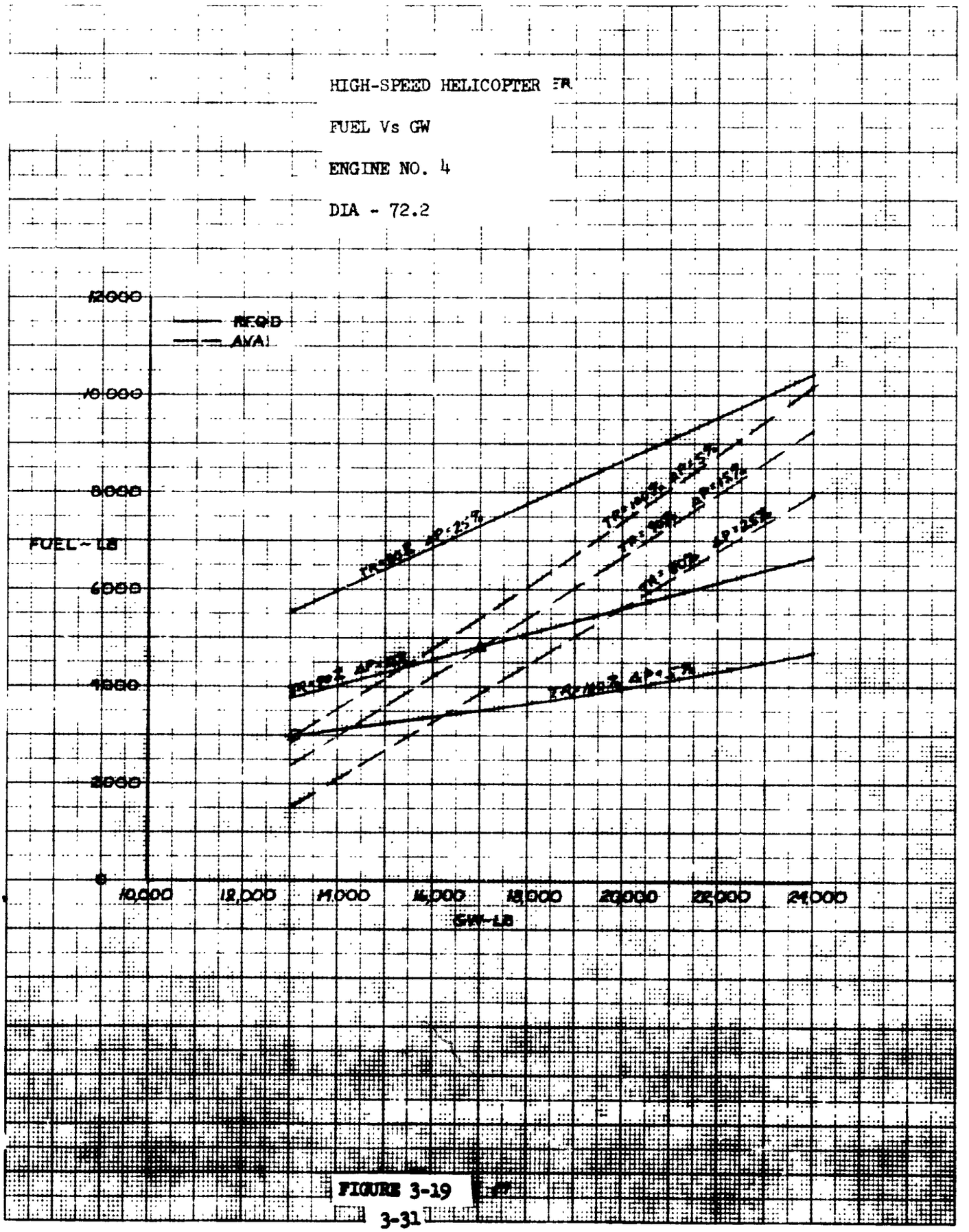

FIGURE 3-19

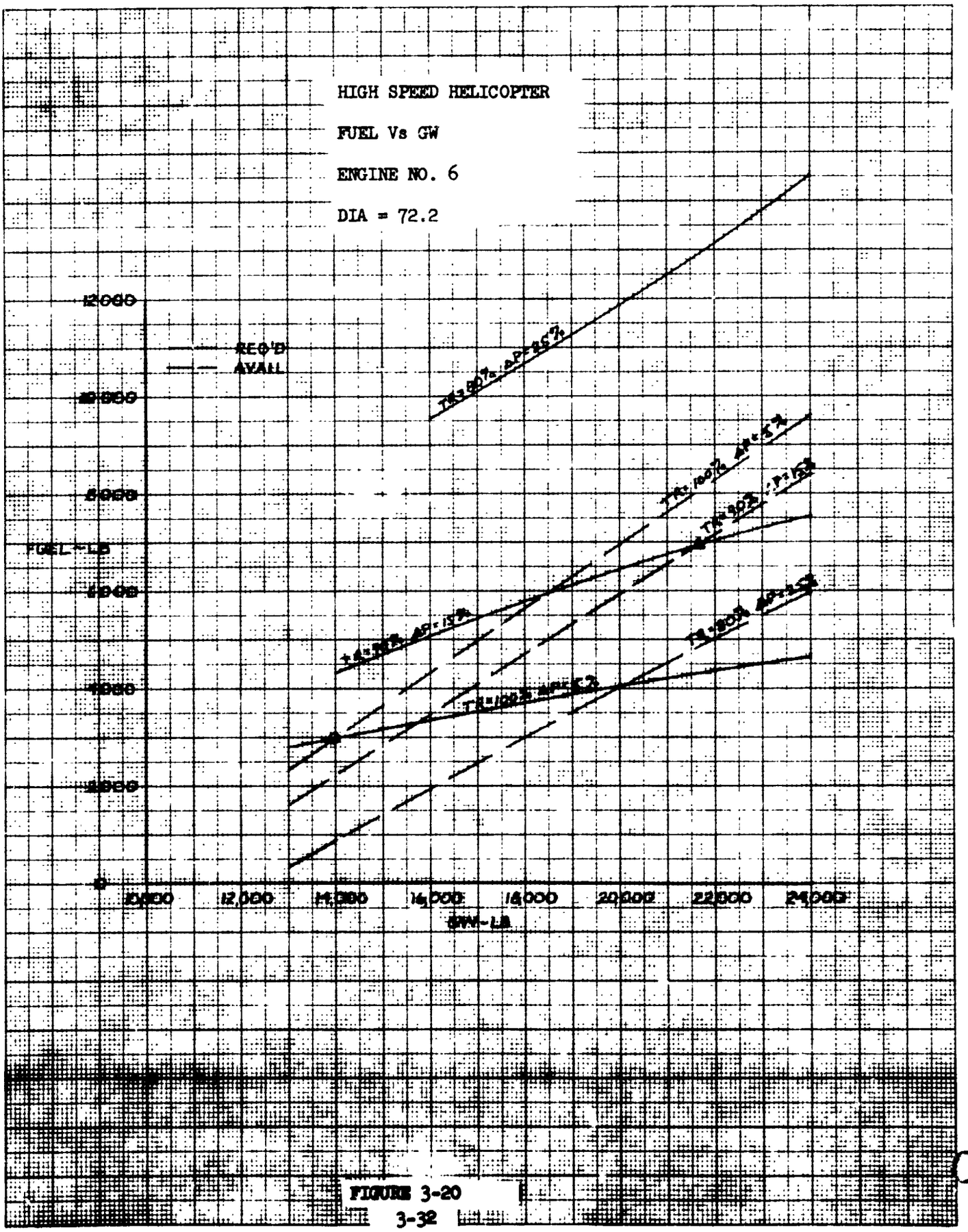
HIGH SPEED HELICOPTER
FUEL Vs GW
ENGINE NO. 6
DIA = 72.2
REQ'D
AVAIL
FUEL-LB
GW-LB
12000
10000
8000
6000
4000
2000
0
10,000
12,000
14,000
16,000
18,000
20,000
22,000
24,000

FIGURE 3-20

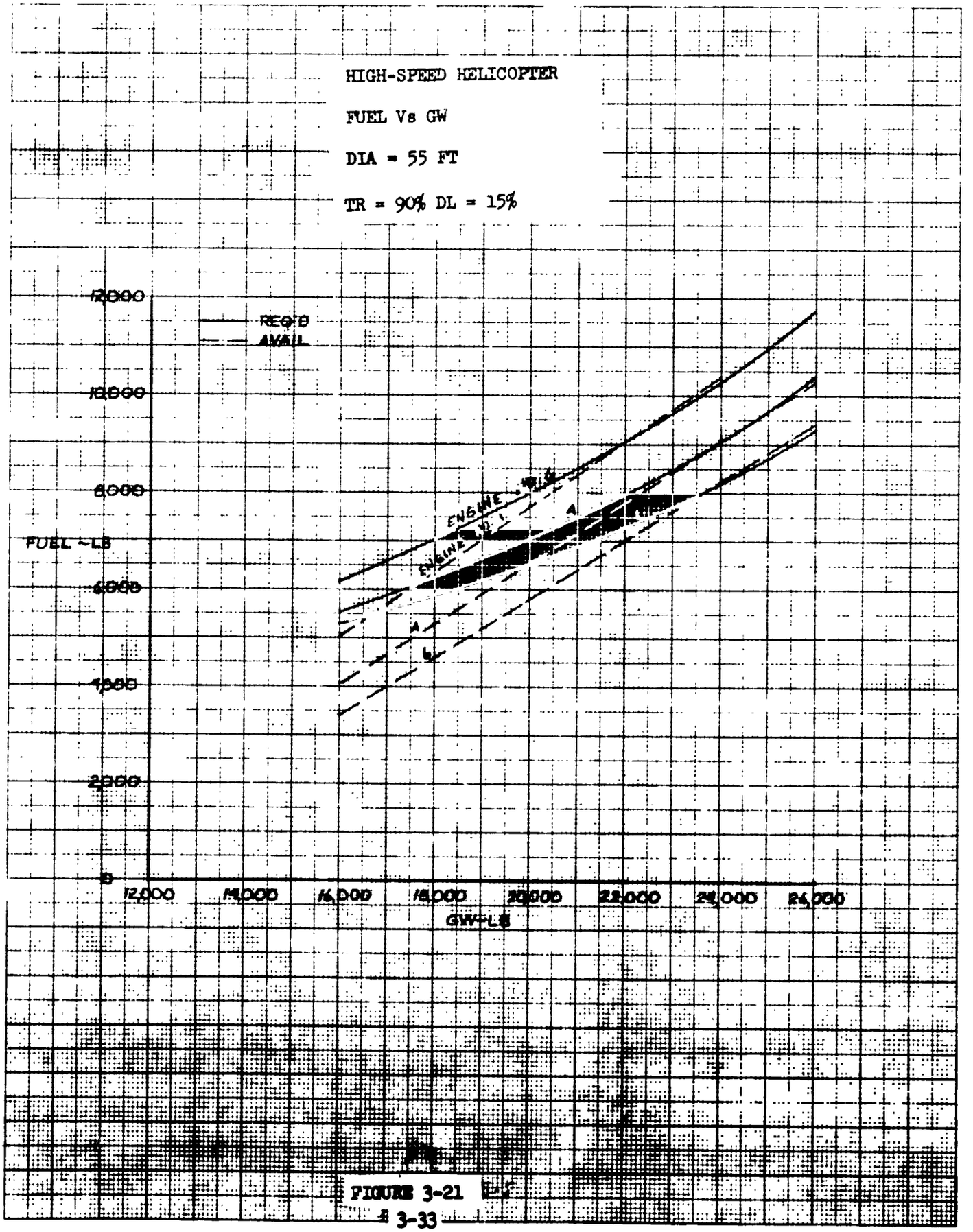
HIGH-SPEED HELICOPTER
FUEL Vs GW
DIA = 55 FT
TR = 90% DL = 15%
REQ'D
AVAIL
ENGINE NO. 1
ENGINE NO. 2
A
B
FUEL ~LB
12,000
10,000
8,000
6,000
4,000
2,000
0
12,000
14,000
16,000
18,000
20,000
22,000
24,000
26,000
GW~LB

FIGURE 3-21

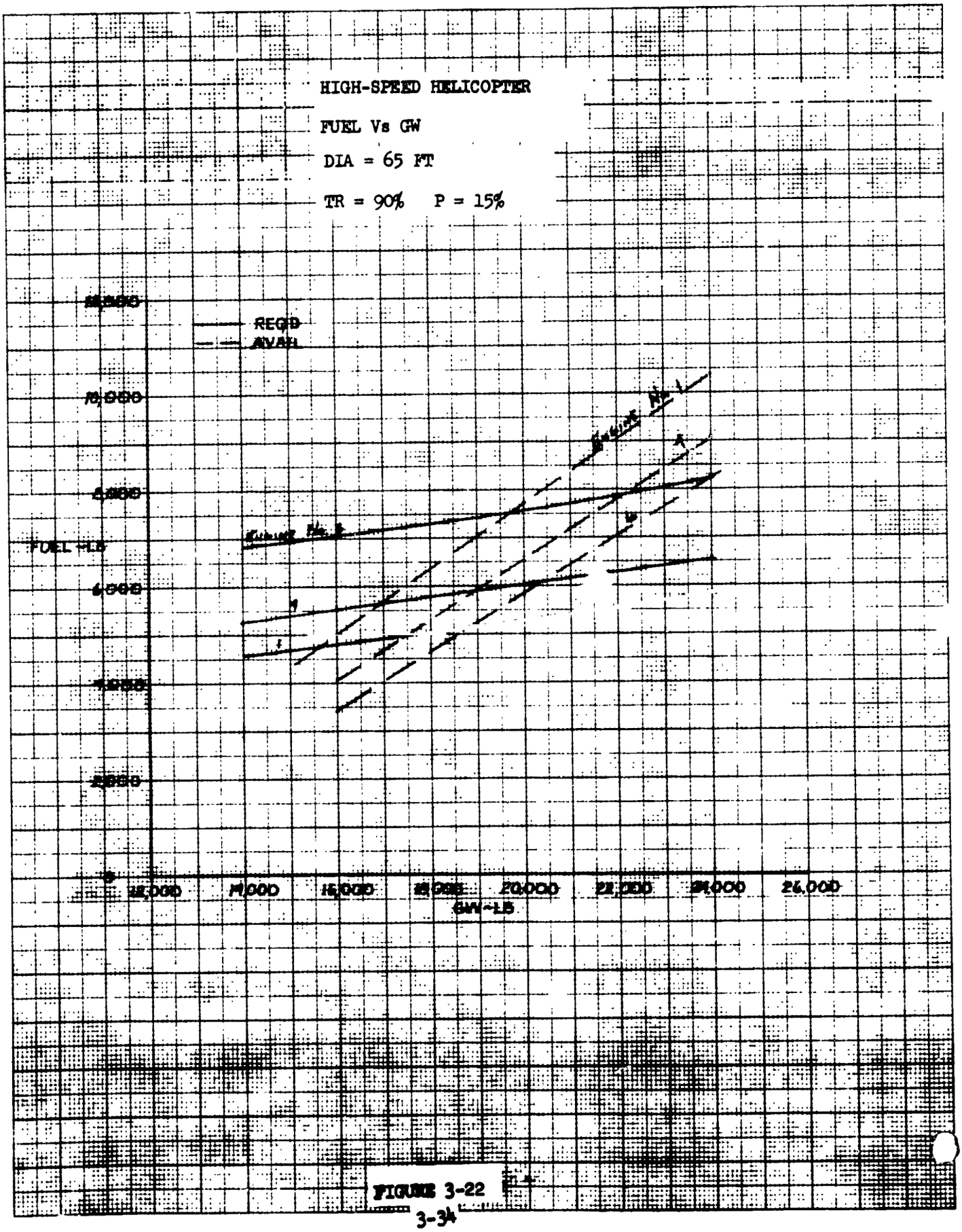
HIGH-SPEED HELICOPTER
FUEL Vs GW
DIA = 65 FT
TR = 90% P = 15%
REQD
AVAIL
FUEL-LB
GW-LB
24,000

FIGURE 3-22

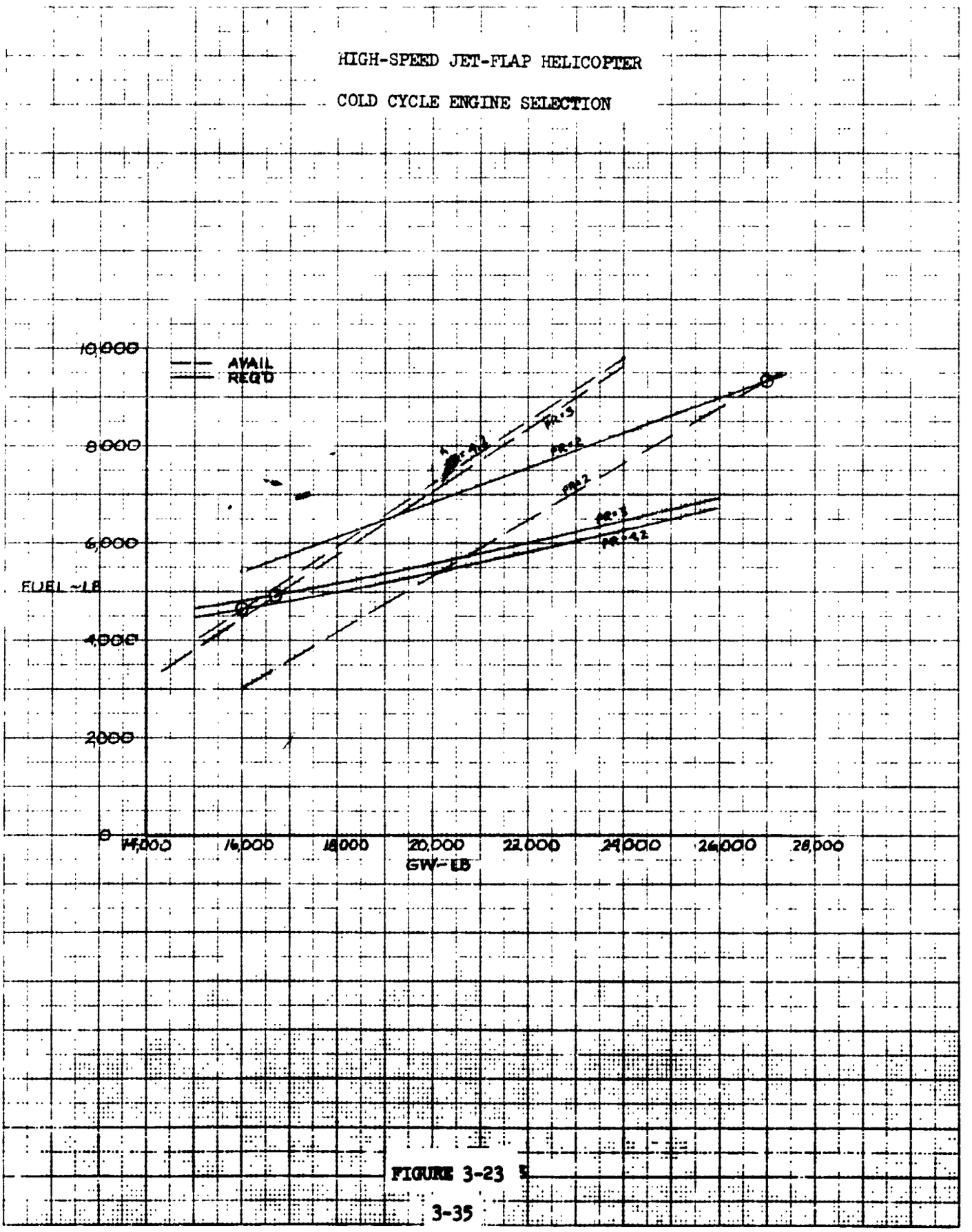
HIGH-SPEED JET-FLAP HELICOPTER
COLD CYCLE ENGINE SELECTION
AVAIL
REQ'D
10,000
8000
6,000
4,000
2000
0
FUEL ~LB
14,000
16,000
18000
20,000
22,000
24,000
26,000
28,000
GW-LB

FIGURE 3-23

Figure 3-24 gives the resulting fuel required and available curves.

3.1.6 High-Speed Tip Jet

The effect on the point design of splitting the gas flow between the flap and tip-jet nozzle was investigated for the high-speed version. Figure 3-25 presents the resulting fuel required-fuel available leading to the minimum gross weights capable of completing the high-speed mission.

3.2 HEAVY-LIFT HELICOPTER PARAMETRIC STUDY

The design mission for both the heavy-lift shaft-driven and jet-flapped helicopters is detailed below:

Payload	=	40,000 lb
Radius of Action	=	10 nm
Cruise Speed	=	40 knots
Power Requirement	=	T/W = 1.1K at SL Std
Warmup & Hover	=	5 min
Mid-Mission Hover	=	2 min
Reserve	=	10% initial fuel

3.2.1 Shaft-Driven Helicopter Optimization

3.2.1.1 Range of Parameters

A limited parametric study was employed in defining the heavy-lift shaft-driven helicopter. Based on the Sikorsky S-64 Sky-Crane, a six-bladed rotor with a disc loading of 10.3 psf and a solidity of 0.106 was employed as typical of present-day heavy-lift helicopters. Thus, by fixing the disc loading, a specific diameter is matched to each of the gross weights used in the study. The range of parameters is shown in Table 3-7 .

FUEL Vs GW

HIGH-SPEED JET-FLAP HELICOPTER with AUXILIARY THRUST

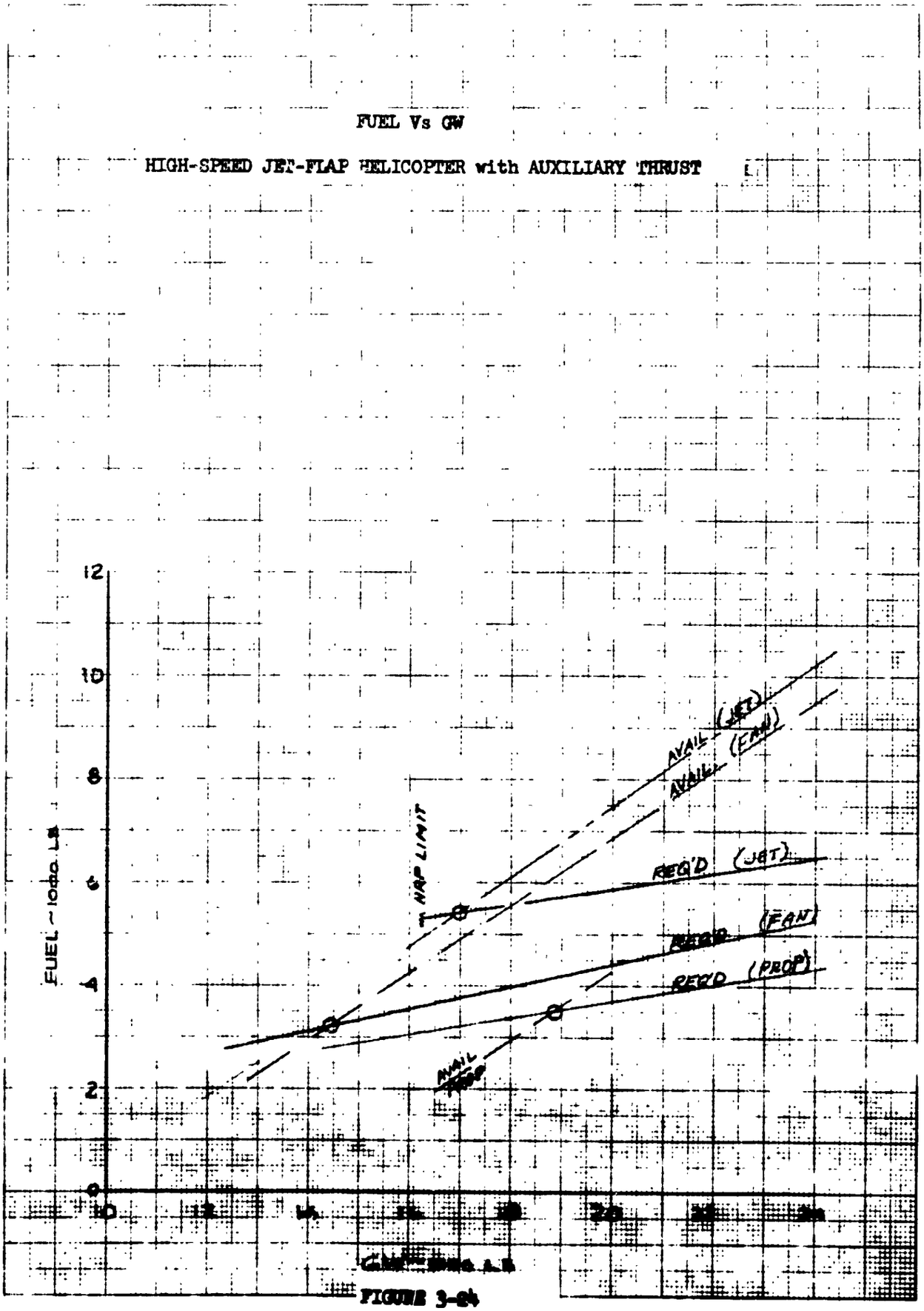

FIGURE 3-24

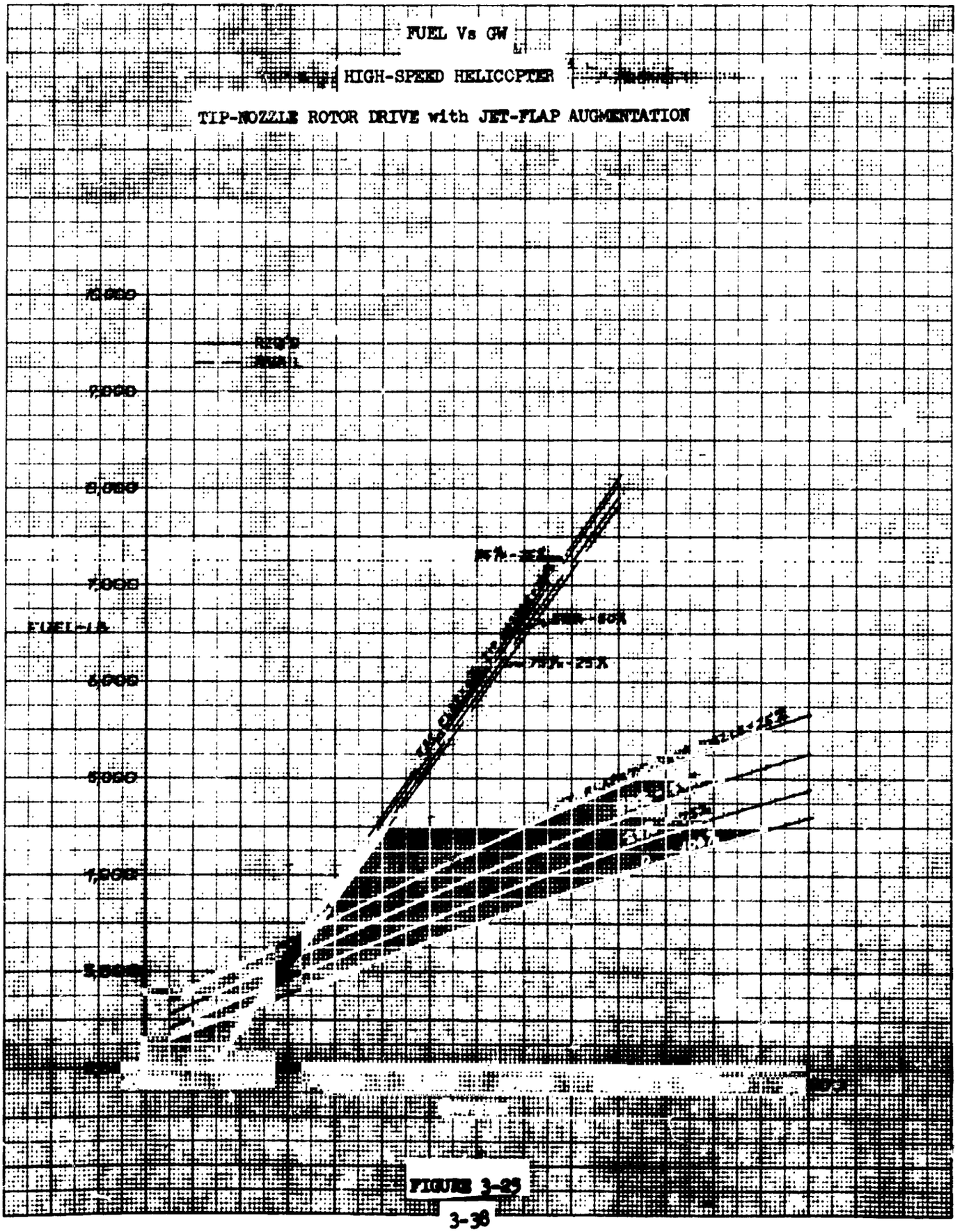
FUEL Vs GW
HIGH-SPEED HELICOPTER
TIP-NOZZLE ROTOR DRIVE with JET-FLAP AUGMENTATION

FIGURE 3-25

It will be noted that for the gross weights corresponding to the 20-ton payload vehicle, the 10.3 psf disc loading results in a rotor diameter of around 100 ft. It will be noted in Paragraph 3.2.2 that the rotor of the optimum heavy-lift jet-flap vehicle is 145 ft with a lower disc loading. Because of torque, reduction gear ratio, and tail rotor-main rotor interference considerations, it is believed that rotor diameters around 100 ft represent a reasonable maximum for shaft-driven vehicles of this class.

TABLE 3-7

HEAVY-LIFT SHAFT-DRIVEN HELICOPTER

PARAMETRIC CONFIGURATIONS

DISC LOADING = 10.3 Lb/Ft^2

NO. OF BLADES = 6

TIPSPEED = 700 Ft/Sec.

GROSS WEIGHT Lbs.	DIAMETER Ft.
70,000	93.0
80,000	99.4
90,000	105.5

A tipspeed of 700 fps was selected in order to yield an average rotor lift coefficient, $\bar{C}_L$ = 0.5, consistent with present technology. By using this approach for the shaft-driven helicopter, i.e., assuming a fixed disc loading and solidity, the resulting point design, if not optimum, can only be conservative.

3.2.1.2 Engine Sizes

The engine sizes for the heavy-lift shaft-driven helicopter are calculated using the LTVAC Rotor Performance Program No. 3 described in Appendix A. Listed in Table 3-8 is the rated horsepower for each gross weight, based on the hover requirement at origin to produce a rotor thrust/gross weight ratio = 1.1 at SL standard conditions .

TABLE 3-8.

ENGINE SIZE

GROSS WEIGHT Lbs	DIAMETER Ft	SHP_{Rated} Hp
70,000	93.0	12,420
80,000	99.4	13,910
90,000	105.5	15,440

3.2.1.3 Fuel Required

The fuel required to perform the design mission is shown in Figure 3-26 versus gross weight. The calculations were accomplished using the LTV Mission Performance Program, described in Appendix A. The fuel available is also presented versus gross weight, with the intersection of the two curves defining the design gross weight, i.e., the minimum gross weight capable of meeting the mission requirements for the disc loading and $\bar{C}_L$ specified.

3.2.1.4 Fuel Available

The fuel available is presented in Figure 3-26 as a function of gross weight for the shaft-driven HLH.

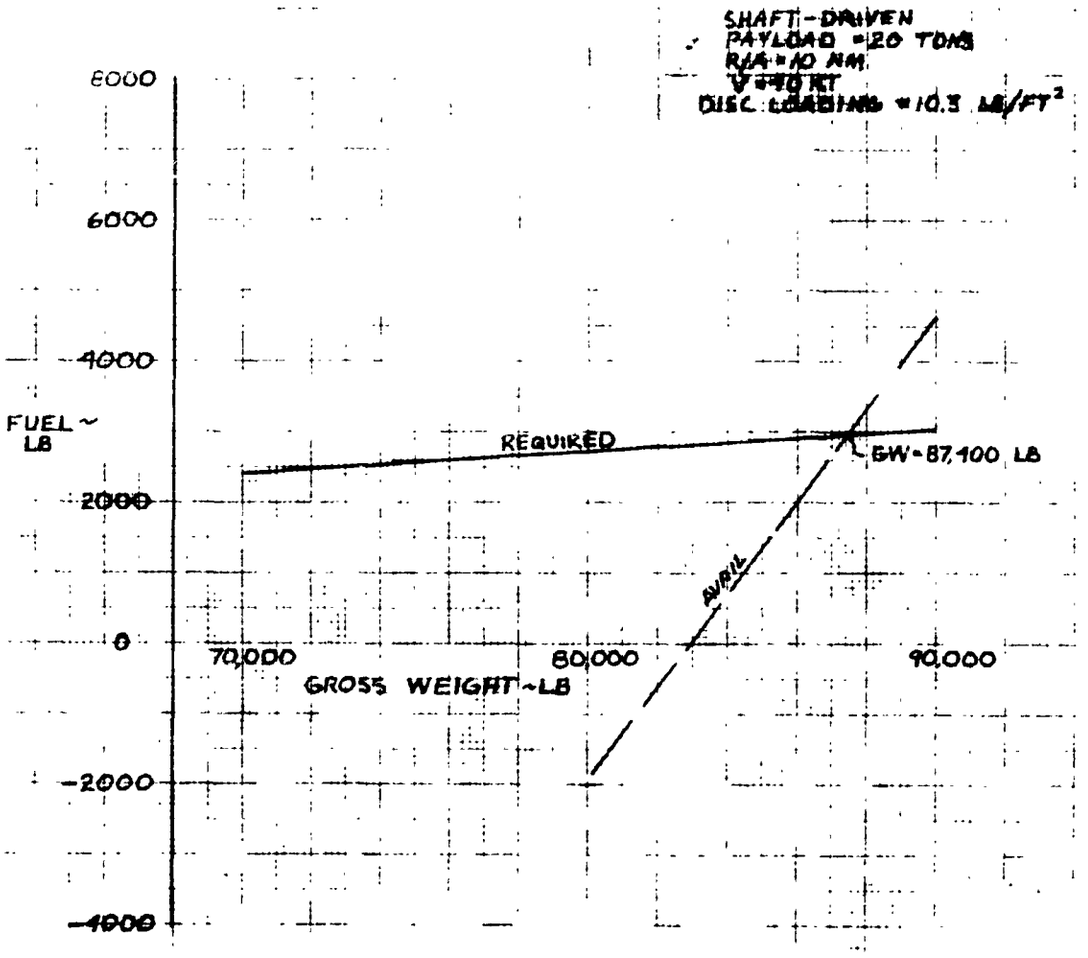

Figure 3-26 Fuel Vs Gross Weight Heavy-Lift Helicopter

3.2.1.5 Point Design Selection

Description. The heavy-lift shaft-driven helicopter is a crane type having a removable pod. The cargo capacity is 20 tons and the pod, when used, is considered a part of the cargo weight.

The 104-foot diameter, six-blade rotor is fully articulated and is driven by two turboshaft engines through the main gearbox transmission which is also provided with an output shaft to drive the antitorque tail rotor.

Shown below are the physical characteristics of the heavy-lift shaft-driven helicopter.

Gross Weight, lbs	87,400
Rotor Diameter, ft	104
Solidity	0.106
No. of Blades	6
Rotor Tipspeed, ft/sec.	700
Rated Horsepower	15,040
Fuel, lbs	2,970
O.W.E., lbs	44,430

3.2.2 Jet-Flap Helicopter Optimization

3.2.2.1 Range of Parameters

As shown in Table 3-9., a range of three gross weights, three rotor diameters, and three solidities resulting in a 27-point matrix was employed in the sizing study. A reasonable tipspeed of 640 fps was used to maintain compatible engine performance data with the high-speed jet-flapped helicopter. Due to the rotor blade duct sizes required to accommodate the mass flow, a three-bladed rotor was selected as being the most practical.

TABLE 3-9

HEAVY-LIFT JET-FLAPPED HELICOPTER

RANGE OF PARAMETERS

Gross Weight, lbs	80,000; 100,000; 120,000
Rotor Diameter, ft	100; 120; 140
Solidity	.06, .11, .16
Rotor Tipspeed, fps	640
No. of Blades	3

The combination of these parameters yielded acceptable values of average rotor lift coefficient within the scope of the Dorand First Series Wind Tunnel Test.

3.2.2.2 Engine Sizes

The rotor power requirement in terms of equivalent shaft horsepower at the rotor exhaust nozzle is presented in Figures 3-27, 3-28, and 3-29 versus solidity for the three diameters and three gross weights of Table 3-9. The power requirement is based on a hover thrust/gross weight ratio T/W = 1.1K at SL standard conditions. As discussed in Paragraph 3.1.2.2, the minimum solidity at each diameter is limited by the chord necessary to accommodate a duct area comparable to the Dorand test rotor. This limit is indicated in the three figures and defines the respective solidity in the remainder of the study. Table 3-10 specifies this solidity and the rated engine horsepower.

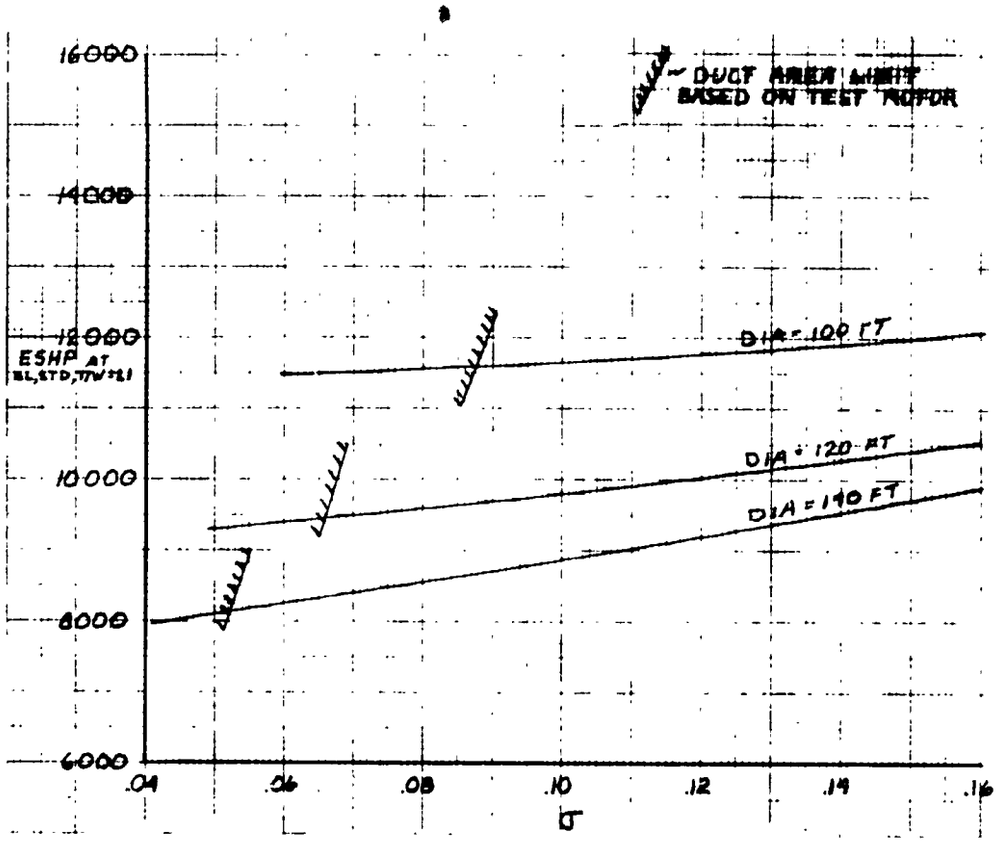

Figure 3-27 Minimum Solidity Heavy-Lift Jet-Flap Helicopter GW=80,000 LB

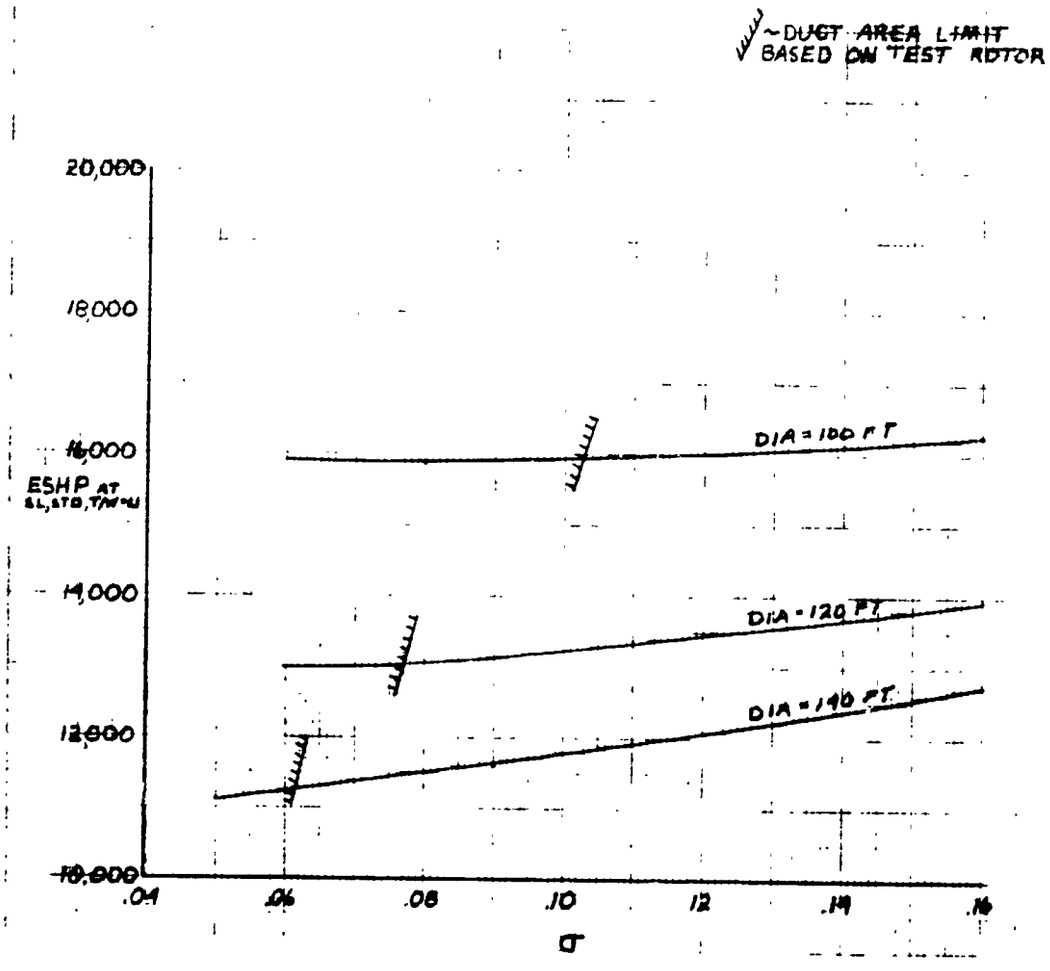

Figure 3-28 Minimum Solidity Heavy-Lift Jet Flap Helicopter GW=100,000 LB

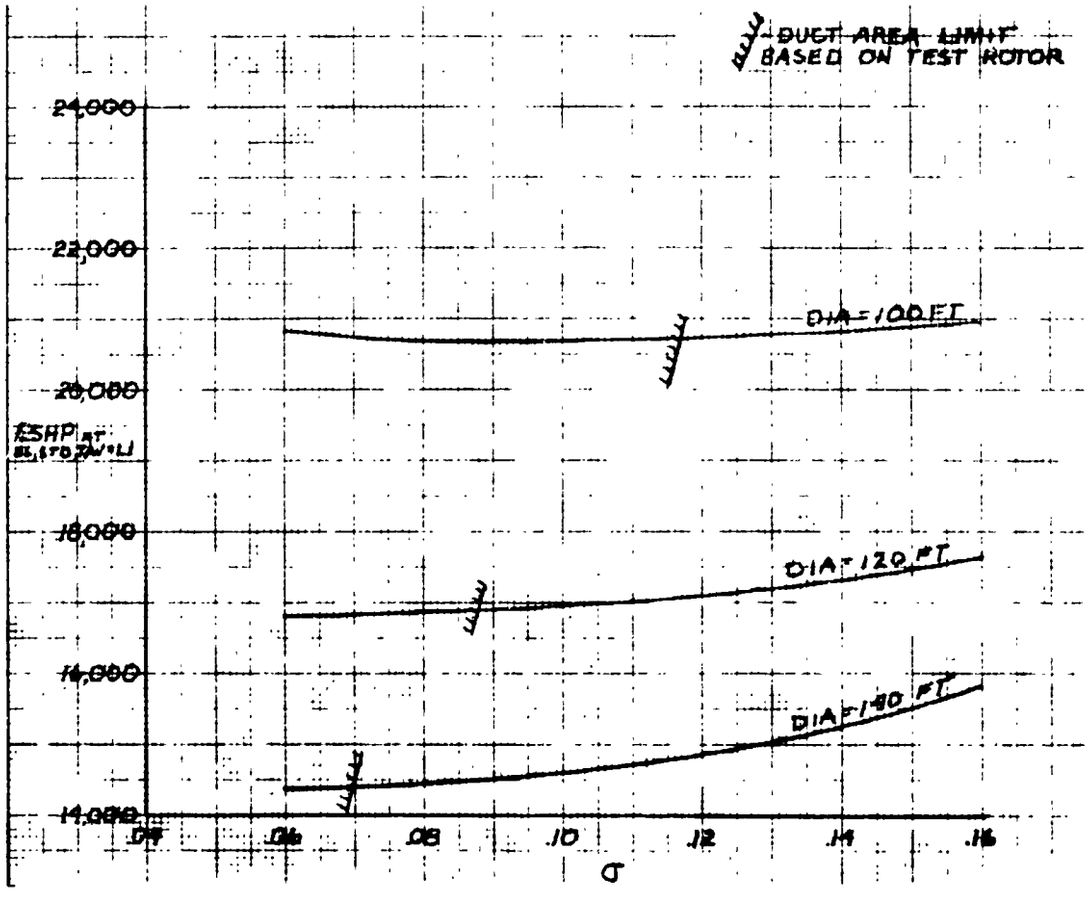

Figure 3-29 Minimum Solidity Heavy-Lift Jet-Flap Helicopter GW=120,000 LB

3.2.2.3 Fuel Required

Presented in Figure 3-30 is the fuel required to perform the design mission calculated by the LTVAC Mission Performance Program, as described in Appendix A.

3.2.2.4 Fuel Available

The fuel available is presented in Figure 3-31 as a function of rotor diameter and gross weight.

TABLE 3-10

HEAVY-LIFT JET-FLAP HELICOPTER

ENGINE SIZES

V_T = 640 Ft/Sec

T/W = 1.1 at SL Std

GW - Lb	DIA - Ft	DL - Psf	σ	ESHP	SHP_{RATED}
80,000	100	10.19	0.0876	11,600	38,337
80,000	120	7.08	0.066	9,500	31,331
80,000	140	5.2	0.0525	8,140	26,869
100,000	100	12.74	0.1025	15,930	52,647
100,000	120	8.85	0.077	13,030	43,096
100,000	140	6.5	0.0615	11,220	37,081
120,000	100	15.3	0.117	20,750	68,544
120,000	120	10.62	0.088	16,920	55,919
120,000	140	7.8	0.0693	14,410	47,657

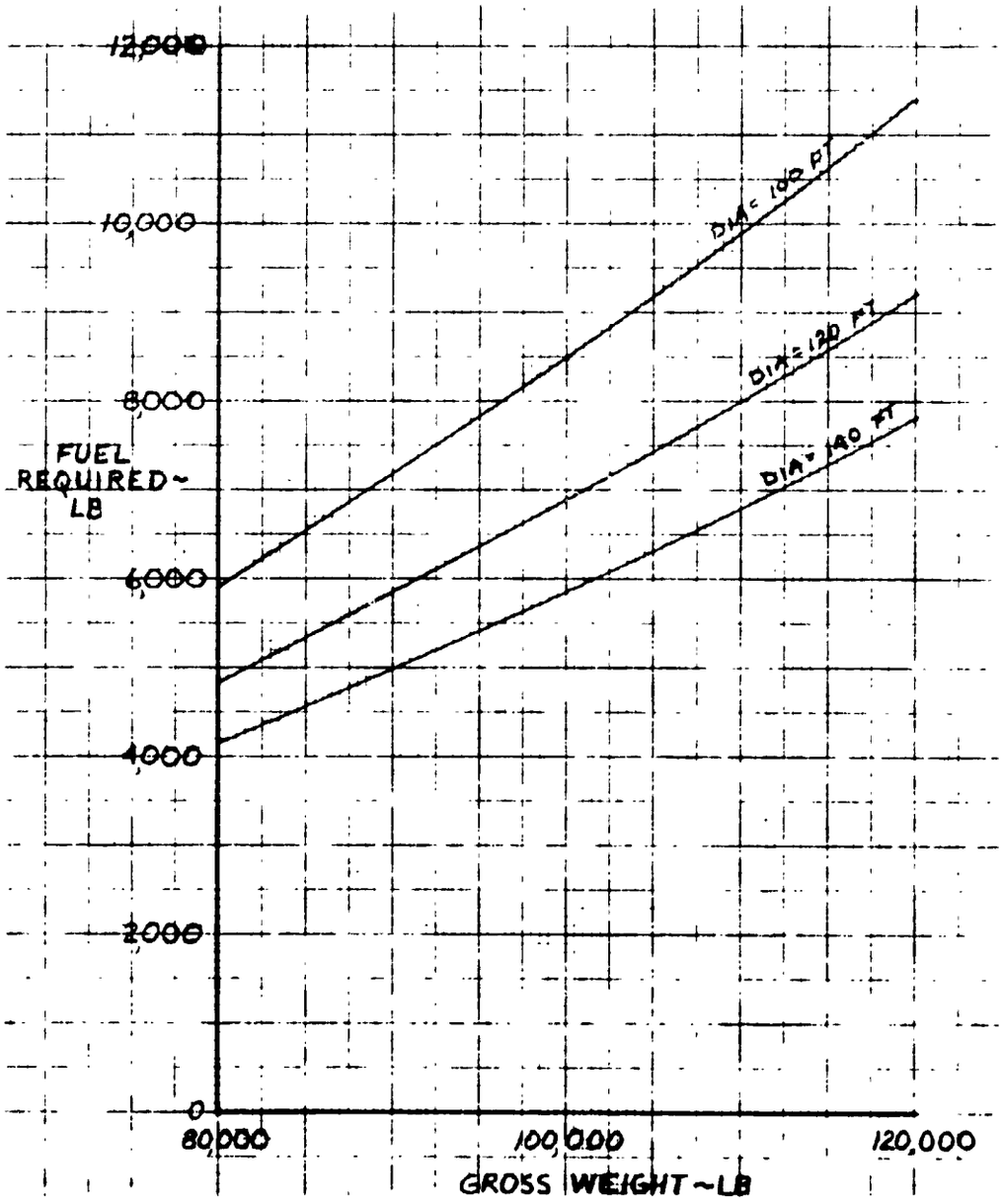

Figure 3-30 Fuel Required Vs Gross Weight Heavy-Lift Helicopter Jet-Flap

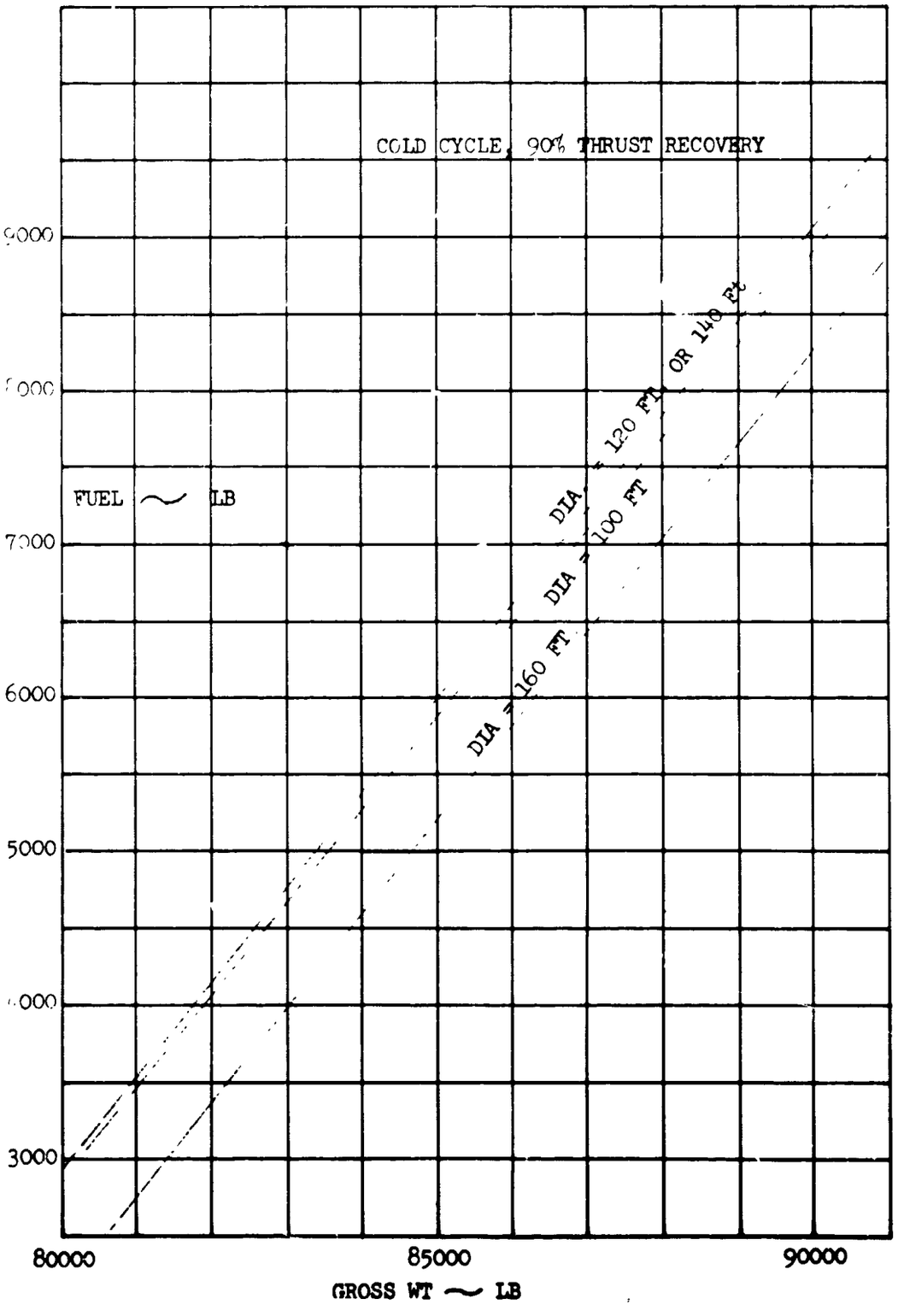

Figure 3-31 Heavy-Lift Jet-Flap Fuel Available Vs Rotor Diameter and Gross Weight

3.2.2.5 Point Design Selection

Procedure. The intersections of the fuel required and fuel available versus gross weight curves of Paragraph 3.2.2.3 and 3.2.2.4, respectively, define a set of gross weights for vehicles capable of meeting the design mission. Figure 3-32 shows these gross weights versus diameter. It is observed that the diameter for the minimum gross weight of 82,500 pounds is 145 feet. From the data of Table 3-10, the corresponding solidity is = 0.0502 and the rated engine horsepower is 27,300 hp.

Description. The 20-ton capacity jet-flap rotor helicopter is the same as the 20-ton shaft-driven helicopter except for the rotor, propulsion, powerplant installation, and tail configuration.

Performance. Shown below in Table 3-11 is a summary of the optimized heavy-lift jet-flap helicopter.

TABLE 3-11

HEAVY-LIFT JET-FLAP HELICOPTER

Gross Weight, Lb	82,500
Rotor Diameter, Ft	145
Solidity	0.0502
No. of Blades	3
Rotor Tipspeed, Ft/Sec.	640
Rated Horsepower, Hp	27,300
Fuel, Lb	4,310
Payload, Lb	40,000
OWE, Lb	38,190

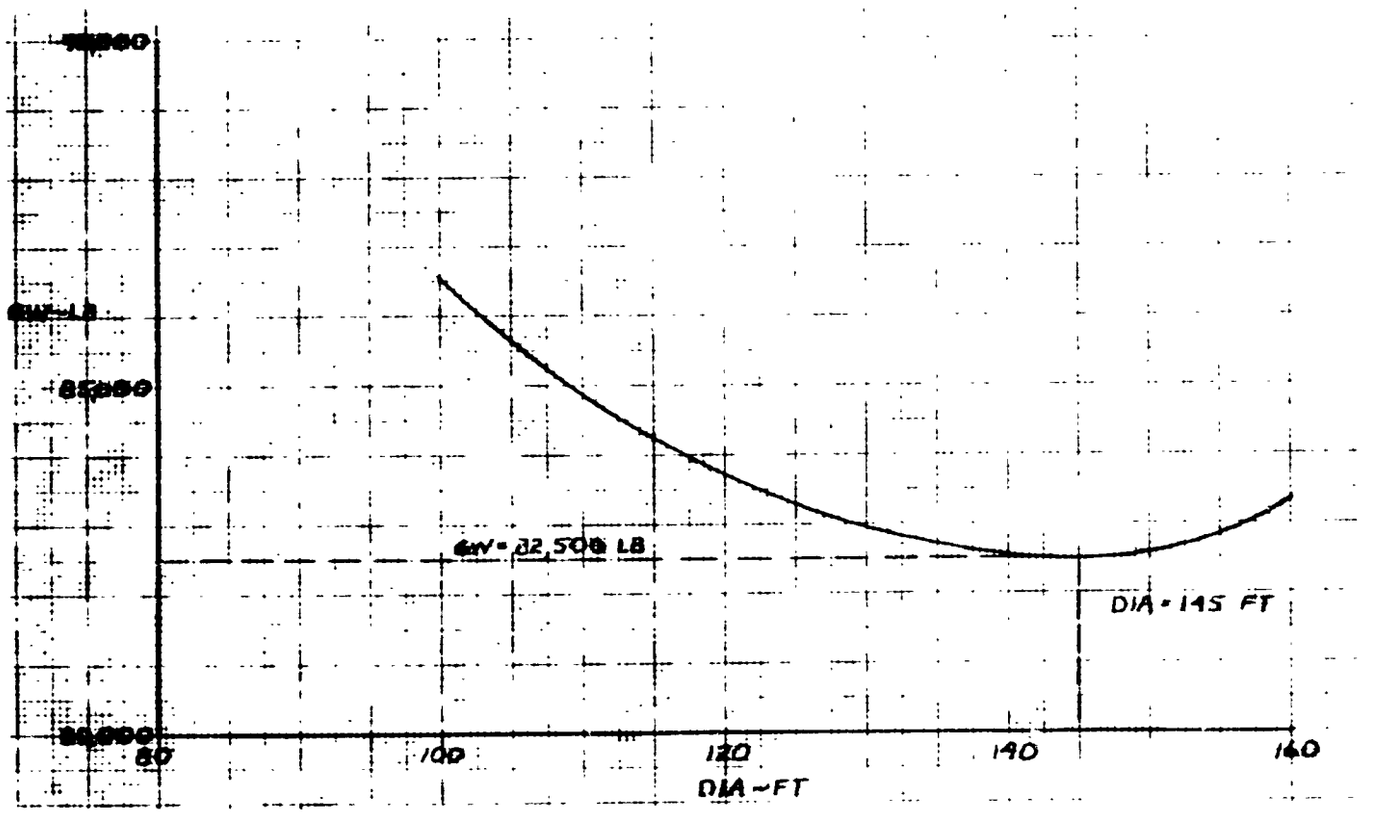

Figure 3-32 GW Vs Dia HLH-Jet Flap

An independent check of the power and fuel requirements was made using the first series extrapolated wind tunnel test data with the following results:

	Pt Design	Ames Test
Rated Horsepower, Hp	27,300	28,400
ESHP at V = 40 kt	4,078	4,120
Fuel, Lb	4,310	4,592

3.2.3 Comparison - Shaft-Driven and Jet-Flap Concepts

The data of Figure 3-33 presents a comparison of the variation of payload with radius-of-action for the shaft-driven vehicle and the jet-flap vehicle with 90 percent thrust recovery. As noted, the operating weight empty and takeoff gross weight is lowest for the jet-flap vehicle. However, the shaft-driven vehicle does have a better load-carrying capability as radius of action increases than the jet-flap vehicle.

3.2.4 Engine Selection

The effect of engine pressure ratio hot/warm cycles on gross weight of the heavy-lift helicopter was determined from a limited parametric study. As in the high-speed study, the most optimistic (100% thrust recovery and 5% static duct pressure loss), intermediate (90% T.R. and 15% D.L.), and pessimistic (80% T.R. and 25% D.L.) cases were employed. The fuel required and fuel available are shown in Figures 3-34, 3-35 and 3-36 for high intermediate, and low pressure ratios of 4.05, 2.42, and 1.91 (Engines No. 1, 4, and 6).

An engine selection parametric was also conducted for the cold cycle. Engine pressure ratios of 4.2 and 3.0 were used. Figure 3-37 presents the fuel required and available curves.

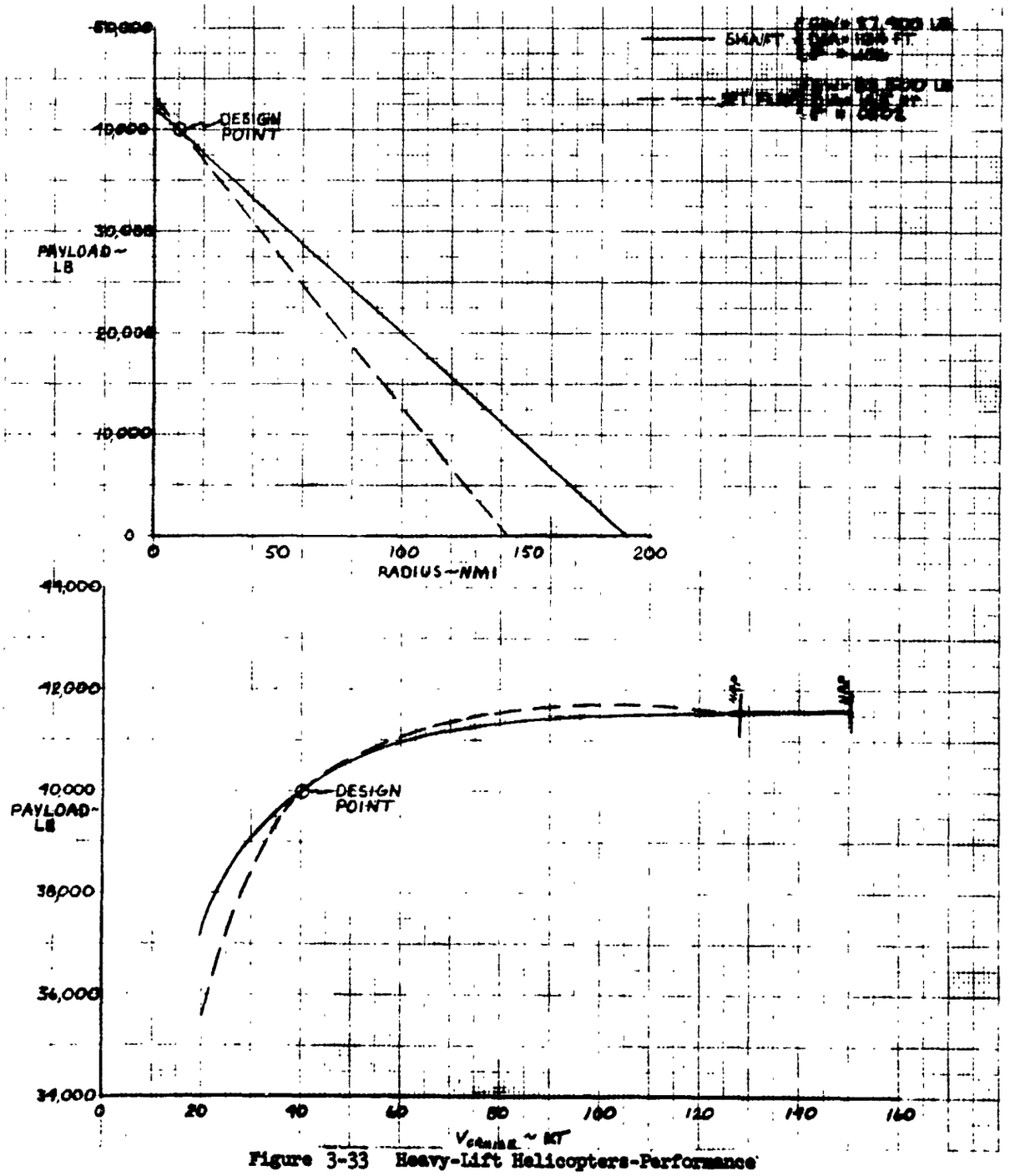

Figure 3-33 Heavy-Lift Helicopters-Performance

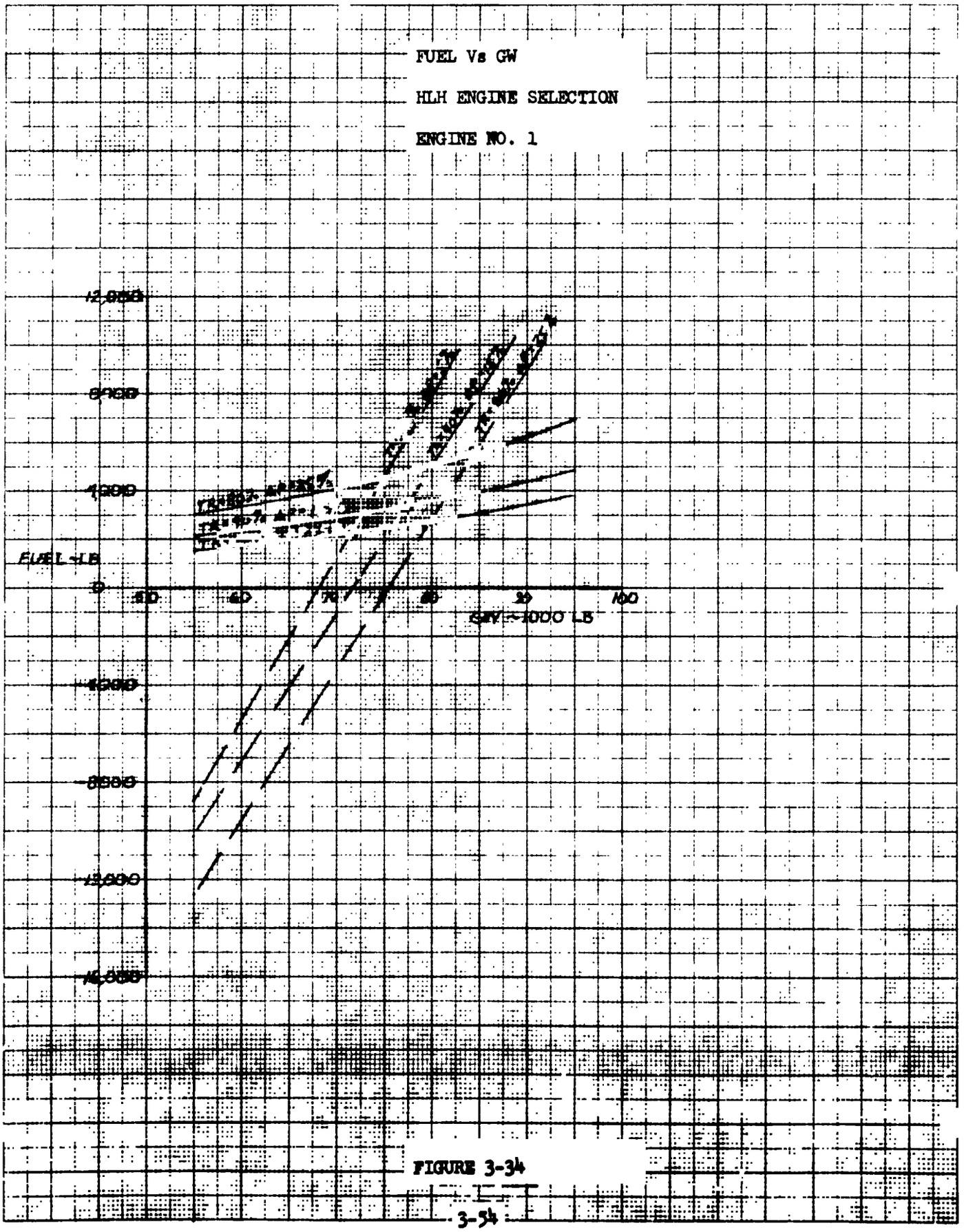

FIGURE 3-34

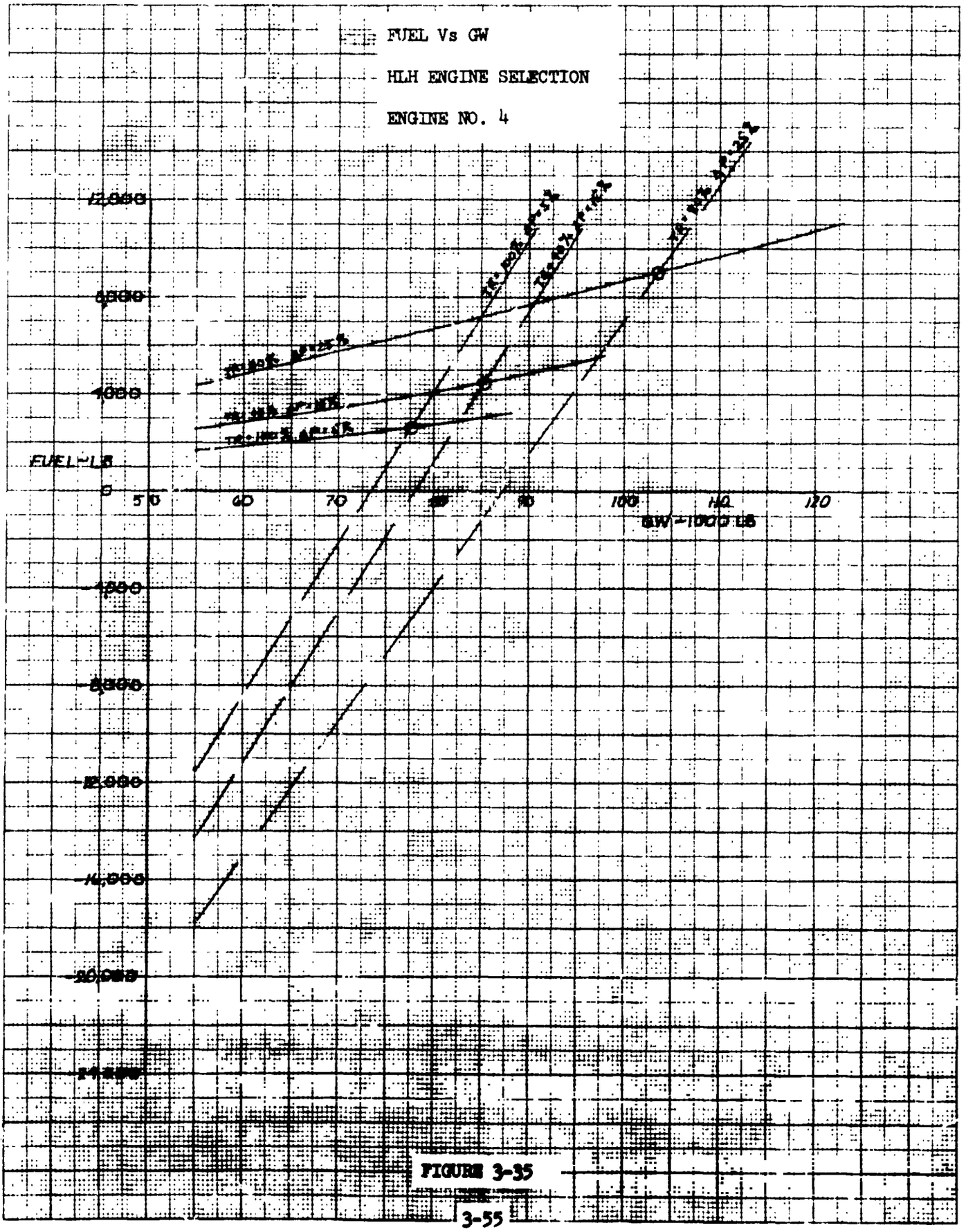
FUEL Vs GW
HLH ENGINE SELECTION
ENGINE NO. 4
FUEL-LB
GW-1000 LB
50
60
70
80
90
100
110
120

FIGURE 3-35

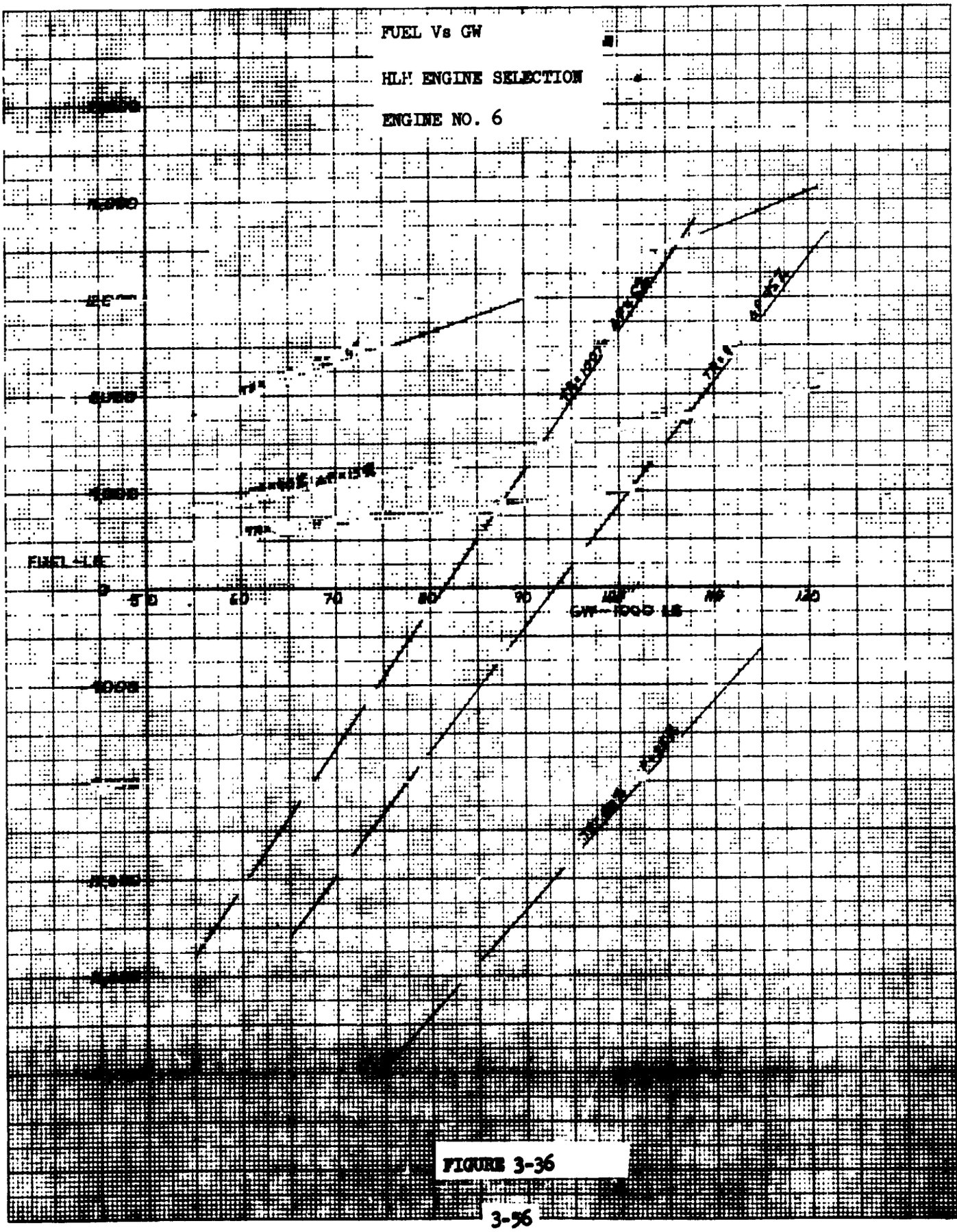

FIGURE 3-36

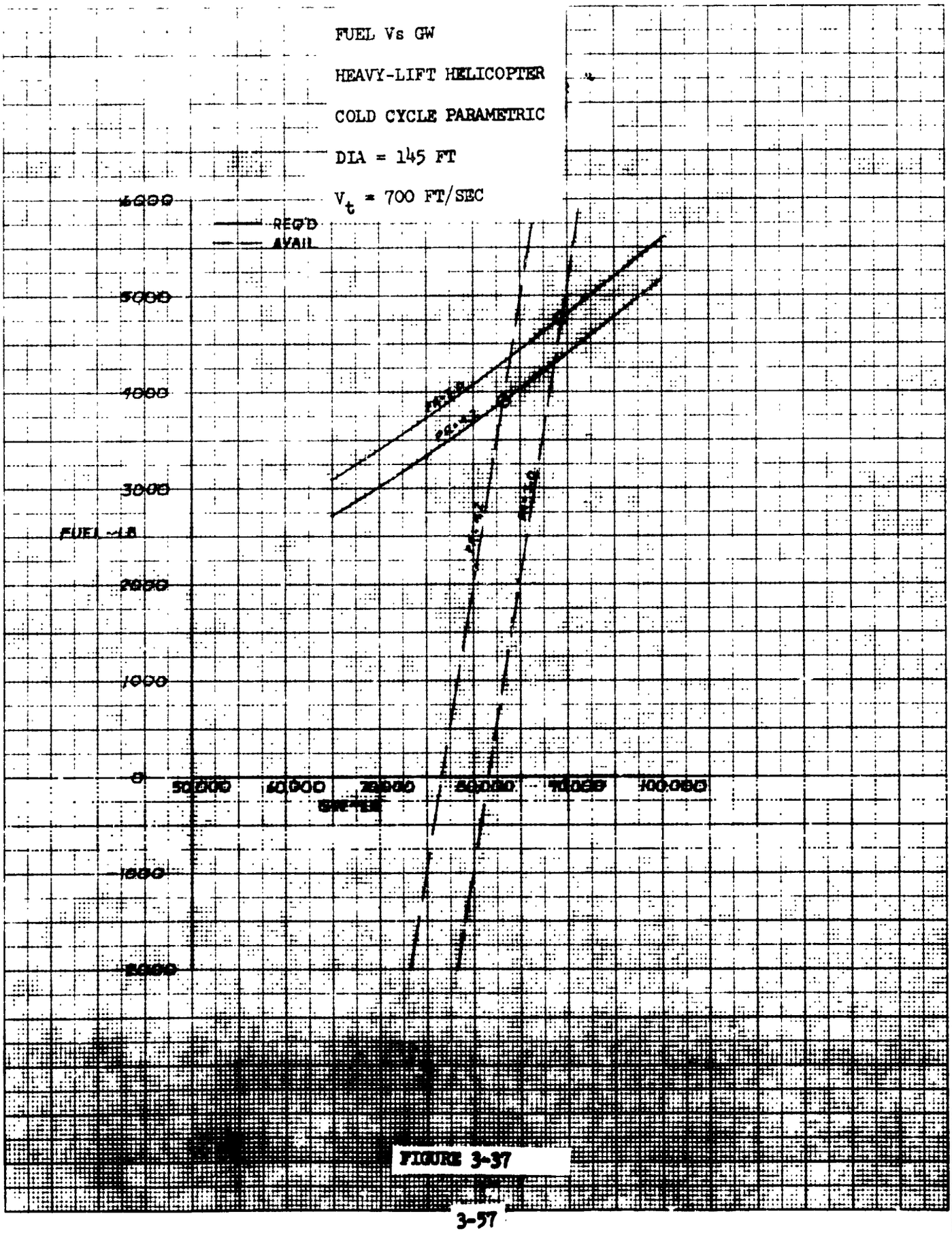
FUEL Vs GW
HEAVY-LIFT HELICOPTER
COLD CYCLE PARAMETRIC
DIA = 145 FT
V_t = 700 FT/SEC
REQ'D
AVAIL
FUEL - LB
GW - LB
6000
5000
4000
3000
2000
1000
0
50,000
60,000
70,000
80,000
90,000
100,000

FIGURE 3-37

3.2.5 Heavy-Lift Tip-Jet

The effect on the point design of splitting the gas flow between the flap and a tip-jet nozzle was investigated for the heavy-lift mission. Figure 3-38 presents the resulting fuel required-fuel available leading to the minimum gross weights capable of completing the heavy-lift mission.

3.2.6 Full Jet-Flap $\bar{C}_L$, Utilization

3.2.6.1 Pure Jet-Flap

A study was conducted wherein the full lifting capability of the jet-flap was utilized. A limited parametric study was conducted to define a minimum weight shaft-driven heavy-lift helicopter for the following design mission:

R/A: 10 nm

V_{CR}: 40 kt

Hover: 2 min

Power based on $\frac{T}{W}$ = 1.1 at SLS

$\bar{C}_{L\ max}$ shaft-driven = 0.5

$\bar{C}_{L\ max}$ jet-flap = 1.0

Payload 20 tons (for shaft-driven helicopter)

The shaft-driven helicopter design was based on the Sikorsky S-64 Sky Crane with a disc loading held at 10.3 psf. In Figure 3-39 the fuel required and fuel available are presented for a gross weight range of 70,000 to 90,000 pounds. Intersection yielded a design gross weight of 81,500 pounds. For the design disc loading, a rotor diameter of 100 feet was selected. The 100-ft diameter was then applied to a jet-flap vehicle

FUEL Vs GW

HEAVY-LIFT HELICOPTER

TIP-NOZZLE ROTOR DRIVE with JET-FLAP AUGMENTATION

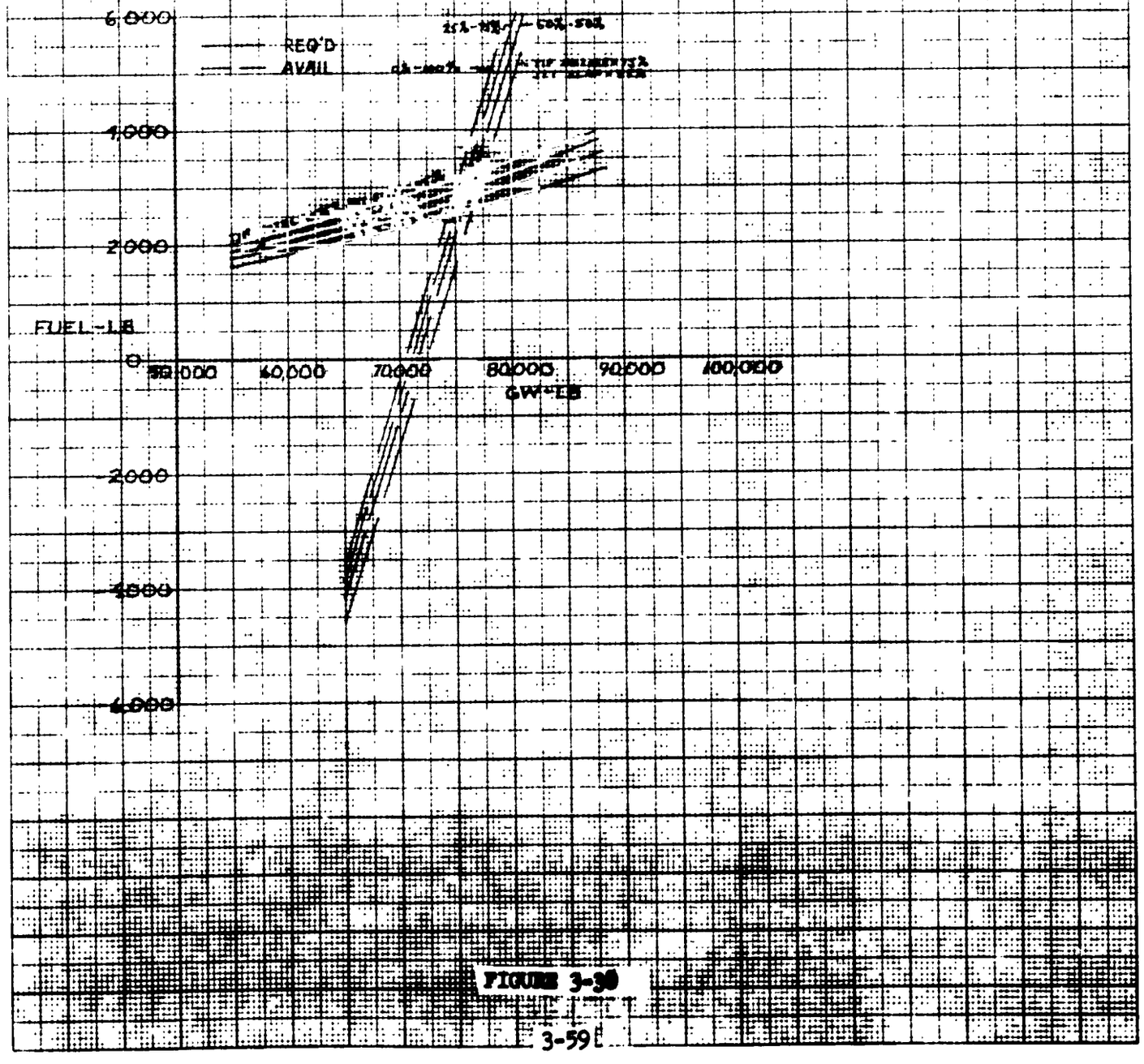

FIGURE 3-30

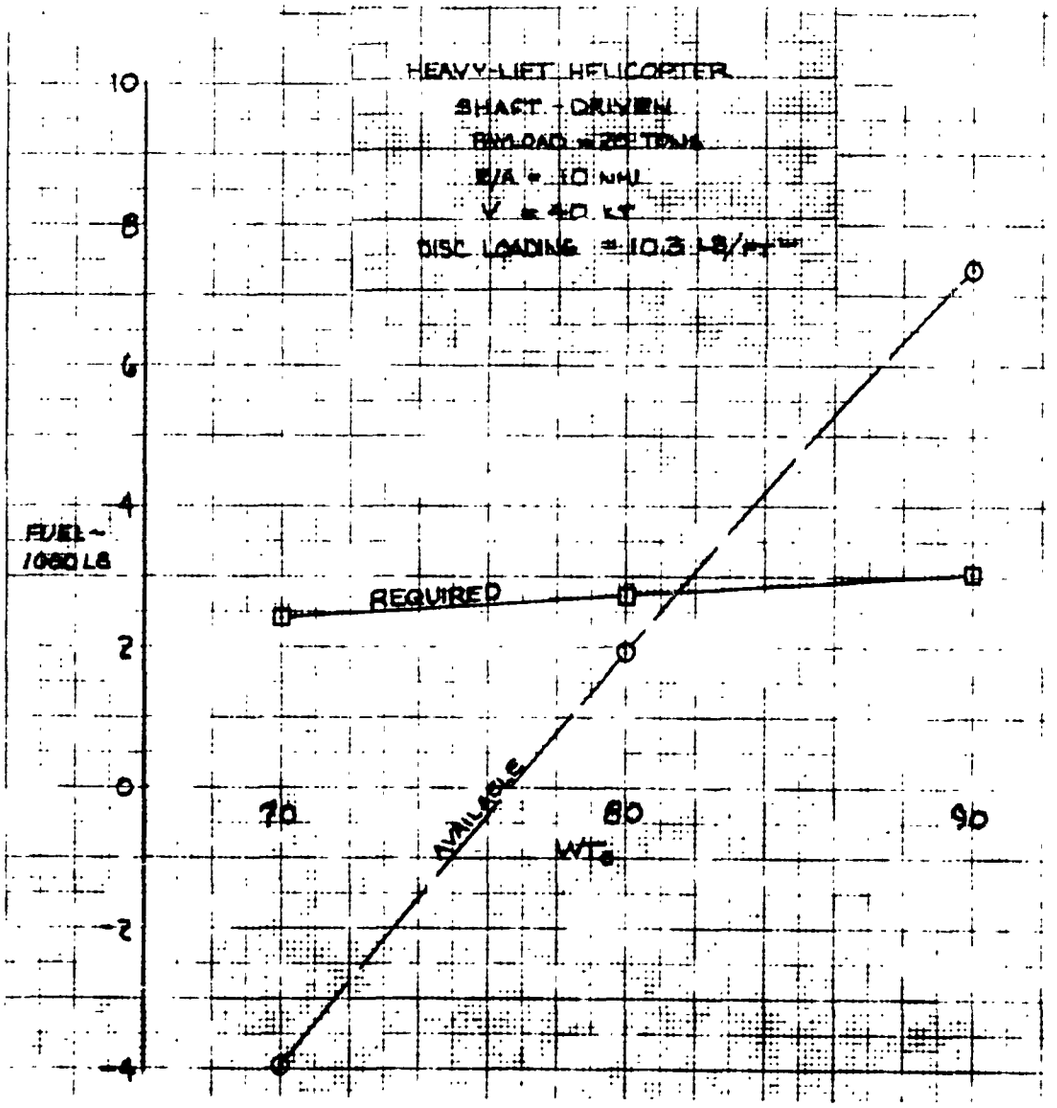

Figure 3-39 Heavy-Lift Helicopter Shaft-Driven

with twice the $\bar{C}_L$ and weighing twice as much as the shaft-driven vehicle. The tipspeed-solidity relationship of the shaft-driven vehicle consistent with a $\bar{C}_L$ = 1.0 was maintained. The fuel required and fuel available intersection shown in Figure 3-40 yielded a payload capability of 76,000 pounds.

The characteristics of the two helicopters are shown below:

	Shaft-Driven	Jet-Flap
Gross Weight, Lb	81,500	163,000
Rated SHP, Hp	14,140	128,000
Diameter, Ft	100	100
Payload, Lb	40,000	76,000
Fuel, Lb	2,800	19,600
OWE, Lb	38,700	67,400
$\bar{C}_L$	0.5	1.0
Cost Effectiveness $/Ton-nm	1.24	1.46

Under these conditions, the rated power required is increased by a factor of approximately nine. This factor is comprised of a 3 to 1 ratio of compressor horsepower to rotor ESHP ($\bar{C}_L$ = 1.0) and a 3 to 1 ratio of ESHP ($\bar{C}_L$ = 1.0) to ESHP ($\bar{C}_L$ = .5). It is interesting to note that momentum theory alone would predict the latter ratio to be 2.8.

In spite of the fact that the jet-flap vehicle carries almost twice the payload of the shaft-driven helicopter, the cost effectiveness of the shaft-driven helicopter in terms of dollars per ton-nm, is still 17 percent more favorable than for the jet-flap. This is attributed to the high installed power and fuel consumed by the jet-flap vehicle.

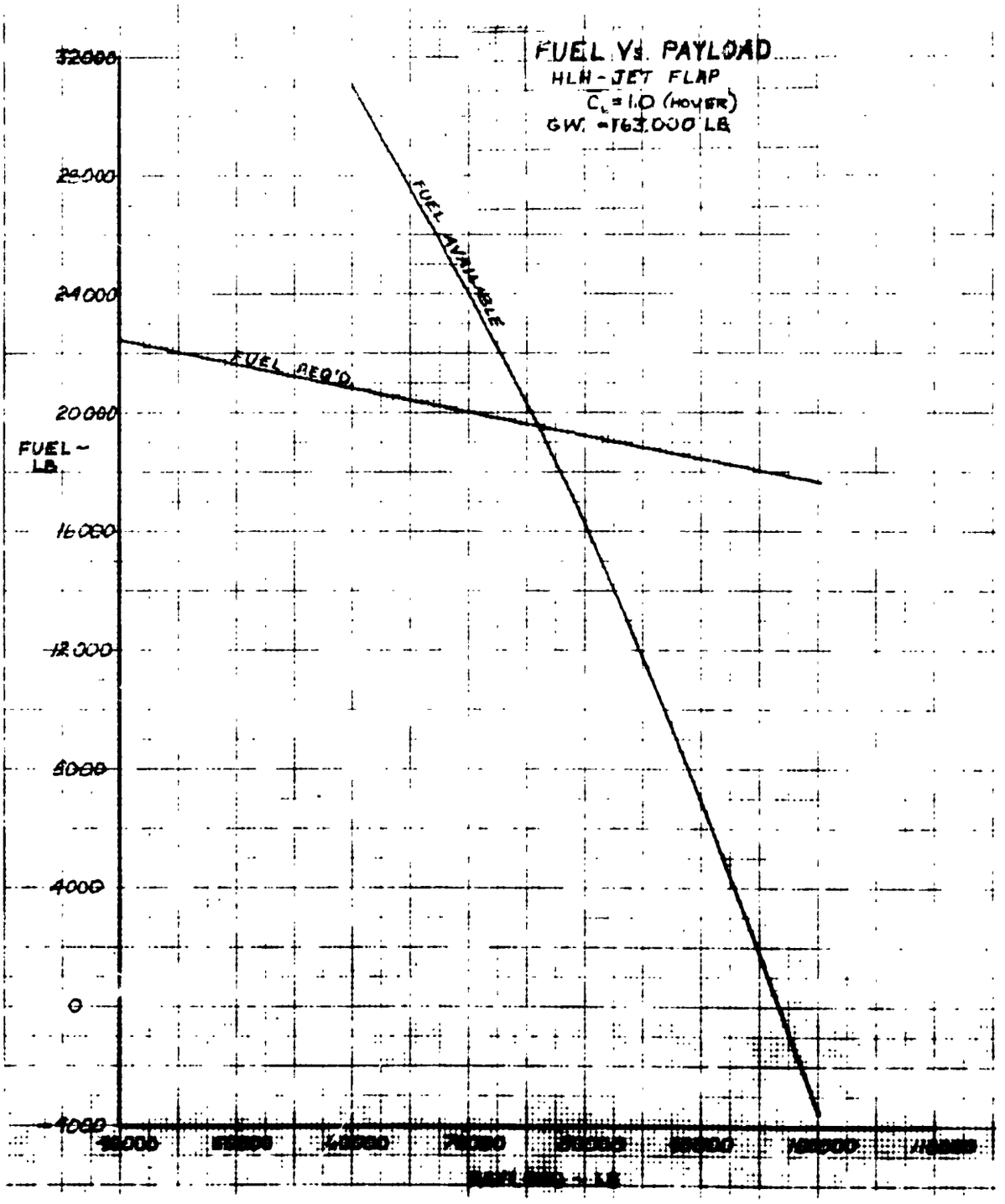

Figure 3-40 Fuel Vs Payload HLH-Jet Flap

3.2.6.2 Equal Empty Weights

Another approach to utilizing the superior lifting capability of the jet-flap was to compare jet-flap vehicles with shaft-driven vehicles of equal empty weight and rotor diameter. The 20-ton vehicle defined in the previous paragraph was taken as a base (100 ft diameter, 38,700 lb operating weight empty). In sizing the vehicles at a takeoff design load factor of 2.5, it was noted that the jet-flap vehicle could only utilize a $\bar{C}_L$ of 0.565. The shaft-driven vehicle was sized to obtain its maximum $\bar{C}_L$ of 0.5 at the design load factor of 2.5. In order to utilize more of the available $\bar{C}_L$ of the jet-flap, a vehicle was sized with an overload design load factor of 2.0. Characteristics of these vehicles are summarized below.

	Shaft-Driven	Jet-Flap	
		Design	Overload
W_{TO}, lb	81,500	92,200	115,200
OWE, lb	38,700	38,700	38,700
Fuel, lb	2,800	7,500	9,500
Installed SHP	14,140	78,300	78,300
Rotor Dia., ft	100	100	100
Payload, lb	40,000	46,000	66,400
$\bar{C}_L$	0.5	0.565	0.707
Takeoff Load Factor, g	2.5	2.5	2.0

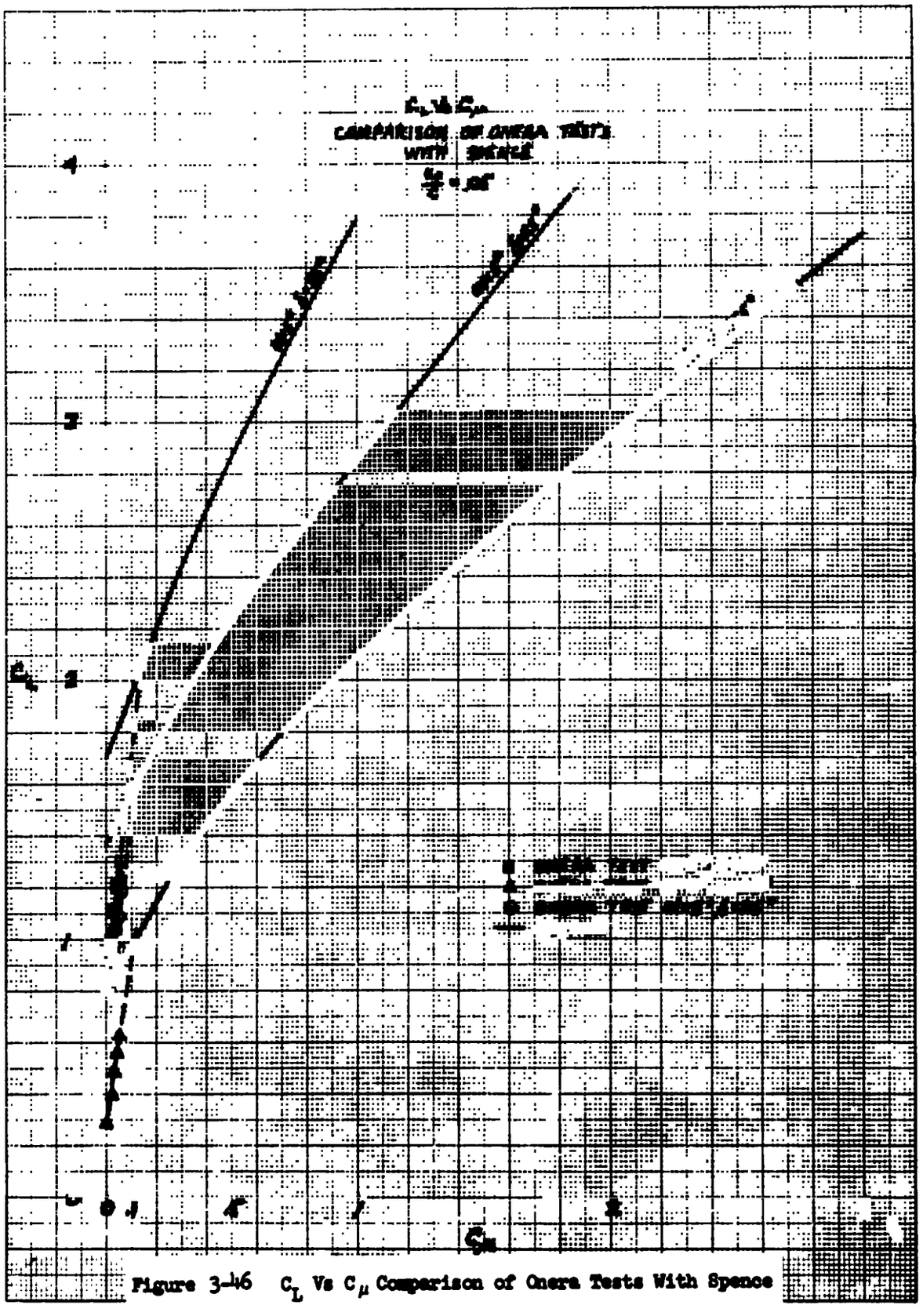

Figure 3-46 C_L Vs C_μ Comparison of Onera Tests With Spence

Reference 5. Since LTV's Rotor Performance Programs are based on Spence's data, a reduced blowing level of C_{μ} = 0.12 is employed as a minimum for accurate flap angle prediction.

A representative heavy-lift helicopter featuring a gross weight of 81,500 lbs, a 100-ft diameter rotor, three rotor blades, a solidity of 0.10 and tipspeed of 640 ft/sec was selected for this trade study. Figure 3-47 presents required rotor blowing coefficient versus the ratio of mechanically supplied shaft horsepower required by the rotor at an airspeed of 40 kt. Converting the C_{μ} = 0.12 into a rotor-blowing coefficient, C_{J_R} = 0.0013, results in a required power split (MECH SHP/ROTOR ESHP) of 40%. The sum of the mechanical horsepower and gas horsepower required at this condition is 17,260 hp. This represents a reduction in total installed horsepower of approximately 29% based on the 100% pneumatic system. Figures 3-48 and 3-49 show the collective, cyclic, and total flap deflection angles required for trim, based on Spence's equations, versus percent power split. Thus, if the power split is 40%, the maximum flap deflection for the case examined is approximately 62°. This indicates that a greater percentage of the required rotor power can be supplied by mechanical means, providing the flap remains installed at C_{μ} = 0.12.

3.2.7.2 Mechanical Considerations - Power Split

Preliminary examination of the mechanization of a drive system in which the installed power is split between a mechanical transmission and a jet-flap indicates that a split of approximately 33 percent for blowing and 67 percent for mechanical transmission is feasible. Such a drive system concept is illustrated in Figure 3-50.

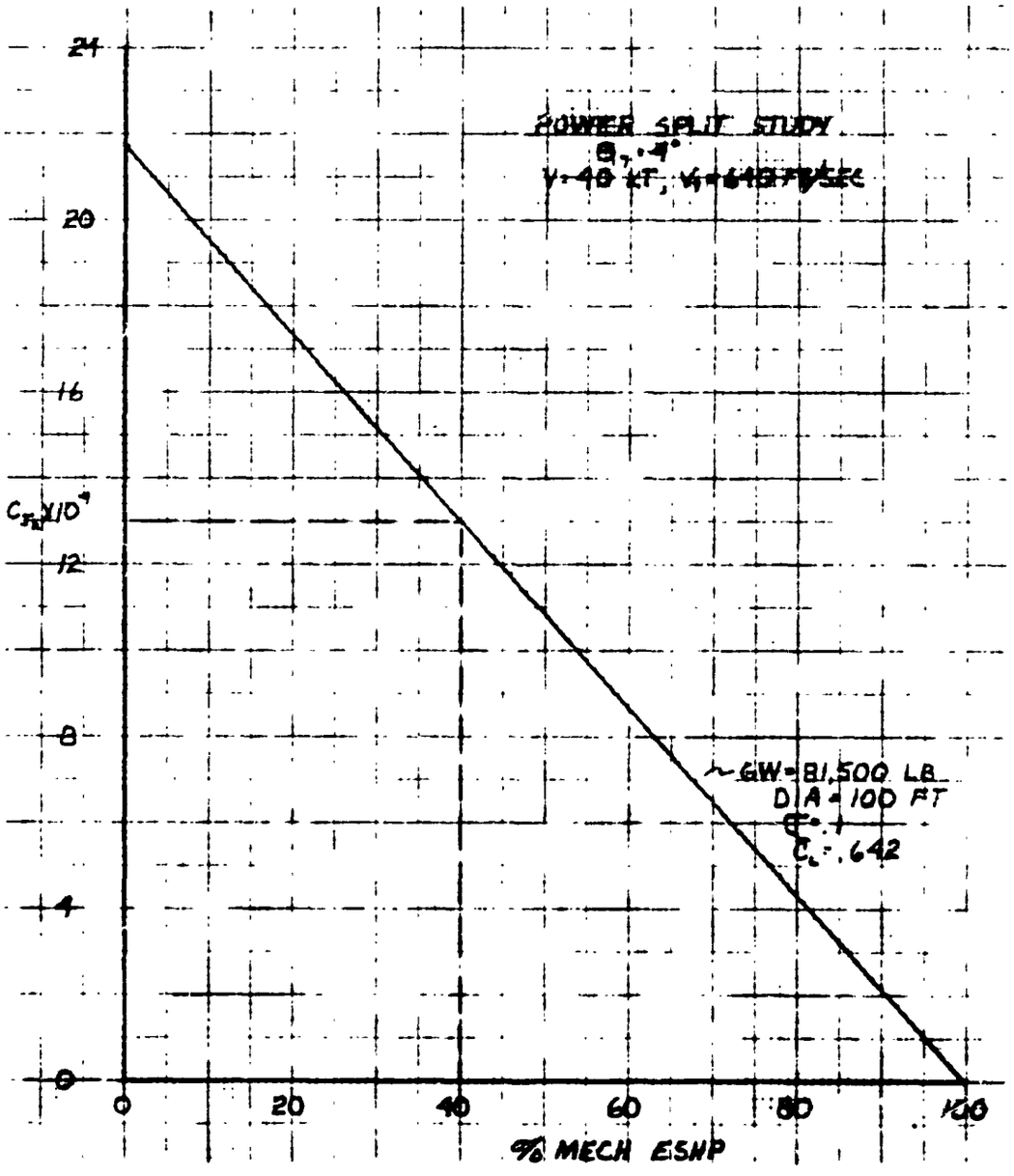

Figure 3-47 Power Split Study

The engine of the 2.5 g jet-flap design was sized to accommodate the overload capability cost effectiveness of the three designs described above, in performing the 10 nm mission were 1.24, 1.40, and 1.07 dollars per ton nm for the shaft-driven, design jet-flap, and overload jet-flap respectively. Payload radius curves for these vehicles are presented in Figure 3-41. Cost-effectiveness in dollars per ton nm and dollars per flight hour are presented in Figure 3-42.

3.2.6.3 Sensitivity of Empty Weight Ratio

One of the parameters that must be considered uncertain because of lack of statistical data is the operating empty weight to takeoff weight ratio. A limited study to determine the sensitivity of this ratio on the jet-flap performance was conducted for a range of operating empty weight ratios from 0.3 to 0.5. The best estimates of this ratio, made at the time of this study are 0.42 for the jet-flap and 0.48 for the shaft-driven vehicle. Results of this study are presented in Figure 3-43. It may be noted in Figure 3-43 that the overload jet-flap design has a more favorable cost-effectiveness value than the shaft-driven vehicle over most of the range considered. Also, the 2.50 design jet-flap cost-effectiveness becomes equal to the shaft-driven vehicle at about 0.38 empty weight ratio.

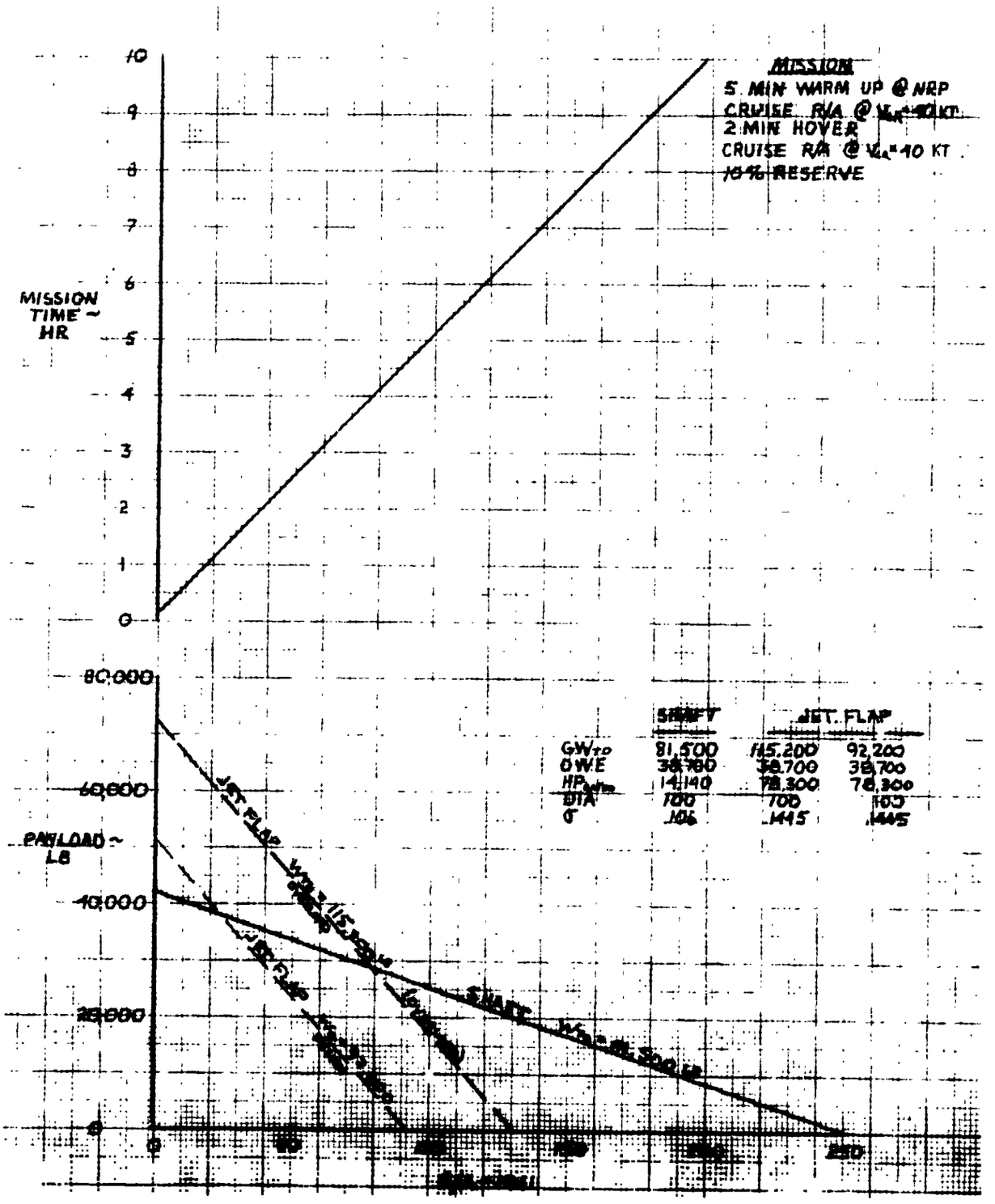

Figure 3-41 Mission Time and Payload Vs R/A

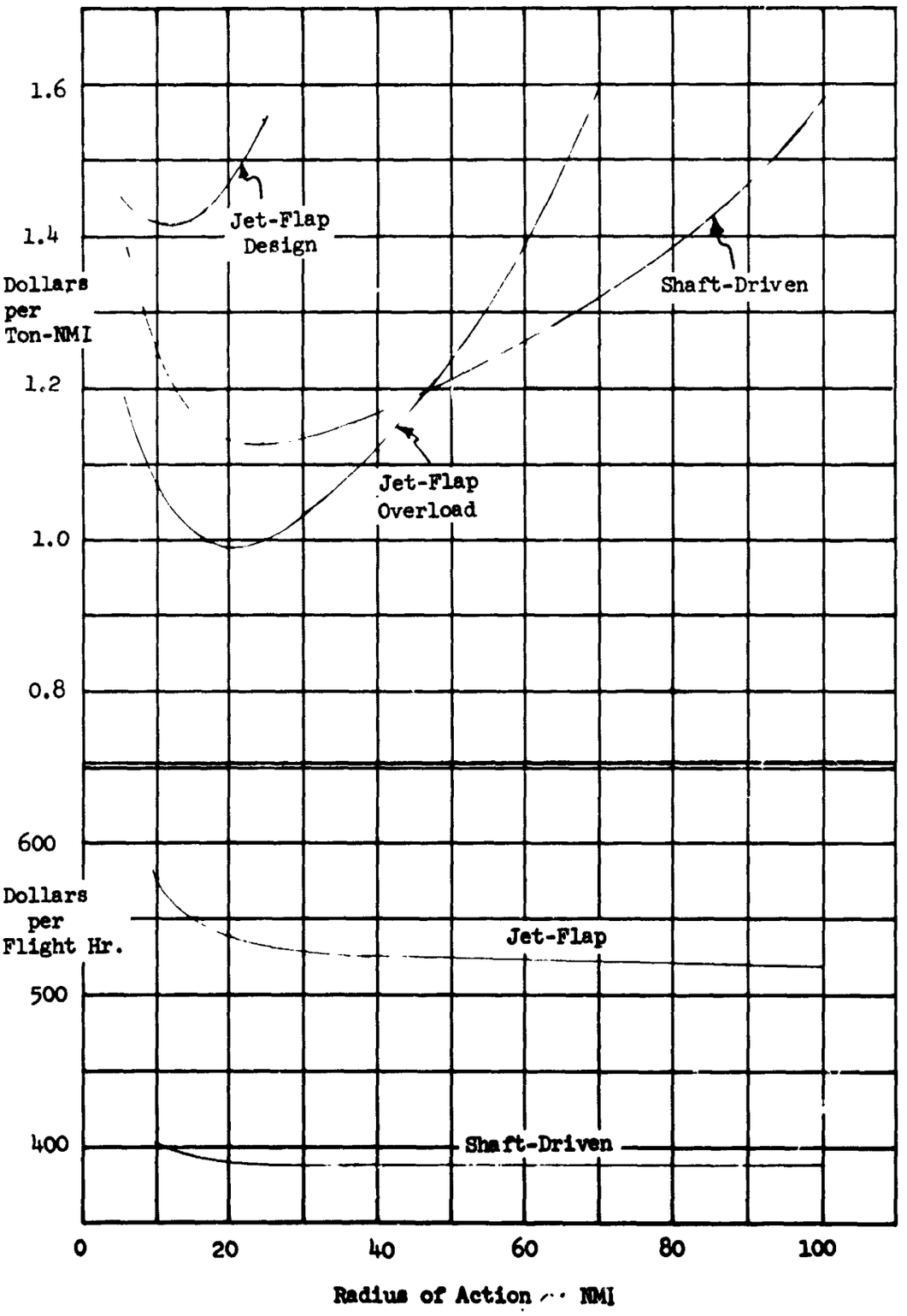

Figure 3-42 Heavy-Lift Helicopter Equal Empty Weight Comparison

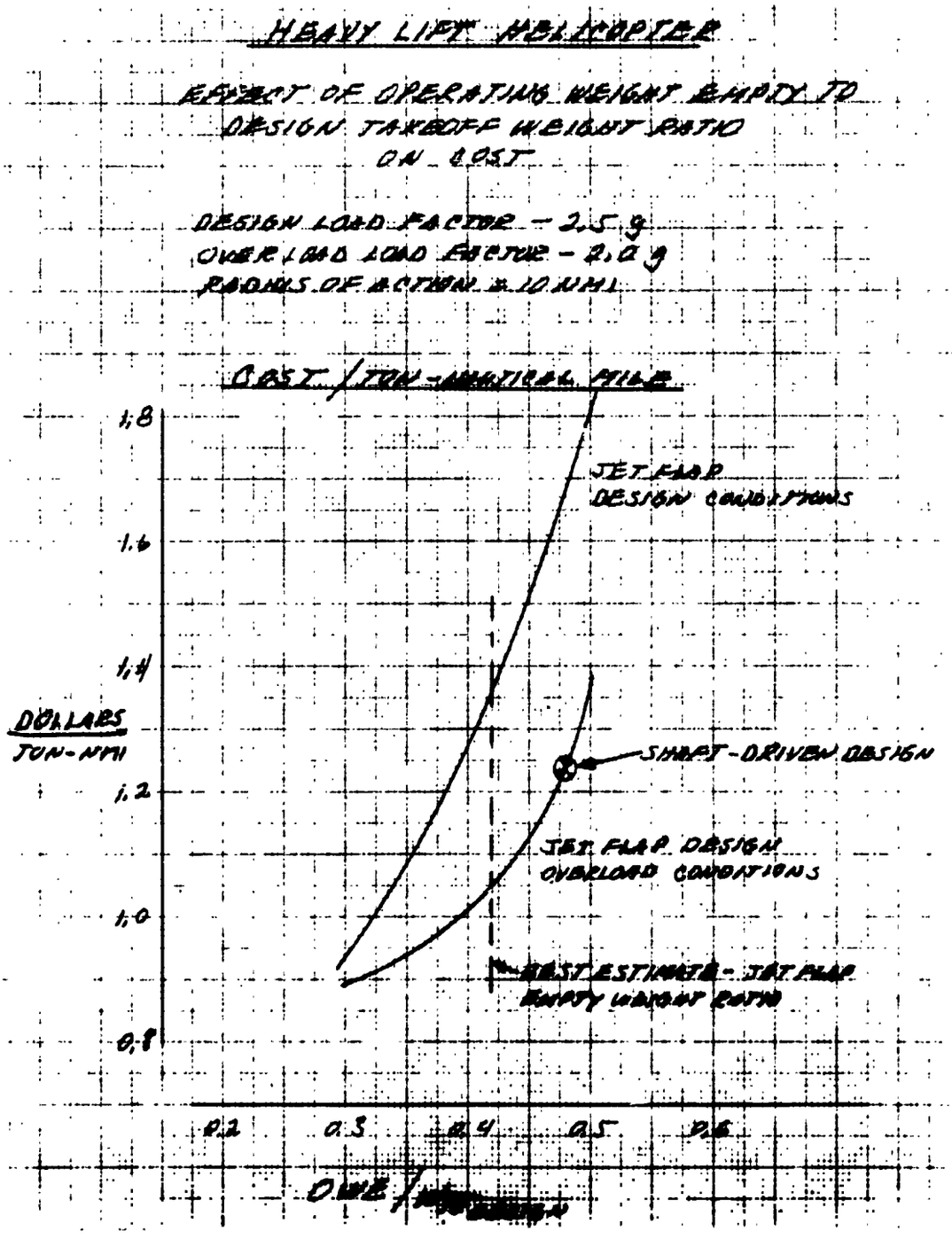

Figure 3-43 Heavy-Lift Helicopter - Effect of Operating Weight Empty to Design Takeoff Weight Ratio on Cost

3.2.7 Jet-Flap Augmentation

3.2.7.1 Analytical Considerations

Since the 100 percent blowing system is relatively low in efficiency in developing rotor shaft horsepower, an obvious alternative is to consider driving the rotor by some more efficient means and using the jet-flap only in an augmentation mode. The classical qualitative relationship between lift coefficient and blowing coefficient is illustrated below.

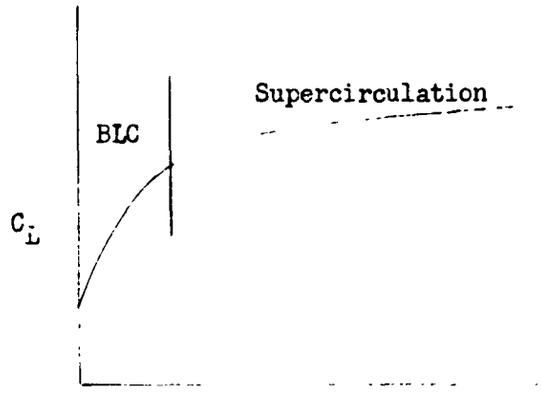

With all of the installed power used for blowing through the jet-flap nozzle, the system is operating in the super-circulation regime with a relatively high blowing coefficient. At low blowing coefficients, in the boundary layer control regime, a better lift coefficient-blowing coefficient relationship is achieved. Where the optimum point is located is subject to a comprehensive trade-off which is beyond the scope of the present study. However, to get an indication of the potential gains of a more favorable power split, a limited study was conducted, in which it

was assumed that the installed power was divided between driving the rotor mechanically and blowing through the jet flap nozzle. Mechanically, this type of split is feasible as indicated in Paragraph 3.2.7.2, but, from a long-range standpoint, a split in power between the jet-flap and more advanced drive systems such as tip jets or turbine-driven rotors may be more attractive.

While lift augmentation is the primary consideration in this type of system, the capability of controlling with the jet-flap alone is also an important consideration. It would be desirable to retain the feature of blade fixed pitch operation.

In the present study, a variation of $\bar{C}_L$ with percent jet-flap augmentation (defined as the percent of the installed power directed to blowing) was postulated based on the limited data available. Power split ranging from pure shaft drive (zero jet-flap augmentation) to pure jet flap (100 percent jet-flap augmentation) was examined and cost-effectiveness calculated for this range for the heavy-lift mission of the parametric study.

The $\bar{C}_L$ variation with augmentation assumed for this study is shown in Figure 3-44. Note that $\bar{C}_L$ varies from 0.5 for the zero augmentation or pure shaft drive to 1.0 for the pure jet flap. Data obtained from Giravions-Dorand personnel generally confirmed the validity of this assumption for $\bar{C}_L$ variation. Utilizing this relationship, along with the basic shaft-driven and jet-flap design data developed in connection with the heavy-lift studies of the previous paragraphs, payload capabilities and cost, as a function of jet-flap augmentation ratio, were developed.

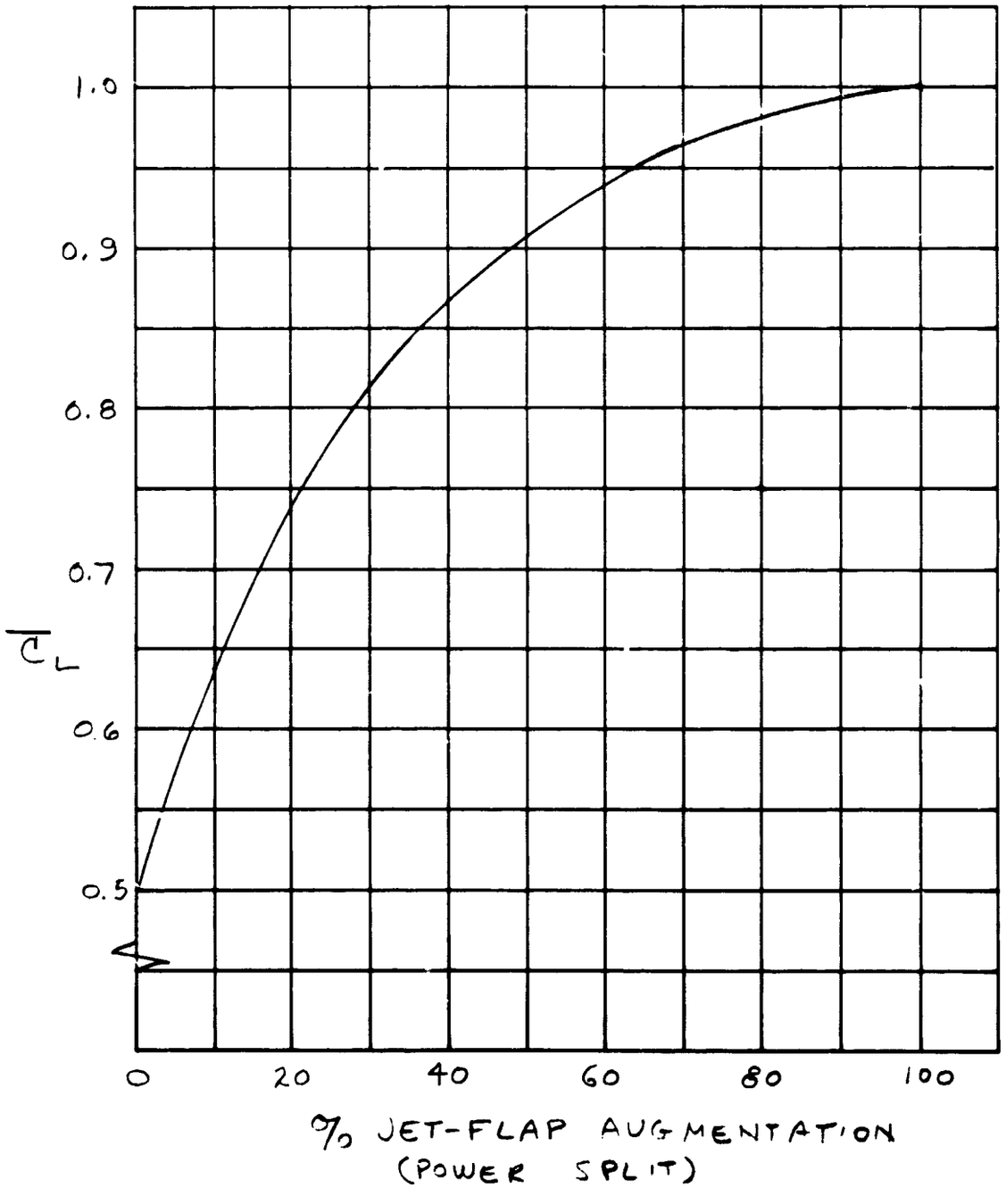

Figure 3-44 Estimated Blowing Effectiveness

Cost-effectiveness results are presented in Figure 3-45 . It may be noted that most favorable cost-effectiveness occurs in the power split ratio regime of 0.15 to 0.30 and that the jet-flap augmentated vehicle shows a favorable cost-effectiveness over the pure shaft-driven helicopter over an appreciable portion of the power split regime.

Late in the study, data were received from Giravions-Dorand on the subject of effectiveness of blowing at low values of blowing coefficient, including some late ONERA test data. The data were received too late in the study time period to be completely incorporated but preliminary examination indicated that reasonable values of lift augmentation can be obtained with a 30 to 70 percent split of installed power. However, it is estimated by Dorand personnel that for complete jet-flap control, some 60 percent or more of the installed power should be directed to the jet-flap. If this is so, it would probably require collective pitch control on the blades with cyclic control being achieved by the jet-flap.

Based on these preliminary studies, it is believed that a system in which only a portion of the installed power is utilized by the jet-flap merits further study, particularly for the heavy lift case.

Aerodynamics Considerations. A brief trade study of a mechanical-pneumatic power split was conducted to evaluate potential reduction of total installed horsepower. In Figure 3-46, two-dimensional ONERA test data (Reference 3) for a jet-flap are compared to theoretical results obtained from Spence's equations (Reference 4). Below C_μ = 0.12, Spence's theory is optimistic with regard to the ONERA tests. Above this value of blowing, Spence's results correlate well with other experimental data as shown in

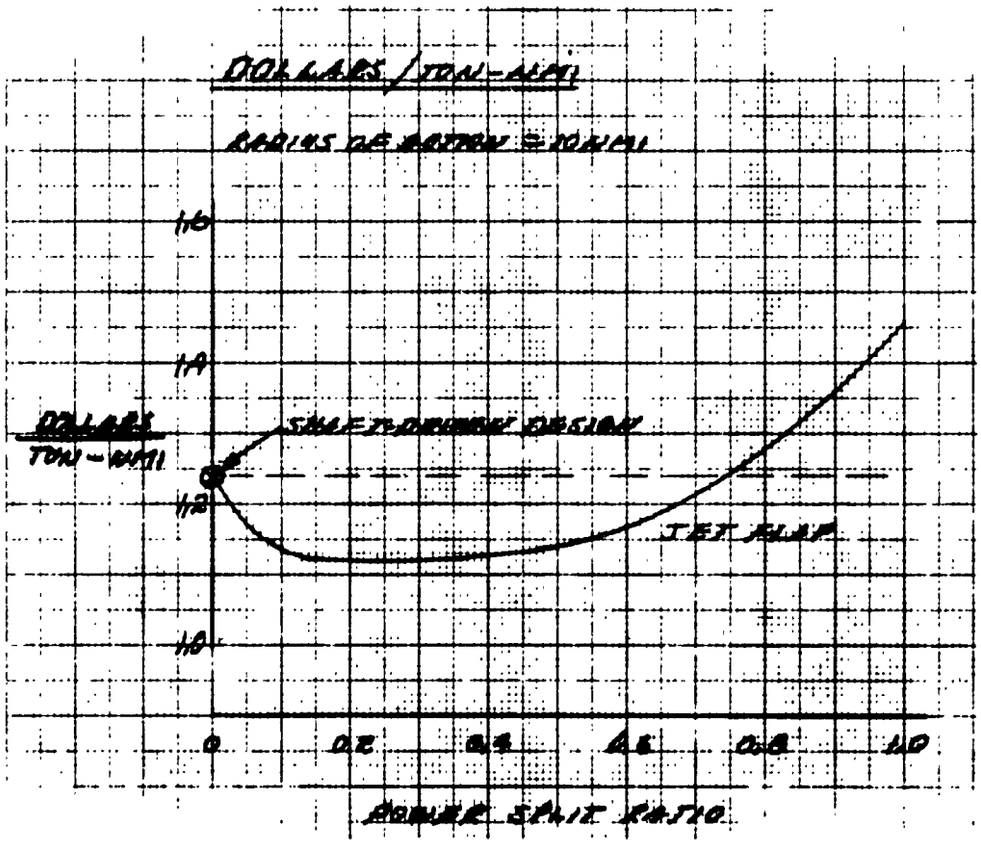

Figure 3-95 Heavy-Lift Helicopter – Effect of Jet-Flap Augmentation for Shaft-Driven Concept on Cost

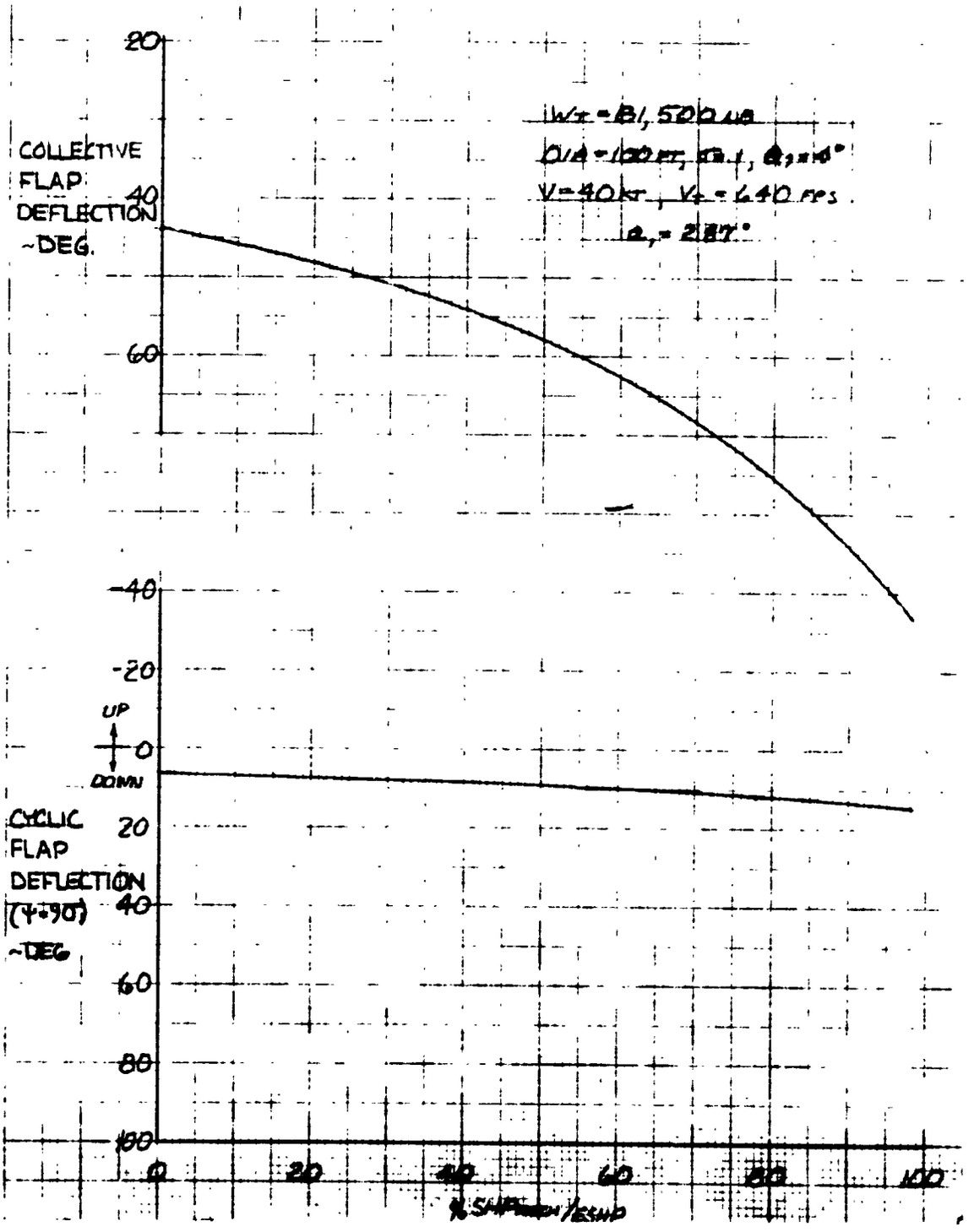

Figure 3-48 Collective and Cyclic Flap Deflections

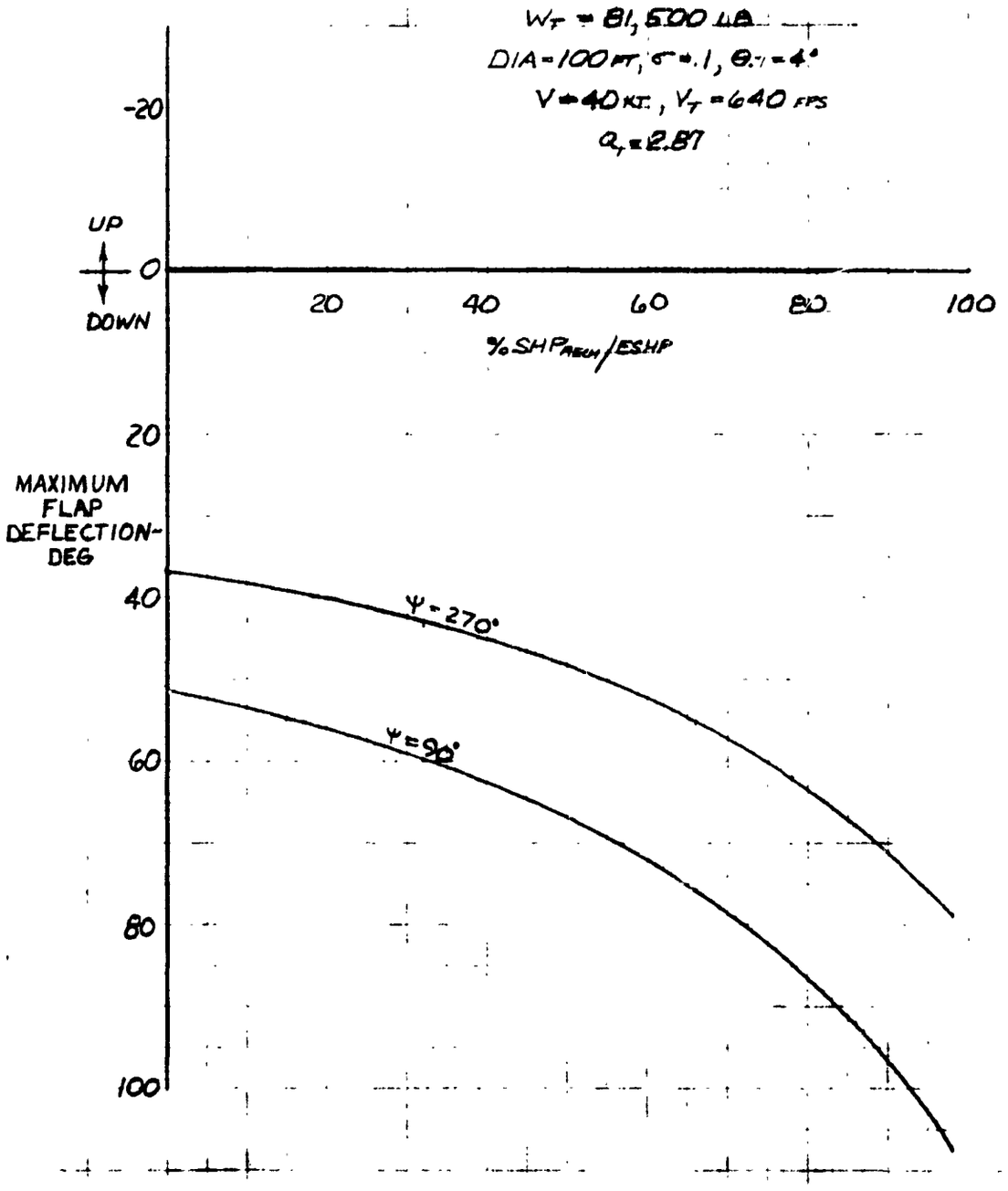

Figure 3-49 Maximum Flap Deflection

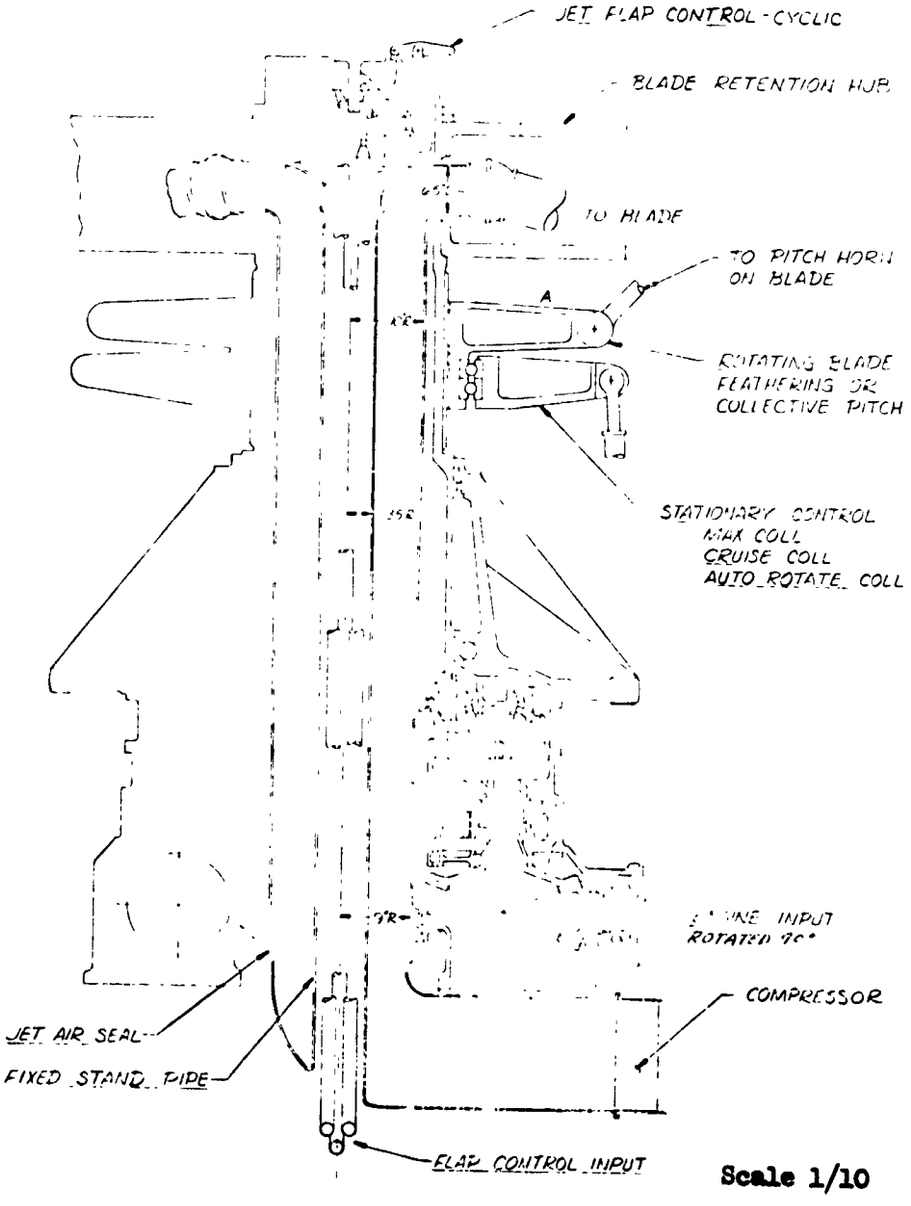

Figure 3-50 20-Ton Jet Flap 33% Jet Flap 67% Shaft Drive

The mechanical transmission is of the conventional type as designed for the 20-ton payload helicopter. One difference is that the rotor mast is supported at the top of the transmission to allow for a larger diameter mast to accept the gas ducts.

The gas ducts from the compressor join with rotating ducts inside the mast sealed by rotating air seals. The rotating gas ducts exit through holes at the hub and continue through the blade to the jet-flaps. In the center of the mast and gas ducts is a stationary standpipe which houses the jet-flap control rods. These control rods come from the pilot's controls through the fuselage, to the standpipe by bellcranks and links. At the top of the mast (rotor hub) a swashplate and linkage assembly provide collective and cyclic control motion to the jet blown flaps in the blade.

The external swashplate (A) of Figure 3-50, provides for feathering of the blade for pitch control in hover, forward flight and autorotation landing.

The gas duct from the compressor is mounted in the fuselage. The rotating gas duct is attached to the hub and has rotating seals at the fuselage junction. At the hub a circular duct to each blade is required and at the flapping axis a swivel joint is employed. Outboard of the swivel joint the duct becomes an oval shape to fit the three ducts in the blade. The three ducts run the entire length of the blade and have expansion joints as required.

3.2.7.3 Blade Sizing - Power Split

Figure 3-51 shows the blade sections sized for a shaft-driven rotor with jet-flap blowing for rotor control. The 6.5-inch diameter blade duct provides for 33 percent of the power to be diverted to the jet-flaps located at the outer 30-percent blade span.

The structural arrangement of the blade provides for mass balance in the leading edge. Blade skin panels of sandwich construction provide adequate stiffness to maintain the airfoil contour in the high speed section of the blade. Vertical web members provide support for the skin panels and support the insulated duct sections which are centered on the 25 percent chord. A series of brackets located between the aft vertical web and the close-out web for the honeycomb trailing edge member support the control rod to the jet-flap. A full depth honeycomb section with 0.020 skins makes up the trailing edge member which completes the blade section structure.

The structural material considered for this configuration is 7075 clad aluminum alloy. Other materials are brass for the leading edge mass balance and stainless steel ducts covered with thermal insulation. This blade configuration provides a ratio of duct area to blade section area of 0.14. Estimated structural weight of the section is 1.235 lb/in., balanced about the 25% chord line.

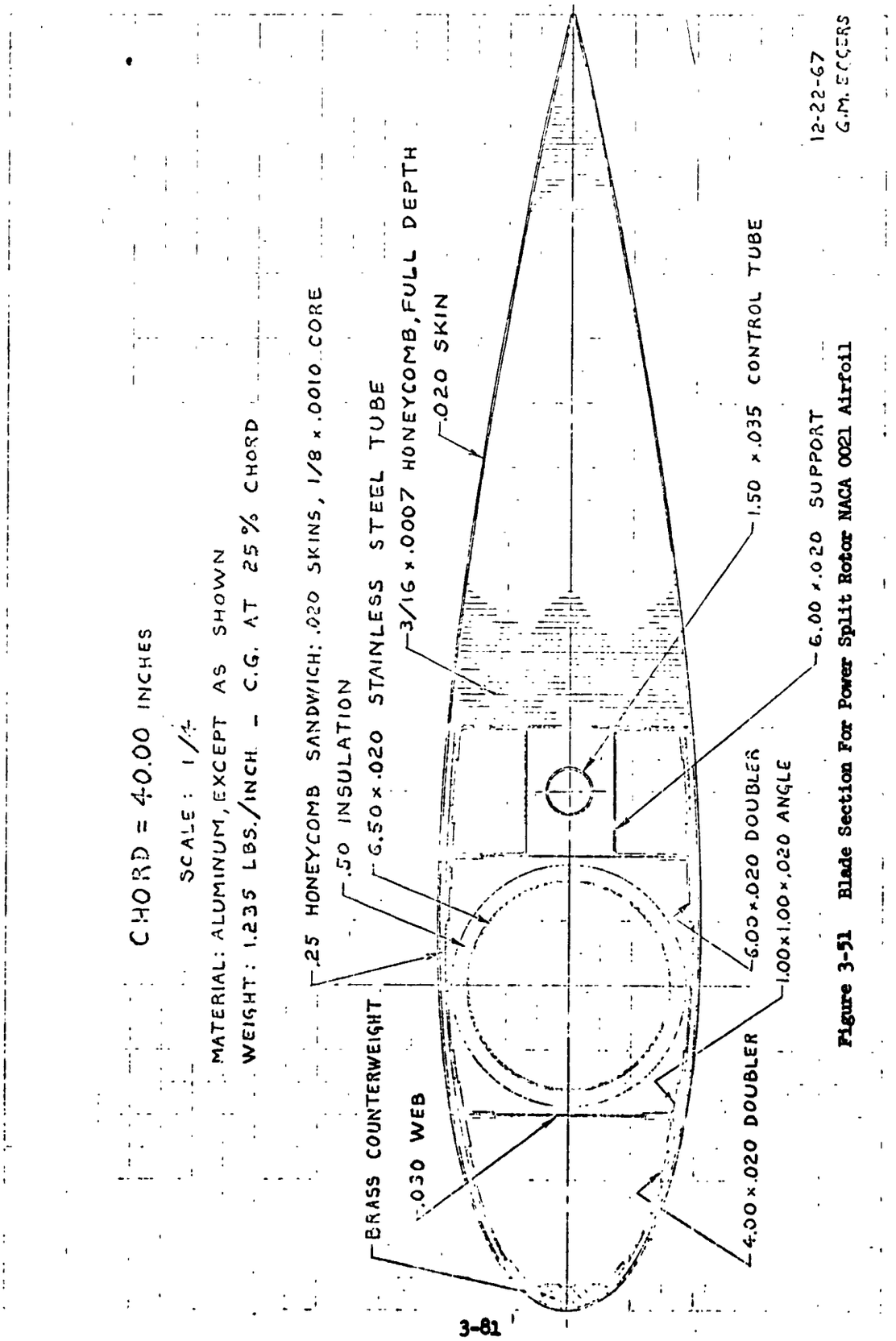

Figure 3-51 Blade Section For Power Split Rotor NACA 0021 Airfoil

3.2.8 Solidity and Disc Loading Sensitivity on ESHP

The sensitivity of power required in hover with solidity and disc loading was investigated for a representative heavy-lift helicopter prior to the parametric study. A configuration featuring a gross weight of 100,000 lb, four rotor blades, and a tipspeed of 700 ft/sec was selected for this study. Takeoff rated power requirements were determined for a shaft-driven and a jet-flapped rotor system based on hover at a T/W = 1.0, SL, STD. Figure 3-52 presents rated power versus solidity for a rotor diameter of 100 ft corresponding to a disc loading of 10. A slight increase in the power requirements is shown for large changes in solidity due to the corresponding profile power increase. For the case examined, the jet-flap propulsion system, due to its inherent greater system losses (explained in Paragraph 8), requires approximately 3.5 times the rated horsepower of a similar shaft-driven rotor. For a solidity of 0.10, Figure 3-53 shows the increase in power with disc loading resulting from the induced power requirements. The relatively large inequality in rated power required for the jet-flapped system as compared to a shaft-driven rotor reflects the propulsion system losses due to compressor efficiency, duct pressure drop and residual energy discharged through the jet-flap nozzle.

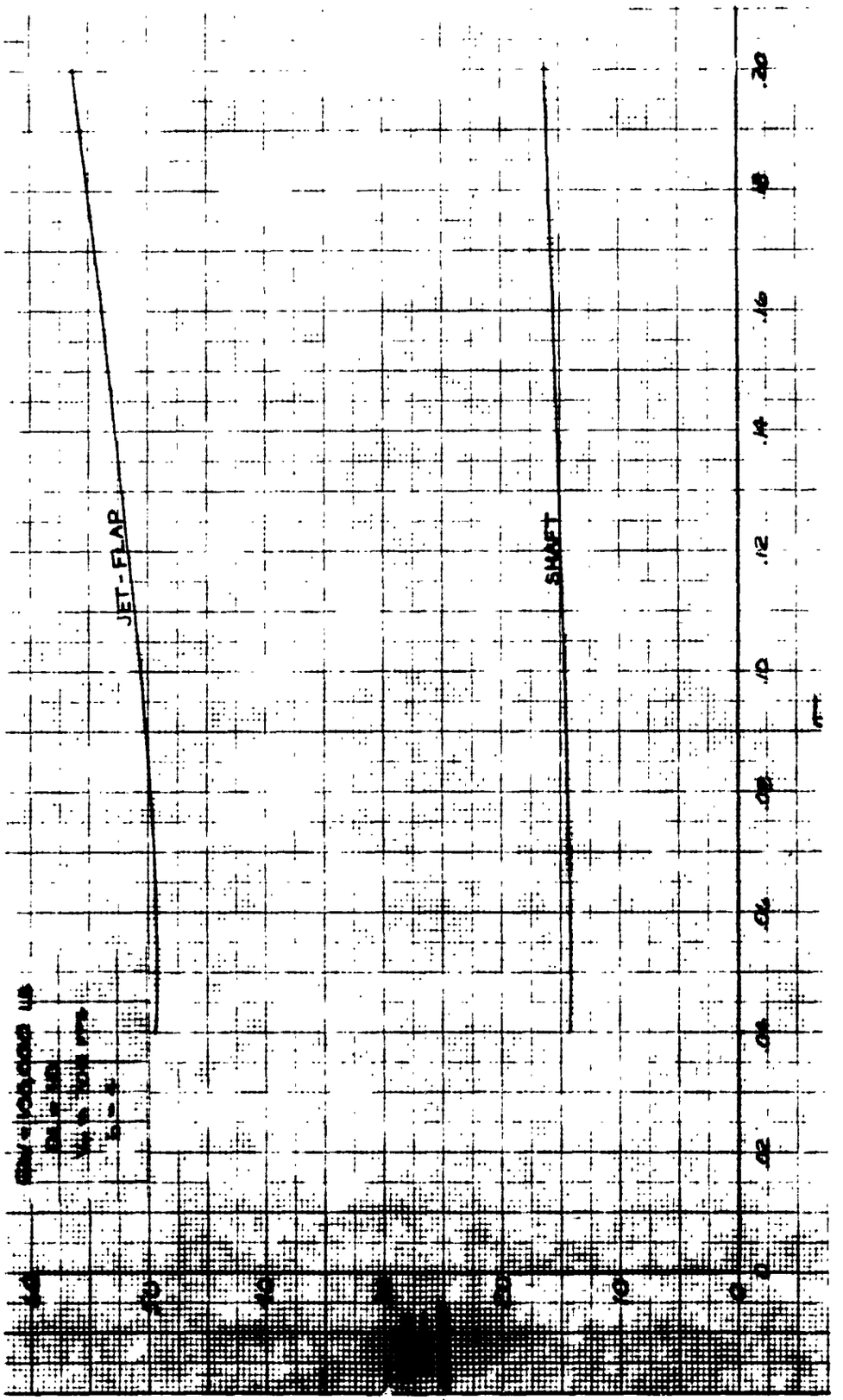

Figure 3-52 Rated SHP Vs σ

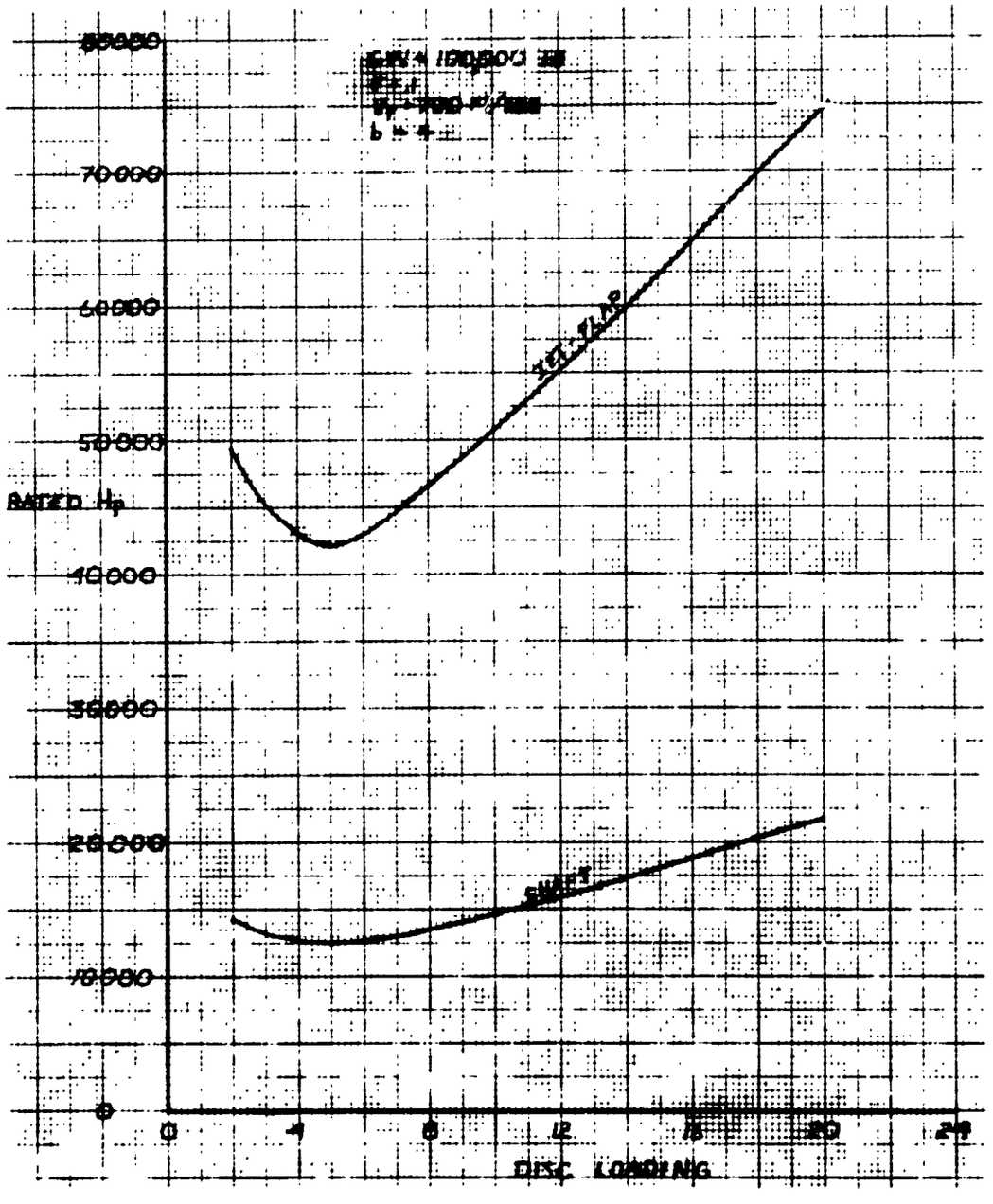

Figure 3-53 Rated Hp Vs Disc Loading

4.0 PROPULSION

Volume I of this report contains details of the following propulsion areas:

- Propulsion Requirements
- Concepts and Data Sources
- Propulsion Parameters and Cycle Comparisons
- Propulsion System Performance Methodology
- Propulsion System Pressure Drop Analysis
- Thrust Recovery Investigation
- Energy Balance

This volume contains the following supplementary material:

- Jet-Flap Propulsion System Analysis Theory
- Effect of System Pressure Loss on Pressure Ratio Selection
- Computer Routine Description

4.1 JET-FLAP PROPULSION SYSTEM PERFORMANCE

4.1.1 Jet-Flap Propulsion System Analysis

Figure 4-1 is a schematic representation of a jet-flap rotor propulsion system with pertinent station notation. In the cold cycle system as shown, a turboshaft engine drives a compressor whose output is ducted through the rotor hub and blades to the nozzles.

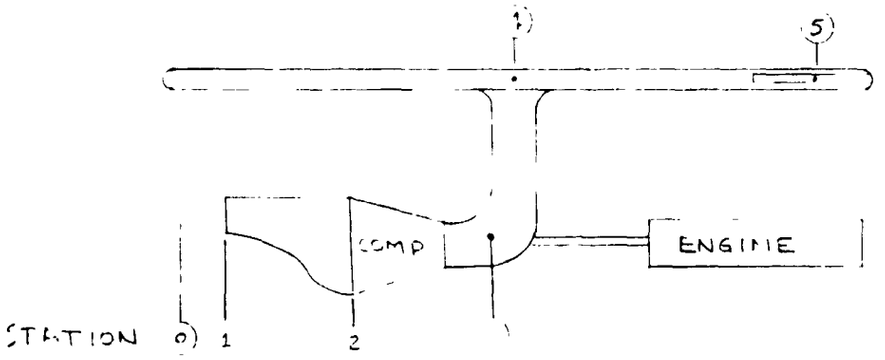

Figure 4-1

Jet Flap Propulsion System Notation

Figure 4-2 shows a section through the rotor blade at the jet-flap. Angle α is the blade angle of attack, and δ is the deflection of the flap relative to the blade chord line. During normal operation, α and δ both vary during a rotor cycle. However, since cyclic rotor pitch is not used, α is considered constant and taken as the effective angle of attack between the rotor blade and the plane of rotation. Flap deflection, δ, varies during forward flight in sweeping the circle. In addition, δ is a function of disc loading.

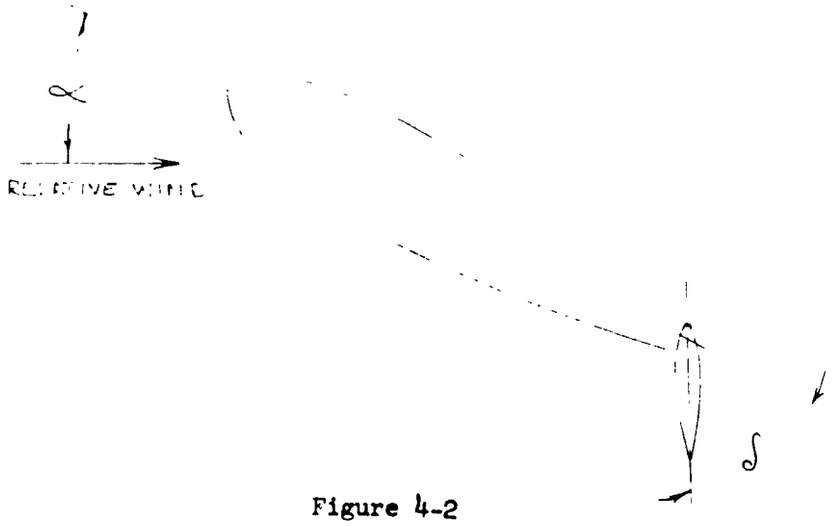

Figure 4-2

Jet Flap Nozzle

4.1.2 ROTOR BLADE INTERNAL FLOW

Figure 4-3 shows the rotor blade internal flow notation:

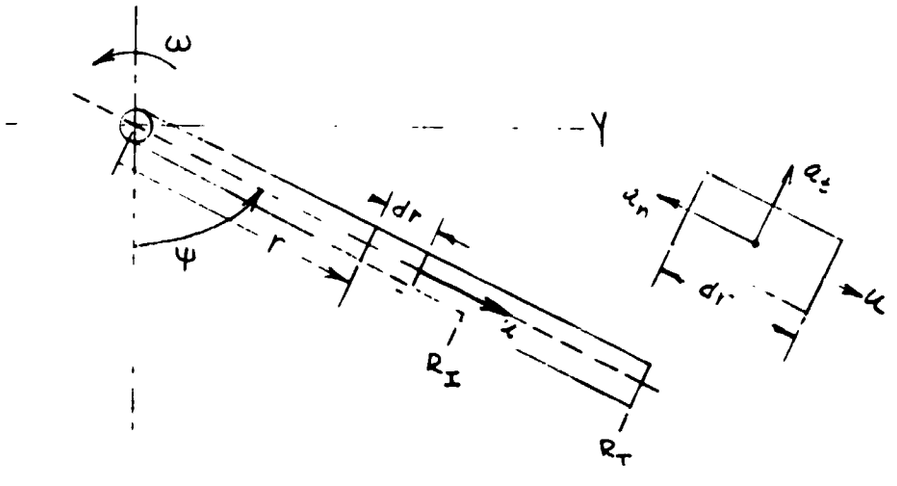

Figure 4-3

Internal Flow Notation

ω = rotational velocity

ψ = blade azimuth angle

r = radial location

R_i = radius at inboard edge of jet slot

R_t = blade radius

a_t = acceleration component tangent to rotor disc

a_n = acceleration component along radius of rotor disc

u = flow velocity inside blade

u_x = component of flow velocity in x direction

u_y = component of flow velocity in y direction

r_x = coordinate of radial location in x direction

r_y = coordinate of radial location in y direction

A = blade flow area

The following assumptions are made:

One dimensional isentropic flow

ω = constant

ρ = constant

A = constant from r = o to = R_i

u = constant = dr/dt

$$r_x = r \cos\psi \quad ; \quad r_y = r \sin\psi$$

$$u_x = dr_x/dt = -r \sin\psi \, d\psi/dt + \cos\psi \, dr/dt$$

$$u_y = dr_y/dt = r \cos\psi \, d\psi/dt + \sin\psi \, dr/dt$$

$$\frac{dr}{dt} = u; \quad \frac{d}{dt} = \omega$$

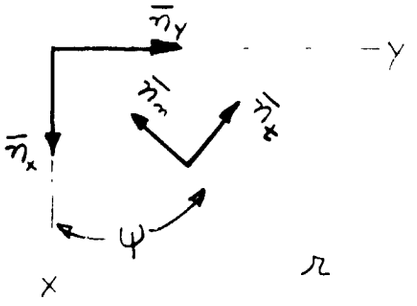

$$u_x = -r\omega \sin\psi + u \cos\psi$$

$$u_y = r\omega \cos\psi + u \sin\psi$$

$$a_x = \frac{du_x}{dt}$$

$$= -\omega \sin\psi \frac{dr}{dt} - r \sin\psi \frac{d\omega}{dt}^{\circ} - r\omega \cos\psi \frac{d\psi}{dt}$$

$$+ \cos\psi \frac{du}{dt}^{\circ} - u \sin\psi \frac{d\psi}{dt}$$

$$= -\omega u \sin\psi - r\omega^2 \cos\psi - u\omega \sin\psi$$

$$= -2\omega u \sin\psi - r\omega^2 \cos\psi$$

$$a_y = \frac{du_y}{dt}$$

$$= \omega \cos\psi \frac{dr}{dt} + r \cos\psi \frac{d\omega}{dt}^{\circ} - r\omega \sin\psi \frac{d\psi}{dt}$$

$$+ \sin\psi \frac{du}{dt}^{\circ} + u \cos\psi \frac{d\psi}{dt}$$

$$= \omega u \cos\psi - r\omega^2 \sin\psi + \omega u \cos\psi$$

$$= 2\omega u \cos\psi - r\omega^2 \sin\psi$$

Defining unit vectors $\bar{n}_x$, $\bar{n}_y$, $\bar{n}_n$ and $\bar{n}_t$ as shown above, the acceleration vector becomes

$$\bar{a} = a_x \bar{n}_x + a_y \bar{n}_y$$

or

$$\bar{a} = (-2\omega u \sin\psi - r\omega^2 \cos\psi) \bar{n}_x + (2\omega u \cos\psi - r\omega^2 \sin\psi) \bar{n}_y$$

From r = R_i to r = R_t, m is assumed to decrease linearly due to discharge through the jet flap nozzle:

$$dm = \rho A \left(\frac{r - R_I}{R_I - R_T} \right) dr, \quad R_I \le r \le R_T$$

F = force; Q = torque.

$$dF_t = a_t d_m \qquad Q = \int_0^{R_I} r\, a_t\, dm$$

$$dQ = r dF_t$$

$$Q = \int_0^{R_I} r 2\omega m \rho A\, dr + \int_{R_I}^{R_T} 2\omega m \rho A r \left(\frac{r - R_T}{R_I - R_T} \right) dr$$

$$= 2\rho A m \omega \left[\int_0^{R_I} r\, dr + \frac{1}{R_I - R_T} \int_{R_I}^{R_T} (r^2 - r R_T)\, dr \right]$$

$$= 2\rho A m \omega \left\{ \left[\frac{r^2}{2} \right]_0^{R_I} + \frac{1}{R_I - R_T} \left[\frac{r^3}{3} - \frac{r^2 R_T}{2} \right]_{R_I}^{R_T} \right\}$$

$$= \frac{\rho A m \omega}{3} \left[\frac{R_I^3 - R_T^3}{R_I - R_T} \right] = \frac{\dot{m} \omega}{3} \left[\frac{R_I^3 - R_T^3}{R_I - R_T} \right]$$

Q is the Coriolis torque required to increase the angular velocity of the flow through the blade passage, i.e., to increase angular momentum.

Qω is the associated Coriolis power:

$$HP_{Coriolis} = \omega Q = \frac{\dot{m} \omega^2}{3} \left[\frac{R_i^3 - R_t^3}{R_i - R_t} \right]$$

This equation can be simplified by substituting an equivalent concentrated jet at the effective center of the jet flap slot, $\bar{R}_t$. In this case:

$$Q = \int_0^{\bar{R}_T} r\, a_t\, dm = \int_0^{\bar{R}_T} r \cdot 2\omega m \cdot \rho A\, dr$$

$$= 2\omega m \rho A \int_0^{\bar{R}_T} r\, dr = 2\omega m \rho A \frac{\bar{R}_T^2}{2} = M_J \omega \bar{R}_T^2$$

$$HP_{CORIOLIS} = \omega Q = M_J \omega^2 \bar{R}_T^2 = M_J \bar{V}_T^2$$

Where $\overline{V}_t$ is the rotor velocity at the effective center of the jet-flap slot. The physical center of the slot can be used as the effective center with negligible error, in which case, for a slot extending over the outer 30 percent of the blade radius, the effective center would be at approximately 85 percent radius.

4.1.4 ROTOR BLADE COMPRESSION DEVELOPMENT

The radial acceleration vector, a_n, passes through the center of rotation and thus requires no additional power input. A development of the gas compression due to centrifugal forces is presented since it contributes to the total enthalpy of the flow at the thrusting nozzle.

$$dF_n = a_n d_m = r\omega^2 \rho A dr$$

4.1.5 POWER RELATIONSHIPS

The net useful power delivered to the rotor is termed Equivalent Shaft Horsepower (ESHP) because it is nominally equivalent to the shaft power required to drive the same rotor mechanically. This power is equal to the gross propulsive thrust horsepower of the jet-flap nozzles, less the Coriolis power:

$$\text{ESHP} = \text{Gross Propulsive THP} - \text{HP Coriolis}$$

$$= M_j V_{J5} \overline{V}_t K_2 - M_j \overline{V}_t^2$$

Where V_{J5} is the ideal nozzle velocity:

$$V_{J5} = \sqrt{2gC_pT_{t5}\left[1 - (P_{amb}/P_{t5})^{r-1/r}\right]}$$

and K_2 is a thrust recovery factor which includes the effect of nozzle thrust coefficient, nozzle thrust vectoring, and deviation of nozzle exit pressure from ambient.

4.2 EFFECT OF SYSTEM PRESSURE LOSSES ON PRESSURE RATIO SELECTION

It is apparent that when system losses are considered, efficiency does not continually increase with decreasing pressure ratio as in the ideal case, but rather reaches an optimum value due to the effect of transmission losses. The reason for transmission losses becoming dominant at low pressures is shown by Figure 4-4. Two simplified air cycle systems are shown, one of relatively low pressure ratio (2.0) and the other fairly high (5.0). In each case system losses are such that 25 percent of the pressure to which the gas is compressed is lost in the ducting. The power put into the systems is shown by "Δ H in", and the gas horsepower remaining at point 3 is shown by "Δ H out". It can be seen that system "efficiency", in terms of Δ H out/Δ H in, is higher for the higher pressure system. The transmission of gas power is analogous to the transmission of electrical power, the efficiency of which increases with electrical pressure (voltage).

4.3 COMPUTER ROUTINE

Propulsion system performance calculations are made by means of a computer routine developed by VAD. The principal inputs to the routine are engine fuel flow, gas conditions entering the aircraft ducting system, and ducting system characteristics. These inputs are made for each combination of ambient conditions, airspeed, and power setting. An engine size factor, such as rated thrust or horsepower is inserted for scaling.

The primary gas conditions are flow rate, temperature, pressure, and specific heat. There are obtained from compressor performance calculations in the case of the cold cycle, and from engine manufacturers' data for the warm and hot cycles.

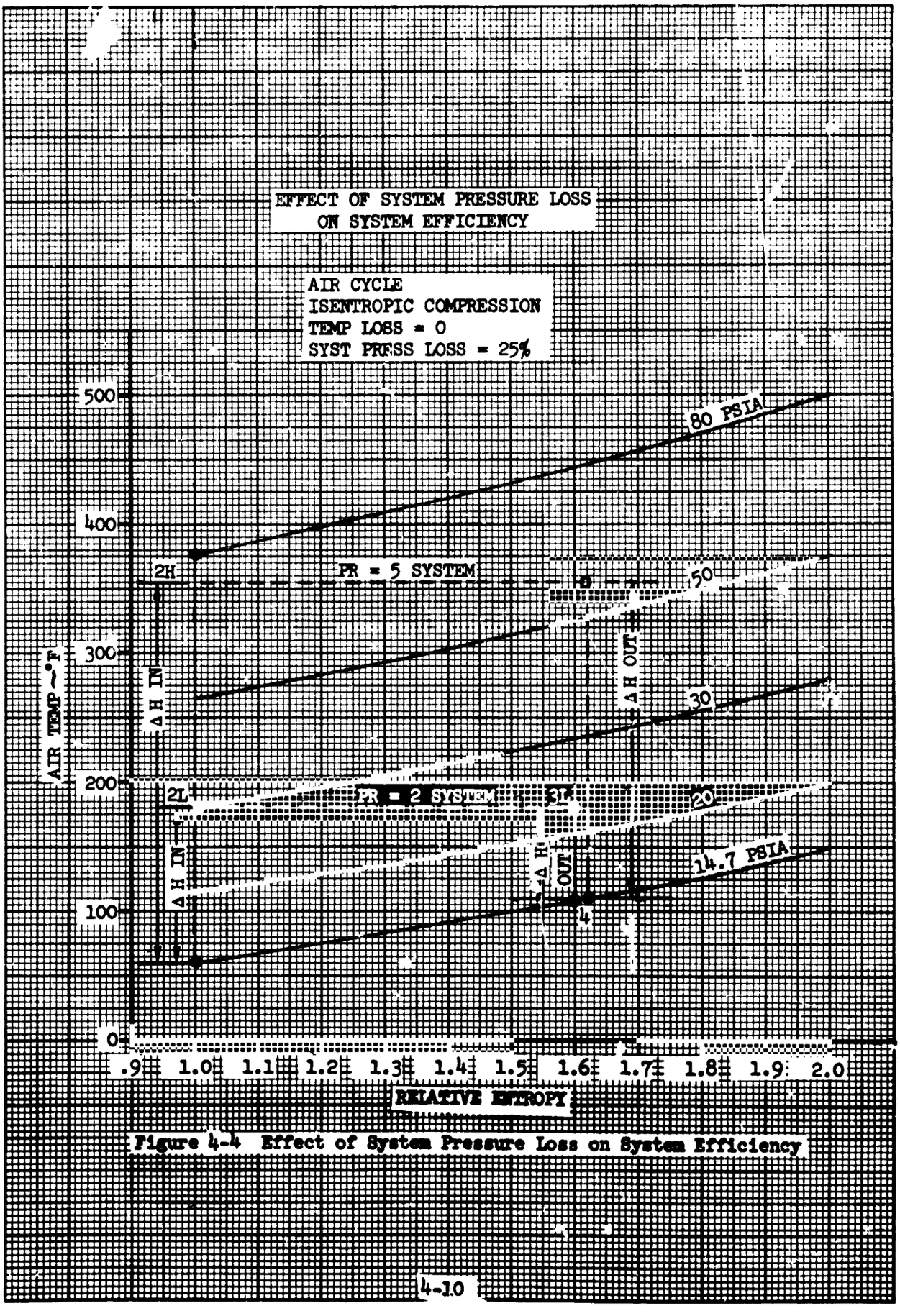

Figure 4-4 Effect of System Pressure Loss on System Efficiency

Ducting system characteristics include pressure drop, thrust recovery, rotor tipspeed, duct Mach number, and control and leakage flow.

These inputs, plus the necessary constants, are used to calculate ESHP available and duct area required. If desired, these outputs can be expressed as a function of rated engine size (such as ESHP/Rated Thrust) so as to cover a range of engine sizes. Other outputs which can be obtained are gas horsepower, nozzle velocity, and nozzle area.

5.0 STRUCTURES AND DESIGN

5.1 HUB AND MAST

The hub and the mast for the HLH 20-ton payload jet-flap helicopter is presented in Figure 5-1. The HSH concept is similar except that the rotor is 2-bladed instead of 3-bladed. The rotor mast is supported in fuselage mounts to react vertical lift loads and moments induced by the rotor. The mast is supported at the bottom to the fuselage by an elastic mount. The mast is non-rotating.

The rotor hub is a one-piece forging supplying the housing for the bearing between it and the mast. The hub provides for the blade attachment and pivot (flapping axis) and centrifugal force restraint and lead-lag restraint. The blade attachment is a clevis-type structure attached to the blade root structural members. The flapping action is provided at the 45-inch blade station by means of two bolts and two bearings around which the blade attachment fittings rotate.

The gas duct from the compressor is mounted in the fuselage. The rotating gas duct is attached to the hub and has rotating seals at the fuselage junction. At the hub a circular duct to each blade is required, and at the flapping axis a swivel joint is used. Outboard of the swivel joint the duct becomes an oval shape to fit the ducts in the blade. The ducts run the entire length of the blade and have expansion joints as required.

5.2 BLADE DESIGN

A study of the structural arrangements for the jet-flap blade was conducted to assist in determining realistic structural weights. The study

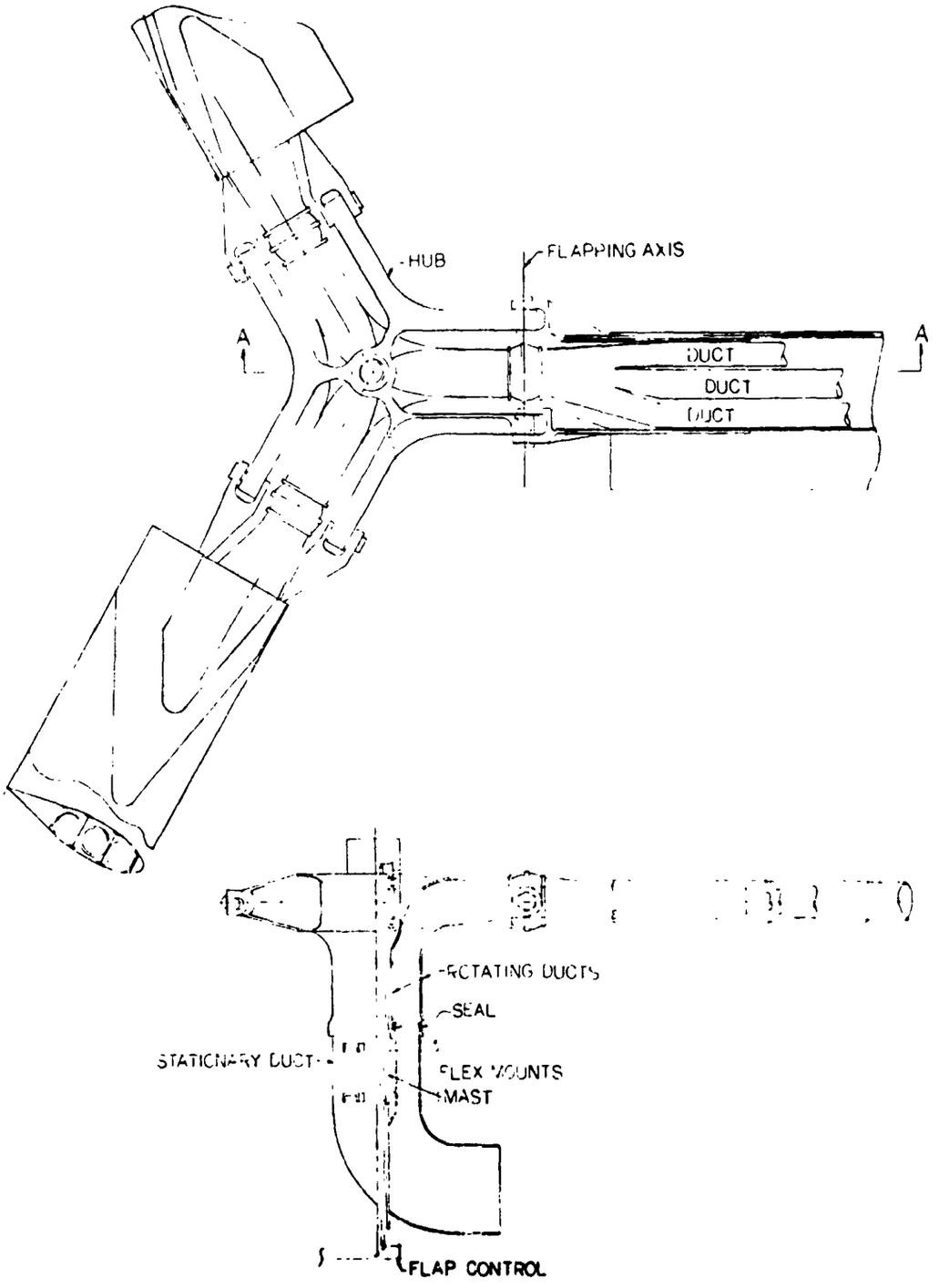

VIEW A-A

Figure 5-1 Jet-Flap Rotor HIH

also investigated and disclosed some of the more obvious structural design problems for the unique jet-flap rotor system. The parameters studied included: duct areas, gas pressures and temperatures, helicopter design gross weight, rotor diameter, and rotor rpm.

The structural design philosophy of making the blade shell the primary structure was selected for the initial design approach for the cold cycle. Blade bending, torsion, and axial loads are carried by the skin panels. Separate internal circular thin wall ducts insulated from the blade skin panels provide for an efficient use of this external structure without degradation of strength due to the temperature of the propulsion gases. The gas ducts are made nonstructural by designing them into short sections and connecting these sections together by flexible joints. In this manner the thermal expansion of the duct sections is compensated, and the thickness of the circular duct walls can be minimized to carry only the hoop tension stresses due to the propulsion gases. The structural concept is discussed in some of the work done by Giravions Dorand on large-diameter rotors, but differs from the DH 2011 test blade, which utilizes its single duct as the main member to carry bending and axial loads.

The NACA 0024 airfoil was used as the basic blade section. Blade chords were selected to obtain sufficient thickness of the blade envelopes to house the warm air ducts. The basic blade section's skin panels, vertical webs, and leading edge member were sized and balanced about the quarter chord line. Representative spanwise distributions of stiffness and blade weight based on several cross-sectional cuts of the blade were used for calculating static blade loads. Blade skin stress levels were

then calculated for the flapwise bending moment and centrifugal force loadings and compared to the allowable limit stress of the material selected for the design.

5.2.1 Basic Blade Description

The structural arrangement of the basic blade cross section for the cold cycle is shown in Figure 5-2. The two configurations of different chord lengths and solidities were sized to accommodate the propulsion system ducting for the jet-flap rotor. An idealized structure of aluminum alloy was used for this study. This tended to simplify details of design and provide an insight to some of the more obvious structural problems associated with large size rotor blades selected for the HSH and HLH jet-flap rotor systems.

The diameters of the ducts were selected to provide a L/D_H ratio of approximately 50 to maintain an acceptable pressure drop in the propulsion system. Where L is the duct length, which is approximately 0.85% rotor radius, and D_H is the hydraulic diameter on the inside diameter of a circular duct. The ratio of duct area to blade cross-sectional area for these blade configurations is 0.38.

Provision has been made inside the trailing edge of the blade for a 1.5-in. control rod to represent a control system for actuation of the mechanical jet flap.

The leading edge member provides the necessary mass balance for the blade section. This structure, wrapped externally with 0.010 stainless steel, provides resistance to any impact loads or erosion that may occur along the leading edge of the blade.

The blade shell design consists of an upper and lower bonded sandwich panel of 0.5-in. honeycomb (5052AL.A) with 0.020-in. thick skins

Figure 5-2 BASIC BLADE SECTION (NACA 0021 AIRFOIL)

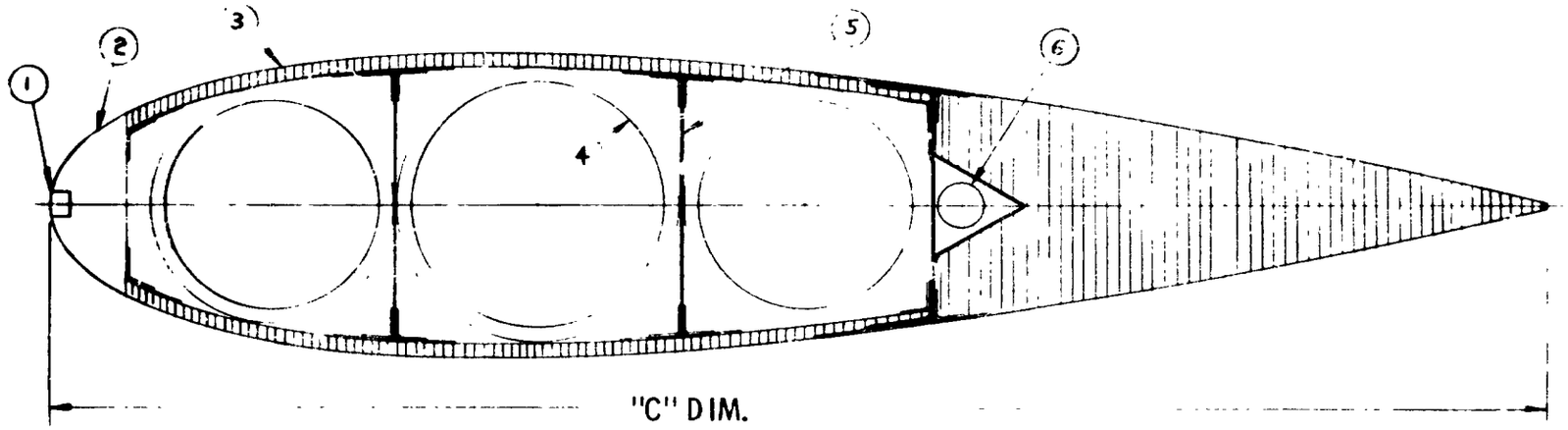

① MASS BALANCE
② NOSE BLOCK EXTRUDED ALUM. ALLOY
③ SKIN PANELS UPPER & LOWER .5 IN. HONEYCOMB WITH .025 IN. ALUM ALLOY SKINS
④ DUCTS -.025 ALUM. ALLOY WITH .5 IN. INSULATION
⑤ VERTICAL WEBS - .020 IN. ALUM. ALLOY
⑥ CONTROL ROD - 1.50 X .035 TUBE ALUM. ALLOY

ROTOR BLADE CONFIGURATION				
CONF.	"C" CHORD	ROTOR DIA.	SOLIDITY	BLADES/ROTOR
HSH	50.0 IN.	72.2 FT.	.106	2
HLH	45.75 IN.	145.0 FT.	.0502	3

of 7075-T6 clad. The skin panels were sized to support an average aerodynamic airload of 4 psi with a minimum deflection of the airfoil surface between the vertical web members. These web members run spanwise between the ducts and support the upper and lower skin panels.

The vertical web members were considered to be made up of two sheets of 0.010 in 7075-T6 clad beaded and bonded together to provide maximum resistance to compression loads on the airfoils shape resulting from blade flapwise bending and airloads normal to the surface. Besides supporting the airfoil surface, the vertical web members support the duct sections and transfer the centrifugal force loading of the duct sections to the skin panels, which form a multibox structure.

Duct walls were sized for 0.02-in. thick aluminum as minimum wall gage. The ducts are considered to be nonstructural except for carrying the warm air from the compressors at 361°F at 46.4 psig. To allow for expansion and flexibility, a joint of silicone tubing is placed at 20-inch intervals along the duct span. An 0.5-inch thick insulation is wrapped around the ducts to prevent heat losses and minimize heat transfer to the basic structures of the blade.

Figure 5-3 shows the spanwise planform of the rotor blade. Details of the rotor hub and blade retention system were not included in this study, but it is envisioned that this structure would be a high strength alloy of steel or titanium to provide the necessary structure to carry the blade loads.

Figure 5-3 JET-FLAP ROTOR BLADE PLAN FORM

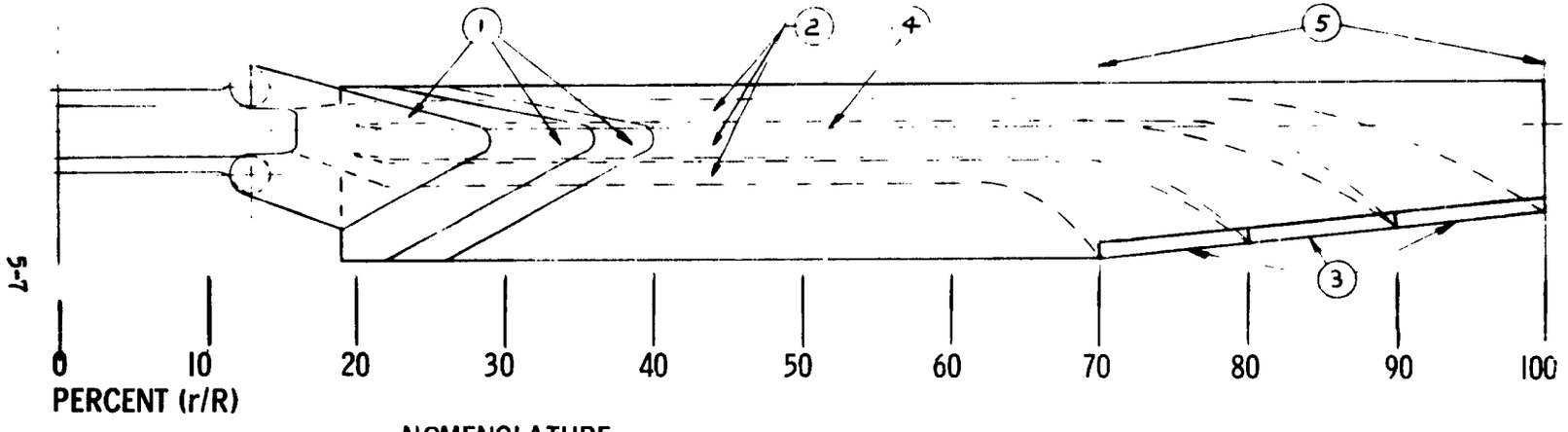

NOMENCLATURE

(1) BLADE DOUBLERS & RETENT'ON PLATE
(2) AIR DUCTS
(3) JET FLAPS
(4) QUARTER CHORD LINE
(5) TIP TAPER RATIO 1.50/1.0

The transfer of blade loads into blade root retention system is accomplished by external doublers and retention plates bonded onto the blade skins. The thickness and the fingerlike shape of these doublers and plates are used to provide adequate bond area and provide a gradual change in structural stiffness. Internal buildup of vertical web members and nose block toward the blade root provides additional means of transferring blade loads into the blade retention member.

The outboard portion of the blade is tapered from the 70 percent station to the tip with a taper ratio of 1.50:1. With the widening-out of the ducts to form the trailing edge nozzle, the blade airfoil can become thinner (less than NACA 0024 airfoil), thus reducing aerodynamic drag at the blade tip. Trailing edge structure in this portion of the blade will necessarily become heavier to support the jet flap and control system.

A study of basic blade section arrangements for the hot cycle rotor was undertaken to determine the maximum duct area ratios achievable and investigate the sensitivity of this ratio to changes of gas pressures and temperature. A number of arrangements of blade shells and ducts were studied. Duct shapes and deflections due to gas pressures were investigated. Duct walls were sized for gas pressure loads at elevated temperatures using selected materials. Of the blade configurations studies, four were selected for comparison and discussion. These four configurations are described in Figure 5-4 through 5-7. These configurations represent three structural concepts which will be discussed below.

The first concept is characteristic of that used for the cold cycle and is represented by configurations No. 1 and 3. The basic blade structure is isolated from the thermal environment of the hot gas duct by insulation. Compression-type bellows join together 30-inch duct sections to

compensate for thermal expansion and eliminate stresses in the duct walls due to centrifugal force and blade bending. Duct shapes were designed to carry the gas pressures in hoop tension thereby minimizing duct wall thickness and deflections. These duct designs result in a ratio of duct area to total blade cross sectional area which is relatively insensitive to gas temperature and pressure. The maximum duct area ratio for configuration 1 was 50 percent. Duct area ratio for configuration 3 was 55 percent.

The second structural concept is represented by configuration No. 2 which utilizes an elliptical-shaped duct of heat-resistance steel. The duct is continuous from the blade retention to the tip. The duct shape is wrapped with insulation and is supported by an envelope of bonded aluminum honeycomb. The duct wall is sized to carry centrifugal force loads, blade bending and gas pressure loads. In addition to supporting the duct shape the aluminum envelope carries its portion of centrigual force and blade bending loads. Differential expansion of duct-to-blade shell is compensated for by permitting the duct to slide inside of its insulation. The shape of the duct and its area are dependent on the interaction of the supporting structure of aluminum shell and the duct wall. This makes the duct area ratio sensitive to gas pressure ratios and temperatures.

The third structural concept is represented by configuration No. 4 which is called the hot blade. Configuration No. 4 uses the blade shell for the hot gas duct and the basic structure. Two half shells of welded stress skin form the blade airfoil. Stress skin is an all-welded honeycomb sandwich structure manufactured entirely by the resistance welding of its components. Inconel 718, heat resistant steel, was selected for this design configuration. The structural thickness of the blade shell depends

on the gas pressures and temperatures. Therefore, the duct area ratio is sensitive to variations of the pressure and temperature of the propulsion gas.

Blade configurations No. 2 and 3 give duct area ratios of 55 percent. For the 48-inch blade sections studied this represents a duct area of 208 square inches compared to the total 378 square inches of the blade cross section. Based on this structural design study of blade configurations it appears that blade configuration No. 3 will give the maximum duct area ratio with the least technical risk of the blade designs studies. However, from the standpoint of wetted area and hydraulic diameter, configuration No. 2 is superior. In a specific design all the factors must be weighed before selecting a particular configuration.

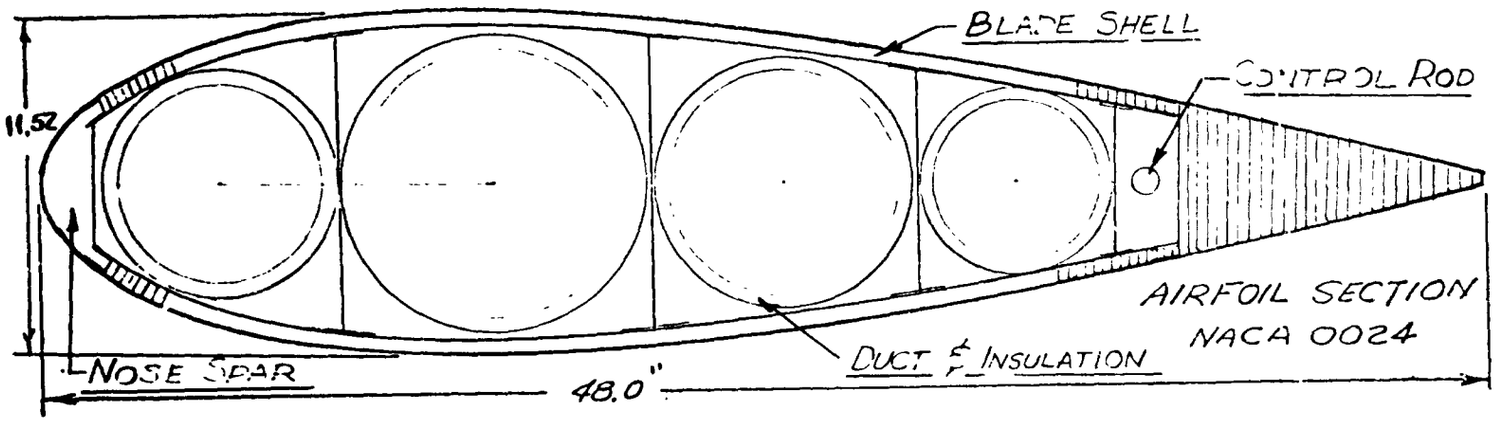

Figure 5-4 BLADE CONFIGURATION NO. 1 (Sheet 1 of 2)

Description:
The blade shell structure utilizes bonded aluminum honeycomb sandwich panels and a full depth honeycomb trailing edge. An aluminum extrusion forms the blade leading edge which is covered with an abrasive resistant material. The hot gas ducts are circular in shape and are fabricated from the thin gage heat resistant steel. Compression type bellows located at every 30 inches in the ducting compensate for thermal expansion. Insulation wrapped around the ducts retain the heat within the ducting to minimize thermal degradation of the load carrying blade shell. A mechanical push-pull rod located in the blade trailing edge section represents the controls for jet-flap actuation. The jet-flaps are located on the outboard 30 percent of the blade radius.

Advantages:

1. The basic blade structure is protected from the heat of the hot gases. This eliminates degradation of the strength of materials and permits the use of metal bonding for the blade shell design.

2. Ratio of duct area to blade cross sectional area is insensitive to duct pressure ratios and temperatures. Duct area ratio is $\simeq 50\%$.

3. Compression type bellows provide flexibility at the duct joints minimizing bending stresses in the duct due to blade bending loads.

Figure 5-4 BLADE CONFIGURATION NO. 1 (Sheet 2 of 2)

4. Isolation of thermal expansion to the duct system facilitates blade jet-flap control design.

5. Basic load carrying structure can be visually inspected for fatigue cracks and structural damage.

Disadvantages:

1. Multiple sections of the four duct system with three vertical web members complicate blade final assembly.

2. Multiple ducts increase wetted area and reduce hydraulic diameter which tend to decrease efficiency of gas flow.

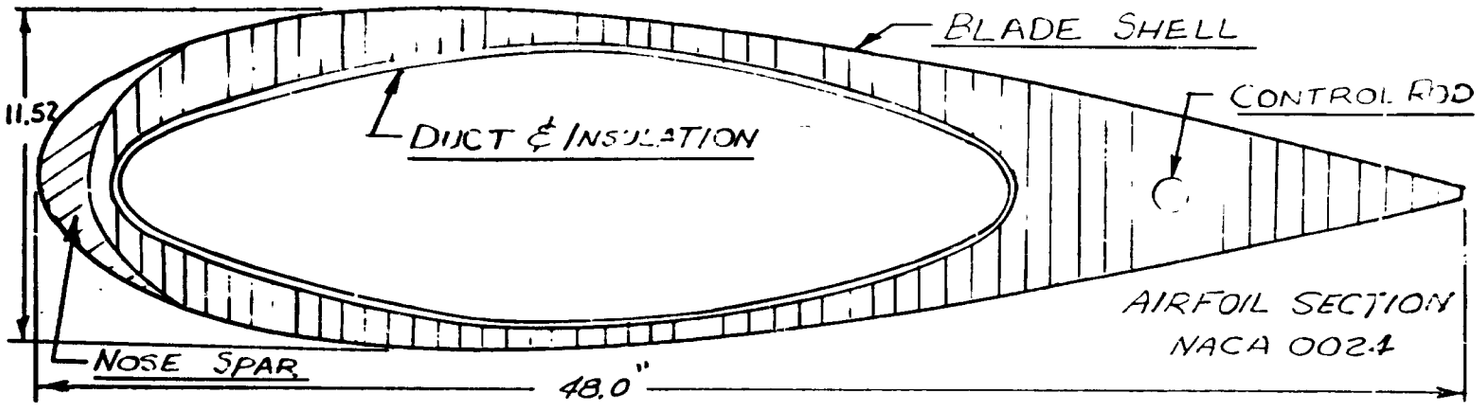

Figure 5-5 BLADE CONFIGURATION NO. 2 (Sheet 1 of 2)

Description:

The blade shell is constructed of adhesive bonded aluminum honeycomb and skins which form the airfoil shape around the elliptical duct section. The nose spar is aluminum, and the trailing edge is full depth honeycomb. The aluminum structural envelope of the blade is protected from the high temperatures of the gas duct by a layer of insulation wrapped around the outside of the duct. A push-pull control rod is located in the trailing edge section of the blade.

Advantages:

1. **Aluminum structure is protected from the high temperatures of the gas ducts which provides for maximum strength of material and permits use of adhesive bonding for structural design.**

2. **Duct is a simple elliptical shape.**

3. **Ratio of duct area to blade cross sectional area is sensitive to duct pressures and temperatures. Duct area ratio for hot cycle blade is about 55% and would increase for the warm and cold cycle blades with decreased gas pressures and temperatures.**

4. **Single duct reduces wetted area and increases hydraulic diameter for more efficient gas flow.**

Figure 5-5 BLADE CONFIGURATION NO. 2 (Sheet 2 of 2)

Disadvantages:

1. Ducting and insulation are subjected to bending and centrifugal force loads in addition to gas pressure loading.

2. Duct wall, which is considered as primary structure, cannot be visually inspected for fatigue cracks without disassembling blade.

3. The slip fit of the aluminum shell over the duct accounts for the thermal expansions of the duct. This is questionable and presents design problems for the blade controls to the jet-flap.

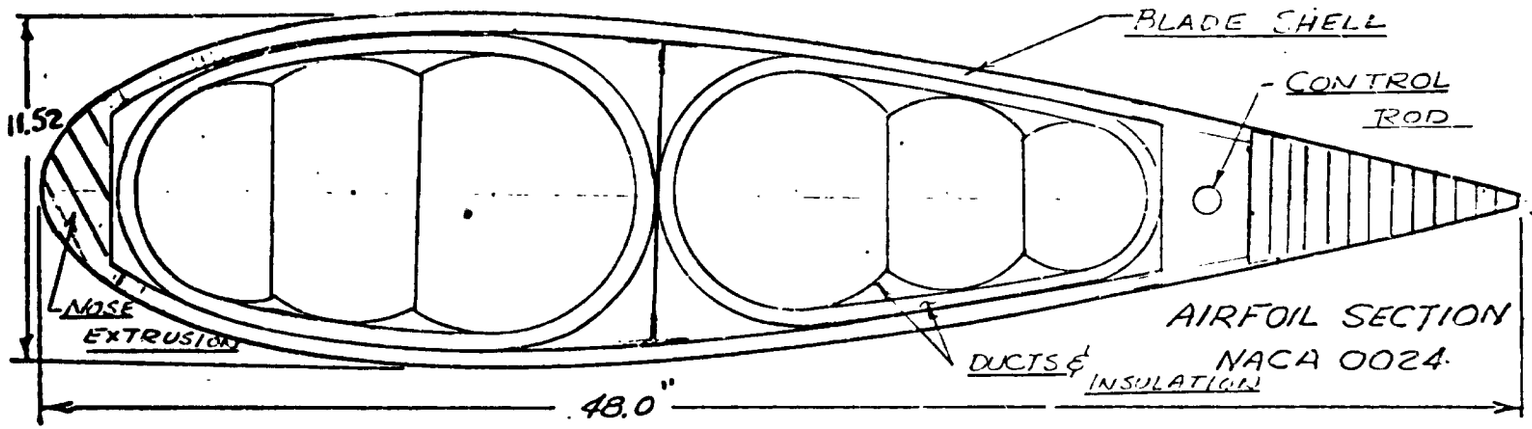

Figure 5-6 BIADE CONFIGURATION NO. 3 (Sheet 1 of 2)

Description:
The blade shell structure is made up of bonded aluminum honeycomb sandwich panels and a full-depth honeycomb trailing edge. An aluminum extrusion forms the blade leading edge which is covered with an abrasive resistant material. The hot gas ducts are fabricated from heat resistant steel in 30-inch lengths. Insulation wrapped around the outside of the ducts serve to retain the heat within the ducts. This provides an acceptable level of temperature on the blade structural shell. Compression type bellows at the 30-inch joints of the ducting compensate for the thermal expansion of the ducts. A mechanical control system is located in the trailing edge section of the blade.

Advantages:

1. The basic blade structure is protected from the heat of the duct gases. This eliminates degradation of the strength of blade shell materials and permits the use of metal bonding.

2. Ratio of duct area to blade cross sectional area is insensitive to duct pressure ratios and temperatures. Duct area ratio is 55%.

3. Compression type bellows provide flexibility at the duct joints which minimizes bending stresses in the duct due to blade bending moments.

Figure 5-6 BLADE CONFIGURATION NO. 3 (Sheet 2 of 2)

4. Isolation of thermal expansion to the duct system facilitates blade jet-flap control design.

5. Basic load carrying structure can be visually inspected for fatigue cracks and structural damage.

Disadvantages:

1. Fabrication triple ring duct and oval shape bellows are feasible, but could be a source of design problems.

2. Gas flow efficiency is reduced by increased wetted area of ducts.

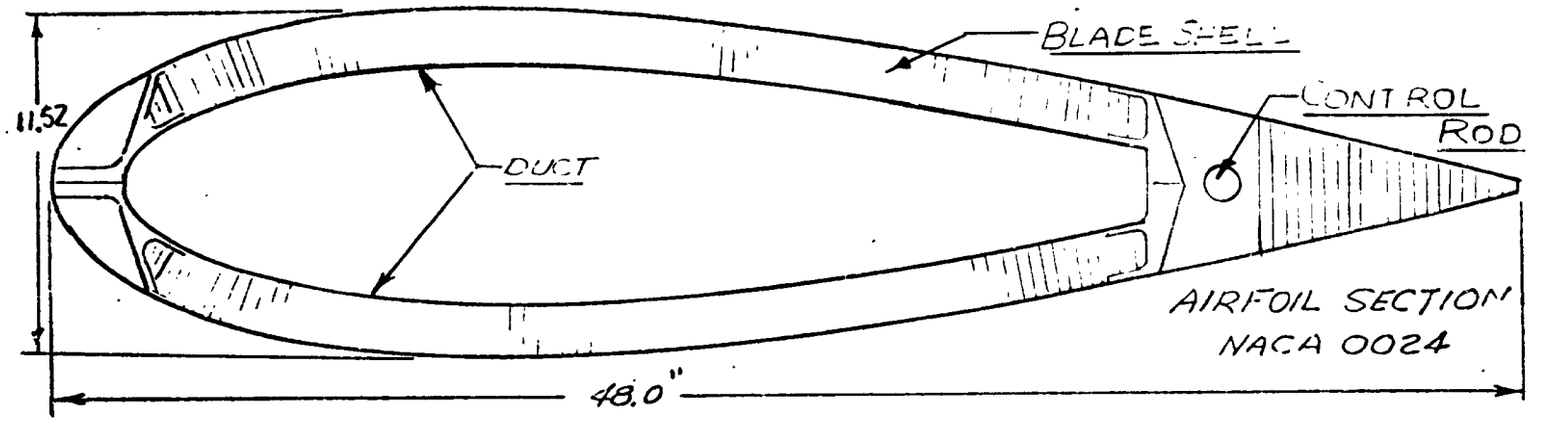

Figure 5-7 BLADE CONFIGURATION NO. 4 (Sheet 1 of 2)

Description:
The blade shell is constructed of stresskin sandwich using Inconel 718 heat resistant steel for the core and face skins. The shell forms the duct for the hot gases and carries centrifugal force and blade bending loads. The blade shell is fabricated in two halfs using heat resistant steel attachment members and mechanical fastners to complete the basic structure of the blade. A bracket and push-pull rod attached to the trailing edge member provides a control to the jet-flap. A nonstructural full depth aluminum honeycomb trailing edge completes the blade section.

Advantages:

1. Blade assembly is simple and contains relatively few parts.

2. Duct area is clean and efficient for transporting gases to the rotor jet-flaps. Reduced wetted area and increased hydraulic diameter.

Disadvantages:

1. Strength-weight ratio of basic structure is degraded at least 25 percent due to the thermal environment.

2. The ratio of duct area to blade cross sectional area of the hot cycle (1300°F, 45 psig) is less than 45 percent. This ratio for this configuration is sensitive to changes in the gas temperature and pressure. It will increase with reduced pressure and temperature.

Figure 5-7 BLADE CONFIGURATION NO. 4 (Sheet 2 of 2)

3. Blade structure is subject to thermal stresses and warping.

4. Control system design is complicated by the thermal expansion of the basic blade structure.

5.2.2 Rotor Blade Loads

A design condition for symmetrical flight is a vertical takeoff requirement of Paragraph 3.2.2.4 of Reference 6. This condition, generally referred to as a jump-takeoff, requires the helicopter to be capable of withstanding loads developed by displacing the main rotor jet flap from minimum to maximum lift angle in not more than 0.4 second with the helicopter on the ground. The resultant load factor on the helicopter's cg shall be the maximum limit design load factor. The load factors used were 3.5 for the HSH configuration and 2.5 for the HLH configuration at normal rotor speeds. The steady rotor loads for this design requirement were selected to investigate the blade stresses for the jet-flap rotor, since it results in maximum blade bending loads on the rotor with centrifugal force loads.

A triangular thrust distribution along the blade span was assumed. This distribution approximates the distribution obtained using the Vortex theory, Reference 7. Rotor blade bending loads for the normal and maximum load factor conditions are plotted in Figures 5-8 and 5-9 for the HSH and HLH rotors, respectively. Centrifugal force distributions for normal rotor rpm are plotted in Figures 5-10 and 5-11.

Spanwise distributions of weight and stiffness were calculated on the basis of several cross sections of the blade assembly. These distributions are plotted for the HSH and HLH in Figures 5-12 and 5-13.

5.2.3 Blade Stresses

The point of maximum stress on the basic blade section due to beamwise bending occurs on skin panels at point of maximum blade thickness.

FIGURE 5-8

HSH ROTOR BLADE BEAMWISE BENDING
MOMENT DISTRIBUTION
LOAD FACTORS(n) 1.0 & 3.5
LIMIT LOALS

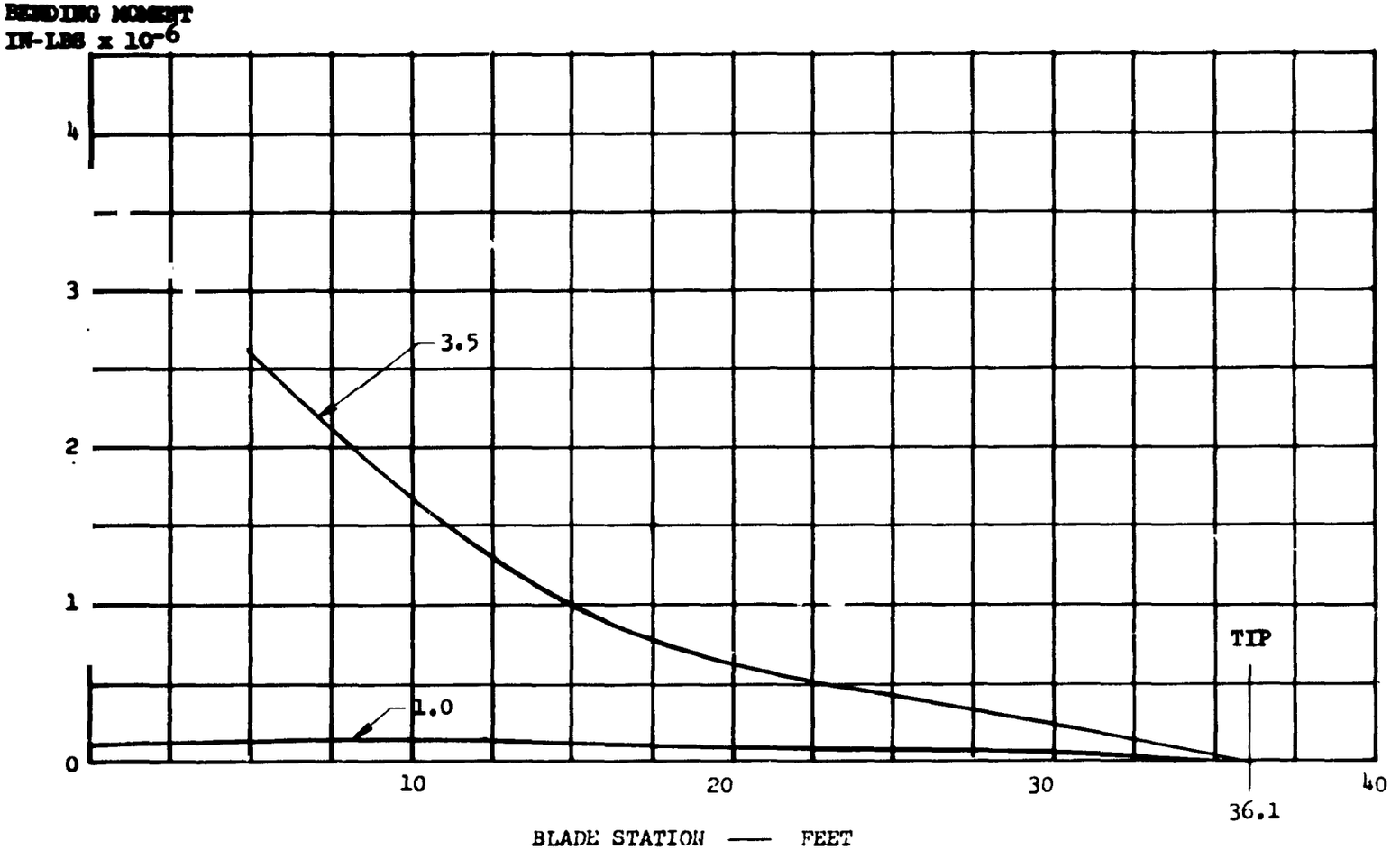

FIGURE 5-9

HLH ROTOR BLADE BEAMWISE BENDING
MOMENT DISTRIBUTION
LOAD FACTORS(n) 2.5 & 1.0
LIMIT LOADS

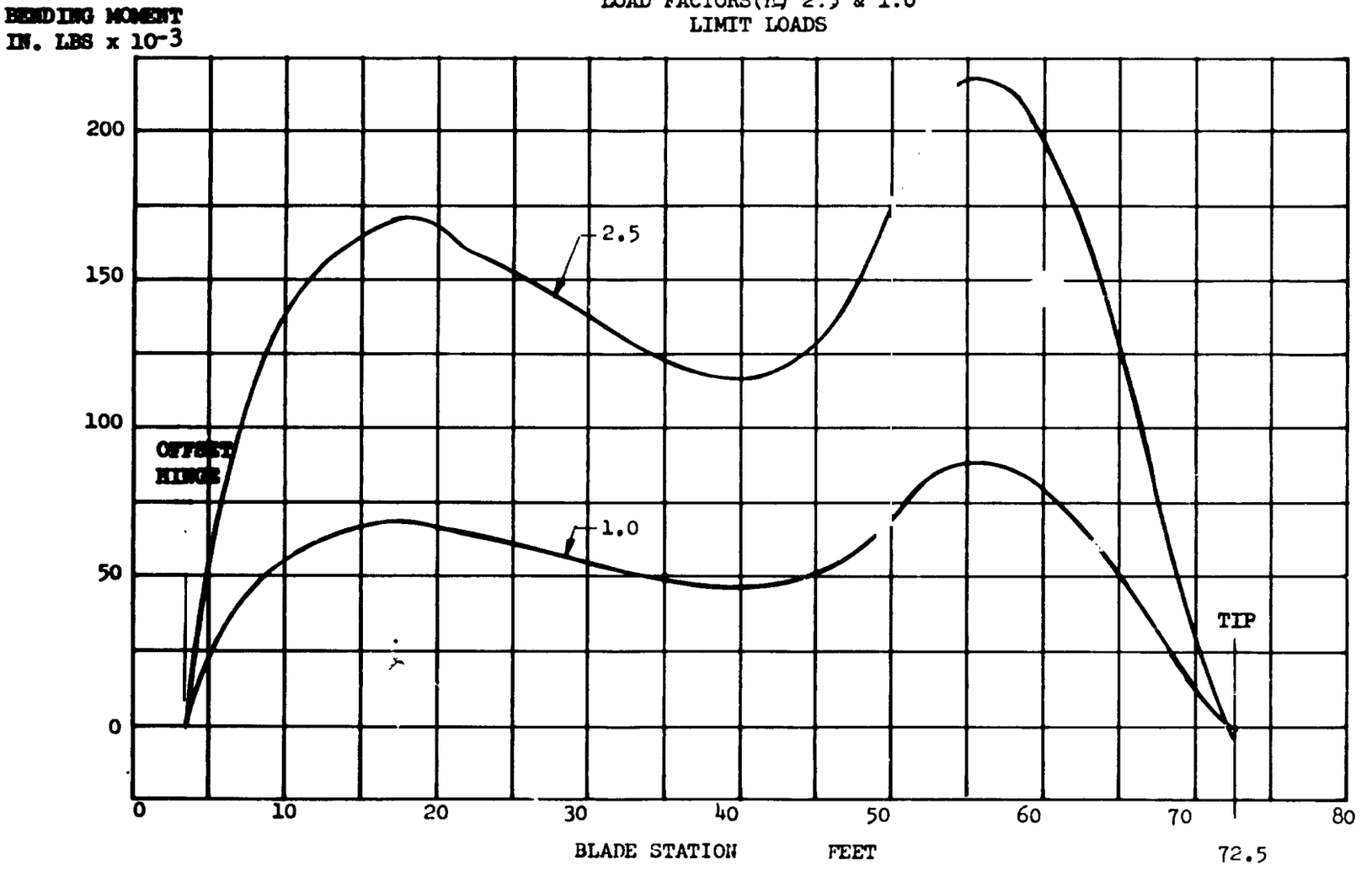

FIGURE 5-10

HSH ROTOR BLADE CENTRIFUGAL FORCE DISTRIBUTION
36.1 FT. BLADE RADIUS - 50.0 IN. CHORD
640 FT./SEC. TIP SPEED (197 R.P.M.)
LIMIT LOAD

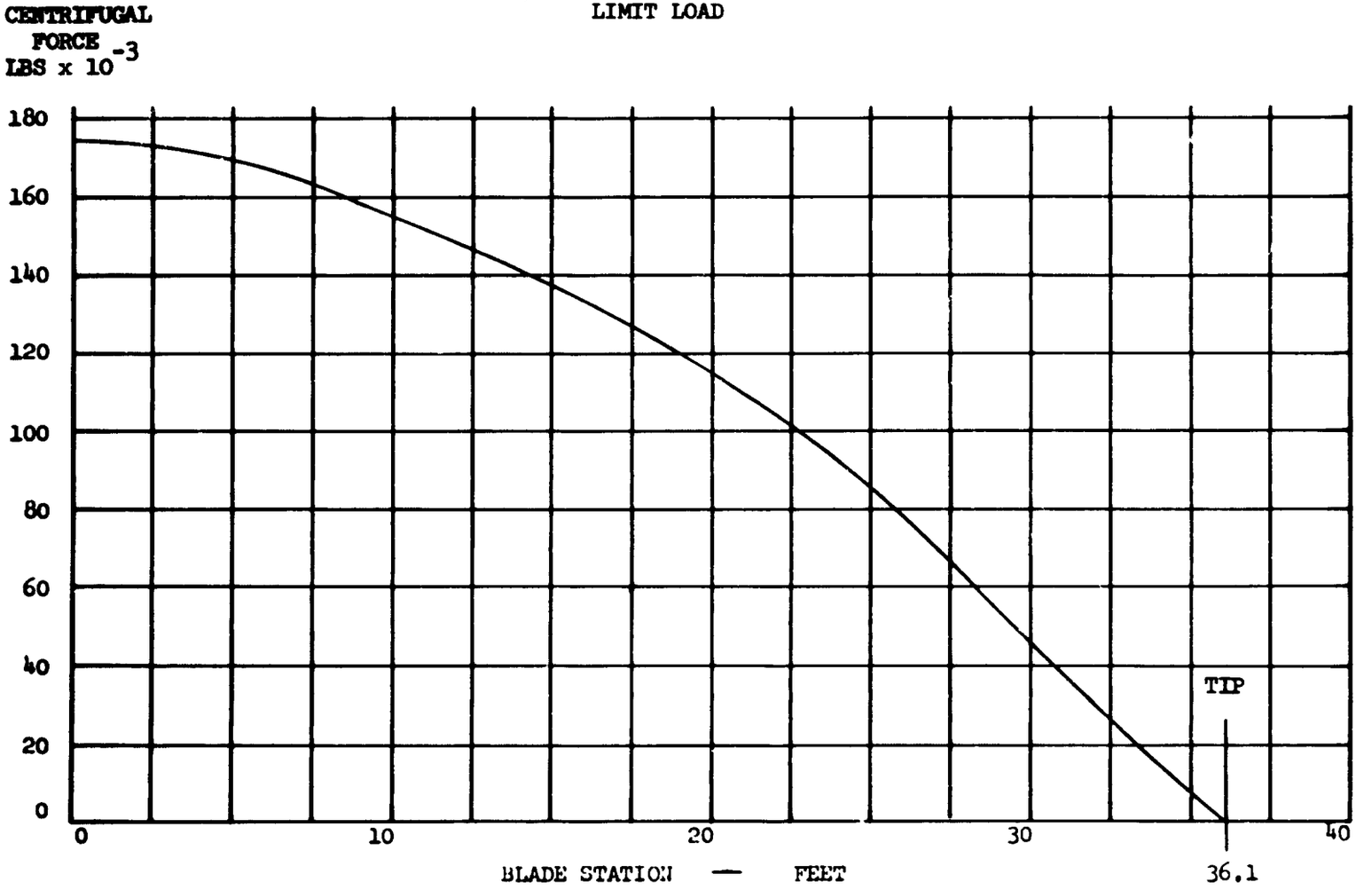

FIGURE 5-11

HLH ROTOR BLADE CENTRIFUGAL FORCE DISTRIBUTION
72.5 FT. BLADE RADIUS - 45.75 IN. CHORD
640 FT./SEC. TIP SPEED (85 R.P.M.)
LIMIT LOAD

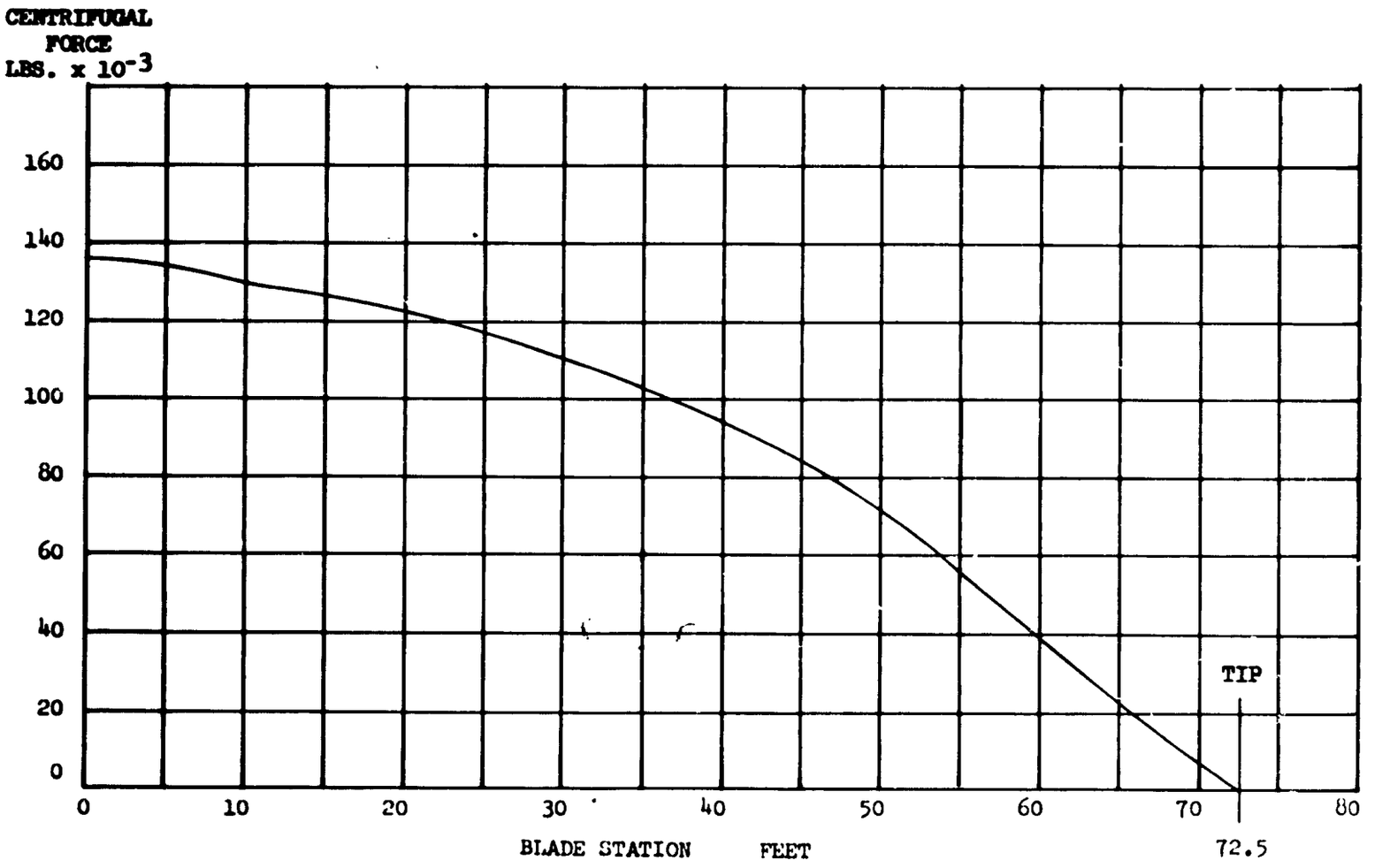

FIGURE 5-12

HSH BLADE WEIGHT
& STIFFNESS DISTRIBUTION
SEMI RIGID ROTOR

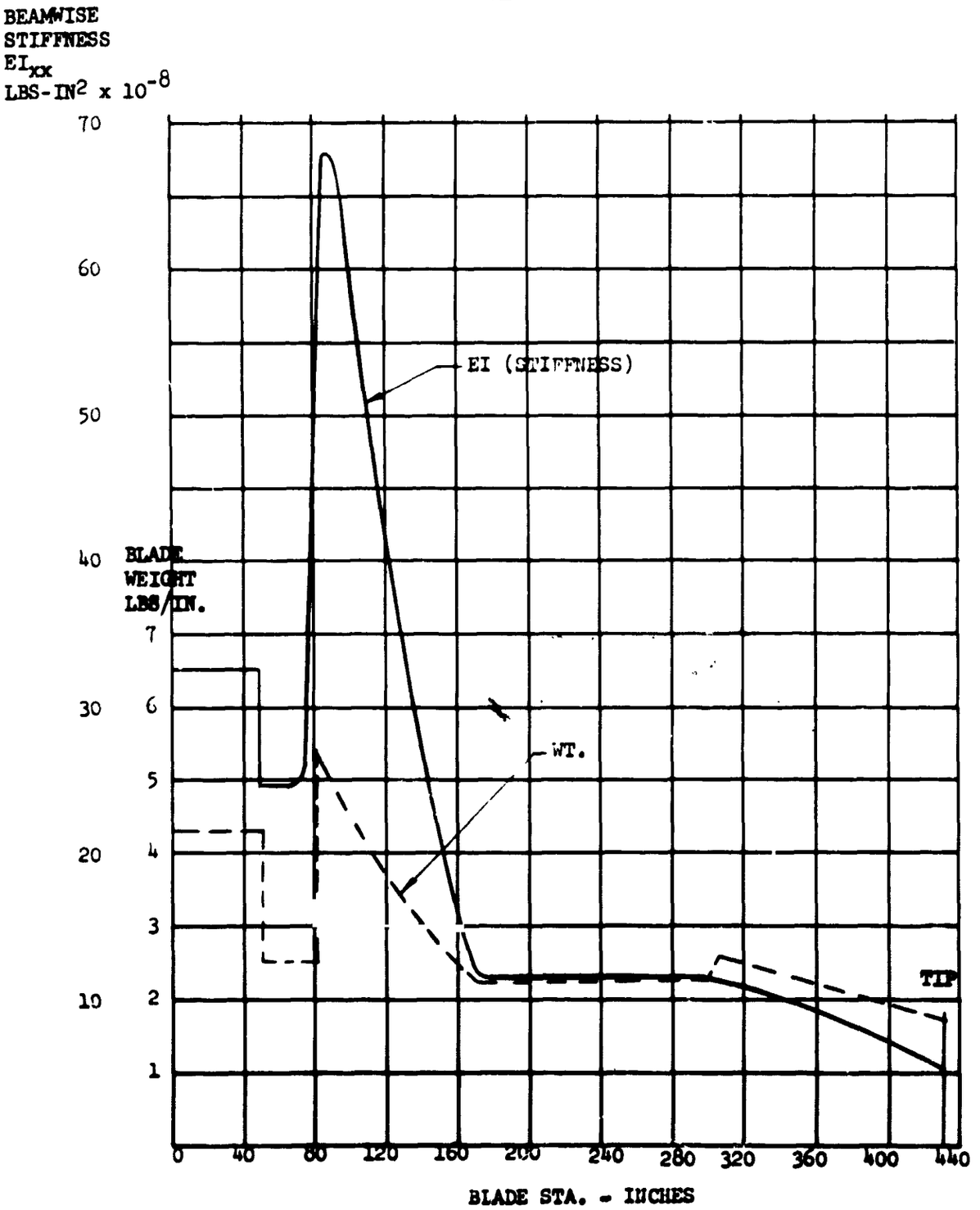

FIGURE 5-13

HLH BLADE WEIGHT
& STIFFNESS DISTRIBUTION
FLAPPING HINGE ROTOR

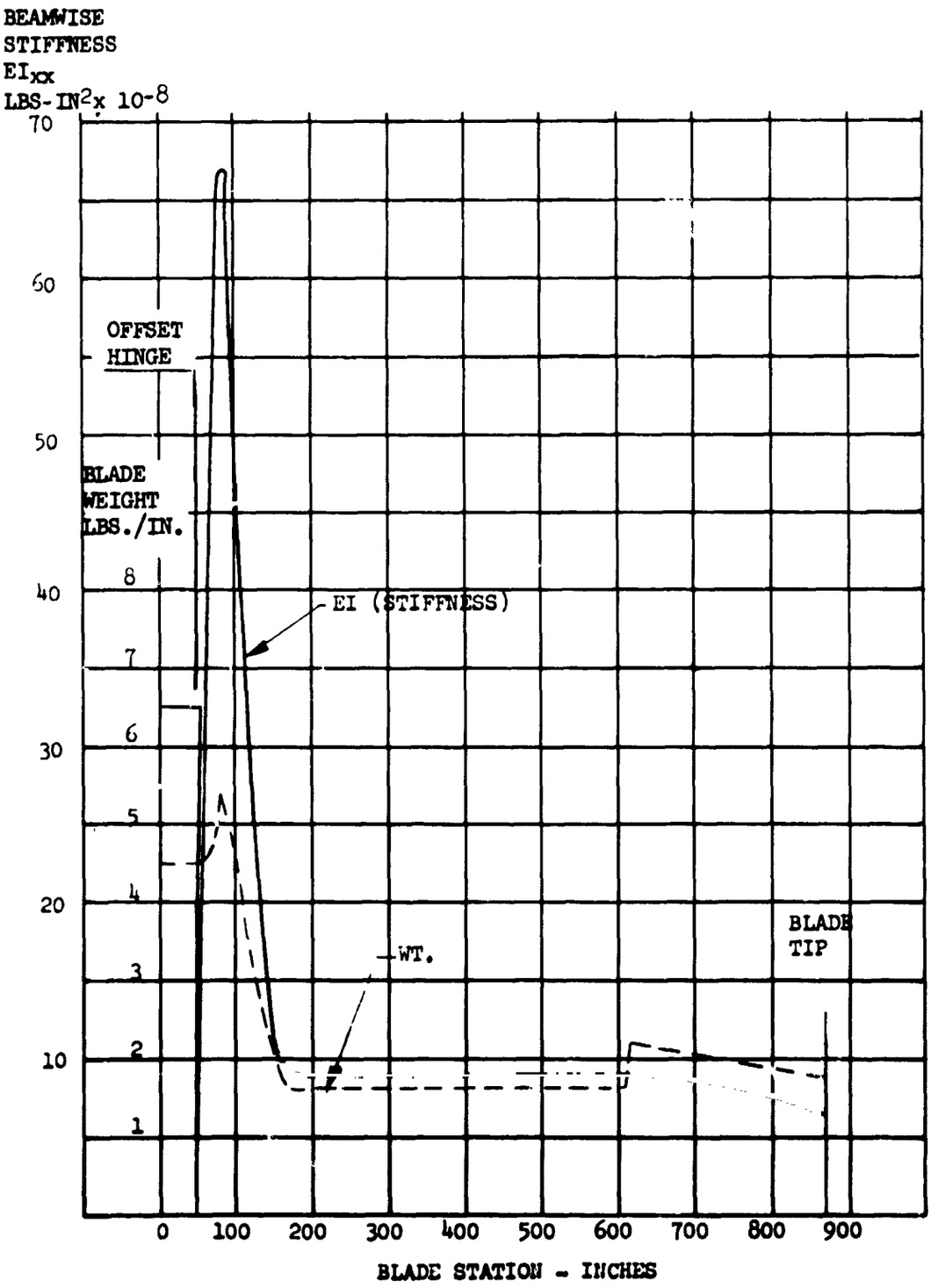

This is at the 30 percent chord station for the NACA 0024 airfoil. Using this point on the blade for calculating maximum bending stresses, assuming that tension stresses resulting from centrifugal force are equally distributed over blade cross-sectional area, stresses for several spanwise stations were calculated. Spanwise distributions for bending stresses and tension stresses for both the HSH and HLH blades are plotted in Figures 5-14 and 5-15. In addition, these figures show the combined stresses ($f_{total} = f_{C.F.} + f_b$) for the upper and lower skin panels.

A comparison of these skin panel stresses to the limit allowable stress of the skin material, 7075 clad, indicate large static strength margins of safety except for the 40 percent station on the HSH blade. Skin gages in the blade portions showing large static margins can be justified as follows:

a. The skins on the outer portion of the blades (.5R-1.0R) were sized for local chordwise airloads. This portion is the high speed section of the blade.

b. The skin gages on the inboard section of the HLH are needed to provide blade stiffness (EI). One design requirement for blade stiffness is static droop. Table 5-1 shows the tabulated results of the computed bending moment and deflection for blade droop at zero rotor rpm due to blade weight. The blade tip deflection (Station 72.2) is 72.4 inches, which results in blade root bending moments of 600,000 inches.

FIGURE 5-14

3.5 g JUMP TAKEOFF COND.
HSH ROTOR BLADE STRESSES

$f_{TOTAL} = f_{C.F.} \pm f_{BENDING}$

$f_{C.F.}$ (CENTRIFUGAL FORCE STRESS)

$f_{BENDING}$ (BEAMWISE BENDING STRESS)

f_{TOTAL} (COMBINED STRESS)

(LIMIT STRESSES)

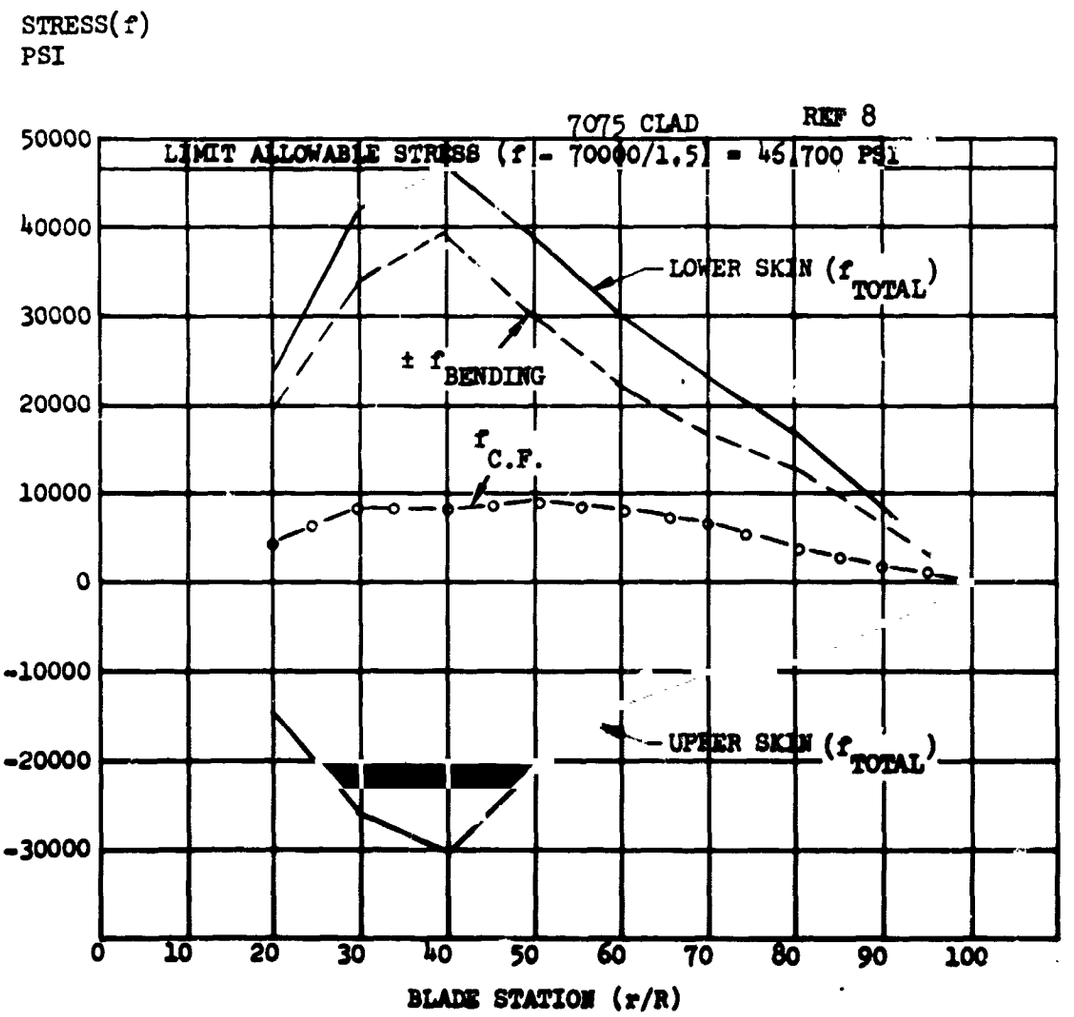

FIGURE 5-15

2.5 g JUMP TAKEOFF COND.
HLH ROTOR BLADE STRESSES

$f_{TOTAL} = f_{C.F.} \pm f_b$

$f_{C.F.}$ (CENTRIFUGAL FORCE STRESS)

f_b (BEAMWISE BENDING STRESS)

f_{TOTAL} (COMBINED STRESS)

(LIMIT STRESSES)

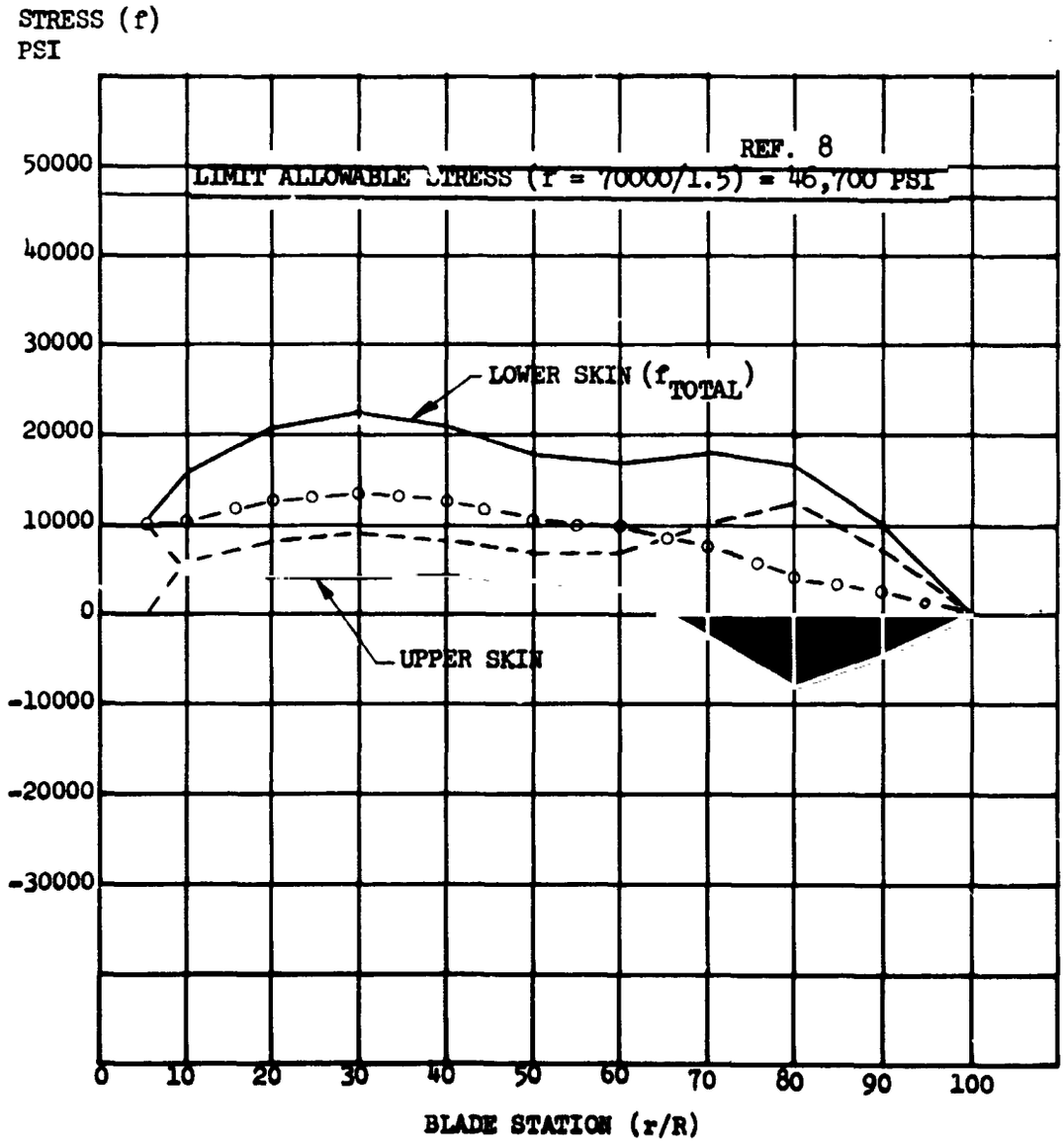

TABLE 5-1 HLH BLADE STATIC DROOP

STATIC DROOP BENDING AND TIP DEFLECTION

NACA 0021 AIRFOIL 72.2FT ROTOR RADIUS 45.75INCHES CHORD

STA. NO.	BENDMO	DEFL.
0.0	0.76643E 06	0.0
3.6	0.68166E 06	0.0
7.2	0.60599E 06	0.45500E 00
10.8	0.53839E 06	0.13626E 01
14.4	0.47590E 06	0.28814E 01
18.0	0.41726E 06	0.50216E 01
2..7	0.36247E 06	0.77069E 01
25.3	0.31152E 06	0.10866E 02
28.9	0.26442E 06	0.14452E 02
32.5	0.22117E 06	0.18344E 02
36.1	0.18176E 06	0.22545E 02
39.7	0.14620E 06	0.26985E 02
43.3	0.11449E 06	0.31616E 02
46.9	0.86628E 05	0.36404E 02
50.5	0.62751E 05	0.41327E 02
54..	0.42910E 05	0.46369E 02
57.8	0.27009E 05	0.51501E 02
61.4	0.14955E 05	0.56694E 02
65.0	0.65610E 04	0.61924E 02
68.6	0.16384E 04	0.67172E 02
72.2	0.0	0.72426E 02

5.3 FUTURE JET-FLAP ROTOR DESIGN DEVELOPMENT

The results of the blade structural design study provide preliminary data on blade sizing and weights which were justified on the basis of calculated loads and stress levels for the jet-flap rotor point designs selected for the HLH and HSH flight vehicles. While the blade structural design was based on a single approach to meet the requirements for the jet-flap rotor, it serves as a design point from which structural design tradeoffs can be generated. Several of these are recommended for any new jet-flap rotor design development activity. They are listed below.

a. Investigate blade structural arrangements to achieve a more optimum design of blade structure and ducts. Duct arrangements should result in a higher ratio of duct area to blade cross-sectional area which is desirable for the jet-flap blade. The blade structure should be optimized to provide maximum strength and stiffness for minimum weight with considerations for mass balance to include the weight of the ducts and mechanical control system. Structural arrangement should consider methods of fabrication to assure that the composite design is feasible.

b. Investigate structural dynamics requirements for blade stiffness and mass balance with the jet-flap forces acting on the outer blade section.

c. Investigate structural dynamic requirements for the mechanical control system to be installed in the blade. Structural considerations should include deflections and loads resulting from the aerodynamic, elastic, and centrifugal forces acting on the jet-flap system installed on the blade trailing edge structure.

5.4 DRIVE SYSTEMS

Drive system concepts were studied for the purpose of sizing the components in order to determine their weights, configuration, and compatibility with the aircraft.

Drive system configurations were determined using conventional state-of-the-art technology. Estimation of gear sizes were calculated using "Dudley's Practical Gear Design Manual" and "Strength of Bevel and Hypoid Gears," Gleason Works, Rochester, New York, 1963. A tentative gear size was obtained using the "Q" factor method.

$$Q = \frac{\text{Horsepower}}{\text{pinion RPM}} \times \frac{(m_G + 1)^3}{m_G}$$

where m_G = speed ratio

Then $$d^2 F = \frac{126{,}000\ Q}{(m_G + 1)^2 K}$$

where d = diameter of gear

F = face width

K = surface durability of gear teeth = 1,000 for aircraft gears having a pitch line velocity between 3,000 and 10,000 fpm.

Using Gleason's method, the bending and compressive stresses may be estimated using:

Bevel Gears

$$\text{Bending stress } S_t = \frac{W_t K_o}{K_v} \times \frac{Pd}{F} \times \frac{K_s K_m}{J}$$

where

W_t = Transmitted tangential load in pounds

K_o = overload factor

K_v = dynamic factor

TOOTH SIZE

Pd = diametrical pitch

F = face width

STRESS DISTRIBUTION

K_s = size factor

K_m = load distribution factor

J = geometry factor

Compressive Stresses

$$S_c = C_p \sqrt{\frac{W_t C_o}{C_v} \times \frac{1}{Fd} \times \frac{C_s C_m C_f}{I}}$$

MATERIAL

C_p = elastic coefficient

LOAD

W_t = transmitted tangential load

C_o = overload factor

C_v = dynamic factor

GEAR SIZE

d = pinion pitch diameter

F = face width

C_s = size factor

STRESS DISTRIBUTION

C_m = load distribution factor

C_f = surface condition factor

I = geometry factor

SPUR GEARS

Compressive stresses

$$S_c = 5715 \sqrt{\frac{W_t}{Fd} \left(\frac{m_G + 1}{m_G} \right)}$$

The allowables used here for gearing steel were:

S_t = 30,000 psi.

S_c = 200,000 psi.

The estimations made here were to highlight any problem areas rather than to define an optimum configuration.

An efficient design from a subsystem weight and stress standpoint is to reduce any given ratio by load-sharing meshes, rather than by transmitting the full load through one mesh. By the use of dual input shaft drives, the load is halved and the size and peripheral speed of the gears is reduced.

Considerable progress in uprating conventional gearing systems could be available in the 1975 era, which will allow higher stress levels in gear teeth, improvements in tooth finish, high speed-high load and lighter bearings, and more efficient lubrication systems.

Progress is likely in the use of helical gears in the planetary systems. Allison Division of General Motors has developed a high speed reduction gearcase for their current T-56 engine using helical gears in both the primary and secondary stages of reduction, resulting in larger load-carrying capability and improved reliability. The use of titanium for shafts and planetary gear carriers will reduce the weight of the drive systems in the near future.

As shown in Figure 5-16 and Figure 5-17, for the 20- and 50-ton payload helicopters, respectively, the gears in the second and third stage planetary are quite large. The industrial equipment to cut these gears is not currently in the inventory, but modified gear cutters could be made available in the time period required for future helicopters.

A review of the available proposals (References 9 and 10) did not show any new drive systems such as the harmonic drive, roller gear drive,

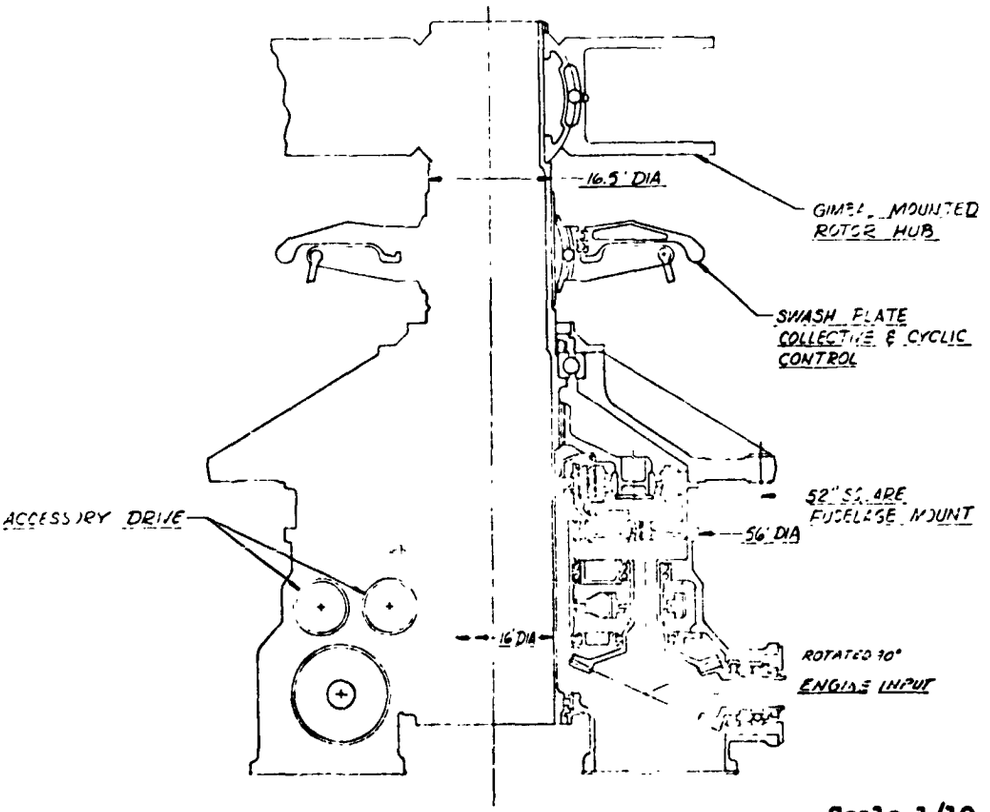

Scale 1/10

Figure 5-16 Transmission Schematic-20-Ton Shaft Drive

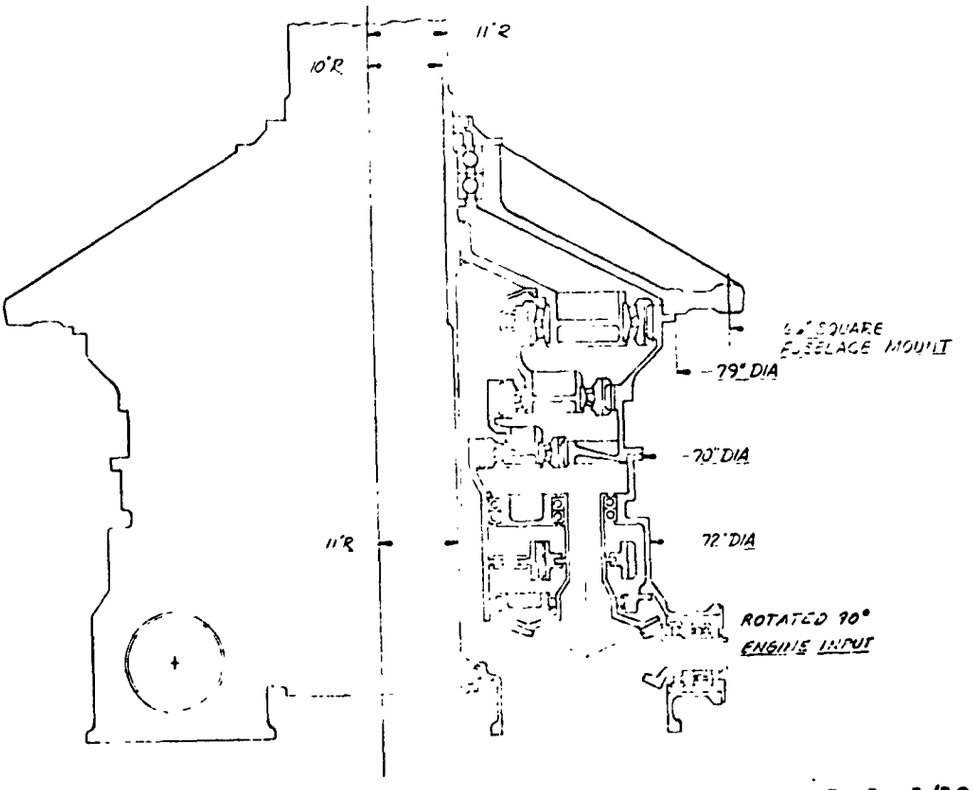

Scale 1/10

Figure 5-17 Transmission Schematic-50-Ton Shaft Drive

and roller friction drive, as having an advantage over the conventional planetary system in the time period discussed here. The harmonic drive and friction roller drive may hold promise in the future but must wait for development and testing of bearings and flexure materials. The roller gear concept does show an efficiency and weight advantage but must have further design and development before it becomes practical for high load and speed application.

5.4.1 HSH 2-Ton Payload Shaft-Drive

The rotor for this helicopter is designed to be 67 feet in diameter and a 640-ft/sec tipspeed which provides 190 rotor rpm.

The installed hp requir l is 2,400 with an output speed of 19,000 rpm.

The configuration presented in Figure 5-18 proposes two engines of 1,200 hp each. This requires a total reduction ratio of 100:1 which is obtained through four gear meshes consisting of two spiral bevel meshes which turn the engine output shaft 90° and provide 2.5:1 reduction ratio. The next mesh is a straight spur gear and bull gear with a ratio of 3.5:1 reduction. The bull (center) gear receives power from both engines; therefore, its output is the sum of the two or 2,400 hp. Two stages of planetary gears complete the speed reduction for a rotor rpm of 190.

The lift of the rotor is reacted through the thrust bearing at the top of the gearcase. Mast bending moments induced by the rotor are reacted through the upper mast bearing and the lower mast bearing housed by the gearcase. The gearcase is shock-mounted to the fuselage at four points.

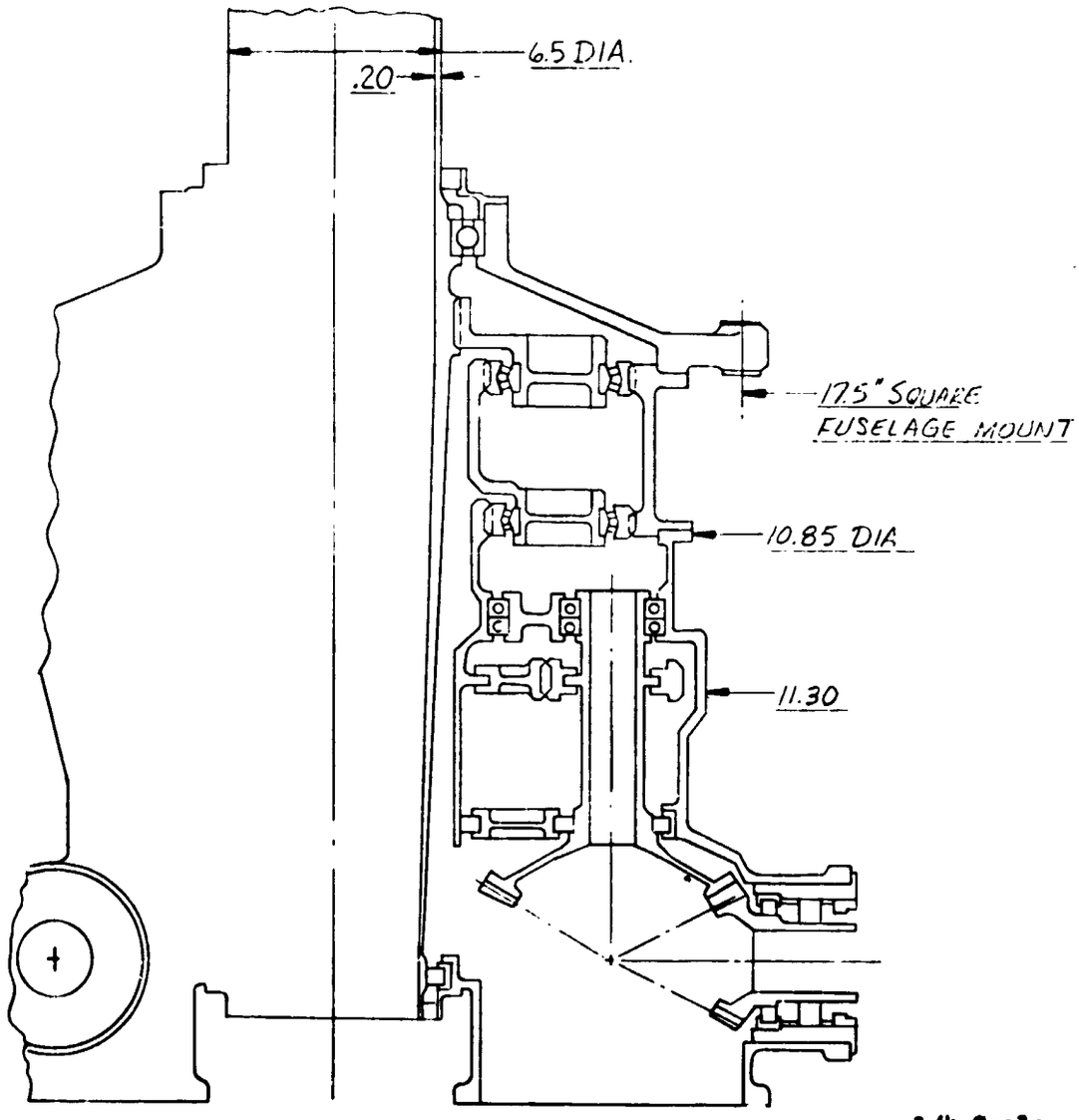

Figure 5-18 Transmission Schematic High Speed Shaft Driven

This gearcase arrangement would be suitable for either forward or aft drive engines and has the advantage of combining the power of the engines after the first two stages of reduction which keeps the high speed meshes smaller in diameter and lighter in weight.

The accessory drives and tail rotor drive is driven by the bull (center) gear. The arrangement of these drives is not defined in detail as they will have little effect on the size or weight of the system.

5.4.2 20-Ton Payload Shaft Drive

The rotor for this size helicopter is designed to be 104 feet in diameter and having a 700 ft/sec tipspeed which gives a 128.5 rotor rpm. The drive system is illustrated in Figure 5-16.

The power plants required are two 7,520 hp turbine engines at 8,200 rpm output with a torque of 58,000 in.-lb at full rpm. The overall speed reduction ratio is 60:1 which is obtained through four gear meshes consisting of a spiral bevel mesh which turns the engine output shaft 90° and provides a 2.5:1 reduction ratio. The next mesh is a straight spur gear mesh of 3.0:1 reduction ratio. The bull (center) gear of this mesh is receiving power from both engines; therefore, its output is the sum of both engines or 15,040 hp. Two stages of planetary gears complete the speed reduction for a rotor rpm of 128.5.

This gearcase arrangement would be suitable for either forward or aft shaft engines and has the advantage of combining the power of the engines after the first two stages of reduction, which keeps the high speed meshes lighter.

The accessory drives and tail rotor drive is driven by the bull (center) gear. The arrangement of these drives was not defined as they will have little effect on the size or weight of the system.

The lift of the rotor is reacted through the thrust bearing at the top of the gearcase. Mast bending moments induced by the rotor are reacted through the upper mast bearing and the lower mast bearing housed by the gearcase. The gearcase is shock-mounted to the fuselage.

5.4.3 50-Ton Payload-Shaft Drive

The main transmission gearcase for a 50-ton payload heavy lift helicopter was sized using current gear technology, and layouts were made to allow for estimation of weights. It is illustrated in Figure 5-17.

This transmission requires a total of 46,000 shaft horsepower, and it was assumed that this power would be available using four advanced design engines of 11,500 hp each. Engines of this size are expected to operate at a shaft speed of 19,000 rpm to keep the shaft torque to a reasonable value.

The 140-foot diameter rotor requires that the rpm be kept to 94 to maintain a tipspeed of 700 feet per second. A total speed reduction of 200 to 1 is required to accomplish this task. An added third stage planetary in the gearcase is required.

The gearcase is arranged so that each of the four engine inputs is turned 90° through a spiral bevel mesh with a 2.1:1 gear reduction.

A straight spur pinion is mounted on the vertical shaft from each engine and drives the bull (center) gear at 3.1:1 reduction. The center shaft of the bull gear provides the sun gear for the first stage preliminary

set. Three stages of planetary gears complete the speed reduction to give a rotor rpm of 94.

The gears to handle this power and gear reduction are large and require special consideration in future transmissions. Large gears may be manufactured on specially built gear cutters. Special gear cutters would be one of the first long lead-time procurements required for large shaft-driven helicopters.

5.4.4 HSH Jet Flap Power Train

The drive system presented in Figure 5-19 is one concept for the jet-flap power train.

Two engines drive into a common gearcase with an output to a compressor to provide cold air to the rotor.

The engines are 7,020 hp each with output shafts speeds of 8,154 rpm. The compressor has 14,040 hp with an input speed of 5,730. A speed reduction ratio of 1.42:1 is required. The most direct approach is to provide this reduction ratio through a set of spur gearing. Any number of configurations could be designed, and two concepts are given here. The alternate design is lighter in weight but has problems in the peripheral speed of the center spur gear. The center gear could be made a double helical gear, thus reducing the tooth load.

5.5 CONTROL SYSTEMS

The control system for the shaft-driven helicopters will be typical of current industry practice in which a swash plate is used to

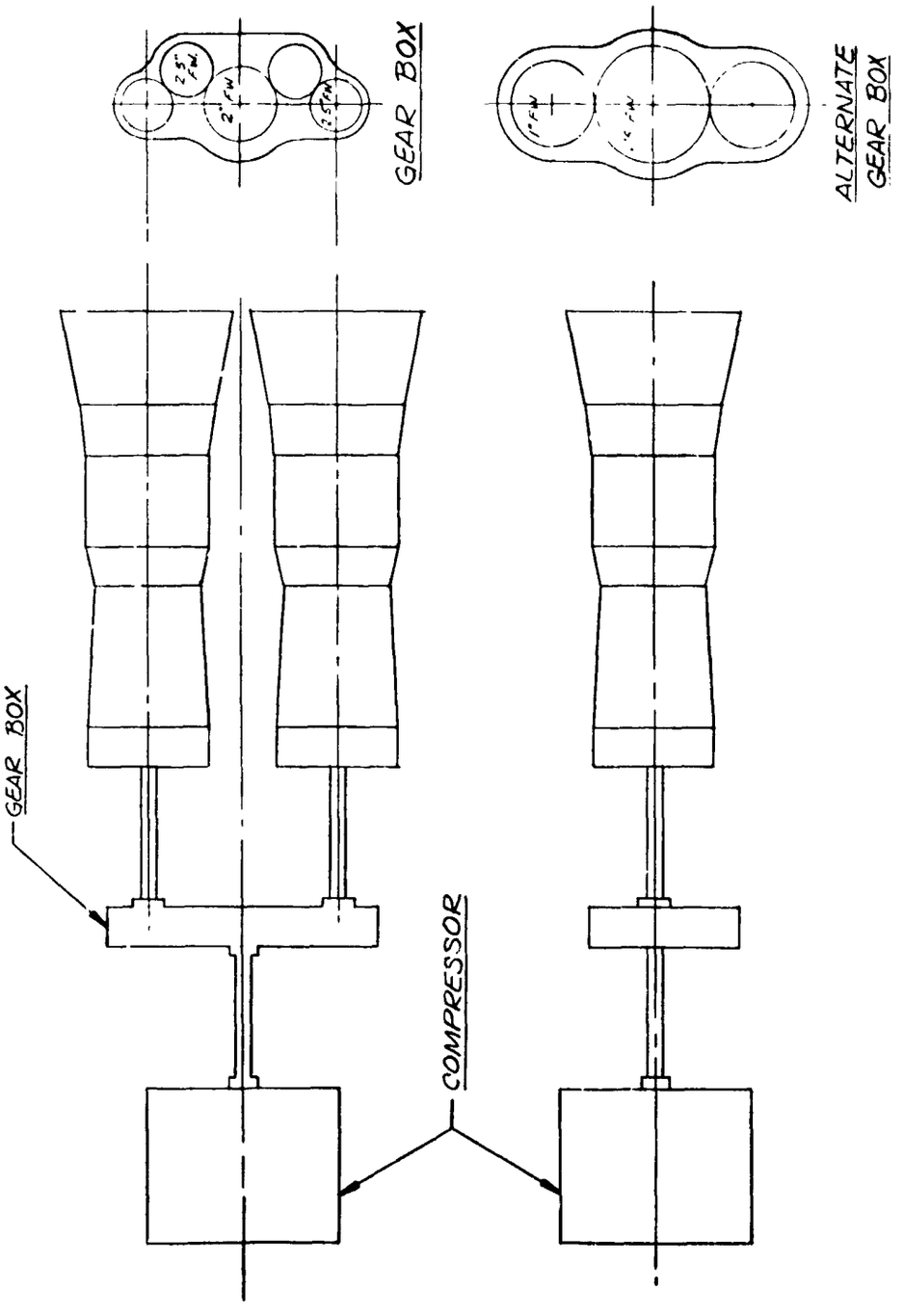

Figure 5-19 High Speed Jet Flap Power Train

provide cyclic blade pitch for lateral and longitudinal control and collective pitch for thrust control. Directional control is provided by rudder pedal-actuated collective pitch on the anti-torque rotor.

In the Dorand jet-flap rotor control system, cyclic and collective actuation of the jet flaps provides the same control functions as does blade pitch actuation on the shaft-driven helicopter; therefore, blade feathering is not required on the jet-flap rotor. However, except for this difference, the two systems are quite similar in that the jet-flap control system also uses a swash plate for lateral and longitudinal cyclic and collective thrust control.

The jet-flap rotor is driven pneumatically so no power shafting to the rotor is required. This makes it possible to provide a hollow stationary mast inside the air ducting on which the rotor hub is mounted. In this design, pushrods from the pilot controls are routed up through the hollow mast to a swash plate mounted on the mast above the rotor hub. The blade flaps are connected to the swash plate by linkage routed through the blade. Because of rotation of the rotor, the control linkage in the blade is subjected to centrifugal forces so a counterbalance will be required to counteract this force.

Although the control loads in the jet-flap rotor system are low compared to those in the shaft-driven helicopter, power actuation will probably be required to prevent cyclical load feedback to the pilot controls.

Directional control is provided through jet reaction of the exhaust by means of valving at the rear of the fuselage. This directional control valve is actuated by the rudder pedals.

As noted previously, blade feathering is not required for cyclic and collective inputs, but would be required if autorotation is to be provided.

5.6 LANDING GEAR

The landing gear of a helicopter serves two purposes: (a) to absorb the kinetic energy due to vertical descent rate during landing; and (b) to provide a means for ground maneuver with or without power. Due to the extreme importance of weight versus performance on a helicopter, the most efficient components to fulfill the above capabilities are required. These include a conventional air-oil shock absorber for energy absorption and a wheel and tire for ground maneuver. Because of the ability to land and takeoff vertically, any small clear area becomes a potential landing site regardless of the ground condition. Therefore, the ground maneuvering capability should be based upon relatively poor soil conditions. Tires best adapted for this ground maneuver are large diameter, low pressure tires. These tires, however, can be operated at near flat condition because of the slow speeds and short rolls normally required. In order to reduce drag at higher speeds, the landing gears are made retractable and are enclosed by doors or fairings.

5.7 MATERIALS CONSIDERATIONS

5.7.1 Cold Cycle

Materials were reviewed for application to the cold cycle rotary blade. The environmental parameters of the cold cycle system are such that conventional airframe materials and processes may be utilized for blade

fabrication. Maximum predicted structural temperatures are under 300°F. The following aluminum alloys meet the structural criteria: 7075, 2024, and 2219. The 7075 alloy would be used as skins for conventional aluminum core honeycomb construction. A modified epoxy adhesive, such as Metlbond 328, is selected for bonding skins to the core material. Either 2024 or 2219 alloy is suitable for the gas ducts within the blade. Although these materials are fairly similar in elevated temperature properties, the 2219 alloy offers distinct advantages if fusion welding should be desired as a fabrication technique. The ducts require insulation to keep the external structure of the blade at efficient strength levels. Study revealed that an 8 lb/cu ft 1/8-in.-thick alumina-silica fiber insulation material would provide the thermal drop required. Johns-Manville's Thermoflex is an example of this type material.

5.7.2 Warm Cycle

Materials considered suitable for the warm cycle blade, except for the duct, are the same as those mentioned in the cold cycle discussion above. The duct material selected (due to temperatures around 900°F) will be a precipitation-hardening stainless steel. PH 15-7 Mo alloy exemplifies this class of material. In order to keep the blade structure cool, the insulation thickness will be increased to approximately one-half inch.

5.7.3 Hot Cycle

The thermal environment and element life desired are of primary importance in selecting a material for the hot ducting. At 1300°F Inconel 718 is a ..d choice because of its strength, density, and fabrication characteristics. As duct temperatures increase to the range of 1400°F to 1600°F the materials available for selection weigh a little more, decrease in strength and become more difficult to fabricate. Rene' 41 is typical of the type of materials available for this thermal region. In particular the welding and forming of these materials becomes increasingly difficult. In the temperature range of 1600°F to 1700°F it becomes a trade-off as to whether nickel or cobalt based superalloys should be used. Here again strength is decreasing and in the case of cobalt based materials (Haynes 25 is an example) density is increasing.

Additionally above 1600°F the problem of dynamic oxidation will be encountered. Alloys containing considerable amounts of chromium are subject to the volatilization of Cr_2O_5. This can greatly shorten the life of a component. Of course, it is dependent on amount of oxygen available, temperature and velocity of gas flow.

In summary from a materials viewpoint, there are definite advantages in keeping the duct temperature reasonably low. Any of the classes of materials discussed above can be fabricated into ducting. In general, though, the lower the temperature the higher will be the material strength. Above 1600°F dynamic oxidation will be encountered and appropriate penalties paid. It is recommended that this thermal region be avoided if at all possible and that duct temperatures be kept no higher than other requirements dictate.

5.7.4 DH 2011 American Equivalent Materials

American equivalents of the materials called out in the Giravions-Dorand Drawing No. 2011-1.40.203 are noted. The Bell's asbestos silicone is equivalent to MIL-R-5847D Class II grade 60 material. Examples of this material would be Dow Corning's Silastic 746U or General Electric's SE 3613U. Equivalents to the adhesive called out as CAF-4 are GE's RTV 102 and DC's 732. Primaire MB is the primer used on the metal surfaces. Similar American materials are GE's SS-4004 and DC's Q-2-1011. The metal used in the laminate is a grade 300 stainless steel.

5.8 DYNAMICS CONSIDERATIONS

The intent of this preliminary applications study was to conduct the research effort planned for the jet-flap rotor concept, rather than to provide a detailed preliminary design. Therefore, extensive efforts in the areas of rotor dynamic behavior, vibration, and acoustics were not required. Only preliminary assessments are made in these areas to determine their potential impact upon weight, performance, and problem areas.

5.8.1 Rotor Dynamic Behavior

Dynamical review of the jet-flap concept reveals no critical problem areas inherent in the design. There are, however, many areas of dynamical considerations requiring thorough investigation to ensure a feasible aircraft once the Dorand concept is finalized. Specifically, flap control and hub design dynamical problems will require state-of-the-art

PARAGRAPH NUMBER & TITLE	PART I 6/67 to 4/68	PART II 7/68 to 2/69	REMARKS
Par. 6.3 STUDY RESULTS	X		Part I Study Presents data generated for: (a) Fuel available curves (b) Weight, balance and inertia summaries (c) Group Weight Statements
		X	Part II Study Presents data generated for: (a) Sensitivity Study (b) Power Split (c) Re-optimization of cold cycle analysis of Part I Data will consist of: (a) Fuel available curves (b) Weight summaries of Point Designs
Par. 6.4 WEIGHT DERIVATION	X		Part I Data presented includes: (a) Statistical equations used to derive the estimated weight of various components (b) Assumptions & Design Data (c) Sample calculations of the estimated weight of one point design using items (a) & (b) above.
		X	Part II Data presented includes: (a) Same statistical equations used as in Part I. However, fuselage equation is new for Part II study. (b) Assumptions and Design Data (c) Sample calculations will not be repeated in Part II since this is demonstrated in Part II.
Par. 6.5 WEIGHT STUDIES	X		Part I (a) Transmission Systems for various payloads. (b) Warm Cycle Configurations Part II See paragraph 6.3

dynamics. The main advantage of the jet-flap concept is the elimination of dynamical problems associated with whirling shafts and gearboxes associated with the shaft-driven concept.

5.8.2 Acoustical and Vibrational Environment

No critical problem areas exist from an acoustics and vibration standpoint for the jet-flap concept. A potential lower vibration level exists for the jet-flap concept when compared to a shaft-driven concept. One of the factors contributing to this reduction is the absence of stall on the retreating blade. No pronounced acoustical differences are apparent between the two concepts. High frequency noise generated by the compressor and turboshaft engines can result in high acoustical levels near the cockpit in either concept. Proper engineering design and soundproofing, if required, can result in acceptable noise levels.

6.0 WEIGHT CONSIDERATIONS

6.1 INTRODUCTION

The jet-flapped rotor system application study contract does not call for the submission of specific types of weight data. However, a certain minimum amount of data must be included for an adequate understanding of the methodology used to derive the weight data. Since a considerable amount of these data were generated in support of the mission studies, it becomes a question of presenting the correct types of weight analysis data. Accordingly, the data selected for presentation include:

- Fuel available curves versus gross weight
- Group weight statements for each point design
- Weight, balance, and inertia summaries for each point design
- Weight studies

The data presented in this report will cover two study periods: (a) Part I, June 1967 to April 1968, and (b) Part II, July 1968 to February 1969. Organization of the data is as presented in the following table.

PARAGRAPH NUMBER & TITLE	PART I 6/67 to 4/68	PART II 7/68 to 2/69	REMARKS
Par. 6.2 METHODOLOGY	X	X	Part I & II Studies Description of the philosophy used in deriving the estimated weights.

The weight data described above were derived for two concepts: (a) a shaft-driven helicopter, and (b) a jet-flap helicopter. Each concept has a high speed and a heavy lift configuration. Type of mission (heavy lift or high speed) dictated the fuselage design. For the heavy lift configuration, a crane-type fuselage arrangement is used; whereas, the high speed configuration had a conventional fuselage arrangement.

The major differences between concepts occur in the propulsion components. The rotor on the jet-flap concept is driven by cold air (≈400°F) supplied by a compressor located in the fuselage. Air is directed from the compressor through the rotor blade to the nozzle and is then blown over the trailing edge flap. Power to drive the single compressor is obtained from the main turboshaft engines through a shaft and gearbox arrangement. No tail rotor is required with the jet-flap concept. A transmission system and tail rotor, however, is required to drive the rotor blade on the shaft-driven concept.

6.2 METHODOLOGY – PART I AND II

Methods which may be used to derive and justify helicopter component weights are technically limited at present by the amount of detail design. Detail design for the subject study was very limited, requiring only enough technical depth to permit the selection of the mission best suited to utilize the capabilities and potentials of the jet-flap rotor. Thus, sizing of the propulsion arrangement of each concept has received the major emphasis. The enclosing structure and fixed equipment items received less detailed attention. Therefore, only one of the standard estimating methods, semianalytical, statistical, and component sizing, is used extensively in this study to derive

the estimated weights. The method used is statistical analysis, which consists of using statistical weight estimating equations and certain design data in deriving the estimated weights. Statistical weight estimating equations are used for as many as possible of the major helicopter components of each concept studied. The statistical weight estimating equations were selected so that the same equation was used for identical components of both concepts, thus eliminating any optimism or conservatism which is induced when identical component weights are derived by two different statistical weight estimating equations. It was necessary to deviate from this philosophy only once in deriving the estimated weight; this conflict occurred in deriving the weight of the transmission system. For the shaft-driven rotor, a conventional shaft and gearbox arrangement is used. The jet-flap rotor concept, however, is driven by a hot gas system plus shaft and gearbox arrangement. Drawings of rotor-driven systems are presented in Section 5.0.

For those few situations where it was not possible to use statistical methods of weight estimating, component weights were derived by other methods. These methods consist of using data obtained from:

- Vendors
- Contemporary helicopters
- Calculations based on preliminary drawings.

Utilizing the estimating methods described previously, sample calculations are presented in Paragraph 6 .4.2 showing how the estimated weights were derived for the components of the Heavy Lift Jet Flap Point Design.

An accuracy analysis was performed to demonstrate the efficiency of the weight estimating procedures used in the subject study. The same equations presented in Paragraph 6.4.2 were used to estimate the weight of various components of twenty-five contemporary helicopters. The estimated weights derived are compared to the actual weights of these models in Tables 6-1A through 6-1C. The derivation of the mean ($\bar{X}$) and the standard deriva-tion is shown in these same tables. A plot of the ratio of actual weight to the estimated weight of the models is presented in Figures 6-1A, 6-1B, 6-1C. The limits shown are 95% confidence that 90% of all future estimates of $\frac{Wt_{act}}{Wt_{est}}$ will lie within this band.

6.3 STUDY RESULTS

6.3.1 Part I

This section contains fuel available curves derived for the parametric study. In addition, it contains the following data for each of the four point designs derived from the parametric study: (a) group weight summaries, and (b) mass properties summaries.

The fuel available data was obtained from a parametric weight-analysis routine using the statistical weight estimating equations described in Paragraph 6.4. Parameters studied were: (a) gross weight, (b) rotor diameter, (c) disc loading, and (d) solidity factor. Plots of these data are presented in Section 3. Four point designs were selected from a sizing study utilizing these data and fuel required data.

TABLE 6-1A ACCURACY ANALYSIS - DERIVATIONS OF MEAN RATIO OF $\frac{WT_{ACT}}{WT_{EST}}$ 2

ROTOR GROUP, HORIZONTAL TAIL, SURFACE CONTROLS,

BODY GROUP, LANDING GEAR, DRIVE SYSTEM, HYDRAULIC AND PNEUMATIC

		Actual Weight	Estimated Weight	$\frac{\text{Act. Wt.}}{\text{Est. Wt.}}$	$\frac{X^2_J}{\frac{\text{Act. Wt.}}{\text{Est. Wt.}}}$
No.	Model	(1)	(2)	(3)	(4)
1	UH-1B	2998	2880	1.0410	1.0837
2	UH-1C	2880	2973	0.9687	0.9384
3	UH-1E	2842	2736	1.0387	1.0790
4	UH-1F	2748	2895	0.9492	0.9010
5	COBRA	962	873	1.1019	1.2143
6	OH-4A	921	843	1.0925	1.1936
7	OH-13L	886	918	0.9651	0.9315
8	OH-13S	938	885	1.0599	1.1234
9	NH-41A	820	723	1.1342	1.2863
10	OH-23G	969	1153	0.8404	0.7063
11	OH-6A	586	695	0.8432	0.7109
12	AH-56A	5510	5578	0.9878	0.9758
13	SH-3A	7291	6426	1.1346	1.2873
14	CH-36	8541	7262	1.1761	1.3833
15	UH-19C	2141	2395	0.8939	0.7991
16	HH-52A	3295	3015	1.0929	1.1944
17	269A	291	372	0.7618	0.5803
18	CH-21C	4245	4246	0.9998	0.9995
19	CH-34A	4534	4843	0.9362	0.8765
20	CH-37A	10210	10039	1.0170	1.0344
21	CH-53A	15941	15448	1.0319	1.0648
22	UH-2B	3966	3684	1.0765	1.1590
23	CH-54B	15875	15854	1.0013	1.0027
24	CH-54A	12853	10772	1.1932	1.4237
25	XV-9A	5189	4730	1.0970	1.2035
	TOTAL			25.4348	26.1527

$$\bar{X} = \frac{(3)}{\text{No. of Models}(n)} = \frac{25.4348}{25} = 1.0174$$

$$\bar{X}^2 = 1.0351 \quad * 1 = 2.208$$

$$S_x = \sqrt{\frac{X^2_J - n\bar{X}^2}{n-1}} = \sqrt{\frac{26.1527 - 25(1.0351)}{n-1}} = \sqrt{0.01147} = 0.1071$$

Upper Limit = $\bar{X} + 1S_x = 1.0174 + 2.208(0.1071) = 1.2539$

Lower Limit = $\bar{X} - 1S_x = 1.0174 - 2.208(0.1071) = 0.7809$

* Taken from Ref.

Accuracy Analysis Table

TABLE 6-1B ACCURACY ANALYSIS - DERIVATIONS OF MEAN RATIO OF $\frac{WT_{ACT}}{WT_{EST}}$ 2

ROTOR GROUP + DRIVE S' STEM

No.	Model	Actual Weight (1)	Estimated Weight (2)	$\frac{\text{Act. Wt.}}{\text{Est. Wt.}}$ (3)	X_J^2 $\frac{\text{Act. Wt.}}{\text{Est. Wt.}}$ (4)
1	UH-1B	1482	1463	1.0130	1.0261
2	UH-1D	1325	1469	0.9020	0.8136
3	UH-1E	1321	1313	1.0061	1.0122
4	UH-1F	1311	1469	0.8924	0.7965
5	OH-4A	409	387	1.0568	1.1169
6	OH-13L	433	441	0.9819	0.9640
7	OH-13S	435	417	1.0432	1.0882
8	OH-23G	509	474	1.0734	1.1531
9	OH-6A	294	323	0.9102	0.8285
10	SH-3A	4091	3601	1.1361	1.2907
11	CH-3C	3850	3842	1.0021	1.0042
12	HH-52A	1483	1632	0.9087	0.8257
13	CH-34A	2427	2381	1.0193	1.0390
14	CH-37A	6082	5719	1.0635	1.1310
15	CH-53A	8546	8469	1.0091	1.0183
16	UH-2B	2028	1942	1.0443	1.0905
17	CH-54B	9298	9312	0.9985	0.9970
18	CH-54A	7662	6866	1.1159	1.2453
		TOTAL		18.1765	18.4408

$$\bar{X} = \frac{(3)}{\text{No. of Models (n)}} = \frac{18.1765}{18} = 1.0098$$

$$\bar{X}^2 = 1.0197 \qquad * \; l = 2.366$$

$$S_x = \sqrt{\frac{X_J^2 - n\bar{X}^2}{n-1}} = \sqrt{\frac{18.4408 - 18(1.0197)}{17}} = 0.0748$$

Upper Limit = $\bar{X} + l\,S_x$ = 1.0098 + 2.366(0.0748) = 1.1868

Lower Limit = 1.0098 - 2.366(0.0748) = 0.8328

* Taken from Ref.

Accuracy Analysis Table

TABLE 6-1C ACCURACY ANALYSIS - DERIVATIONS OF MEAN RATIO OF $\frac{WT_{ACT}}{WT_{EST}}$ 2

TOTAL ROTOR GROUP

No.	Model	Actual Weight (1)	Estimated Weight (2)	Act. Wt. / Est. Wt. (3)	X^2_J Act. Wt. / Est. Wt. (4)
1	UH-1B	931	873	1.0664	1.1372
2	UH-1D	745	823	0.9052	0.8194
3	UH-1E	756	723	1.0456	1.0933
4	OH-13F	740	823	0.8991	0.8084
5	COBRA	962	873	1.1019	1.2142
6	OH-4A	250	231	1.0823	1.1713
7	OH-13L	285	268	1.0634	1.1309
8	OH-13S	257	252	1.0198	1.0400
9	NH-41A	242	242	1.0000	1.0000
10	OH-23G	311	299	1.0401	1.0818
11	OH-6A	181	216	0.8380	0.7022
12	AH-56A	2178	2227	0.9780	0.9565
13	SH-3A	2328	2003	1.1623	1.3509
14	CH-3C	1909	2148	0.8887	0.7898
15	UH-19D	808	860	0.9395	0.8827
16	HH-52A	785	872	0.9002	0.8104
17	269A	115	139	0.8273	0.6845
18	CH-21C	1344	1392	0.9655	0.9322
19	CH-34A	1336	1459	0.9157	0.8385
20	CH-37A	3618	3480	1.0397	1.0809
21	CH-53A	4788	4827	0.9919	0.9839
22	UH-2B	1295	1186	1.0191	1.1923
23	CH-54B	5035	5595	0.8999	0.8098
24	CH-54A	4051	3461	1.1705	1.3700
25	XV-9A	2805	2660	1.0545	1.1120
	TOTAL			24.8874	25.2931

$$\bar{X} = \frac{(3)}{\text{No. of Models}(n)} = \frac{24.8874}{25} = 0.9955$$

$$\bar{X}^2 = 0.9910 \qquad * 1 = 2.208$$

$$S_x = \sqrt{\frac{X^2_J - n\bar{X}^2}{n-1}} = \sqrt{\frac{25.2931 - 25(.9910)}{24}} = \sqrt{0.02158} = 0.1469$$

Upper Limit = $\bar{X} - 1\, S_x = 0.9955 + 2.208(0.1469) = 1.3199$

Lower Limit = $\bar{X} - 1\, S_x = 0.9955 - 2.208(0.1469) = 0.6711$

* Taken from Ref.

Accuracy Analysis Table

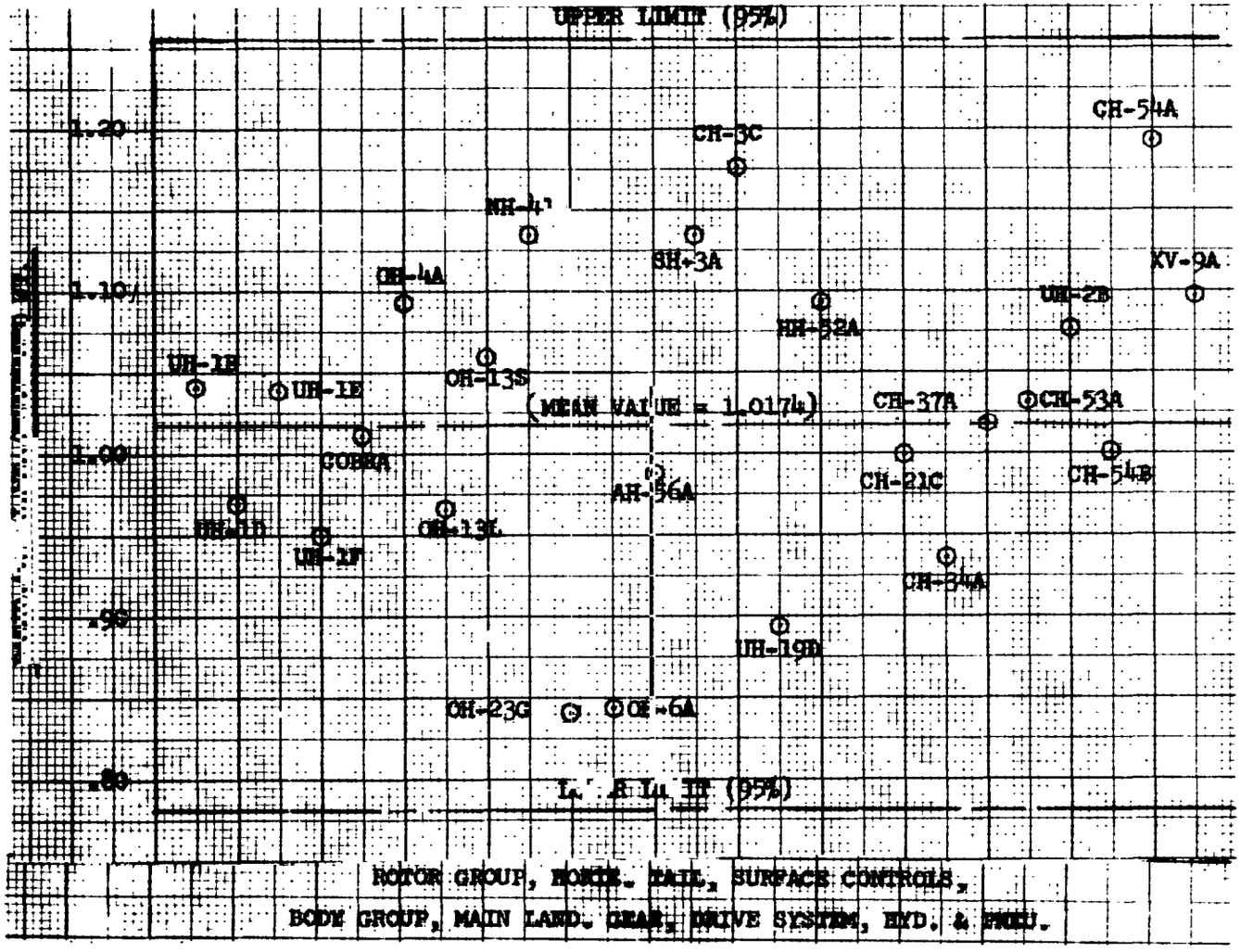

Figure 6-1A Comparison of $\frac{Wt_{actual}}{Wt_{est}}$ Ratio

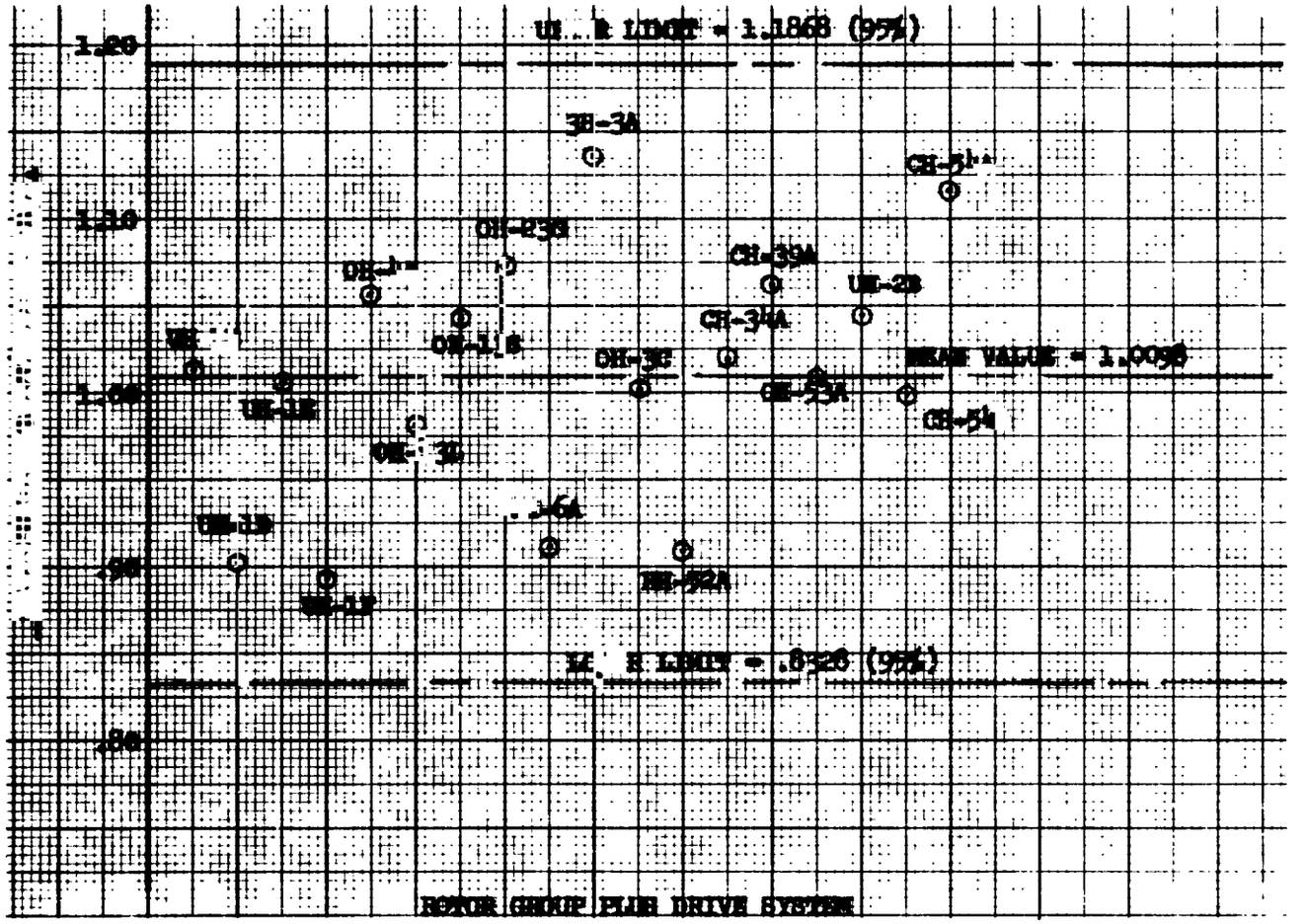

Figure 6-1B Comparison of $\frac{Wt_{actual}}{Wt_{est}}$ Ratio

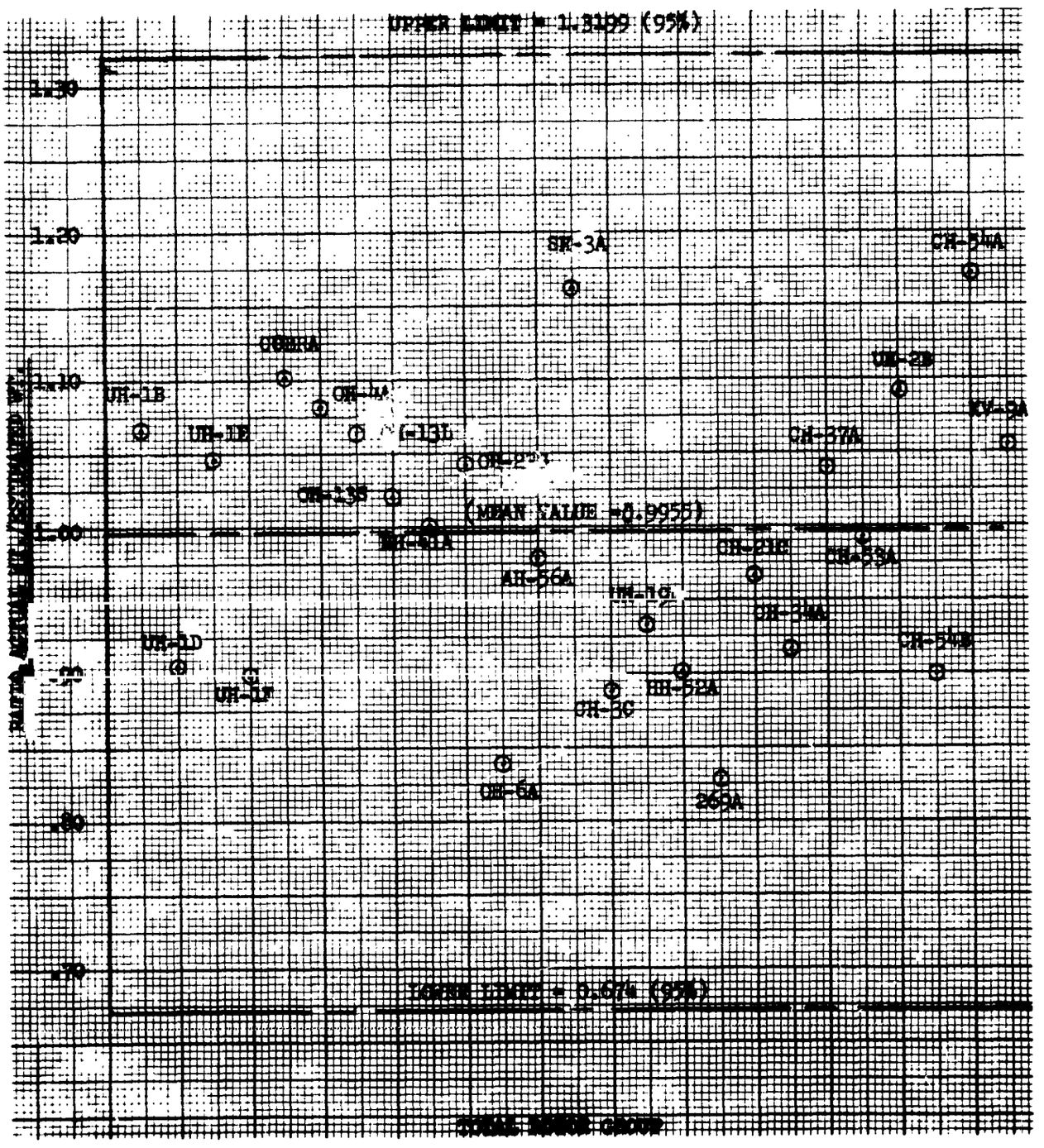

Figure 6-1C Comparison $\frac{Wt_{actual}}{Wt_{est}}$ Ratio

Table 6-1 is a summary of the estimated weight distributions of the various point designs.

The mass properties data for the four point designs are summarized in Table 6-2. Values are shown for: (a) takeoff gross weight, (b) zero fuel, and (c) operating weight empty. Figure 6-1 shows the reference axis system for the four point designs. The mass properties data was derived using: (a) the inboard profile drawings, (b) the weight summaries shown in Table 6-1, and (c) a computer routine.

6.3.2 Part II

The results obtained from the completion of three tasks are summarized in this section. Tasks completed are: (a) Sensitivity Study, (b) Power Split, and (c) Reoptimization of Cold Cycle Analyses of Part I. This data consists of: (a) Fuel available curves, and (b) Group weight summaries for point designs derived from the parametric study. The fuel available data was obtained from a parametric weight analysis routine using the statistical weight estimating equations described in Paragraph 6.4. Parameters studies were: (a) gross weight, (b) rotor solidity, (c) engine cycle, (d) thrust recovery and pressure loss, (e) thrust augementation, and (f) power split between jet flap and a tip jet.

These data are presented in Section 3. Point designs were selected from a sizing study utilizing these data and the fuel required data of Section 3.0.

Table 6-1 is a summary of the estimated weight distributions for the various point designs.

TABLE 6-1 GROUP WEIGHT SUMMARY

FOUR POINT DESIGNS

	Jet Flap		Shaft Driven	
	Heavy Lift	High Speed	Heavy Lift	High Speed
Main Rotor Blade Assembly	9,583	2,566	11,552	2,167
Tail Rotor	---	---	701	106
Horizontal Tail	270	43	242	47
Vertical Tail	491	51	458	41
Basic Body	8,584	2,058	8,779	1,811
Main Landing Gear	2,739	590	2,887	381
Nose Landing Gear	796	171	841	102
Surface Controls	2,083	672	2,181	503
Engine Section	757	240	436	119
Total Structure	(25,303)	(6,391)	(28,077)	(5,277)
Engine	3,440	1,090	1,980	540
Air Induction System	140	65	141	50
Exhaust System	85	94	99	66
Lubricating System	256	126	192	69
Fuel System - Tanks and Plumbing	312	605	218	121
Engine Controls	60	60	60	60
Starting System	60	60	60	60
Drive System	3,730	400	9,256	1,425
Compressor	510	265	---	---
Total Propulsion	(8,593)	(2,766)	(12,006)	(2,391)
Instrument and Navigation Equip.	300	96	300	96
Hydraulic and Pneumatic	131	70	135	56
Electrical	1,000	220	1,000	220
Electronics	290	274	290	274
Furnishings	350	280	350	280
Heat and Ventilation	50	96	50	96
Aux. Gear	1,500	---	1,500	---
Total Fixed Equipment	(3,621)	(1,036)	(3,625)	(1,022)
Total Weight Empty	(37,517)	(10,193)	(43,708)	(8,690)
Crew	600	400	600	400
Fuel - Unusable	43	83	30	18
Fuel - Usable	4,270	8,284	2,992	1,742
Oil Engine	70	20	70	20
Cargo	40,000	4,000	40,000	4,000
Total Useful Load	(44,983)	(12,787)	(43,692)	(6,180)
Gross Takeoff Weight	82,500	22,980	87,400	14,870

TABLE 6-1 (Contd) GROUP WEIGHT SUMMARIES POINT DESIGNS

	LTV HIGH SPEED HELICOPTER				LTV HEAVY LIFT HELICOPTER
	AUXILIARY THRUST TURBOJET	AUXILIARY THRUST CRUISE FAN	AUXILIARY THRUST TURBOPROP	SPLIT POWER 50% FLOW TO FLAPS 50% FLOW TO TIPS	SPLIT POWER 25% FLOW TO FLAP 75% FLOW TO TIP
Main Rotor Blade Assembly	1248	1073	1373	1121	8766
Horizontal Tail	37	33	39	32	257
Vertical Tail	40	35	44	33	473
Basic Body	1258	1166	1311	1113	8213
Main Landing Gear	436	369	483	335	2475
Nose Landing Gear	119	98	134	87	707
Surface Controls	540	477	581	445	1956
Engine Section	75	59	303	51	220
Total Structure	(3753)	(3310)	(4347)	(3216)	(23,067)
Engine	342	266	376	230	960
Air Induction	86	66	69	59	294
Exhaust System	1214	958	700	518	3500
Lubricating System	126	126	126	126	134
Fuel System-Tanks and Plumbing	395	234	256	224	200
Engine Controls	60	60	60	60	120
Starting System	60	60	60	60	60
Drive System	--	--	--	--	--
Auxiliary Thruster	--	600	3779	--	--
Total Propulsion	(2283)	(2370)	(5426)	(1275)	(5268)
Instrumentation and Navigation	96	96	96	96	300
Hydraulic and Pneumatic	70	70	70	70	125
Electrical	220	220	220	220	1000
Electronics	274	274	274	274	290
Furnishings	280	280	30	280	350
Heat and Ventilation	96	96	96	96	50
Auxiliary Gear	--	--	--	--	1500
Total Fixed Equipment	(1036)	(1036)	(1036)	(1036)	(3615)
Total Weight Empty	(7071)	(6716)	(10,809)	(5527)	(31,950)
Crew	400	400	400	400	600
Fuel - Unusable	108	64	70	61	28
Fuel - Usuable	5400	3200	3501	3067	2752
Oil - Engine	20	20	20	20	70
Cargo	4000	4000	4000	4000	40,000
Total Useful Load	(9929)	(7684)	(7991)	(7548)	(43,450)
Gross Take-off Weight	(17,000)	(14,400)	(18,800)	(13,075)	(75,400)

TABLE 6-1 (Contd) GROUP WEIGHT SU

	HIGH SPEED HELICOPTER			
	LTV Hot Cycle	Dorand Hot Cycle	Dorand Warm Cycle	LTV Cold Cy
Main Rotor Blade Assembly	1,099	663	1,322	1,226
Horizontal Tail	34	30	31	3[illegible]
Vertical Tail	36	31	32	3[illegible]
Basic Body	1,185	1,069	1,104	1,21[illegible]
Main Landing Gear	381	306	328	411
Nose Landing Gear	101	78	85	111
Surface Controls	488	416	439	516
Engine Section	63	41	88	17[illegible]
TOTAL STRUCTURE	(3,388)	(2,634)	(3,430)	(3,72
Engine	286	188	402	782
Air Induction	71	38	68	5[illegible]
Exhaust System	580	350	590	9[illegible]
Lubricating System	126	126	126	126
Fuel System - Tanks and Plumbing	319	203	176	35[illegible]
Engine Controls	60	60	60	6[illegible]
Starting System	60	60	60	60
Drive System	-	-	-	496
Compressor	-	-	-	126
TOTAL PROPULSION	(1,502)	(1,025)	(1,482)	(2,13[illegible]
Instrument and Navigation	96	96	96	96
Hydraulic and Pneumatic	70	70	70	70
Electrical	220	220	220	220
Electronics	274	274	274	274
Furnishings	280	280	280	280
Heat and Ventilation	96	96	96	9[illegible]
Auxiliary Gear	-	-	-	-
TOTAL FIXED EQUIPMENT	(1,036)	(1,036)	(1,036)	(1,03[illegible]
TOTAL WEIGHT EMPTY	(5,926)	(4,695)	(5,949)	(6,897
Crew	400	400	400	40[illegible]
Fuel-Unusable	88	56	48	4[illegible]
Fuel-Usable	4,376	2,779	2,413	4,6[illegible]

A

PART II

UP WEIGHT SUMMARIES POINT DESIGNS

	HEAVY LIFT HELICOPTER					
le	LTV Cold Cycle	LTV Hot Cycle	LTV Cold Cycle	Dorand Hot Cycle	Dorand Warm Cycle	LTV Warm Cycle
	1,226	8,705	9,432	4,605	9,764	15,427
	35	260	270	239	257	274
	39	483	511	427	474	521
	1,219	8,349	8,732	6,857	8,235	8861
	411	2,543	2,735	1,950	2,486	2802
	111	727	793	603	708	815
	516	1,995	2,104	1776	1,962	2141
	172	262	722	187	396	510
	(3,728)	(23,324)	(25,299)	(16,647)	(24,284)	(31,351)
	782	1,192	3,280	852	1,800	2320
	50	283	283	283	283	283
	44	4,264	198	1,590	1,970	3295
	126	147	250	124	183	208
	338	251	287	151	183	220
	60	120	120	120	120	120
	60	60	60	60	60	60
	496	-	4629	0	-	-
	126	-	530	-	-	-
	(2,133)		(9,636)	(3,188)	(4,598)	(6507)
	96	300	300	300	300	300
	70	127	131	117	125	133
	220	1,000	1,000	1,000	1,000	1000
	274	290	290	290	290	290
	280	350	350	350	350	350
	96	50	50	50	50	50
	-	1,500	1,500	1,500	1,500	1500
	(1,036)	(3,617)	(3,621)	(3,607)	(3,615)	(3623)
	(6,897)	(33,258)	(38,557)	(23,443)	(32,497)	
	400	600	600	600	600	600
	46	34	39	21	25	30
	4,636	3,438	3,934	2,066	2,507	3019

6-15/6-16

1 6

TABLE 6-1 (Contd) GROUP WEIGHT

	HIGH SPEED HELICOPTER			
	LTV Hot Cycle	Dorand Hot Cycle	Dorand Warm Cycle	LT Cold
Useful Load(Continued)				
Oil Engine	60	20	20	
Cargo	4,000	4,000	4,000	4,(
TOTAL USEFUL LOAD	(8,924)	(7,255)	(6,881)	(9,
GROSS TAKEOFF WEIGHT	(14,850)	(11,950)	(12,830)	(16,(

PART II

ROUP WEIGHT SUMMARIES POINT DESIGNS

	HEAVY LIFT HELICOPTER					
le	LTV Cold Cycle	LTV Hot Cycle	LTV Cold Cycle	Dorand Hot Cycle	Dorand Warm Cycle	LTV Warm Cycle
	20	70	70	70	70	70
	4,000	40,000	40,000	40,000	40,000	40,000
	(9,103)	(44,142)	(44,643)	(42,757)	(43,203)	(43,719)
	(16,000)	(77,400)	(83,200)	(66,200)	(75,700)	(85,200)

TABLE 6-2 POINT DESIGN MASS PROPERTIES DATA
JET-FLAP AND SHAFT-DRIVEN CONCEPTS

Condition	Blade Direction	Pounds	$\bar{X}$ Inches	$\bar{Y}$ Inches	$\bar{Z}$ Inches	I_{XX} Slug-Ft^2	I_{YY} Slug-Ft^2	I_{ZZ} Slug-Ft^2	U_{XZ} Slug-Ft^2
HEAVY LIFT SHAFT DRIVEN									
Takeoff Gross Wt.	-	87,400	619	0	156	288,437	1,244,908	1,202,682	66,642
Zero Fuel	-	84,407	618	0	154	286,546	1,192,483	1,151,072	66,071
OWE	-	44,408	635	0	221	178,625	737,187	782,990	43,845
HEAVY LIFT - JET FLAP									
Takeoff Gross Wt.	-	82,500	602	0	150	351,224	1,114,917	1,285,912	24,094
Zero Fuel	-	78,230	600	0	147	347,744	1,038,578	1,211,155	22,320
OWE	-	38,230	600	0	196	288,545	730,930	942,000	22,253
HIGH SPEED - JET FLAP									
Takeoff Gross Wt.	long.	22,980	200	0	91	10,847	72,701	64,564	2,607
	lat.	22,980	200	0	91	31,540	52,008	64,564	2,607
Zero Fuel	long.	14,696	199	0	98	9,237	52,727	45,299	2,853
	lat.	14,696	199	0	98	29,930	32,034	45,299	2,853
OWE	long.	10,696	198	0	117	5,793	47,605	43,291	2,941
	lat.	10,696				26,486	26,913	43,291	2,941
HIGH SPEED - SHAFT DRIVEN									
Takeoff Gross Wt.	long	14,870	194	0	102	8,638	46,843	40,745	1,183
	lat.	14,870	194	0	102	21,167	34,314	40,745	1,183
Zero Fuel	long.	13,128	193	0	98	7,972	45,962	40,305	1,099
	lat.	13,128	193	0	98	20,501	33,433	40,305	1,099
OWE	long.	9,128	191	0	118	4,693	37,326	34,282	1,475
	lat.	9,128	191	0	118	17,222	24,797	34,282	1,475

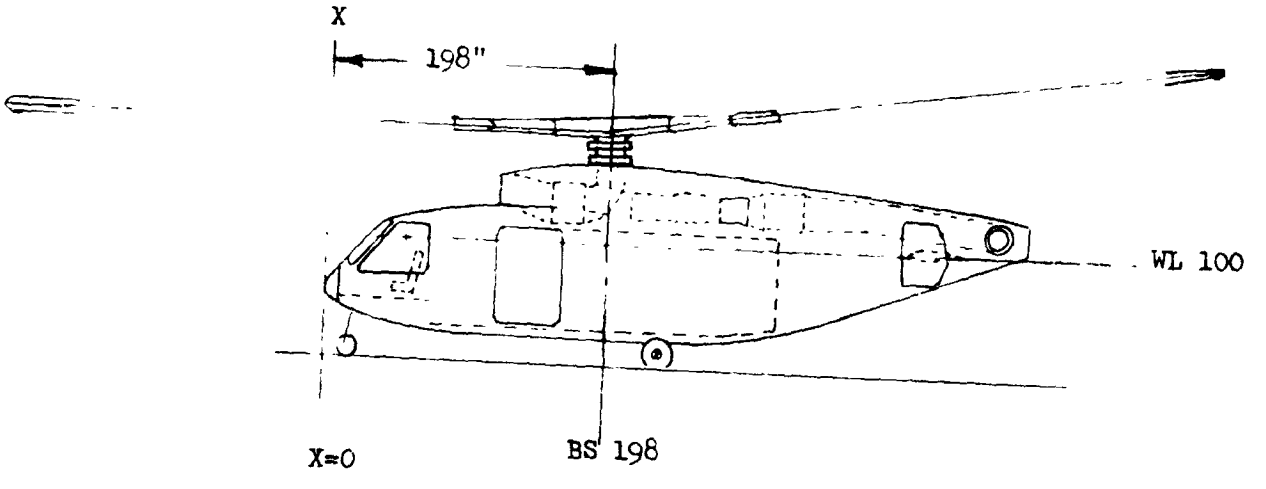

HIGH SPEED HELICOPTER JET FLAP

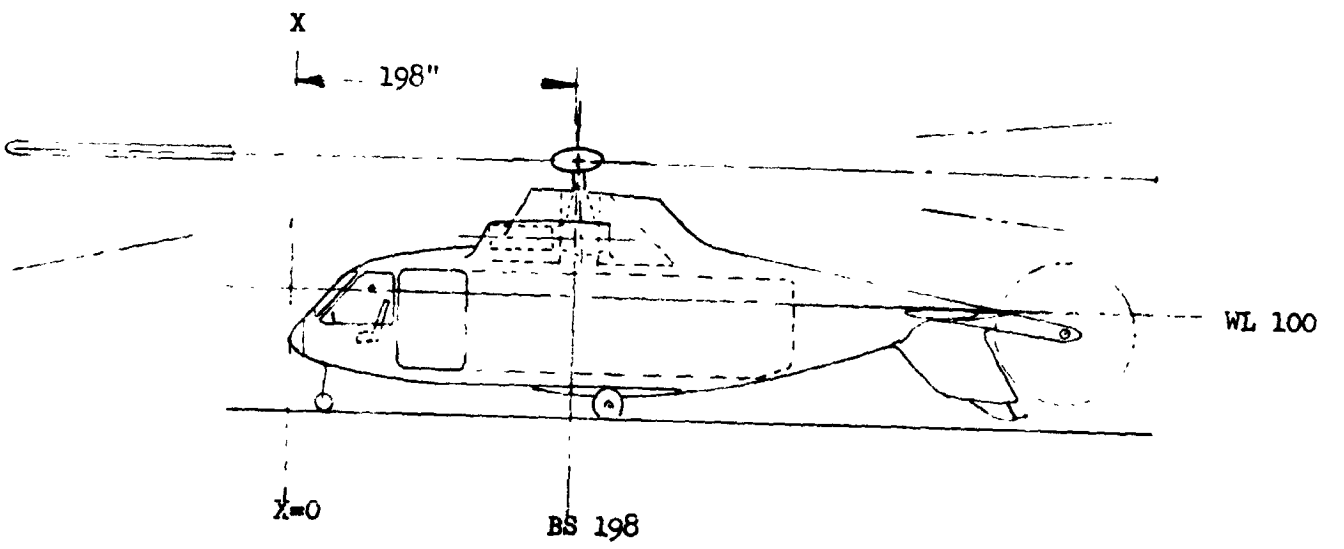

HIGH SPEED HELICOPTER SHAFT DRIVEN

NOTE: $\bar{X}$ = HORIZONTAL C.G. - INCHES AFT OF REFERENCE DATUM XX
= LATERAL C.G. - INCHES OUTBOARD OF AIRCRAFT CENTERLINE
= VERTICAL C.G. - INCHES ABOVE REFERENCE DATUM Z Z (WL 100)

FIGURE 6-1. DIMENSIONAL REFERENCE DATA

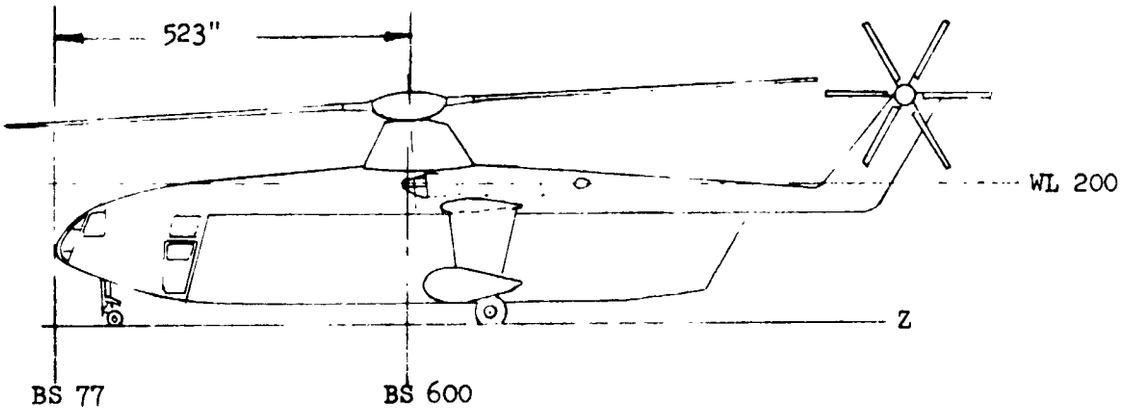

HEAVY LIFT HELICOPTER ~ SHAFT DRIVEN

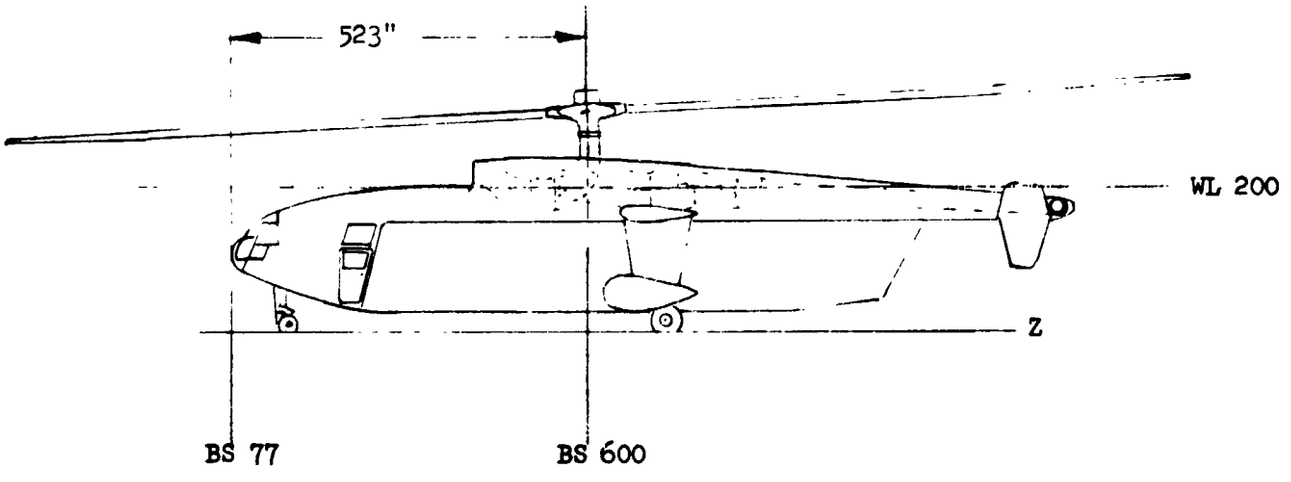

HEAVY LIFT HELICOPTER ~ JET FLAP

NOTE: $\bar{X}$ = HORIZONTAL C.G. - INCHES AFT OF REFERENCE DATUM XX
$\bar{Y}$ = LATERAL C.G. - INCHES OUTBOARD OF AIRCRAFT CENTERLINE
Z = VERTICAL C.G. - INCHES ABOVE REFERENCE DATUM Z Z

FIGURE 6-1 (CONT'D)

6.4 WEIGHT DERIVATION

This section contains a tabulation of the weight estimating methods and the design data used to derive the estimated weight of the four point designs. Pertinent remarks, assumptions, and necessary backup data are included. Any modification or change required in a particular weight estimating method is noted.

Table 6-3 contains all the design data necessary for the complete use of the weight estimating methods utilized.

A practical application of the weight derivation procedure appears in the sample calculations contained in a later section of this report. The jet-flap rotor heavy lift configuration is used for this application.

A statistical weight comparison of major structural, propulsion, and equipment components of other helicopters is made. These weight comparisons are presented in Figures 6-2 through 6-8.

6.4.1 Weight Estimation Methods and Equation

6.4.1.1 Rotor Group - All Concepts

$$W_{RG} = 0.00956 \left| (W_{DG})^{.238} (N_Z)^{.525} (R_M)^{.417} (S_{BLA})^{.955} (R_{RPM})^{.524} \right| K_1$$

where

W_{DG} = Design Gross Weight

N_Z = Ultimate Load Factor

R_M = Radius of Main Rotor Blade

PART II

TABLE 6-3 DESIGN DATA – POINT DESIGNS – ALL CONCEPTS

ITEM	JET FLAP			SHAFT DRIVEN	
	HLH-WARM	HLH-COLD	HSH	HSH	HLH
Design Gross Weight	82,100	82,500	22,980	14,870	87,400
Design Landing Weight	82,100	82,500	22,980	14,870	87,400
Ultimate Load Factor	3.75	3.75	3.75	3.75	3.75
Landing Load Factor	3.75	3.75	3.75	3.75	3.75
Number of Crew	3	3	2	2	3
Number of Engines	2	2	2	2	2
Cargo	40,000	40,000	4,000	4,000	40,000
Fuselage Length	103	103	40	46.2	103
Fuselage Depth	5.7	5.7	9.5	9.5	5.7
Fuselage Width	11.7	11.7	5.3	5.3	11.7
Fuselage Wetted Area	2,500	2,500	720	850	2,500
Horizontal Tail Area	121	121	17	30	96
Vertical Tail Area	94	94	18.6	21.8	78
Main Rotor Tip Velocity	640	640	640	640	700
Main Rotor Blade Diameter	145	145	72.2	67	104
Main Rotor Cord	5.24	3.81	4.17	4.13	2.88
Rotor Solidity	0.069	0.0502	0.0735	0.0785	0.106
Main Rotor Blade Area	1,139	829	301	275	900
Tail Rotor Diameter	-	-	-	8.0	10
Distance between Rotors	-	-	-	28.5	60
Rotor RPM	84.5	84.5	172	190	129
Number of Blades	3	3	2	2	6
Horsepower per Engine	7,525	6,280	7,020	1,198	7,520
Shaft RPM		20,000	18,980	19,000	8,000

PART II

TABLE 6-3 (Contd) DESIGN DATA-POINT DESIGNS-ALL CONCEPTS

	HIGH SPEED HELICOPTER				HEAVY LIFT HELICOPTER
	AUXILIARY THRUST TURBOJET	AUXILIARY THRUST CRUISE FAN	AUXILIARY THRUST TURBOPROP	SPLIT POWER 50% FLOW TO FLAPS 50% FLOW TO TIPS	SPLIT POWER 25% FLOW TO FLAPS 75% FLOW TO TIPS
Design Gross Weight	17,000	14,400	18,800	13,075	17,400
Design Landing Weight	17,000	14,400	18,800	13,075	17,400
Ultimate Load Factor	3.75	3.75	3.75	3.75	3.75
Landing Load Factor	3.75	3.75	3.75	3.75	3.75
Number of Crew	2	2	2	2	3
Number of Engines	2	2	2	2	4
Cargo	4000	4000	4000	4000	40,000
Fuselage Length, Ft	40	40	40	40	103
Fuselage Depth, Ft	9.5	9.5	9.5	9.5	5.7
Fuselage Width, Ft	5.3	5.3	5.3	5.3	11.7
Fuselage Wetted Area, Sq Ft	720	720	720	720	2500
Horizontal Tail Area, Sq Ft	17	17	17	17	121
Vertical Tail Area, Sq Ft	18.6	18.6	18.6	18.6	94
Main Rotor Tip Velocity, Ft/Sec	640	640	640	640	700
Main Rotor Blade Dia. Ft	72.2	72.2	72.2	72.2	145
Main Rotor Chord, Ft	2.13	1.9	2.3	72.2	4.45
Rotor Solidity	.0376	.0336	.0405	.0295	.039
Main Rotor Blade Area, Sq Ft	154	137	166	121	644
Rotor RPM	170	170	170	170	92
Number of Blades	2	2	2	2	3
Thrust/Engine	1485	1135	1640	965	2120
Horsepower/Engine	--	--	--	--	--

TABLE 6-3 (Contd) DESIGN DATA-F

	HIGH SPEED HELICOPTER			
	LTV Cold Cycle	LTV Hot Cycle	Dorand Hot Cycle	Dor Warm C
Design Gross Weight	16,000	14,850	11,950	12,8
Design Landing Weight	16,000	14,850	11,950	12,8
Ultimate Load Factor	3.75	3.75	3.75	3.
Landing Load Factor	3.75	3.75	3.75	3.
Number of Crew	2	2	2	
Number of Engines	2	2	2	
Cargo	4000	4000	4000	4C
Fuselage Length, Ft.	40	40	40	
Fuselage Depth, Ft.	9.5	9.5	9.5	
Fuselage Width, Ft.	5.3	5.3	5.3	
Fuselage Wetted Area, Sq. Ft.	720	720	720	7
Horizontal Tail Area, Sq. Ft.	17	17	17	
Vertical Tail Area, Sq. Ft.	18.6	18.6	18.6	18
Main Rotor Tip Velocity, Ft/Sec.	640	640	720	7
Main Rotor Blade Diameter, Ft.	72.2	72.2	67	
Main Rotor Chord, Ft.	2.1	1.9	1.2	2
Rotor Solidity	.0375	.034	.023	.C
Main Rotor Blade Area, Sq. Ft.	153	139	81	1
Rotor RPM	170	170	203	2
Number of Blades	2	2	2	
Thrust/Engine		1185	775	1
Horsepower/Engine	3125	-	-	

A

PART II

IGN DATA-POINT DESIGNS-ALL CONCEPTS

	HEAVY LIFT HELICOPTER					
	Dorand Warm Cycle	LTV Cold Cycle	LTV Hot Cycle	Dorand Warm Cycle	Dorand Hot Cycle	LTV Warm Cycle
	12,830	83,200	77,400	75,700	66,200	85,200
	12,830	83,200	77,400	75,700	66,200	85,200
	3.75	3.75	3.75	3.75	3.75	3.75
	3.75	3.75	3.75	3.75	3.75	3.75
	2	3	3	3	3	3
	2	4	4	4	4	4
	4000	40000	40000	40000	40000	40000
	40	103	103	103	103	103
	9.5	5.7	5.7	5.7	5.7	5.7
	5.3	11.7	11.7	11.7	11.7	11.7
	720	2500	2500	2500	2500	2500
	17	121	121	121	121	121
	18.6	94	94	94	94	94
	720	700	700	720	720	700
	67	145	145	145	145	145
	2.4	3.5	3.3	3.7	1.9	5.8
	.046	.0465	.0435	.0485	.0245	.076
	164	767	718	800	404	1254
	203	92	92	95	95	92
	2	3	3	2	2	3
	1400		2660	3230	1875	4120
	-	6480	-	-	-	-

B

6-25/6-26

FIGURE 6-2

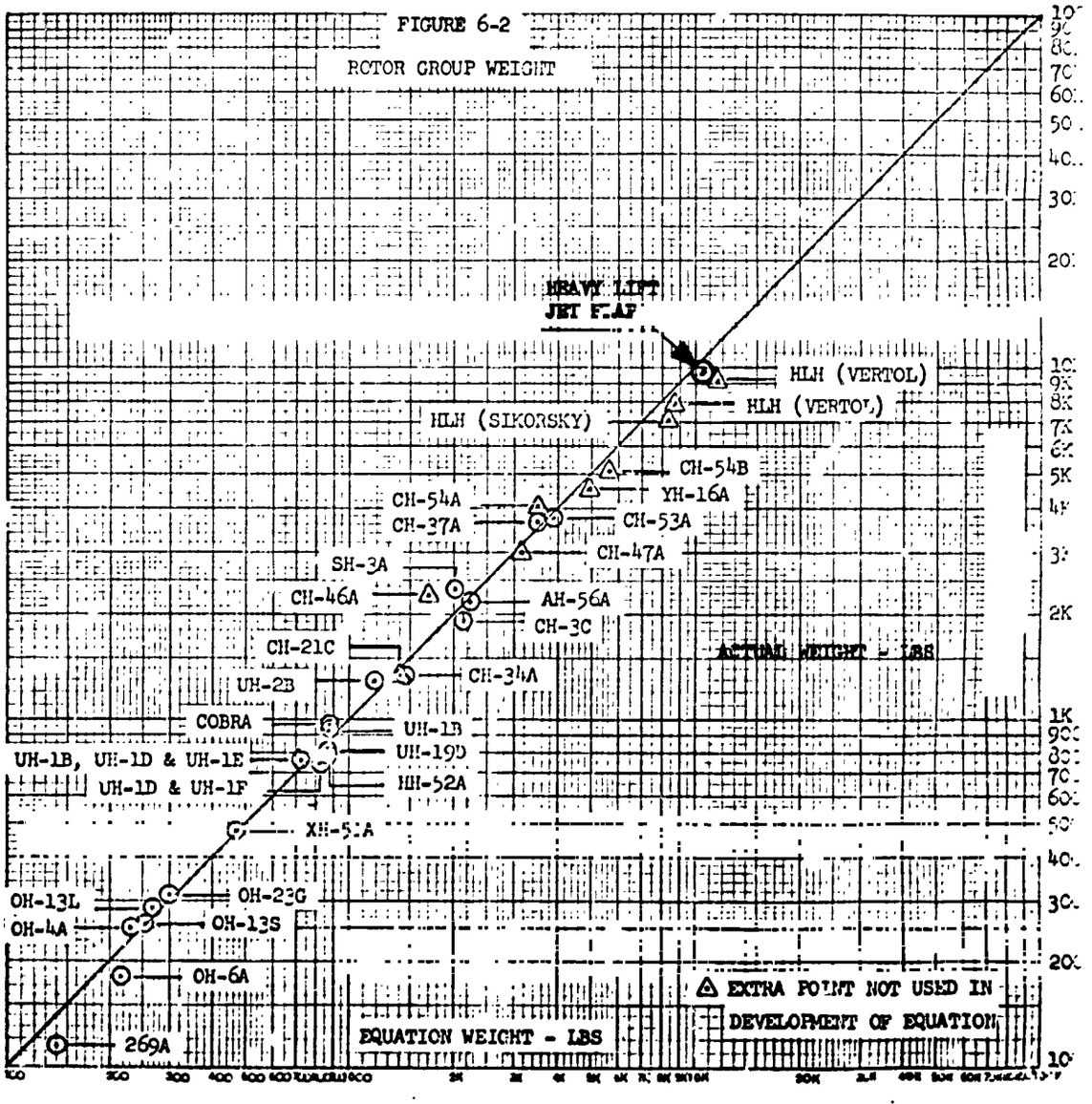

$$W_{RG} = .00956\ W_{DG}^{*.238}\ N_Z^{.525}\ P^{.417}\ S_{BLA}^{*.955}\ R_{BLA}^{.524}$$

FIGURE 6-3

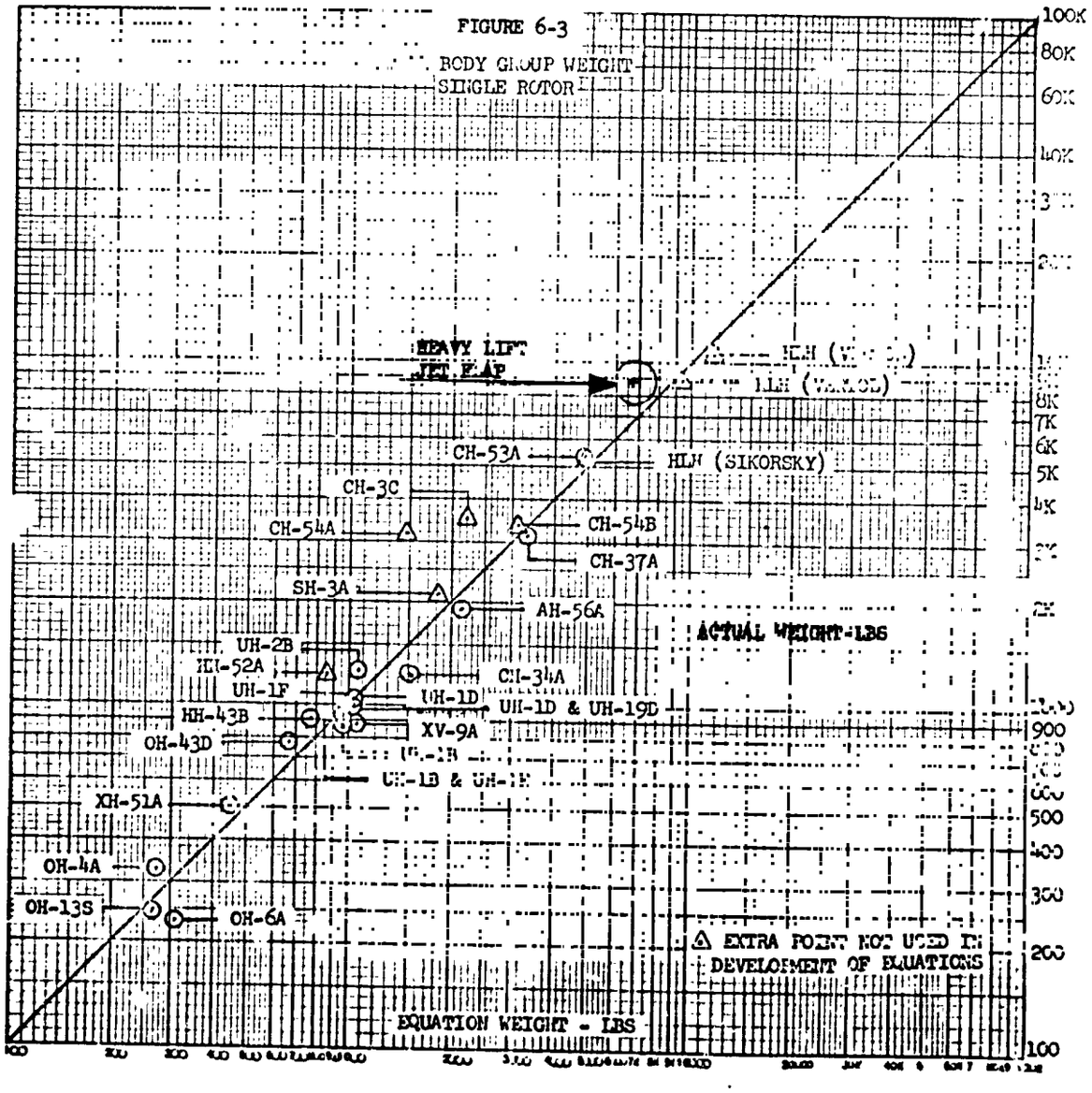

$$W_T = .020445\, W_{DG}^{.62}\, N_Z^{1.49}\, S_T^{.15}\, L^{.19}\, D^{.45}\, B^{.36}$$

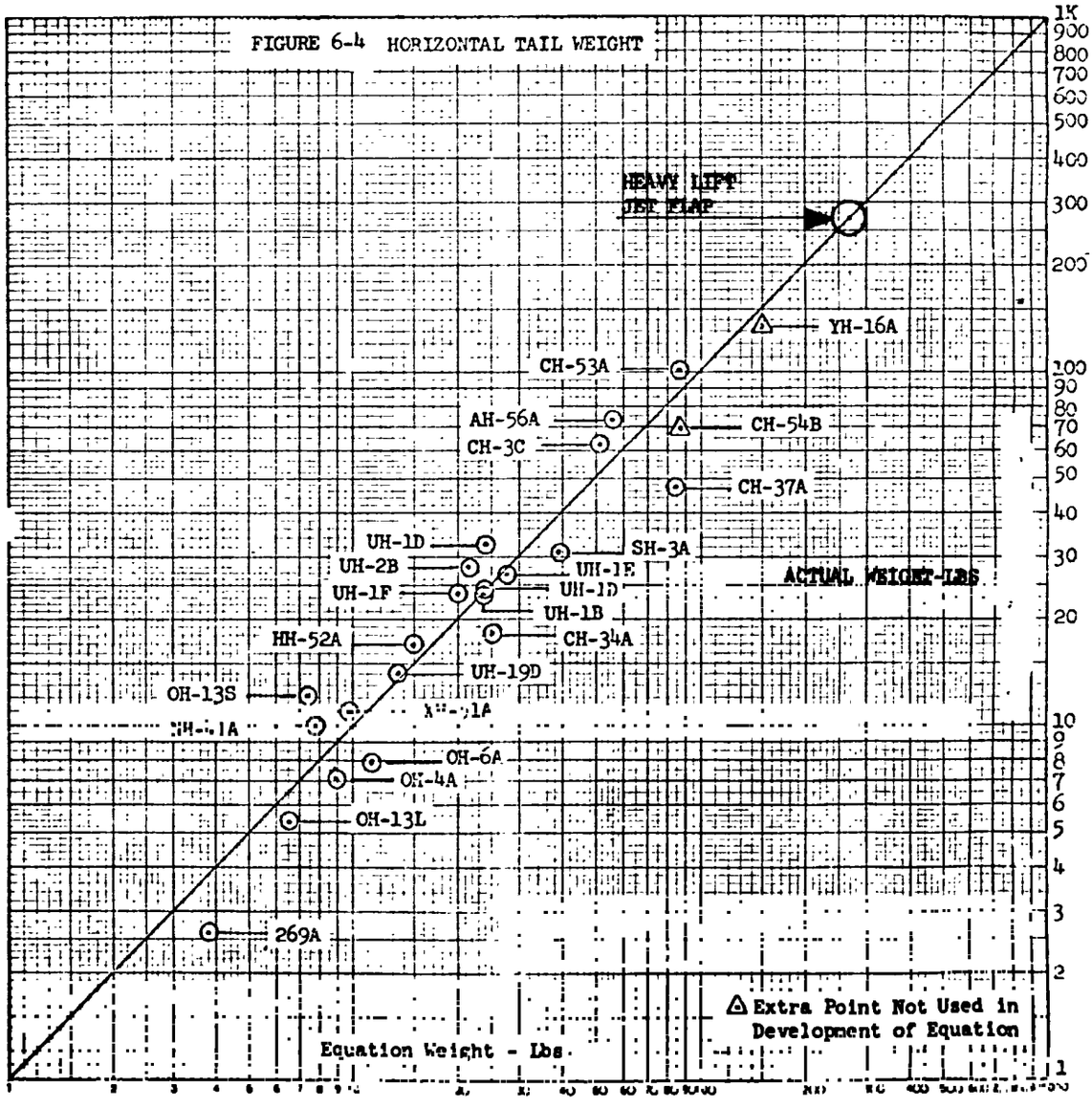

Equation 3

$$W_{HT} = .03725\ W_{DG}^{.537}\ S_{HT}^{.585}$$

COEFFICIENT OF CORRELATION 95.04

FIGURE 6-5

WEIGHT OF MAIN LANDING GEAR
OLEO TYPE GEAR

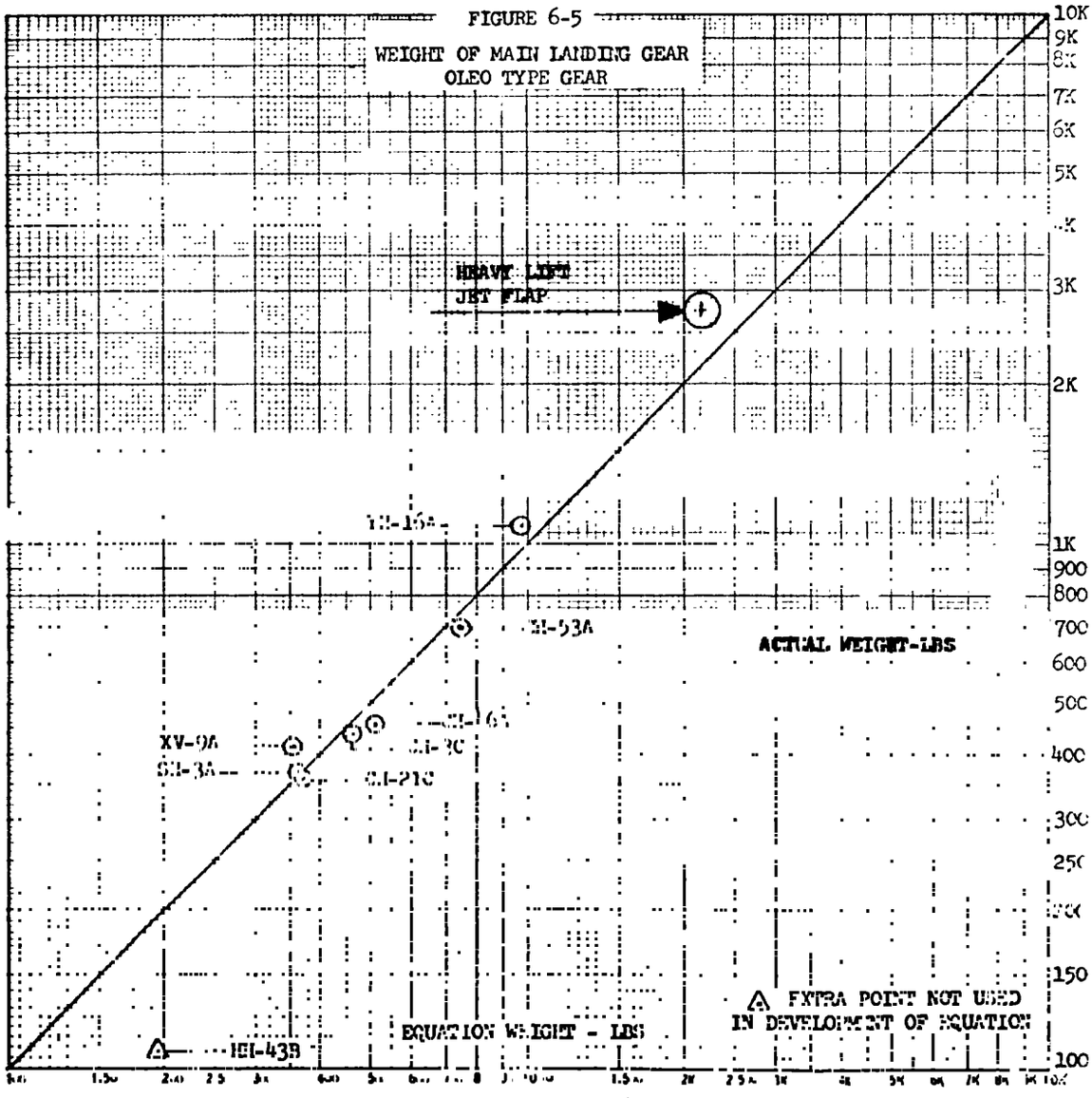

$$W_{MLG} = .005300\ W_{DL}^{1.01}\ N_L^{1.12}$$

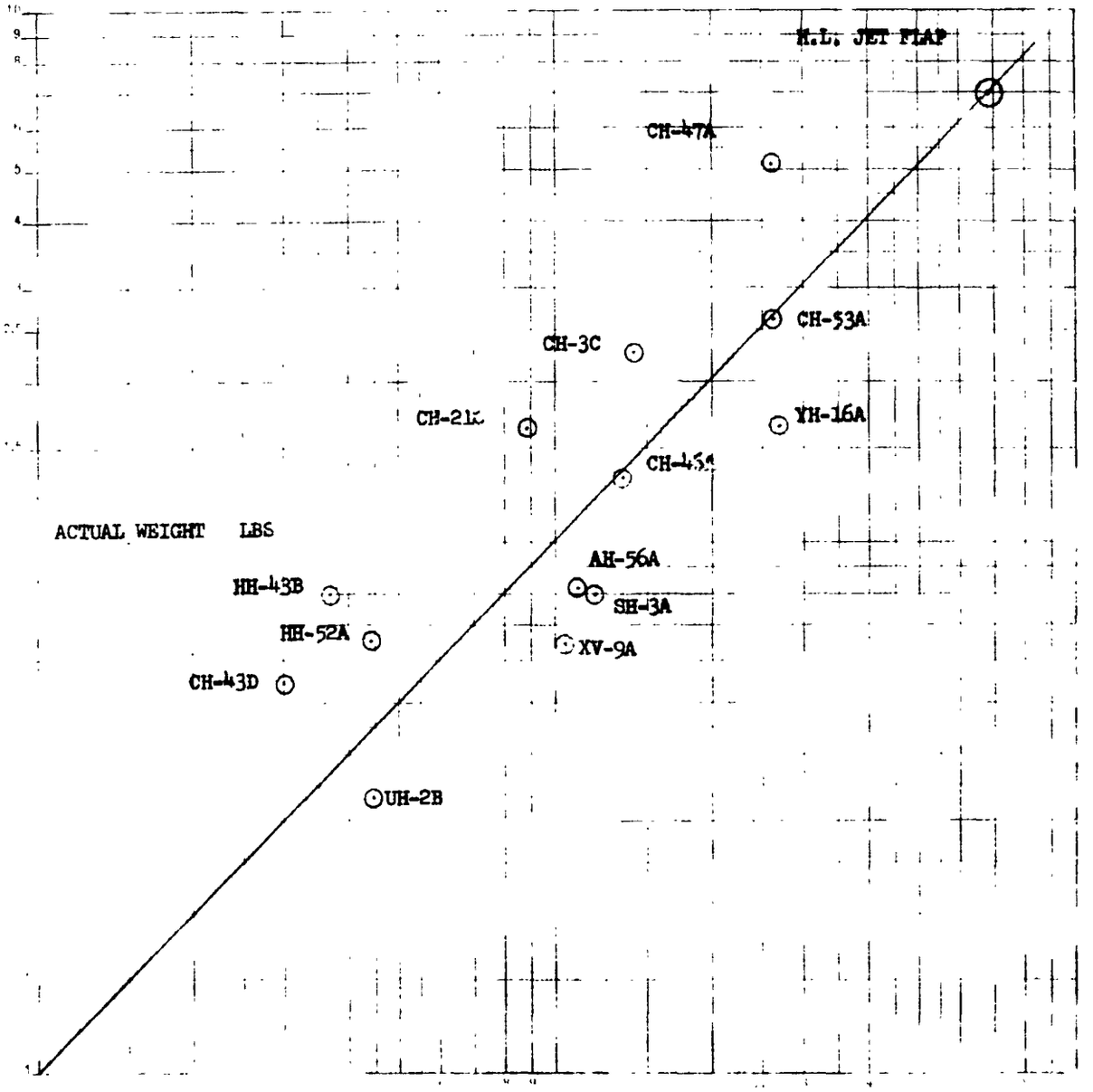

EQUATION

$$W_{NLG} = 0.00107 \times W_{D.L.}^{1.193}$$

FIGURE 6-6 NOSE LANDING GEAR

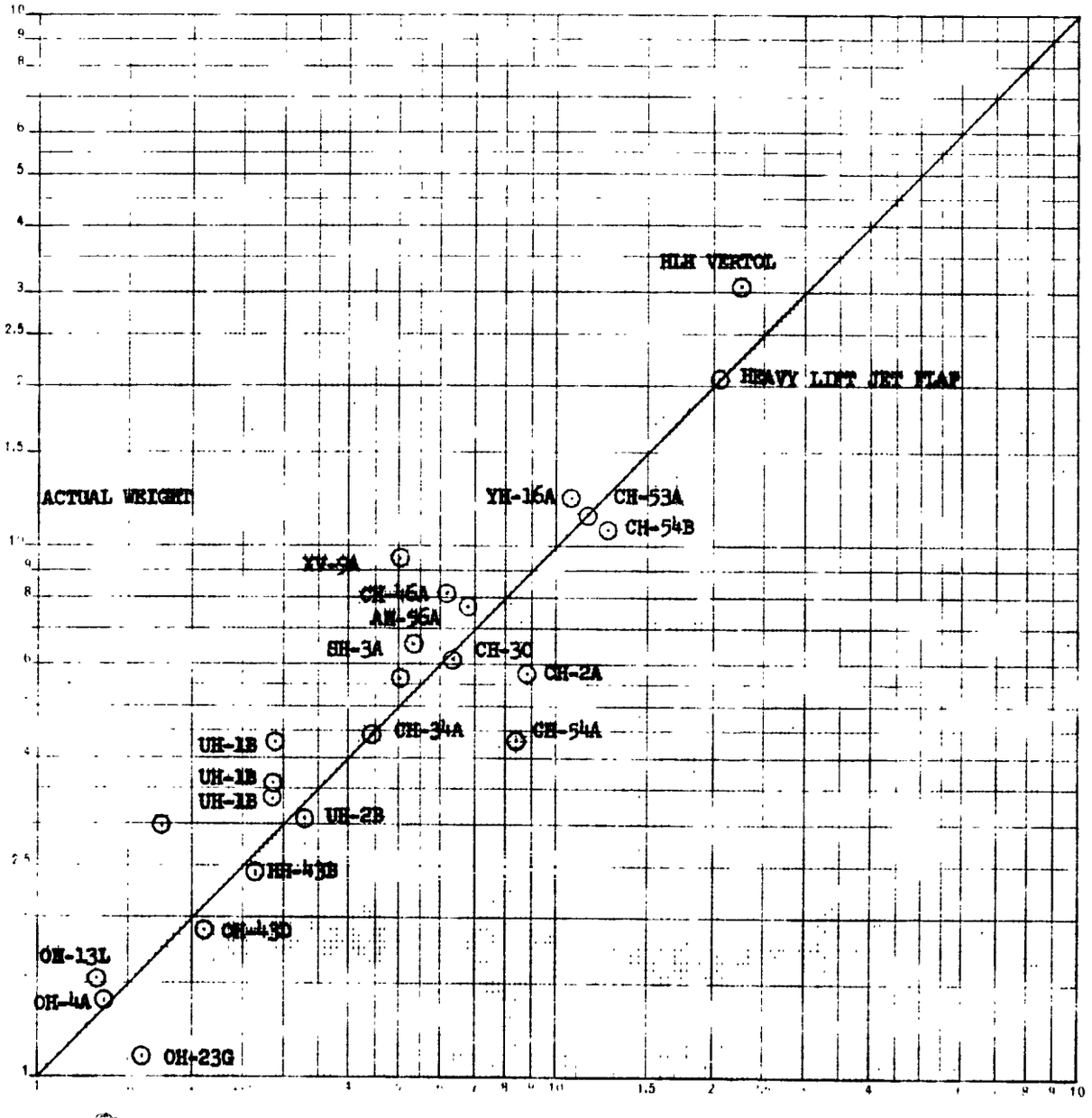

EQUATION

$$W_{SC} = .089815 \ (W_{DG})^{.736} (N_z)^{.592} (L_f)^{.203}$$

FIGURE 6-7 SURFACE CONTROLS

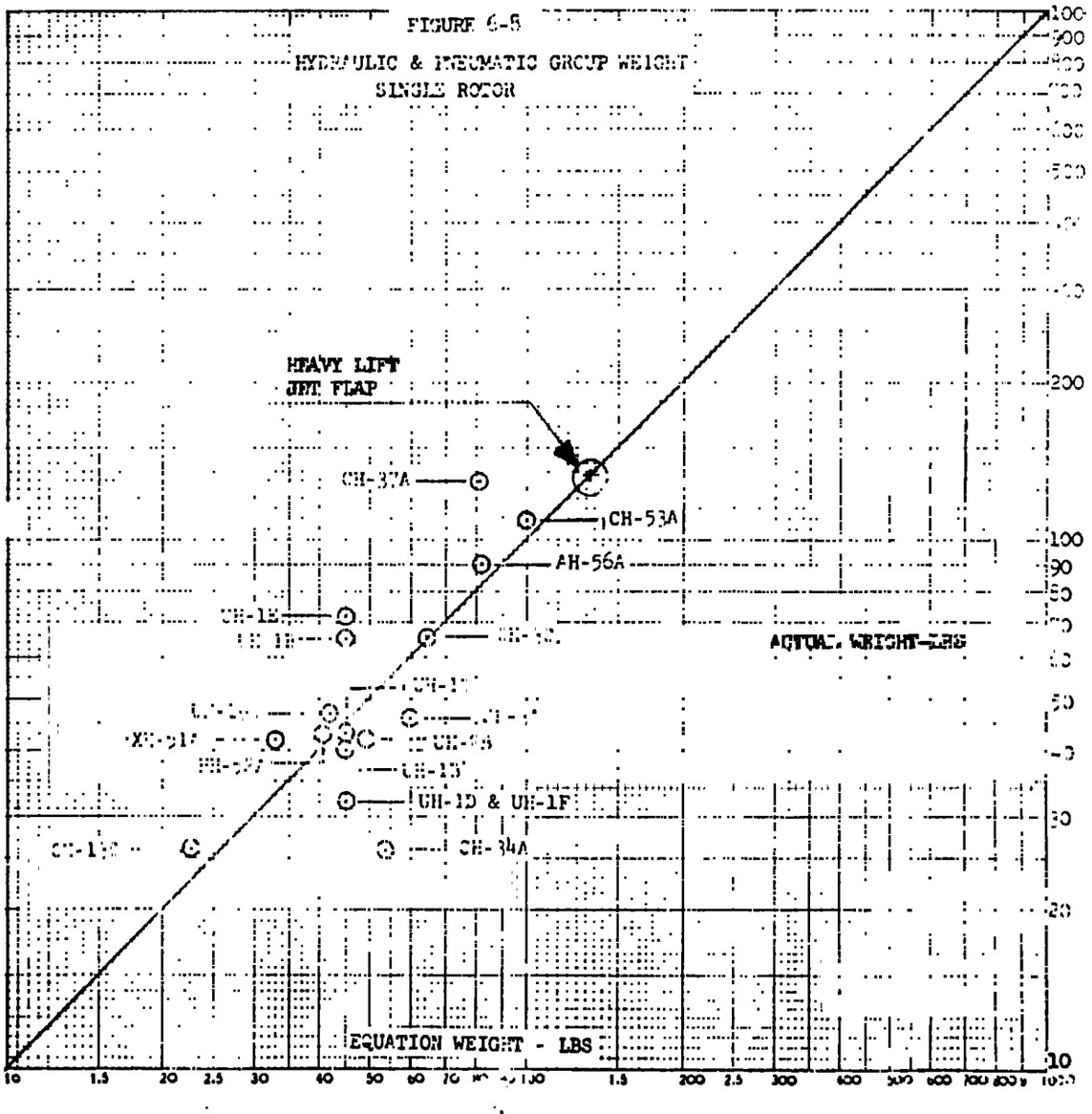

FIGURE 6-5
HYDRAULIC & PNEUMATIC GROUP WEIGHT
SINGLE ROTOR

$$W_{HPG} = .15881 W_{DG}^{.489} N_Z^{.891}$$

S_{BLA} = Total Blade Area

R_{RPM} = Rotor RPM

K_1 = 0.797 for Gross Weights from 10,000 - 39,999

= 0.857 for Gross Weights from 40,000 - 69,999

= 0.916 for Gross Weights from 70,000 - 99,999

6.4.1.2 Wing Group

Not applicable.

6.4.1.3 Tail Group

a. Tail Rotor - All Shaft-Driven Concepts

$$W_{TR} = .18637 \left| \left(\frac{HP}{V_T}\right)^{.500} (W_{DG})^{.476} (R_T)^{.709} (R_M)^{.036} \right|$$

where

$\frac{HP}{V_T}$ = Total Horsepower/Tip Velocity

W_{DG} = Design Gross Weight

R_T = Radius Tail Rotor

R_M = Radius Main Rotor

b. Horizontal Tail - All Concepts

$$W_{HT} = .03725 \left| (W_{DG})^{.537} (S_{HT})^{.585} \right|$$

where

W_{DG} = Design Gross Weight

S_{HT} = Area Horizontal Tail

c. Vertical Tail - All Concepts

$$W_{VT} = .00184 \left| (W_{DG})^{.788} (S_{VT})^{.794} \right|$$

where

W_{DG} = Design Gross Weight

S_{VT} = Area Vertical Tail

6.4.1.4 Body Group - All Configurations

$$W_{BG} = 0.020445 \left| (W_{DG})^{.62}(N_Z)^{1.49}(S_F)^{.15}(L)^{.19}(D)^{.46}(B)^{.36} \right| K_1$$

where

W_{DG} = Design Gross Weight

N_Z = Ultimate Load Factor

S_F = Wetted Area Basic Body (Ft^2)

L = Length of Body (Ft)

D = Depth of Body (Ft)

B = Width of Body (Ft)

K_1 = 1.0 for Gross Weights from 10,000 - 39,999

= 1.14 for Gross Weights from 40,000 - 69,999

= 1.26 for Gross Weights from 70,000 - 99,999

6.4.1.5 Alighting Gear - All Concepts

a. Main Landing Gear

$$W_{MG} = 0.0053 \left| (W_{DL})^{1.01}(N_L)^{1.12} \right| K_1$$

where

W_{DL} = Design Landing Weight

N_L = Landing Load Factor

K_1 = 1.0 for Gross Weights from 10,000 - 39,999

= 1.14 for Gross Weights from 40,000 - 69,999

= 1.26 for Gross Weights from 70,000 - 99,999

b. Nose Landing Gear

$$W_{DL} = .00107(W_{DL})^{1.193}$$

where

W_{DL} = Design Landing Weight

6.4.1.6 Surface Controls - All Concepts

$$W_{SC} = .08915\left|(W_{DG})^{.736}(N_Z)^{.592}(L_F)^{.203}\right|$$

where

W_{DG} = Design Gross Weight

N_Z = Ultimate Load Factor

L_F = Length of Body

6.4.1.7 Engine Section - All Concepts

$$W_{ES} = .22\ (W_E)$$

where

W_E = Weight of Engines

6.4.1.8 Engine - All Concepts

The engine weights were read from curves supplied by Allison. This data is presented as Figure 6.9.

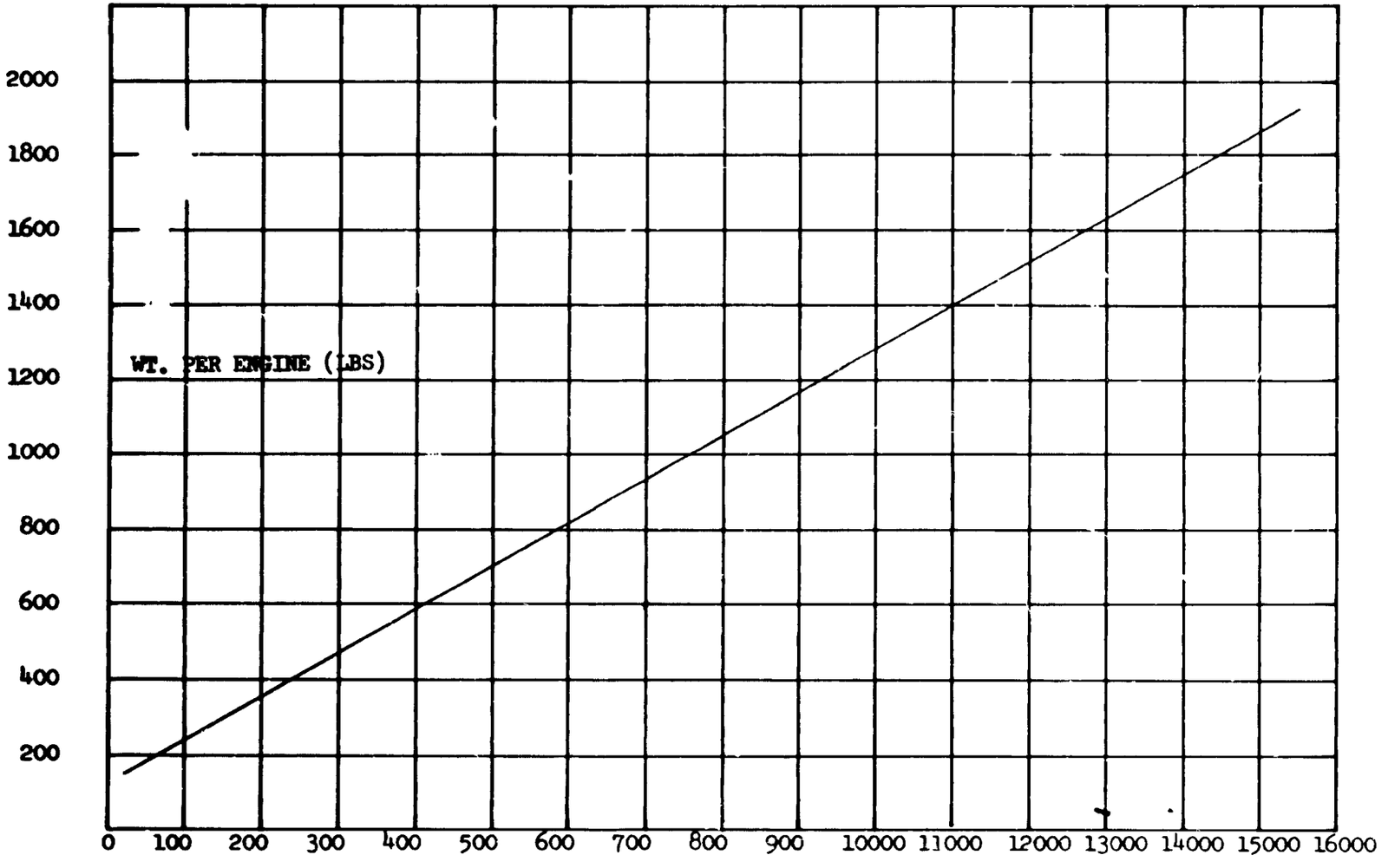

FIGURE 6-9 ENGINE WEIGHT VS MRP SHP. ALLISON TURBOSHAFT ENGINE MODEL 548-C13
HIGH SPEED & HEAVY LIFT JET-FLAP & SHAFT DRIVEN CONCEPT

6.4.1.9 Air-Induction System - All Concepts

$$W_{AI} = (1 \text{ lb/ft}^2)(\text{Length})(\text{Dia})\ (\pi)$$

6.4.1.10 Exhaust System - All Concepts

$$W_{EXH} = (1.25 \text{ lb/ft}^2)(\text{Length})(\text{Dia})(\pi)$$

6.4.1.11 Lubricating System - All Concepts

$$W_{LS} = 3.7062(W_{ENG})^{.52}$$

where

W_{ENG} = Total Engine Weights

6.4.1.12 Fuel System - All Concepts

$$W_{FS} = .073(W_{UF})$$

where

W_{UF} = Weight Usable Fuel

6.4.1.13 Engine Controls - All Concepts

$$W_{EC} = 30 \text{ lb/engine}$$

The estimated weight for this component is held constant per engine. It is derived from statistical data taken from the following helicopters:

XH-15, YH-12, HSL-1, XH-17, XHCH-1, XH-16, H-37

6.4.1.14 Starting System

W_{SS} = 30 lb/engine

The estimated weight for this component is held constant per engine. It is derived from statistical data taken from the following helicopters:

XH-15, YH-12, HSL-1, XH-17, XHCH-1, XH-16, H-37

6.4.1.15 Drive System

a. Shaft Driven - Heavy Lift and High Speed

$$\text{Weight Drive System} = 0.3024 \left| (HP)^{.413} (L_R)^{1.246} (HP/RPM)^{.176} (R)^{.307} \right| K_1$$

where

HP = Total Horsepower

L_R = Length between Rotors

$HP/RPM = \frac{HP/Engine}{Shaft\ RPM}$

R = Reduction Gear Ratio

K_1 = 1.15 for Gross Weights from 10,000 - 39,999

= 1.08 for Gross Weights from 40,000 - 69,999

= 1.00 for Gross Weights from 70,000 - 99,999

b. Jet Flap - Concept Only

The estimated weight for the jet-flap configurations is derived from a buildup of component parts as shown below:

Heavy Lift

$$\text{Gearbox Weight} = 896 \left| \left(\frac{HP\ In}{RPM\ In}\right)^{.65} \left(\frac{RPM\ In}{RPM\ Out}\right)^{.67} \right| (\text{No. Engines})$$

$$= 896 \left| \left(\frac{13,750}{5,900}\right)^{.65} \left(\frac{5,900}{9,242}\right)^{.67} \right| 2$$

$$= 896 \left| (1.73)(.74) \right| 2 \qquad 2,294$$

Installation of Gearbox = 21.5% of Gearbox Weight = 494

Shafts

Engine = $.283\left|(28.27 - 23.76)(2)(36)\right|$ = 92

Compressor = $.283\left|(12.57 - 9.62)(60)\right|$ = 50

Support Bearings

Assumed 20% of shaft weight

$\left|(142)(.20)\right|$ = 28

Ducts

To Rotor = (π) (Dia)(Length)(Wall Thickness)(2)(.1)

= (3.14)(34)(140)(.05)(2)(.1) = 150

Through Blade (3 blades)

$(3)(\pi)(7.58)(72.5)(.05)(2)(.1)$ = 52

$(3)(\pi)(6.36)(72.5)(.04)(2)(.1)$ = 70

Drive System Weight

Cooling System for Gearbox = (.166)(Weight Gear Box)

= (.166)(2,294) = 380

Override Clutch = 60 lb/engine = (60)(2) = 120

Total Weight for Heavy Lift Jet Flap 3,730

High Speed Jet Flap

$$\text{Gearbox} = 228\left|\left(\frac{\text{HP In}}{\text{RPM In}}\right)^{.65}\left(\frac{\text{RPM In}}{\text{RPM Out}}\right)^{.67}\right|(\text{No. Engines})$$

$$= 228\left|\left(\frac{1,197.5}{8,154}\right)^{.65}\left(\frac{8,154}{5,730}\right)^{.67}\right|(2)$$

$$= 228\left|(.278)(1.264)\right|(2) = 160$$

Gearbox Installation 28

Shafts	
Engine = $.283\|(7.069 - 5.309)(14)(2)\|$ =	14
Compressor = $.283\|(12.57 - 10.18)(70)\|$ =	48
Support Bearings (assume 20% shaft weight) = (62)(.2)	12
Ducts	
To Rotor = (.1)(625)(.025)(π)(20) =	10
In Blades (.1)(36)(.04)(π)(8.4)(2)(2) =	15
(.1)(36)(.04)(π)(7.08)(2)(4) =	26
Cooling System = (.166)(Wt Gearbox) =	27
Override Clutch = (30 lb/engine)(2) =	60
Total Weight for High Speed Jet Flap	400

6.4.1.16 Compressor Weights - Jet-Flap Concept - Only

The estimated weight for this component was read from data supplied by the General Electric Co. Figure 6-10 is a plot of compressor weight versus shaft horsepower.

6.4.1.17 Instrument and Navigational Equipment Weight

a. Heavy Lift Helicopters - All Concepts

The estimated weight of these items for the heavy lift configurations is derived from statistical data taken from the following helicopters:

CH-53A, CH-54B, Sikorsky HLH, Vertol HLH

CH-53A	357 pounds
CH-54B	286

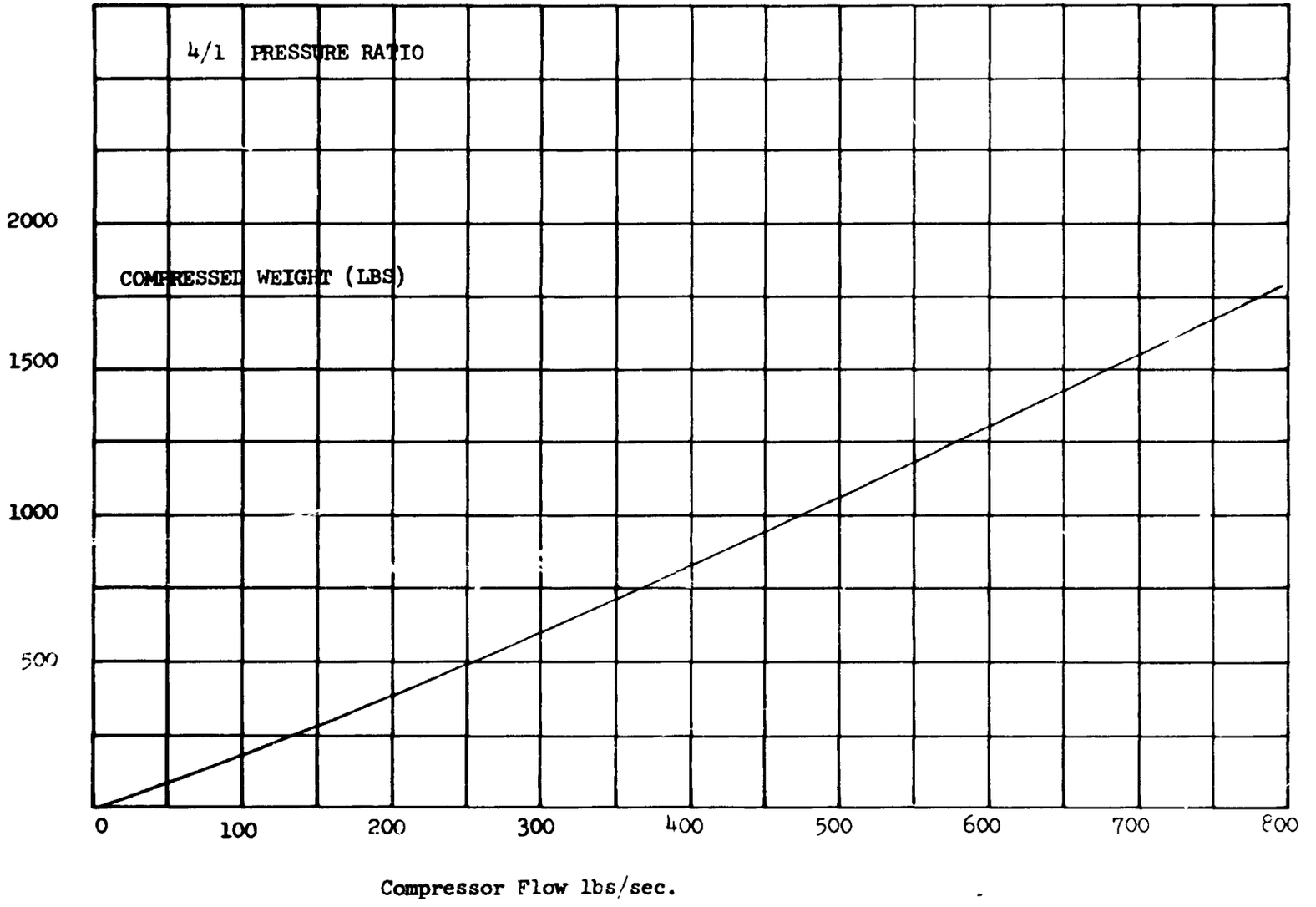

FIGURE 6-10 COMPRESSOR WEIGHT VS COMPRESSOR FLOW JET-FLAP HEAVY LIFT & CONCEPT (GENERAL ELECTRIC DATA)

Sikorsky HLH	277 Pounds
Vertol HLH	248
Average Weight	292 pounds

This average shows the reasonability of the 300 pounds used for the heavy lift configurations.

b. High Speed Helicopters - All Concepts

The estimated weight for these items for the high speed configurations is derived from statistical data taken from the following helicopters:

AH-56A, CH-34A, CH-21C, UH-19D, UH-25B

AH-56A	140 pounds
CH-34A	108
CH-21C	134
UH-19D	70
UH-25B	62
Average Weight	103

This average shows the reasonability of the 96 pounds used for the high speed configurations.

6.4.1.18 Hydraulic and Pneumatic Weights - All Concepts

$$W_{H\&P} = .158817 \left| (W_{DG})^{.489} (N_Z)^{.891} \right|$$

where

W_{DG} = Design Gross Weight

N_Z = Ultimate Load Factor

6.4.1.19 Electrical Weight

a. Heavy Lift Helicopters - All Concepts

The estimated weight for the electrical group for the heavy lift configurations is derived from statistical data taken from the following helicopters:

Vertol HLH, XH-17, Sikorsky HLH, Lockheed HLH

Vertol HLH	995 pounds
XH-17	920
Sikorsky HLH	610
Lockheed HLH	1,402
Average weight	982 pounds

This average shows the reasonability of the 1,000 pounds used for the heavy lift configurations.

b. High Speed Helicopters - All Concepts

The estimated weight for the electrical group for the high speed configurations is derived from the following helicopters:

CH-34A, XV-9A, OH-43D, UH-25B

CH-34A	327 pounds
XV-9A	201
OH-43D	205
UH-25B	192
Average weight	231 pounds

This average shows the reasonability of the 220 pounds used for the high speed configurations.

6.4.1.20 Electronics

a. Heavy Lift Helicopters - All Concepts

The estimated weight for the electronics group for the heavy lift configurations is derived from statistical data taken from the following helicopters:

CH-54A, CH-47A, Sikorsky HLH, Vertol HLH, Lockheed HLH, YH-16A

CH-54A	292 pounds
CH-47A	302
Sikorsky HLH	290
Vertol HLH	280
Lockheed HLH	200
YH-16A	303
Average Weight	278 pounds

This average shows the reasonability of the 290 pounds used for the heavy lift configurations.

b. High Speed Helicopters - All Concepts

The estimated weight for the electronics group for the high speed configurations is derived from statistical data taken from the following helicopters:

CH-34A, CH-21C, CH-46A, CH-37A

CH-34A	269 pounds
CH-21C	247
CH-46A	354
CH-37A	231
Average Weight	275 pounds

This average shows the reasonability of the 274 pounds used for the high speed configurations.

6.4.1.21 Furnishing Weights

a. Heavy Lift Helicopters - All Concepts

The estimated weight for the furnishing group for the heavy lift configurations is derived from statistical data taken from the following helicopters:

HH-52A, CH-47A, YH-16A, UH-25B, UH-1E

HH-52A	216 pounds
CH-47A	810
YH-16A	425
UH-25B	125
UH-1E	217
Average Weight	358 pounds

This average shows the reasonability of the 350 pounds used for the heavy lift configurations.

b. High Speed Helicopters - All Concepts

The estimated weight for the furnishings group for the high speed configurations is derived from statistical data taken from the following helicopters:

AH-56A, SH-3A, CH-21C, UH-19D

AH-56A	255 pounds
SH-3A	405

CH-21C	258 pounds
UH-19D	205
Average Weight	280
Total furnishings used for high speed configuration	280 pounds

6.4.1.22 Heating and Ventilation Weight

a. Heavy Lift Helicopters - All Concepts

The estimated weight for the heating and ventilation group for the heavy lift configurations is derived from statistical data taken from the following helicopters:

Vertol HLH, UH-25B, UH-2B, HH-43B, UH-1E

Vertol HLH	128 pounds
UH-25B	27
UH-2B	81
HH-43B	39
UH-1E	49
Average Weight	65 pounds

This average shows the reasonability of the 50 pounds used for the heavy lift configurations.

b. High Speed Helicopters - All Concepts

The estimated weight for the heating and ventilation group for the high speed configurations is derived from statistical data taken from the following helicopters:

SH-3A, CH-21C, UH-19D, CH-34A

SH-3A	109 pounds
CH-21C	137
UH-19D	77
CH-34A	72
Average Weight	99 pounds

This average shows the reasonability of the 96 pounds used for the high speed configurations.

6.4.2 Sample Weight Calculations

Paragraphs 6.4.2.1 through 6.4.2.24 contain sample calculations showing the use of the estimating methods of Paragraph 6.4.1. The configuration used for this application is the heavy lift jet flap point design. A tabulation of the derived component weights is presented in Table 6-1.

6.4.2.1 Rotor Group

$$\text{Weight Rotor Group} = 0.00956 \left| (W_{DG})^{.238} (N_Z)^{.525} (R_M)^{.417} (S_{BLA})^{.955} (R_{RPM})^{.524} \right| K_1$$

W_{DG}	=	Design Gross Weight	= 82,500
N_Z	=	Ultimate Load Factor	= 3.75
R_M	=	Radius of Main Rotor Blade (Ft)	= 72.5
BLA	=	Total Blade Area (Ft^2)	= 829
RPM	=	Rotor RPM	= 84.5
K_1	=		= 0.916

$$W_{RG} = 0.00956 \left| (82{,}500)^{.238} (3.75)^{.525} (72.5)^{.417} (829)^{.955} (84.5)^{.524} \right| \times 0.916$$

$$= 0.00956 \left| (14.77)(2)(5.96)(602)(10.3) \right| \times 0.916$$

$$= 9{,}583 \text{ pounds}$$

6.4.2.2 Horizontal Tail

$$\text{Weight Horizontal Tail} = 0.3725 \left| (W_{DG})^{.537} (S_{HT})^{.585} \right|$$

W_{DG}	=	Design Gross Weight	= 82,500
S_{HT}	=	Area Horizontal Tail (Ft^2)	= 121

W_{HT} = $0.03725 \left| (82,500)^{.537} (121)^{.585} \right|$

= $0.03725 \left| (436.2)(16.6) \right|$

= 270 pounds

6.4.2.3 Vertical Tail

Weight Vertical Tail = $0.00184 \left| (W_{DG})^{.788} (S_H)^{.794} \right|$

W_{DG} = Design Gross Weight = 82,500

S_{HT} = Area Vertical Tail (Ft^2) = 94

W_{VT} = $0.00184 \left| (82,500)^{.788} (94)^{.794} \right|$

= $0.00184 \left| (7,358)(36.5) \right|$

= 491 pounds

6.4.2.4 Fuselage

Weight Body Group = $0.020445 \left| (W_{DG})^{.62} (N_Z)^{1.49} (S_F)^{.15} (L)^{.19} (D)^{.46} (B)^{.36} \right| \times K_1$

W_{DG} = Design Gross Weight = 82,500

N_Z = Ultimate Load Factor = 3.75

S_F = Wetted Area of Basic Body = 2,500

L = Length of Body = 103

D = Depth of Body = 5.7

B = Width of Body = 11.7

K_1 = = 1.2287

W_{BG} = $0.020445 \left| (82,500)^{.62} (3.75)^{1.49} (2,500)^{.15} (103)^{.19} (5.7)^{.46} (11.7)^{.56} \right| \times 1.2287$

= $0.020445 \left| (1117)(716)(3.24)(2.41)(2.26)(2.42) \right| \times 1.2287$

W_{BG} = 8,584 pounds

6.4.2.5 Landing Gear Group

a. Main Landing Gear

$$\text{Weight Main Landing Gear} = 0.0053 \left| (W_{DL})^{1.01} (N_L)^{1.12} \right| K_1$$

W_{DL} = Design Landing Weight = 82,500

N_L = Ultimate Landing Load Factor = 3.75

K_1 = = 1.26

$$W_{MG} = 0.0053 \times \left| (82,500)^{1.01} (3.75)^{1.12} \right| \times 1.26$$

$$= 0.0053 \times \left| (92,767)(4.4) \right| \times 1.26$$

W_{MG} = 2,739 pounds

b. Nose Landing Gear

$$\text{Weight Nose Landing Gear} = 0.00107 (W_{DL})^{1.193}$$

W_{DL} = Design Landing Weight = 82,500

$$W_{NG} = 0.00107 (82,500)^{1.193}$$

$$= 0.00107 (744,000)$$

W_{NG} = 796 pounds

6.4.2.6 Surface Controls Group

$$\text{Weight Surface Controls} = 0.089815 \left| (W_{DG})^{.736} (N_Z)^{.592} (L_F)^{.203} \right|$$

W_{DG} = Design Gross Weight = 82,500

N_Z = Ultimate Load Factor = 3.75

L_F = Length of Body (Ft) = 103

$$W_{} = 0.089815 \left| (82,500)^{.736} (3.75)^{.592} (103)^{.203} \right|$$

$$= 0.089815 \left| (4,156) (2.18) (2.56) \right|$$

$$= 2,083 \text{ pounds}$$

6.4.2.7 Engine Section

Weight Engine Section = .22 (W_E)

W_E = Total Engine Weight

$W_{ES} = 0.22 (3,440)$

$W_{ES} = 757$ pounds

6.4.2.8 Engine

Engine Weight = 3,400 pounds (Figure 6-9)

This is for two engines and was obtained from Allison.

6.4.2.9 Air Induction System

Weight Air Induction = (1 lb/ft^2)(Length)(Diameter)(π)(Number of Engines)

$W_{AI} = \left| (1)(9)(2.48)(3.14)(2) \right|$

$W_{AI} = 140$ pounds

6.4.2.10 Exhaust System

Exhaust System = (1.25 lb/ft^2)(Length)(Diameter)(π)(Number of Engines)

$W_{ES} = \left| (1.25)(6)(1.8)(3.14)(2) \right|$

$W_{ES} = 85$ pounds

6.4.2.11 Lubricating (Engine) System

Weight Lubricating System = $3.7062 (W_E)^{.52}$

W_E = Total Engine Weight = 3,440

$W_{LS} = 3.7062 (3,440)^{.52}$

$= 3.7062 (69)$

$W_{LS} = 256$ pounds

6.4.2.12 Fuel System

Weight Fuel System = 0.073 (Weight Usable Fuel)

Weight Usable Fuel = 4,270

W_{FS} = 0.073 (4270)

W_{FS} = 312 pounds

6.4.2.13 Engine Controls

Weight Engine Controls = 30 lb/engine

W_{EC} = (30)(2)

W_{EC} = 60 pounds

6.4.2.14 Starting System

Weight Starting System - 30 lb/engine

W_{SS} = (30)(2)

W_{SS} = 60 pounds

6.4.2.15 Drive System

Weight Drive System

W_{DS} = 3,730 pounds (See Paragraph 6.4.1.15 for Derivations)

6.4.2.16 Compressor – For Jet Flap

Weight Compressor

W_C = 510 pounds (Figure 6-10)

6.4.2.17 Instrumentations and Navigational Group

Weight Instrumentation and Navigation Equipment

W_{IN} = 300 pounds (See Paragraph 6.4.1.17)

6.4.2.18 Hydraulic Group

Weight Hydraulic and Pneumatic = $0.158817 \left| (W_{DG})^{.489} (N_Z)^{.891} \right|$

W_{DG} = Design Gross Weight = 82,500

N_Z = Ultimate Load Factor = 3.75

W_{H+P} = 131 pounds

6.4.2.19 Electrical Group

Electrical Weight

W_{ELECT} = 1,000 pounds (See Paragraph 6.4.1.19)

6.4.2.20 Electronics

Electronics Weight

W_{AV} = 290 pounds (See Paragraph 6.4.1.20)

6.4.2.21 Furnishings Group

Furnishings Weight

W_{FURN} = 350 pounds (See Paragraph 6.4.1.21)

6.4.2.22 Heat and Ventilation

Heat and Ventilation

W_{H+V} = 50 pounds (See Paragraph 6.4.1.22)

6.4.2.23 Auxiliary Gear Group

Hoist Equipment

W_{HOIST} = 1,500 pounds

6.4.2.24 Useful Load Components

	JET FLAP		SHAFT DRIVEN	
	HIGH SPEED	HEAVY LIFT	HIGH SPEED	HEAVY LIFT
CREW (2)/(3)	400	600	400	600
FUEL - UNUSABLE	83	43	18	30
FUEL - USABLE	8,284	4,270	1,742	2,992
OIL - ENGINE	20	70	20	70
CARGO	4,000	40,000	4,000	40,000
TOTAL	(12,787)	(44,983)	(6,180)	(43,692)

6.4.3 Weight Estimation Methods and Equations - Part II

Weight estimating methods used in Part I and Part II design studies are the same with one exception. This exception applies to the statistical equation used to derive the fuselage structural weight. In Part I the fuselage structural weight of the High Speed and Heavy Lift Configurations were derived using the same statistical equation only with the K_1 factor changed. In Part II, however, two equations are used to estimate the fuselage structural weight. One is used for the High Speed Configuration (new) and the other (the same one used in Part I) for the Heavy Lift Configurations. In this manner, a better match occurs between the type of fuselage and the statistical data used to estimate the weight of the fuselage component.

The statistical equation used to derive the structural weight of the fuselage for the High Speed Configurations (Part II only) is as follows:

$$Wt_{Body} = 0.031795\ Wt_{DG}^{.45}\ L_B^{1.58} \times D_B^{-.1}\ N_Z^{.45}$$

Where: Wt_{DG} = Design Gross Weight

L_B = Body Length (ft)

D_B = Body Depth (ft)

N_Z = Ultimate Load Factor

6.5 WEIGHT STUDIES

6.5.1 Introduction

This section contains the results of a drive system weight study, and an estimated weight distribution of warm cycle jet-flap configuration.

These studies were conducted in order to form a reasonable technical base from which weight changes caused by conceptual variations can be evaluated. The drive system study consists of designing and conducting a weight analysis of a drive system sized for a payload of: (a) 2 tones, (b) 6 tons, (c) 20 tons, and (d) 50 tons. A more detailed discussion of these designs is presented in Paragraph 6.5.2. Table 6-4 is a weight summary of all the designs. Tables 6-5 through 6-9 contain the detailed weight calculations of each design.

Replacing the cold cycle propulsion arrangement with a warm cycle system results in a heavier design. The heavy lift jet-flap configuration

is used for this study. A more detailed discussion is given in Paragraph 6.5.3 Table 6-10 is a tabulation of the estimated weights of the warm cycle configuration.

6.5.2 Drive System Design and Weight Study

The variations in drive system weight was determined for the high speed shaft-driven configuration with payloads of 2 and 6 tons. Payloads of 20 and 50 tons were analyzed for the heavy lift shaft-driven configuration. For the 20-ton configuration, two concepts were analyzed: (1) totally shaft-driven, and (2) power split of 75 percent from shaft drive and 25 percent from the jet-flap system.

A summary of the weight results of this study are shown in Table 6-4, and a more detailed discussion of the various designs is given in Section 5.0. Component weight calculations are presented in Tables 6-5 through 6-9.

6.5.3 Warm Cycle Jet Flap Study

A parametric weight analysis as described in Paragraph 6.3.1 was conducted for a warm cycle, heavy lift jet-flap configuration. This data was combined with aerodynamic data; from the resulting sizing study, a point design was selected. The warm cycle concept consists of a turbofan engine exhausted directly into the rotor duct.

The estimated weight of the warm cycle configuration is given in Table 6-10.

Table 6-4 Weight Summary Drive System Study

COMPONENT	HOW WEIGHT DERIVED	HEAVY LIFT SHAFT DRIVEN		HEAVY LIFT JET-FLAP	HIGH SPEED HELICOPTER		
		20-TON	50-TON	20-TON 25%-75% SPLIT	2-TON		6-TON
					No. 1	Alternate	
Gears							
Bevel		518	302	-	141	54	5
Spur		134	452	-			
Bull		550	2,160	320			12
Planetary		974	4,653	1,076			98
Ring		907	2,660	615			44
Sun		352	2,368	484			142
Spline				-			
Misc.				148		56	28
Bearing							
Shaft and Bearing		298	-				
Roller		40	-				
Main		212	1,910	498			28
Misc.		100	200	14			
Clutch		-	-	80			
Shafting		1,737	2,790	2,275			66
Housing Case		2,789	3,288	769	54	66	105
Miscellaneous		861	2,130	1,291			79
Rotor Brake				200			
Lub System				150			
Total Drive System		9,472	22,913	7,920	195	176	607

Table 6-5 Gearbox Weight Derivation

High Speed Configuration Two-Ton Payload

COMPONENT	CALCULATIONS	WEIGHT
	Design No. 1	
GEARS		
Dia = 8 In.	Vol = $(\pi)(r^2)(t)$	
No. = 4	Vol = $3.14 \left\|(4)^2(2.5)\right\| = 126$ in.^{3}	
t = 2.5 in.		
	Wt = $\left\|126 - (0.3 \times 126)\right\|$ (4) (0.283)	
	Wt = $\left\|'88 \text{ in.}^3) (4) (0.283)\right\|$	100.00
Dia = 11.4 In.	Vol = $(\pi)(r^2)(t)$	
No. = 1	Vol = $3.14 \left\|(5.7)^2 (2)\right\| = 204$ in.^{3}	
t = 2 in.		
	Wt = $\left\|204 - (.3)(204)\right\|$ (0.283)	
	Wt = (143 in.^{3}) (0.283)	41.0
HOUSING		
	Wt = $(\pi)(4)^2(2)$ + (14 x 30 x 1.0)	
MAGN.	+ (5 x 26 x 1.0) + $\left\|(100)(5)(0.5)\right\|$	
	(0.063)	54.0
	TOTAL WEIGHT PER GEARBOX	(195.0)

Table 6-5 Gearbox Weight Derivation

High Speed Configuration Two-Ton Payload (Continued)

COMPONENT	CALCULATIONS	WEIGHT
	ALTERNATE DESIGN	
GEARS		
Dia = 13.2 In.	$Vol = (\pi)(R)^2(t)$	
No. = 2	$= (\pi)(6.6)^2(1.0)(2) = 272\ In.^3$	
t = 1.0 In.		
	$Wt = \lvert 272 - (.3)(272) \rvert (0.283)$	
	$= \lvert (190\ in.^3)\ (0.283) \rvert$	54.0
Dia = 18.8 In.	$Vol = (\pi)(R)^2(t)$	
No. = 1	$= (\pi)(9.4)^2(1)(1) = 280\ in.^3$	
t = 1.0 In.		
	$Wt = \lvert 280 - (.3)(280) \rvert (0.283)$	
	$= \lvert (196\ in.^3)\ (0.283) \rvert$	56.0
HOUSING		
MAGN.	$Wt = (6.6)^2(1) + (32)(20)(1)$	
	$+ \lvert (109)(5)(.5) \rvert (0.063)$	66.0
	TOTAL WEIGHT PER GEARBOX	(176.0)

Table 6-6 Gearbox Weight Derivations
High Speed Configuration 6-Ton Payload

COMPONENT	CALCULATIONS	WEIGHT POUNDS
HOUSING PWR. GEAR (2) Req.	|(0.6 x 0.8 x 2π x 2.8) + (2.8 x .32 x 2π x 2.6)| x 0.063 (1.5 lb x 2)	3.0
	|(0.4 x 6.8 x 2π x 12.8) (0.3 x 4 x 2π x 4.4) + (0.2 x 2.4 x 2π x 3.6)| x 0.063	17.0
	|(2.4 x 0.36 x 2π x 11.8) + (0.36 x 12 x 2π x [illegible]| x 0.063	23.0
	|(0.36 x 4 x 2π x 9.6) + (.8 x 1.6 x 2π x 10)| x 0.063	11.0
	|(3.6 x 1.6 x 2π x 11.6) +(5.2 x .4 x 2π x 7.6) + (.8 x 2.4 x 2π x 5)| x 0.063	37.0
GEAR BULL		
Dia = 11.2 in.	(1.8 x .96 x 2π x 5.6 x .7) x 0.283	12.0
PINIONS-IN/OUT	(0.8 x 1.0 x 2π x 1.76 x .7) x 0.283	3.0
(2) Req		
GEAR-LOWER	|(0.4 x 4.4 x 2π x 4.4) + (0.8 x .24 x 2π x 4.2)	
SUN (1) Req	+ (6 x 0.2 x 2π x 3.8)| x 0.283	23.0
SHAFT-INPUT		
PINION (2) Req	|(0.32 x 8.0 x 2π x 0.88) +(2.8 x 0.2 x 2π x 2.0)	
	+ (0.6 x 1.0 x 2π x 3.[illegible])| x 0.283	20.0
GEAR-PLANET		
LWR (6) Req	|(2.0 x 0.6 x 2π x 2.0) + (0.52 x 0.6 x 2π x 1.44)| x 0.283	30.0
SHAFT-ROTOR	|(5.2 x 0.6 x 2π x 3.36) +(0.48 + 0.28) x 0.5 x 2π x 2.88)| x 0.283	48.0
MAIN	(12 x 0.2 x 2π x 3.2) x 0.283	18.0
BEARING-LOWER SHAFT	|(0.72 x 0.6 x 2π x 3.2) + (0.4 x 0.88 x 2π x 3.0)| x 0.283	4.0

Table 6-6 Gearbox Weight Derivations
High Speed Configuration 6-Ton Payload (Contd)

COMPONENT	CALCULATIONS	WEIGHT POUNDS
BEARING-UPPER SHAFT	(1.0 x 1.2 x 2π x 4.16) x 0.283	9.0
SEALS-UPPER	(0.6 x 0.6 x 2π x 3.6) x 0.028	1.0
LOWER	(0.6 x 0.6 x 2π x 3.6) x 0.028	1.0
BEARING RET.	(0.8 x 0.8 x 2π x 1.6) x 0.283	4.0
(2) Req	(0.6 x 1.08 x 2π x 1.28) x 0.283	3.0
GEAR UPPER PINION-IDLER (2) Req	(1.2 x 0.8 x 2π x 0.6) x 0.063	1.0
BEARINGS	(0.6 x 1.08 x 2π x 5.3) x 0.283	6.0
GEAR CTR SUN	|(0.6 x 2.0 x 2π x 4.4) + (2.6 x 0.32 x 2π x 4.24) + (1.4 x 0.4 x 2π x 5.0) + (1.6 x 0.4 x 2π x 5.6) + (2.0 x 1.6 x 2π x 7.0 x 0.6)| x 0.283	49.0
GEAR RING		
LOWER	(1.4 x .6 x 2π x 9.6) x 0.283	14.0
UPPER	(2.5 x .72 x 2π x 9.6) x 0.283	30.0
GEAR SUN	|(0.6 x 3 x 2π x 4) + (1.8 x 0.4 x 2π x 5.2)	
UPPER	+ (2.8 x 2.2 x 2π x 6.8 x 0.7)| x 0.283	70.0
IDLER-LWR (2) Req	(2.6 x 0.8 x 2π x 1.28) x 0.062 x 2	2.0
IDLER-BRG	(0.56 x 4.8 x 2π x 4.2) x 0.283	2.0
HOUSING-PWR GEAR (2) Req	(3.2 x 1.2 x 2π x 1.6 x 0.6) x 0.283 x 2	14.0
GEAR PWR BEVEL (2) Req	|(0.2 x 2.0 x 2π x 1.0) + (0.8 x 0.4 x 2π x 1.0) + (0.8 x 1.0 x 0.5 x 2π x 1.5)| x 0.283 x 2	5.0
GEARS-UPPER PLANET (8) Req	|(3.0 x 0.6 x 2π x 2.0) +(0.6 x 1.2 x 2π x 1.6)| x 0.283 x 8	68.0
	HARDWARE AND MISC (15%)	79.0
	TOTAL WEIGHT PER GEARBOX	607.0

Table 6-8 Gearbox Weight Derivation Jet Flap Concept
20-Ton Payload 25% - 75% Power Split (Contd)

COMPONENT	CALCULATIONS	WEIGHT POUNDS
OVERRUNNING CLUTCH (2 Req)		80
INPUT GEARS (2 Req)	From Engines $W = \left\|(7)(4)(0.3)(\pi) + 4(1)(3)(2\pi)\right\|\ (0.283)$ = 29 lb each	58
BEARINGS AND RETAINERS (2 Req)		10
GEAR TO BULL GEAR (2 Req)	$W = \left\|(0.4)(10)(4.5)(\pi) + (0.4)(6)(12)(\pi) + (2)(1)(18)(\pi)\right\|\ 0.283 \times 1.10 = 81$ lb	162
BEARING SET (2 Req)	OD = 5.4 ID = 3.7 N = 2.5 $W = 0.18(5.4^2 - 3.7^2)(2.5) = 7$ lb	14
SUPPORT MAG (1 Req)	$W = (15.5)(36)(\pi)(0.5)(0.065)(1.10) = 63$ lb	63
SUPPORT BEARING (1 Req)	OD = 20 ID = 17.5 N = 1 $W = 0.18(20^2 - 17.5^2)(1) = 17$ lb	17
SPLIT GEAR SET (2 Req)	$W = (3.0)(1.8)(7.6)(\pi)(0.283)(1.10) = 40$ lb	80
BEARING SUPT. TO GEAR (2 Req)	OD = 6.9 ID = 4.5 N = 1 $W = 0.18(6.9^2 - 4.5^2)(1) = 5$ lb	10
SLEEVE (2 Req)	$W = (5.5)(5.0)(0.5)(\pi)(0.283) = 12$ lb	24
BULL GEAR (1 Req)	$W = (2)(3)(27)(\pi)(0.283)(1.10) = 158$ lb	158
SUNGEAR-LOWER (1 Req)	$W = (19)(0.5)(\pi)(20)(0.283)(1.10) = 186$ lb	186
SUNGEAR BEARING (1 Req)	OD = 23.5 OD = 21 N = 2.1 $W = (0.18)(23.5^2 - 21.0^2)(2.1) = 43$ lb	43

Table 6-8 Gearbox Weight Derivation Jet Flap Concept
20-Ton Payload 25% - 75% Power Split (Contd)

COMPONENT	CALCULATIONS	WEIGHT POUNDS
UPPER PLANETS	90.1 lb each	721
(8 Req)	Inner Race (1)	
	$W = (2.5)(0.8)(4.5)(\pi)(1.10)(0.283) = 8.8$	
	Lower Retainer (1)	
	$W = (4.5)^2(0.5)(0.7854)(0.283) = 2.3$	
	Gear (1)	
	$W = (4)(2)(9)(\pi)(1.10)(0.283) = 70.4$	
	Bearing (1)	
	$W = 0.18(7^2 - 5^2)(2) = 8.6$	
ROTOR BRAKE (1 Req)	Allowance	200
ACCESSORY DRIVE	Allowance	500
SECTION (1 Req)		
TAIL ROTOR DRIVE	Allowance	500
SECTION (1 Req)		
LUB SYSTEM		150
	Oil Pumps 50	
	Cooler Inst. 75	
	Lines and Fitting 25	
CENTER DUCT/SUPPORT (1 Req)	$W = \pi(15)(87)(0.25)(0.101) = 103$	
	Misc. 10%	720
	TOTAL	(7920)
	Use 8,000 pounds	

Table 6-9 Gearbox Weight Derivation
Heavy Lift Configuration 50-Ton Payload (Contd)

COMPONENT	CALCULATION	WEIGHT POUNDS
LOWER CASE	$(7 \times 1.5)\ 2\pi\ (38)\ (0.064)$	160
	$(7 \times 2)\ 2\pi\ (35)\ (0.064)$	197
	$(7 \times 1.5)\ 2\pi\ (33)\ (0.064)$	139
	$(7 \times 2)\ 2\pi\ (30)\ (0.064)$	121
	$(3 \times 5)\ 2\pi\ (27)\ (0.064)$	163
	$(5 \times 1.5)\ 2\pi\ (30)\ (0.064)$	90
	$(4 \times 4)\ 2\pi\ (34)\ (0.064)$	218
	$(6 \times 2)\ 2\pi\ (35)\ (0.064)$	169
	$(3 \times 4)\ 2\pi\ (34)\ (0.064)$	164
LOWER MAIN BRNG (1 Req) R = 15 in.	Cross Section $2 \times 3 = 6$ in.^{2} $2\pi(15)(6)(0.283) =$	160
LOWER SEAL HOUSING (POWER) BEVEL GEAR R = 7 in. (4 Req)	Cross Section $1 \times 5 = 5$ in.^{2} $2\pi(7)(5)(0.064) \times 4 =$	56
LOWER SEAL (POWER BEVEL GEAR) R = 5 in. (4 Req)	Cross Section $2.5 \times 3 = 7.5$ in.^{2} $2\pi(5)(7.5)(0.05)(4) =$	47
MISCELLANEOUS BRINGS, HOUSING, ETC.		200
SHAFTING	Wt/Linear Inch = Density (lb/in.^{3}) $= \pi/4\ (D_o^2 - D_i^2)$ $= 0.283\ (0.785)(22^2 - 20^2)100$	
LENGTH = 100 in.	$0.283\ (0.785)(84)(100) =$	1,870
	Add 10%	2,083
	Total 50-ton Drive System Weight	22,913

TABLE 6-10 HELICOPTER WEIGHT ANALYSIS APRIL 5, 1968 POINT DESIGN
SEA LEVEL STANDARD TAKEOFF THRST/WT = 1.1,0 DEGREES F
WARM CYCLE HEAVY LIFT JET FLAP HELICOPTER THREE BLADES

1	Main Rotor Blade Assembly	13,116
2	Main Rotor Hub and Hinge	0
3	Tail Rotor	0
4	Horizontal Tail	268
5	Vertical Tail	506
6	Basic Body	8,421
7	Booms/Other Structure	0/0
9	Main Landing Gear	2,711
10	Nose Landing Gear	780
11	Surface Controls	2,083
12	Engine Section	436
13	Other Structure	0
14	Total Structure	(28,321)
15	Engine	1,980
16	Tip Burners	0
17	Air Induction System	614
18	Exhaust System	2,275
19	Cooling System	0
20	Lubricating System	192
21	Fuel System - Tanks and Plumbing	349
22	Fuel System - Other	0
23	Engine Controls	60
24	Starting System	60
25	Drive System	0
26	Compressor	0
27	Total Propulsion	(5,530)
28	Auxiliary Power Plant	0
29	Instrument + Navigation Equipment	300
30	Hydraulic and Pneumatic	130
31	Electrical/Electronics	1,000/290
33	Armament	0
34	Furnishings	350
35	Air-conditioning + Anti-icing	50
36	Auxiliary Gear	1,500
37	Other Fixed Equipment	0
38	Mfg. Variations (Contingency)	0
39	Total Fixed Equipment	(3,620)
40	Total Weight Empty	(37,472)
41	Crew/Passengers *	600/0
43	Fuel - Unusable/Internal *	48/4,810
45	Oil - Unusable/Engine	0/70
47	Cargo Handling*/Cargo*	0/40,000
49	Ammunition*/Other*	0/0
51	Guns/Other Useful Load	0/0
53	Total Useful Load	(45,528)
54	Gross Takeoff Weight	(83,000)

*Excluded from Operating Weight Empty

7.0 REFERENCES

1. Study of Future Mission Requirements for High Speed and Heavy Lift, LTVAC Report No. 2-55400/7R-50424, 8 August 1967

2. Tanner, Watson H., Charts for Estimates Rotary Wing Performance in Hover and at High Forward Speeds, NASA CR-114, Washington, D.C., November 1964

3. "Two Dimensional Jet-Flap Test Results," ONERA, Unpublished, January 1959

4. McCormick, Barnes W., Aerodynamics of V/STOL Flight, Academic Press Inc., New York, 1967

5. Spence, D. A., "The Lift of a Thin, Jet-Flapped Wing," Proc. Roy. Soc., A238,46-68, 1956

6. MIL-HDBIC-5 "Metallic Materials and Elements for Flight Vehicle Structures" dated 24 July 1967

7. A. A. Nikolsky "Helicopter Analysis," Published by John Wiley & Sons, Inc. dated 1951

8. Power Transmission Studies for Shaft-Driven Heavy Lift Helicopters, USAAVLABS Technical Report 66-40, Sikorsky Aircraft, U. S. Army Material Laboratories, Fort Eustis, Virginia, October 1965

10. Parametric Analysis and Preliminary Design of a Shaft-Driven Rotor System for a Heavy Lift Helicopter, USAAVLABS Technical Report 66-56, Sikorsky Aircraft, U. S. Army Material Laboratories, Fort Eustis, Virginia, February 1967

Table 6-7. Gearbox Weight Derivation
Heavy Lift Shaft Driven Concept 20-Ton Payload

COMPONENT	CALCULATION	WEIGHT POUNDS
POWER BEVEL GEAR	$W_{GSB} = 138.487\ (SHP/RPM)^{1.21} = 138.487 \left(\frac{8500}{3000}\right)^{1.21}$	
SHAFT AND BEARINGS (2 Req)	= 149 2 x 149 =	298
POWER BEVEL GEAR CASE (2 Req)	Use .42857 (Gear, Shaft and Bearing Wt) W_e = .42857 (298) =	128
BEVEL GEAR SHAFT	$W_{GSE} = 138.487 \left(\frac{8500}{3200}\right)^{1.21} = 455$	
	2 x 455	910
UPPER BEVEL GEAR CASE (2 Req)	W_e = .42857 (910) =	390
SPUR GEAR (2 Req) R=6 in. h=3 in.	Solid Gear = $\pi R^2 h = \pi(6)^2\ 3 = 338$ in.^{3} 338 - 30% (338) = 236 in.^{3} 236 x 0.283 = 67 67 x 2	134
BULL GEAR (1 Req) R=21 in. h=2 in.	Solid Gear = $\pi(21)^2\ 2 = 2780$ 2780 - 0.30 (2780) = 2780 - 834 = 1946 in.^{3} 1946 x 0.283 =	550
LOWER BEARING R=11 in. (1 Req)	Cross Section 3 x 2 = 6 in.^{2} 6 x 2π x 0.283 =	118
LOWER SUN GEAR R=9.5 in. (1 Req)	Cross Section 0.9 x 10 = 9 in.^{2} Wt. = 2π (9.5)(9)(0.283) =	152
PLANETARY GEAR LOWER (6 Req) R=5 in. h=4 in.	Solid Vol = πR^2 h = $\pi(5)^2$ 4 = 314 in.^{3} 314 - 0.30 (314) = 220 (0.283) (6) =	374
RING GEAR (LWR) (1 Req) R=21 in.	Cross Section = 4 x 2.5 = 10 in.^{3} 2π (21)(10)(0.283) =	374
ROLLER BRNG (LWR PLANETARY GEAR R=10 in. (1 Req)	Cross Section = 2.25 in.^{2} Wt. = 2π (10) (2.25)(0.283)	40
CASE (LWR PLANETARY GEAR) R=15 in. (2 Req)	Cross Section = 8 x 1 = 8 in.^{2} Wt. = 2π (15)(8)(0.283) = 214 214 x 2	428

Table 6-7 Gearbox Weight Derivation
Heavy Lift Shaft Driven Concept 20-Ton Payload (Contd)

COMPONENT	CALCULATION	WEIGHT POUNDS
HOUSING BETWEEN RING GEAR R=24 in. h=5 in. (1 Req)	Cross Section = 0.8 x 6 = 5 in.^{2} Wt. = 2π (24)(5)(0.283) =	223
UPPER PLANETARY GEARS R=5.5 in. h=4 in. (8 Req)	Solid = $\pi R^2 h = \pi(5.5)^2\ 4 = 380$ in.^{3} $\lvert 380 - 0.30\ (380) \rvert$ = 266 in.^{3} 266 x 0.283 x 8 =	600
CASE (UPPER PLANETARY) (2 Req)	Wt. = 2π (18)(9) x 0.283 x 2 =	576
UPPER RING GEAR R=25 in. (1 Req)	Cross Section = 3 x 4 = 12 in.^{2} Wt. = 2π (25)(12)(0.283) =	533
UPPER SUN GEAR R=12.5 in. (1 Req)	Cross Section = 9 x 1 = 9 in.^{2} Wt. = 2π (12.5)(9)(0.283) =	200
UPPER SPLINE CASE R=12.5 in. (1 Req)	Cross Section (3 x 1) + (6 x 1) = 9 in.^{2} Wt. = 2π (12.5)(9)(0.283) =	200
UPPER MAIN BEARING R=11 in. (1 Req)	Cross Section Bearings 1.5 x 3.2 = 4.8 in.^{2} Wt. = 2π (11)(4.8)(0.283) =	94
LOWER BRNG CASE R=11 in. (1 Req)	Cross Section = (6 x 1) + (2 x 1) + (3 x 3) = 17 in.^{2} Wt. = 2π (11)(17)(0.283) =	332
UPPER CASE (OUTSIDE) R=18 in. (1 Req)	Cross Section = (1.5 x 22) = 33 in.^{2} 2π18 (33)(0.101) =	377
CENTER CASE OUTSIDE R=25 in.	Cross Section = (3 x 1) + (4.5 x 1) + (10 x 1) = 17.5 Wt. = 2π (25)(17.5)(0.101) =	277
LWR CASE (OUTSIDE) R=30 in.	Cross Section = (12 x 0.6) = 7.2 in^2 and (7 x 1) + 2 (2 x 1) = 11 in.^{2} Wt. = 2π (30)(7.2)(0.101) = Wt. = 2π (34)(11)(0.101) =	138 238
SHAFT (LOWER) R_o = 9.6 in. R_1 = 9.0 in. = 30 in.	Vol = $\pi(R_o^2 - R_1^2)$ $\pi\lvert(9.6)^2 - (9.0)^2\rvert$ 30 = 1040 in.^{2} Wt. = 1040 (0.283) =	292
SHAFT (UPPER) R_o = 12 in. R_1 = 11.5 in. = 50 in.	Vol = $\pi(R_o^2 - R_1^2)$ $\pi\lvert(12)^2 - (11.5)^2\rvert$ 50 = 600π Wt. = (π)(600)(0.283) =	535
MISCELLANEOUS BRNGS	Estimated	100
	Add 10%	861
	TOTAL WEIGHT PER GEARBOX	9472

Table 6-8 : Gearbox Weight Derivation Jet Flap Concept
20-Ton Payload 25% - 75% Power Split

COMPONENT	CALCULATIONS	WEIGHT POUNDS
HOUSING (1 Req)	Upper - Mag.	346
	$V = \{\|(22)(1)(16.5) + (7)(1)(22) + (1.5)(2.5)(25.5)\| 2\pi + 3 \|(8)(2)(2) + (0.5)(15)(22)\|\} 1.2 = 1.2\ (3849.24 + 591)$	
	$= 5{,}328\ in.^3$	
	$W = 346$ lb	
	Lower - Mag. - outer	369
	$V = \|(2)(0.75)(25.5) + (4.5)(0.5)(25) + (3.5)(1.5)(23) + (2.5)(0.5)(25) + (4.5)(0.5)(26) + (2.0)(1)(26.5) + (4.0)(0.5)(29) + (13.5)(0.5)(30) + (1)(1)(30.5) + 2\ (6.5)(0.5)(5)\| (2\pi)(1.2) + (11)(17)(0.5)(2\pi) = 5{,}672\ in.^3$	
	$W = 369$ lb	
	Lower - Mag. - inner	29
	$V = (10)(0.5)(12)(2)(\pi)(1.2) = 452\ in.^3$	
	$W = 29$ lb	
	Sump Cover - Alum	25
	$V = (20)(2\pi)(20)(0.10)(0.101) =$	
	$W = 25$ lb	

Table 6-8 Gearbox Weight Derivation Jet Flap Concept
20-Ton Payload 25% - 75% Power Split (Contd)

COMPONENT	CALCULATIONS	WEIGHT POUNDS
LOWER BEARING (1 Req)		34
	OD = 20 ID = 16.5 Width = 1.5	
	$W = 0.18\ (20^2 - 16.5^2)(1.5) = 34$ lb	
	Inner Support	28
	$W = (4)(0.5)(8)(2\pi)(0.283) = 28$ lb	
	Lower Support	19
	$W = (3.5)(0.3)(10)(2\pi)(0.283) = 19$ lb	
	Retainer Nut	15
	$W = (1.0)(1.0)(8.5)(2\pi)(0.283) = 15$ lb	
UPPER BEARING (1 Req)		188
	OD = 32.8 ID = 26.5 Width = 2.8	
	$W = 0.18\ (32.8^2 - 26.5^2)(2.8) = 188$ lb	
	Upper Retainer	6
	$W = (0.5)^2\ (13.5)(2\pi)(0.283) = 6$ lb	
	Lower Retainer	
	$W = (2.0)(0.3)(16.5)(2\pi)(0.283) = 18$ lb	18
UPPER BEARING (1 Req)		22
	OD = 29 ID = 26.5 Width = 0.9	
	$W = 0.18\ (29^2 - 26.5^2)(0.9) = 22$ lb	
BEARING SUPPORT (1 Req)		27
	$W = (4)(0.25)(15)(2\pi)(0.283) = 27$ lb	
SEAL (1 Req)	Seal	4
	$W = (1)(1)(13.2)(2\pi)(0.050) = 4$ lb	
ROTOR SHAFT		
	$W = (\pi)(72)(25)(0.9) + 2(7)(1.5)(18)(\pi)(0.283)$	1,775
	$= 1,775$ lb	

Table 6-8 Gearbox Weight Derivation Jet Flap Concept
20-Ton Payload 25% - 75% Power Split (Contd)

COMPONENT	CALCULATIONS	WEIGHT POUNDS
RING GEAR (1 Req)	$V = \left\{(2)(1)(19.5) + (4)(0.5)(22) + (4.2)(6)(24.5) + 2(1.5)(0.8)(25.2) + (3.5)(1.3)(24)\right\}(2\pi)(1.10) = 2{,}172$ in.^{3}	615
	$W = 615$ lb	
UPPER SUN GEAR (1 Req)	$W = \left\{(4.0)(2.2)(11.8) + (2)(1)(11.5) + (3)(0.5)(12.5)\right\}(2\pi)(0.283)(1.10) = 280$ lb	280
UPPER SUN GEAR BEARING (1 Req)	Upper Sun Gear Bearing OD = 20.8 ID = 18.2 Width = 1.0 $W = 0.18(20.8^2 - 18.2^2)(1.0) = 18$ lb	18
UPPER BEARING SUPPORT (1 Req)	Upper Bearing Support $W = (10)(0.4)(10)(2\pi)(1.10)(0.283) = 78$ lb	78
RETAINER (1 Req)	Retainers	20
LOWER PLANETS (8 Req)	Lower Planets 44.4 lb each Center Plates (2) $W = 0.7854(5)^2(0.8)(0.283) = 4.4$ Inner Race (1) $W = (3)(0.9)(4)(\pi)(1.10)(0.283) = 10.6$ Gear (1) $W = (2.2)(1.0)(8)(\pi)(1.10)(0.283) = 17.2$ Bearing (1) OD = 7 ID = 5 Width = 1.8 $W = 0.18(7^2 - 5^2)(1.8) = 7.8$	355

Table 6-9 Gearbox Weight Derivation
Heavy Lift Configuration 50-Ton Payload

COMPONENT	CALCULATION	WEIGHT POUNDS
BEVEL GEAR, SHAFT AND BEARING (4 Req)	$W_{GSB} = 138.487(SHP/RPM)^{1.21}$ $= 138.487\left(\frac{11500}{19000}\right)^{1.21} = 75.5$ 75.5 x 4 =	302
BEVEL GEAR, SHAFT AND BEARING (4 Req)	$W_{GSB} = 138.487\left(\frac{11500}{7600}\right)^{1.21} = 230$ 4 x 230 =	920
SPUR GEAR (4 Req) R = 6 in. L = 5.1 in.	Diameter = 12 inches Solid Gear = $\pi R^2 H = \pi(6)^2(5.1) = 575$ in.^{3} Cutouts - 30% 575 - 575 (0.30) = 402 in.^{3} 402 x 0.283 x 4 =	452
SPUR GEAR BEARINGS (8 Req) R = 6 in.	Cross Section Area 6 in.^{2} $2\pi 5.5(6)$ 0.283 x 8 =	470
BULL GEAR (1 Req) R = 21 in. h = 8 in.	Vol. = $\pi R^2 h = 3.14(21)^2(8) = 11,050$ 11,050 - 0.30 (11,050) = 7,635 in.^{3} 7,635 x 0.283 =	2,160
BULL GEAR BEARING (1 Req) R = 11 in.	Cross Section Area = 7.2 in.^{2} R = 11 in. 7.2 x 2π (11) x -.283 =	141
SUN GEAR-LOWER (1 Req) R = 12 in.	Cross Section (5 x 1.5) + (6 x 3) = 25 in.^{2} 25 x 2π x 12 x 0.283 =	530
PLANETARY GEAR (LOWER) (8 Req) R = 5.7 in. h = 5 in.	Wt. = $\pi(5.7)^2 5$ x 0.283 x (8) - .30%	705
RING GEAR LOWER R = 24.5 in.	Cross Section 5 x 3 = 15 in.^{2} (15) $2\pi(24.5)(0.283)$ =	655
SUNGEAR LOWER BRNG (6 Req)	Cross Section 2 x 3 = 6 in.^{2} (6) $2\pi(11)(0.283)$ =	117
SUNGEAR (CENTER) (1 Req) R = 18 in.	Cross Section = (2x1.5) + (3x1) + (3x6) = 24 in.^{2} $2\pi(18)(24)0.283$ =	765
BRNG. (SUNGEAR CENTER) R = 14 in. (1 Req)	Cross Section = 3.17 x 3 = 9.5 in.^{2} $2\pi(14)(9.5)(0.283)$ =	235

Table 6-9 ; Gearbox Weight Derivation
Heavy Lift Configuration 50-Ton Payload (Contd)

COMPONENT	CALCULATION	WEIGHT POUNDS
PLANETARY GEAR (CENTER) R = 7.1 in. (8 Req) h = 6 in.	$\pi R^2 h$ Cutouts = 30% $\pi(7.1)^2(6)(0.283)$ 8-30% =	1,498
RING GEAR CENTER (1 Req)	Cross Section 6 x 2.5 = 15 $in.^2$ $2\pi(31)(15)(0.283)$ =	830
SUN GEAR (UPPER) R = 18.5 in.	Cross Section (2 x 2) + (1 x 4) + (3 x 7) = 29 $in.^2$ $2\pi(18.5)(29)(0.283)$ =	956
PLANETARY UPPER R = 8.4 in. L = 7 in. (8 Req)	$\pi(8.4)^2(7)0.283$ x 8-30% =	2,450
BRNG, SUN GEAR (UPPER) R = 14 in. (1 Req)	(2 x 2) + (3 x 1) + (2 x 1) = 29 $in.^2$ $2\pi(14)(9)(0.283)$ =	224
SPLINE GEAR CASE (1 Req)	Cross Section 4 x 2 = 8 $in.^2$ 4.5 x 1.5 = 6.8 $in.^2$ 2.5 x 9 = 23 $in.^2$	
R = 20 in.	$2\pi(20)(8)(0.283)$ =	286
R = 17 in.	$2\pi(17)(6.8)(0.283)$ =	206
R = 13.5 in.	$2\pi(13.5)(23)(0.283)$ =	553
TOP MAIN BRNG (1 Req) R = 25.5 in.	Cross Section 3 x 5 = 15 $in.^2$ $2\pi(25.5)(15)(0.283)$	680
RING GEAR (TOP) (1 Req) R = 31.5 in.	Cross Section 7 x 3 = 21 $in.^2$ $2\pi(31.5)(21)(0.283)$ =	1,175
CASE (UPPER)	Cross Section 3 x 10 in.^{2} 26 x 1.5 = 39 $in.^2$ 5 x 1.5 = 8 $in.^2$	
	$2\pi(16)(30)(0.064)$ =	193
	$2\pi(28)(39)(0.064)$ =	438
	$2\pi(41)(8)(0.064)$ =	135

APPENDIX A

PERFORMANCE COMPUTATIONAL METHODS

APPENDIX A

PERFORMANCE COMPUTATIONAL METHODS

LTV has developed five computer programs for estimating the performance of rotorcraft, both jet-flapped and shaft-driven. The computational methods for four of them are based on an approximate solution to the jet-flap rotor developed by Dr. B. W. McCormick for LTVAC during the summers of 1966 and 1967. The solution is described in Appendix B. The fifth program, designated LS 0317, is a general rotor loads and performance program developed recently. Program LS 0317 was not used directly in the present contract but indirectly it was used to provide check and trend data. A description of it is included for information. It is believed that the program will provide a powerful tool for future jet-flap and other rotor design programs. All five computer programs are described below.

LTVAC Rotor Performance Program No. 1. This program was formulated to compare estimated jet-flap rotor performance with experimental data. The approach taken is to simulate a continuous jet-flap rotor by an equivalent jet-flap wing free to flap on the end of a rotating rod. The geometric characteristics of the rotor system, i.e., solidity, blade twist, diameter, etc., are input with section lift and drag data for a representative airfoil section. Input operating conditions include the average flap angle, δ_0, and the flap excursion, δ_2, as well as advance ratio, rotor shaft angle, pressure ratio, and tipspeed. Through an iterative process, the rotor lift force, propulsive force, power requirements, and flapping angles are determined to meet additional input conditions. Also, an azimuth survey can be read out which shows local values of blowing coefficient, blade angle of attack, flap angle, section lift coeffiecient, and

Mach number. Thus, the occurrence of blade stall or compressibility effects beyond which the theory would not be expected to hold can be determined. On the basis of comparisons with test data acquired from the First Series Ames Wind Tunnel Tests of the Dorand DH 2011 rotor, illustrated by Figures A-1 and A-2, it is concluded that the general method developed is capable of predicting the performance of a jet-flap rotor reasonably well.

LTVAC Rotor Performance Program No. 2. This program is essentially the reverse of Program No. 1 in that the lift, drag, and geometric characteristics of the rotor are input, and the flap deflection for trim is calculated. This program is used for determining the detailed performance of a specific helicopter as a function of the flight condition. An azimuth survey of the local conditions on the blade at the 85% radius station is presented in Figure A-3 for the high-speed jet-flapped helicopter point design of Paragraph 7.2.2 of the basic report. Since the estimated maximum lift coefficient at the cruise speed of 200 knots is not exceeded, it is assumed that the stall problem is minimal. An additional feature of this program is illustrated in Figures 3-14 and 3-15 of the basic report showing required control angles versus airspeed for the high-speed jet-flapped helicopter.

LTVAC Rotor Performance Program No. 3. Program No. 3 is a simplified form of No. 2. Power requirements in hover and forward flight are calculated for both the shaft-driven and jet-flap parametric studies with gross weight, equivalent flat plate drag area, disc loading, tipspeed, $\overline{C}_{L_s}$, and pressure ratio as inputs. The profile, parasite, and induced powers are computed for a shaft-driven rotor at the desired operating conditions. To produce this total equivalent shaft horsepower, the blowing requirement for a jet-flapped rotor is then computed.

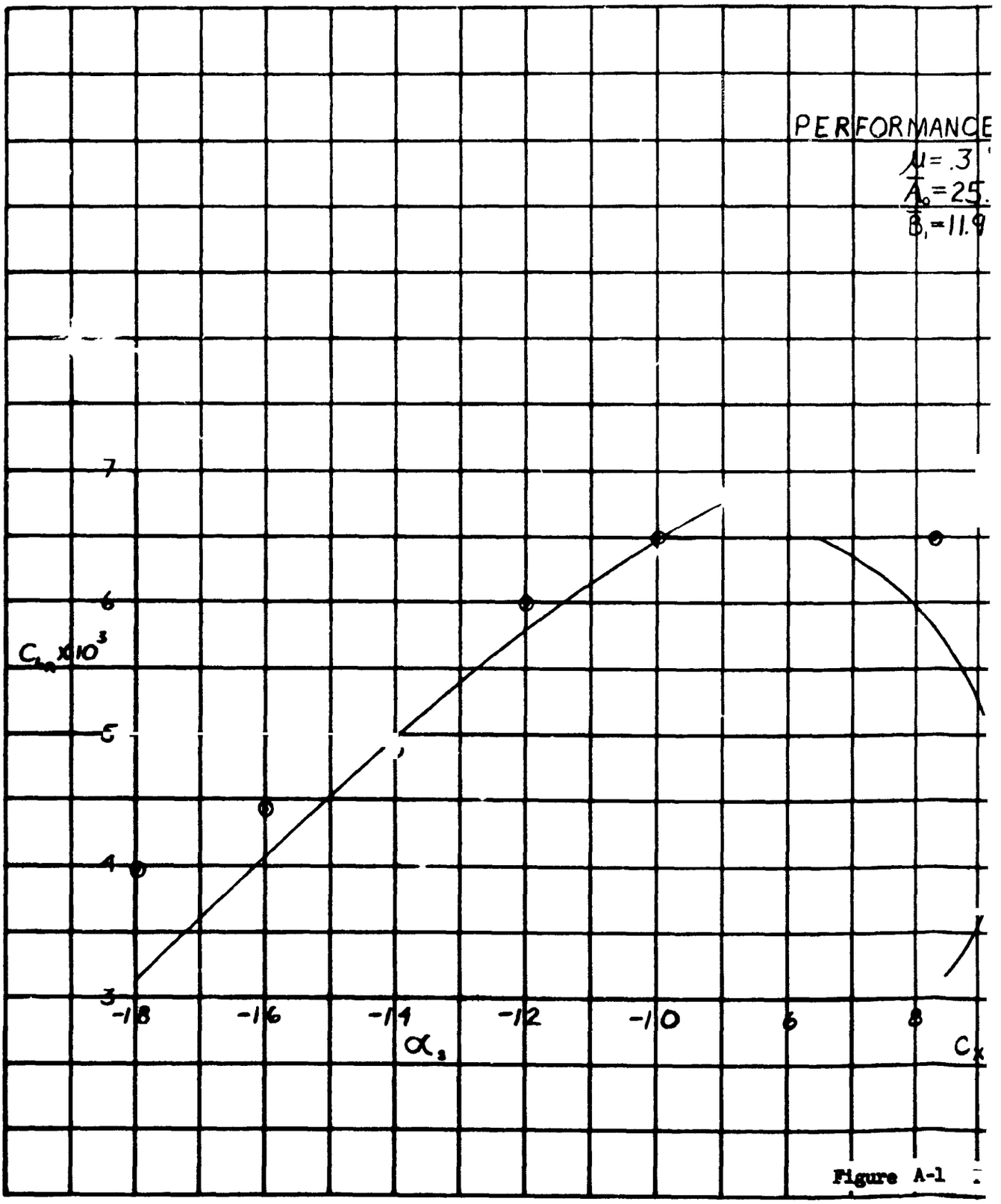
PERFORMANCE
M = .3
A₀ = 25.
B₁ = 11.9
7
6
5
4
3
$C_{l_\alpha} \times 10^3$
-18
-16
-14
-12
-10
6
8
α_s
C_x

Figure A-1

A

MANCE COMPARISONS

$M_1 = .3$

$\frac{L}{D} = 25.3$

$\psi_1 = 11.9$

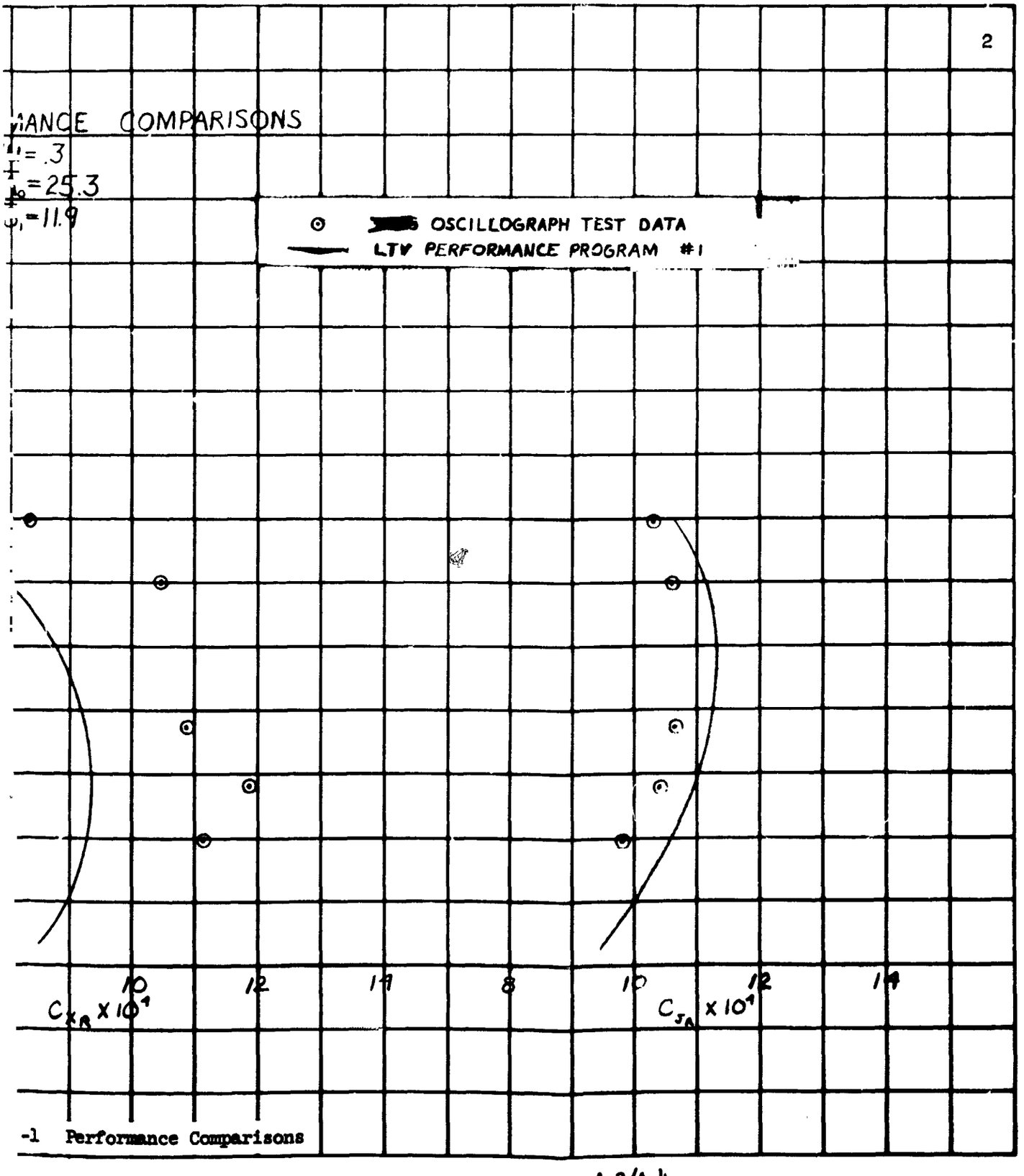

-1 Performance Comparisons

A-3/A-4

B

1

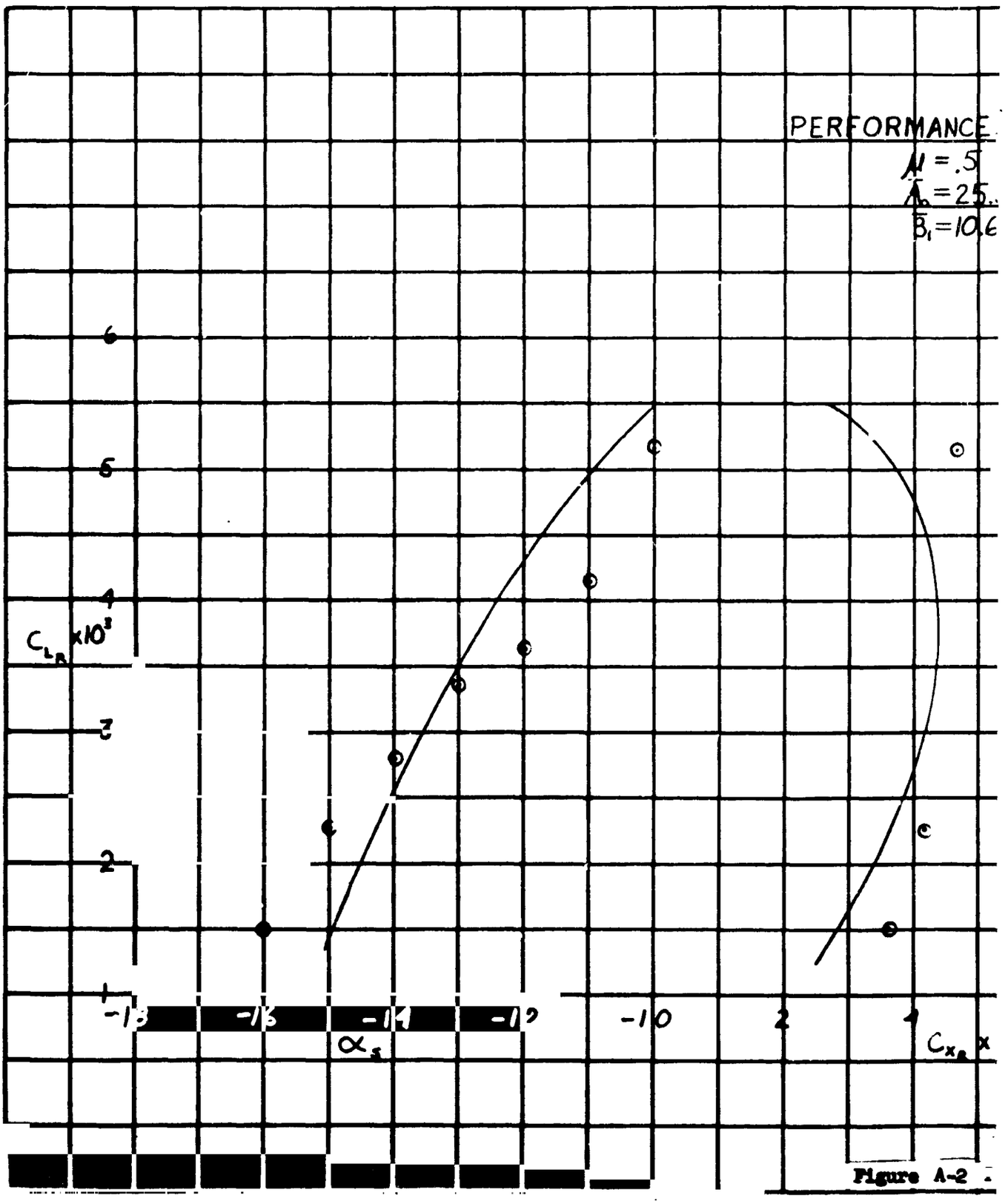

Figure A-2

ANCE COMPARISONS
= .5
= 25.5
B_1 = 10.6

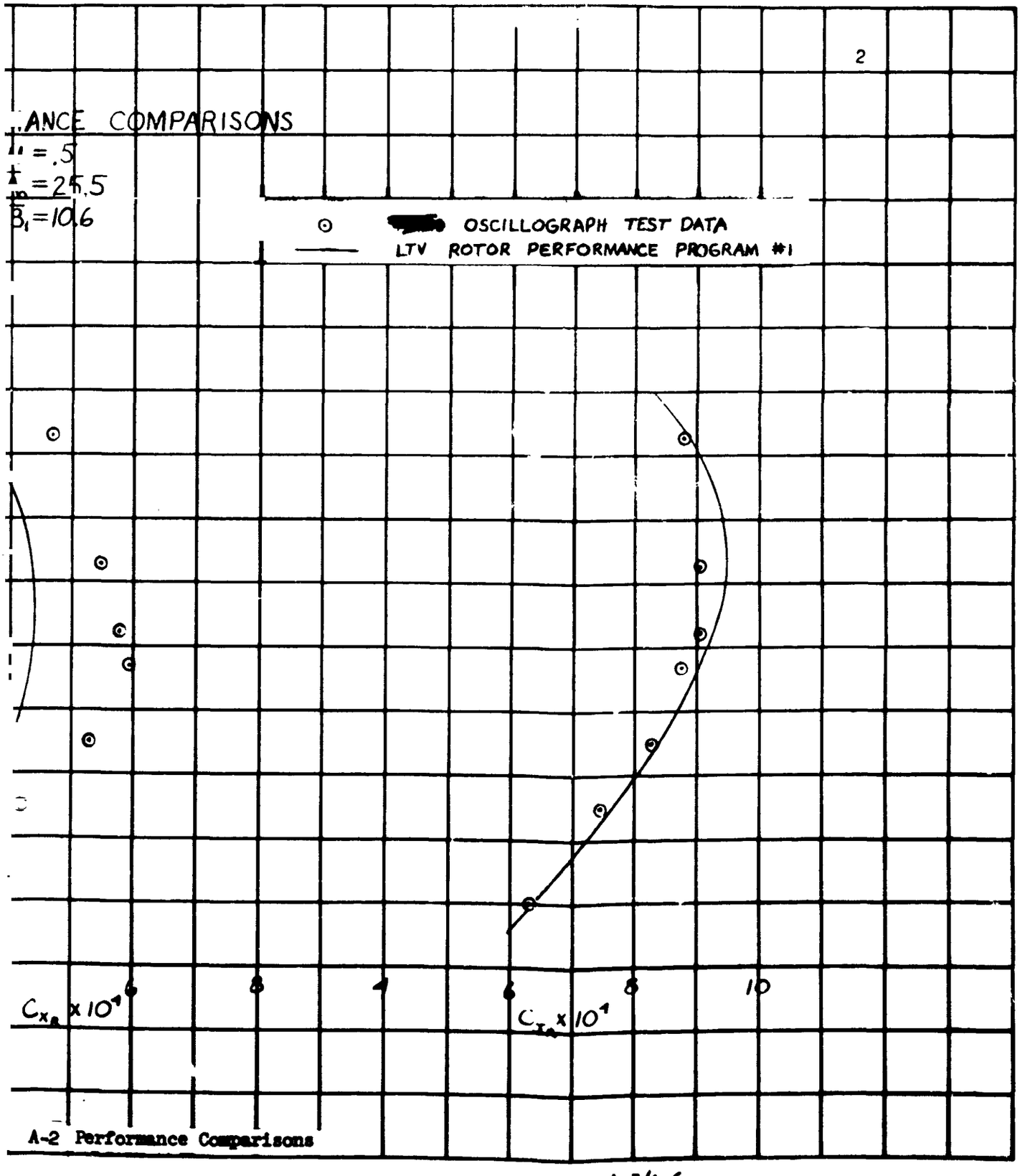

A-2 Performance Comparisons

A-5/A-6

B

1

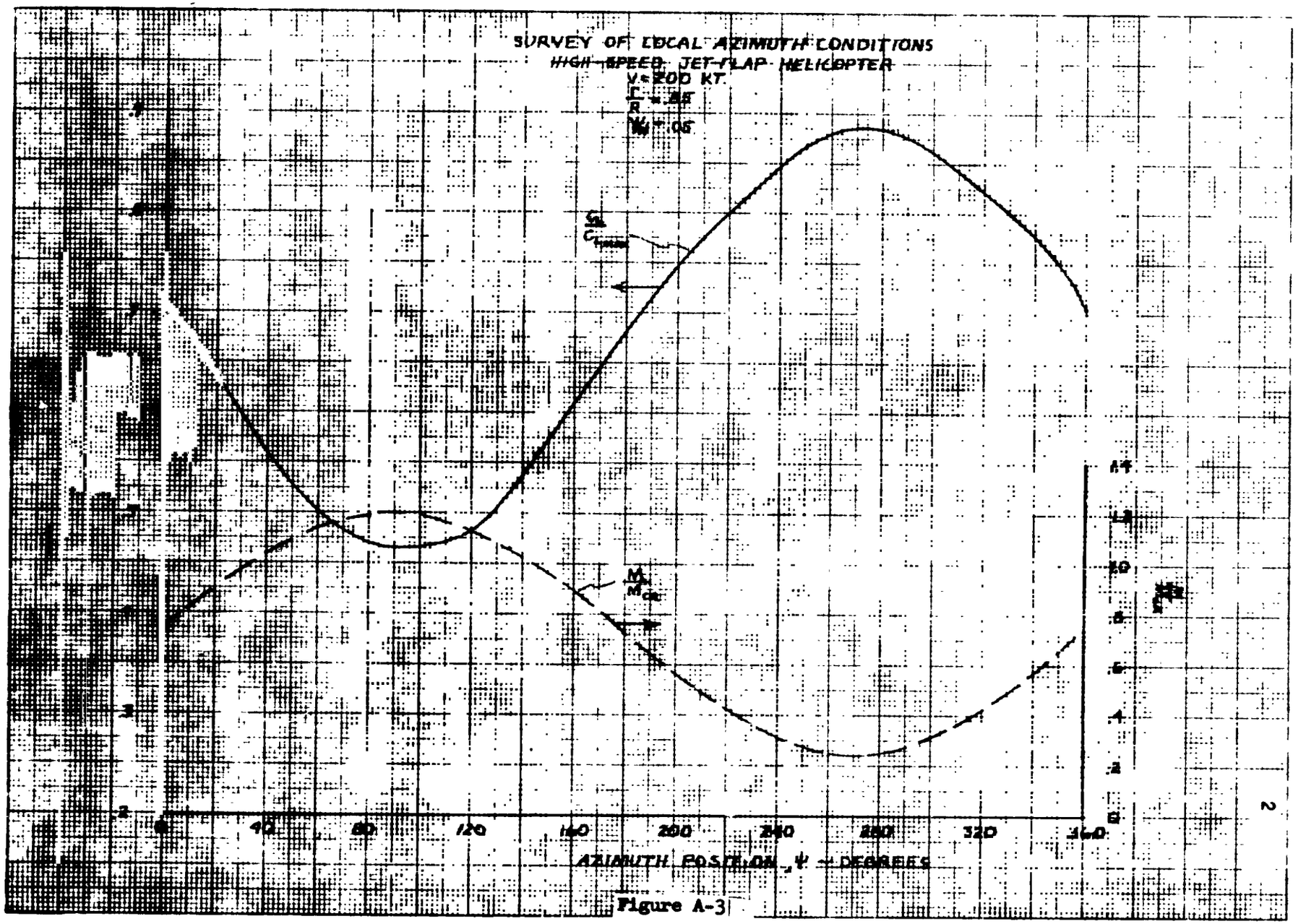
SURVEY OF LOCAL AZIMUTH CONDITIONS
HIGH SPEED JET-FLAP HELICOPTER
V = 200 KT.
μ = .05
AZIMUTH POSITION, ψ - DEGREES
40
80
120
160
200
240
280
320
360

Figure A-3

Programs No. 2 and No. 3 have been modified to include the effects of retreating blade stall and compressibility on power requirements at high speed. For shaft-driven vehicles, the equivalent shaft horsepower was adjusted to agree with Reference 6 of the basic report which includes these effects. Also based on this reference is the prediction of the upper stall limit, beyond which flight is not possible. Figure A-4 shows the power required versus airspeed for the optimum high-speed shaft-driven design predicted by program No. 3 as compared to CR-114. The agreement in results illustrates the capabilities of this program. For jet-flapped rotors, the basic power requirements were adjusted by information obtained from the text Aerodynamics of V/STOL Flight, by B. W. McCormick, Academic Press Inc., New York, 1967.

LTVAC Rotor Performance Program No. 4 (Mission Performance). Program No. 4 incorporates the power required prediction methods of No. 3 and calculates the fuel required to accomplish an input mission profile. Mission capabilities include warm-up at a desired power setting, initial hover time, mid-mission hover time, pickup or drop of payload at mid-mission, cruise at an input power setting or velocity, and a fuel reserve. A takeoff gross weight, rotor geometry, equivalent flat plate area, tipspeed, and rated engine size are also input. The fuel required for each segment of the design mission is obtained from engine data at the required power. This routine was used to generate the fuel requirements and mission performance for all phases of the parametric study.

LTVAC Program LS 0317. LTVAC computer program LS 0317 is a general rotor loads and performance program, written in FORTRAN IV, which finds the rotor variable induced velocity field by treating the problem as a boundary-

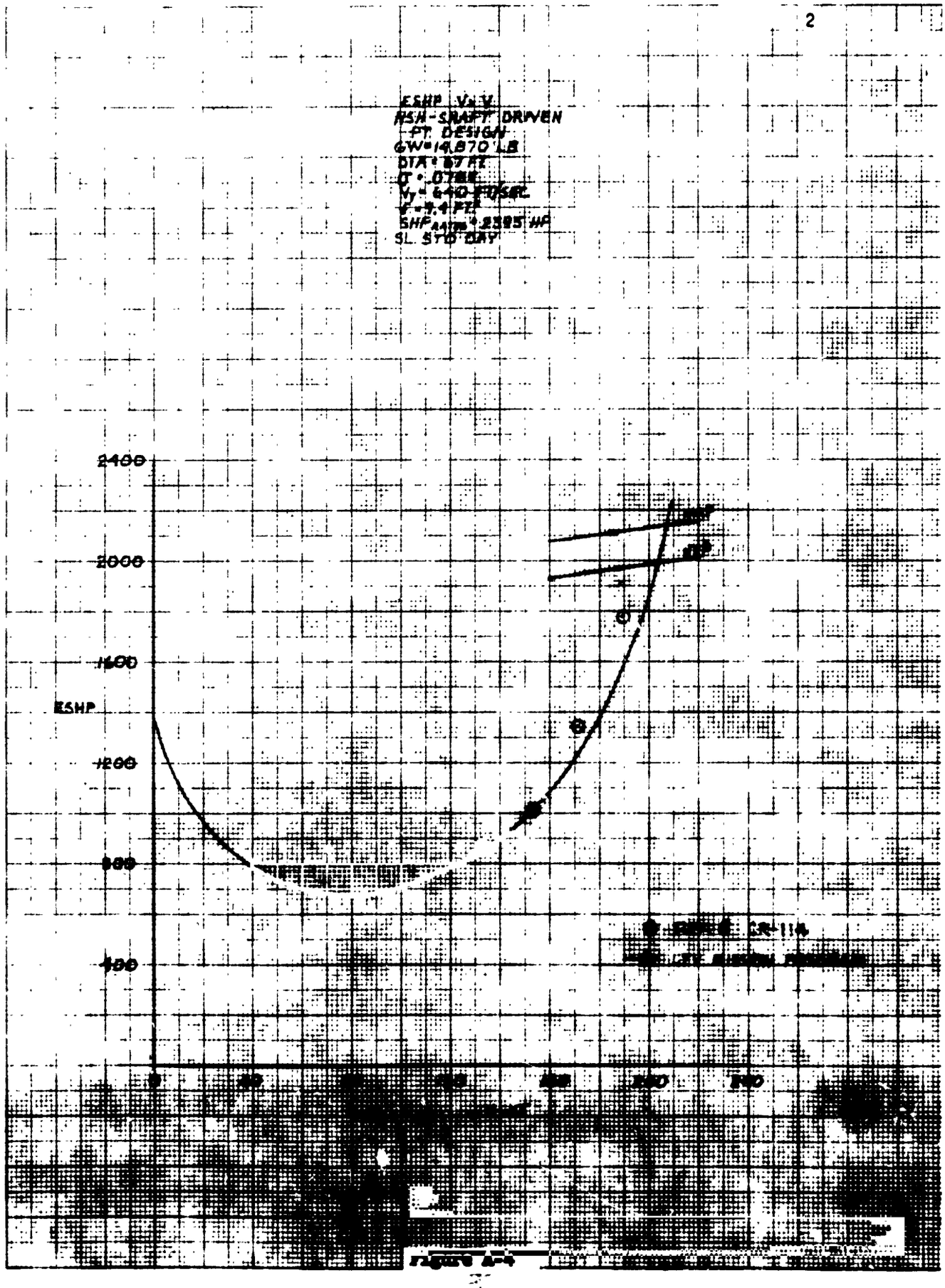
ESHP VS V
ASH-SHAFT DRIVEN
-PT. DESIGN
GW=14,870 LB
DIA=8.7 FT
C=.078E
V=640 KNOTS
F=9.4 FT
SHP=2385 HP
SL STD DAY
2400
2000
1600
ESHP
1200
800
400
CR-114

Figure A-4

valued problem. Boundary options include thrust, horsepower, rolling moment, pitching moment, and/or horizontal thrust component. These boundaries are met by adjusting collective pitch, A_1 control, B_1 control, shaft normal plane tilt, flap angle, and/or slot jet reaction. The program is applicable to propellers, helicopters, autogyros, ship screws, rotors using a blown cyclic flap, and rotors using an adjustable flap with a cyclic jet. Small angle assumptions are not used. The induced velocity at each of 20 blade stations at 24 azimuth stations (480 disc points) is found by converging the equation $L = C_l \frac{\rho}{2} CU^2$ with the equation $L = 2\rho \frac{2\pi r}{b} (V^2 + v^2)^{1/2}$ at each point, using Spence's equations with empirical Mach corrections, flap equations, and airfoil 360° aerodynamic tables having Mach effects. Trim is obtained by using matrix algebra techniques, where a matrix transfer function representing the boundaries and controls concerned is multiplied by a column of boundary errors to obtain a column representing the required simultaneous control changes required to eliminate the boundary errors. Computer time required is 3 minutes to calculate a 7 x 7 array of partial derivatives (which is subsequently partitioned into 12 smaller arrays representing 12 options of control), 2 to 6 minutes to obtain a trimmed solution, and 2 minutes to calculate and print out the detailed load analysis of the solution. The print-out includes harmonic analysis (seven Fourier coefficients) of the blade spanwise loads, shaft load, blade angle, shear distribution, moment distribution, and induced velocity. For propellers, the aerodynamic derivatives and the neutral stability boundary are also calculated. Once calculated for a particular speed, the 7 x 7 array of partial derivatives can be put on cards for reading into core for later problems at the same speed. On demand, damping derivatives (for use in matrix algebra response programs) can also be calculated.

Program uses include parametric studies to study the effect of blade geometry, air density and temperature, airfoil section, jet strength and distribution, flight and tipspeed, power, climb rate, glide angle, turn radius, and general rotor orientation. Hover solutions are obtained in 2 to 30 seconds. Since the tip vortex pattern is not considered (tip loss is shaped empirically), the fourth and higher harmonics are not meaningful.

is program was developed under the VAD Independent Research and Development program. ~~Additional discussion of the program and some results from it are presented in Volume IV.~~

APPENDIX B

AN APPROXIMATE SOLUTION TO THE JET-FLAP ROTOR

APPENDIX B

AN APPROXIMATE SOLUTION TO THE JET-FLAP ROTOR

By Dr. Barnes W. McCormick*

Introduction

This paper deals with a rotor which utilizes a jet-flapped airfoil as its section. The jet-flap serves a three-fold purpose. First, it provides the driving torque to rotate the rotor, secondly, the flap angle is varied to provide both collective and cyclic pitch control; and finally, higher section lift coefficients are obtained as a result of the boundary layer and circulation control afforded by the jet-flap.

The analysis of such a rotor is complicated by the fact that the blowing, jet-flap deflection angles, angular velocity and flapping are all interdependent. An approach to the solution of the jet-flap rotor is presented in Ref. B-1 which requires iteration techniques and numerical integration of the rotor aerodynamic forces utilizing a digital computer. The computer programs which are developed employ a table look-up for the airfoil section data as a function of the angle-of-attack and Mach number. Section lift and drag coefficients thus obtained are modified by adding increments to account for the additional lift and thrust provided by the jet-flap. In the final analysis of a jet-flap rotor, the degree of sophistication offered by the method of Ref. B-1 may be required. However, even it is limited by the assumption of a uniform inflow and that the maximum section lift coefficient can be given as the sum of $C_{l_{max}}$ for the unblown section and the increment

*Dr. McCormick worked at LTVAC on the Jet-Flap Rotor program during the summers of 1966 and 1967.

in C_l due to blowing for the unstalled section. Also, by comparison with the relationships to be used later in this paper, one might question the comparable expressions used in the reference for the section lift and drag coefficients as a function of the section angles-of-attack, flap angle and jet momentum coefficient.

The approximate solution to the jet-flap rotor presented here develops relatively simple, closed-form expressions to describe the rotor's behavior. By comparison with test data it appears that the method is adequate in its description, at least up to the point where the method predicts retreating blade stall or compressibility effects.

The approach which is taken is briefly as follows. The continuous jet-flap rotor is replaced by an equivalent jet-flapped wing free to flap on the end of a long, weightless, dragless, rotating rod. What might appear to be a gross simplication actually results for the shaft-driven rotor in relationships between flapping and pitch angles which require only minor correction as a function of the advance ratio to agree precisely with more exact solutions. These same corrections were assumed to relate the jet-flapped wing to the jet-flapped rotor.

In addition to the flapping, expressions are developed for calculating the required jet mass flow rate and jet velocity. For these, the approximation of the wing is not required.

Development of Flapping Theory

Instead of treating a continuous rotor, consider a wing having a planform area of S rotating on the end of a long, weightless, dragless rod as shown in Fig. B-1. B-1(a) is a view looking down on the planform. B-1(b) is a view in the plane containing the rod and the shaft. B-1(c) is a left-side view showing the disc plane at an angle-of-attack α_s and the tip-path plane tilted back an angle of a_1 from the disc plane due to longitudinal flapping. B-1(d) is a view looking in along the rod. The wing and rod are rotating about the shaft with an angular velocity of ω. At the instant the rod is at the azimuth angle, the free-stream velocity has components of V cos Ψ and V sin Ψ parallel and normal to the span of the wing, respectively. As the wing rotates it flaps up from the disc plane by the angle β. As shown in Fig. B-1(b), relative to the wing, the net downward velocity will be:

$$R\dot{\beta} + w + \beta V \cos\Psi - V\alpha_s$$

w is the downwash induced as a result of the lift of the wing. If the pitch angle of the wing is denoted by θ, then the angle-of-attack of the wing will be given by:

$$\alpha = \theta - \frac{R\dot{\beta} + w + \beta V \cos\Psi - V\alpha_s}{\omega R + V \sin\Psi} \qquad (1)$$

If the rod is pinned at the axis so that the wing and rod are free to flap, then the summation of moments about the flapping axis becomes:

$$\frac{W}{g} R^2 \ddot{\beta} = LR - WR - \frac{W}{g} R^2 \omega^2 \beta$$

or:

$$\ddot{\beta} = \frac{gL}{RW} - \frac{g}{R} - \omega^2 \beta \qquad (2)$$

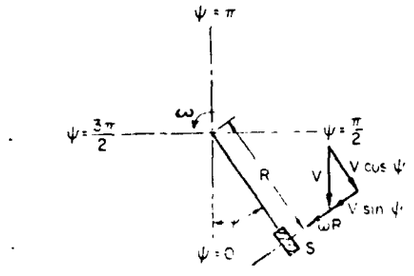

(a)

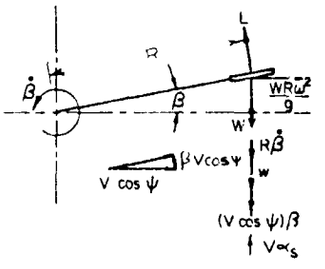

(b)

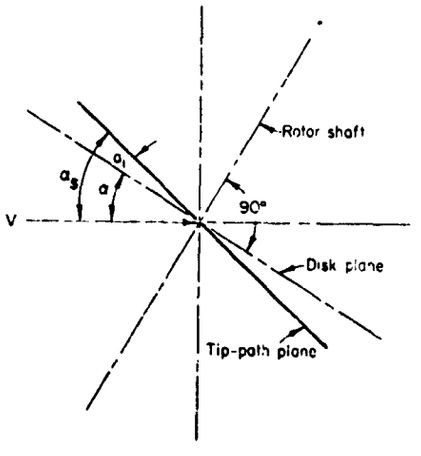

(c)

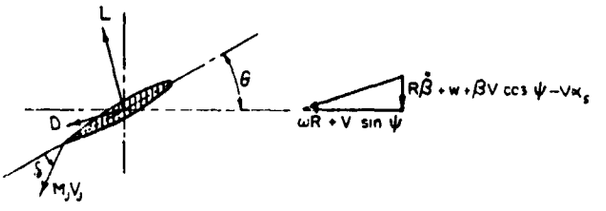

(a)

FIGURE B-1

FLAPPING JET-FLAPPED WING

L is the instantaneous lift on the wing and W is its weight.

Assuming α is a small angle, the lift can be written as:

$$L = \tfrac{1}{2}\rho(\omega R + V \sin\Psi)^2 S \left[C_{L_\alpha}\alpha + C_{L_\delta}\delta\right]$$

δ is the deflection angle of the jet flap. The performance of a jet flap is a function of the dimensionless momentum coefficient C_μ . For this application, C_μ varies with Ψ . For a mass flow of M_J and a jet velocity, V_J

$$C_\mu = \frac{M_J V_J}{\frac{1}{2}\rho S (\omega R + V\sin\Psi)^2} \tag{3}$$

For C_μ values up to at least 5, Spence's results documented in Ref.B-2, can be closely approximated by:

$$\begin{aligned} C_{L_\alpha} &= 2\pi + 18\,C_\mu \\ C_{L_\delta} &= \sqrt{4\pi C_\mu} + 64\,C_\mu \end{aligned} \tag{4}$$

In the above, α and δ are in radians.

Hence, using (1), (3) and (4), the lift becomes:

$$\begin{aligned} L = \tfrac{1}{2}\rho S(\omega R)^2 \Big[& 2\pi\Theta(1+\mu\sin\Psi)^2 + 18\,C_{\mu_R}\Theta \\ & -2\pi(1+\mu\sin\Psi)\left(\frac{\dot\beta}{\omega} - \lambda + \mu\beta\cos\Psi\right) \\ & -18\,C_{\mu_R}\frac{\left(\frac{\dot\beta}{\omega} - \lambda + \mu\beta\cos\Psi\right)}{1+\mu\sin\Psi} \\ & + \delta(1+\mu\sin\Psi)\sqrt{4\pi C_{\mu_R}} + .64\,C_{\mu_R}\delta\Big] \end{aligned} \tag{5}$$

$$C_{\mu_R} = \frac{M_J V_J}{\frac{1}{2}\rho(\omega R)^2 S}$$

where:

$\mu = \dfrac{V}{\omega R}$ = inflow velocity ratio

$\lambda = -\dfrac{w}{\omega R} + \mu\alpha_s$ = tipspeed ratio

Considering first harmonic control and flapping only, i.e., let:

$$\Theta = \Theta_0 + \Theta_1 \cos\Psi + \Theta_2 \sin\Psi \tag{6}$$

$$\delta = \delta_0 + \delta_1 \cos\Psi + \delta_2 \sin\Psi \tag{7}$$

and assume:

$$\beta = \beta_0 - a_1 \cos\Psi - b_1 \sin\Psi \tag{8}$$

Since

$$\dot{\beta} = \frac{d\beta}{dt} = \omega \frac{d\beta}{d\Psi}$$

$$\frac{\dot{\beta}}{\omega} = a_1 \sin\Psi - b_1 \cos\Psi \tag{9}$$

$$\frac{\ddot{\beta}}{\omega^2} = a_1 \cos\Psi + b_1 \sin\Psi \tag{10}$$

Eq. (2) becomes:

$$L = \frac{R\omega^2 W}{g}\beta_0 + W$$

Now remembering that:

$\sin\Psi\cos\Psi = 1/2 \sin 2\Psi$

$\sin^2\Psi = 1/2 (1-\cos 2\Psi)$

$\cos^2\Psi = 1/2 (1+\cos 2\Psi)$

equation (5) can be expanded using (6) through (10) retaining only constant or first harmonic terms in Ψ. From the constant terms,

$$\beta_0 = -\frac{qR}{(\omega R)^2} + \frac{\rho S R}{2W}\left\{2\pi\Theta_0\left(1+\frac{\mu^2}{2}\right)\right.$$
$$+ 1.8 C_{\mu_R}\Theta_0 + 2\pi\lambda + 1.8 C_{\mu_R}\left(\lambda + \mu a_1 + \frac{\mu^2\lambda}{2} + \frac{\mu^2 a_1}{4}\right.$$
$$\left.+ \frac{\mu^3 a_1}{4}\right) + \sqrt{4\pi C_{\mu_R}}\left(\delta_0 + \frac{\mu\delta_2}{2}\right)$$
$$\left. + .64 C_{\mu_R}\delta_0 + 2\pi\mu\Theta_2\right\} \tag{11}$$

Equating coefficients of the sin terms one obtains the longitudinal flapping angle, a_1:

$$a_1 = \frac{\mu\lambda + 2\mu\theta_0 - \frac{1.8\,C_{\mu_R}}{2\pi}\left(\mu\lambda + \frac{\mu^3\lambda}{2}\right) + \frac{\sqrt{4\pi C_{\mu_R}}}{2\pi}\left(\delta_2 + \mu\delta_0\right)}{1 + \frac{1.8\,C_{\mu_R}}{2\pi}\left(1 + \mu^2 + \frac{\mu^4}{4}\right) - \frac{\mu^2}{2}} + \frac{\frac{4\,C_{\mu_R}}{2\pi}\delta_2 + \left(1 + \frac{1.8\,C_{\mu_R}}{2\pi} + \frac{\mu^2}{2}\right)\theta_2}{1 + \frac{1.8\,C_{\mu_R}}{2\pi}\left(1 + \mu^2 + \frac{\mu^4}{4}\right) - \frac{\mu^2}{2}} \tag{12}$$

Equating coefficients of the cos terms results in the lateral flapping angle, b_1:

$$b_1 = \frac{\mu\beta_0 + \frac{1.8}{2\pi}\,C_{\mu_R}\left(\mu\beta_0 + \frac{\mu^2}{2}\beta_0\right) - \delta_1\left(\frac{\sqrt{4\pi C_{\mu_R}}}{2\pi} + \frac{.64\,C_{\mu_R}}{2\pi}\right)}{1 + \frac{1.8}{2\pi}\,C_{\mu_R}\left(1 + \mu^2 + \frac{\mu^4}{4}\right) - \frac{\mu^2}{2}} - \frac{\left(1 + \frac{1.8}{2\pi}\,C_{\mu_R} + \frac{\mu^2}{2}\right)\theta_1}{1 + \frac{1.8}{2\pi}\,C_{\mu_R}\left(1 + \mu^2 + \frac{\mu^4}{4}\right) - \frac{\mu^2}{2}} \tag{13}$$

The average lift, is calculated from:

$$\bar{L} = \frac{1}{2\pi}\int_0^{2\pi} L(\Psi)\,d\Psi \tag{14}$$

Substituting (5) in (14) gives:

$$\frac{2\bar{L}}{\rho S(\omega R)^2} = 2\pi\theta_0\left(1 + \frac{\mu^2}{2}\right) + 1.8\,C_{\mu_R}\theta_0 + 2\pi\lambda + 2\pi\mu\theta_2 + 1.8\,C_{\mu_R}\left(\lambda + \mu a_1 + \frac{\mu^2\lambda}{2} + \frac{\mu^2 a_1}{4} + \frac{\mu^3 a_1}{4}\right) + \delta_0\sqrt{4\pi C_{\mu_R}} + \frac{\mu\delta_2}{2}\sqrt{4\pi C_{\mu_R}} + .64\,C_{\mu_R}\delta_0 \tag{15}$$

Now each term not involving C_{μ_R} (or for $C_{\mu_R} = 0$) in equations (11), (12), (13) and (15) can be compared to the corresponding term obtained by considering an unblown continuous rotor blade. In Reference 2, for example, for a shaft-driven rotor, a_1 is given by:

$$a_1 = \frac{\frac{8\mu}{3}}{1 - \frac{\mu^2}{2}} \theta_0 + \ldots$$

Using the approximation of a finite wing, equation (12) shows the coefficient of the θ_0 term in a_1 to be (for $C_{\mu_R} = 0$)

$$\frac{2\mu}{1 - \frac{\mu^2}{2}}$$

Hence if the coefficient of the θ_0 term in the a_1 equation as obtained by the wing analogy to the rotor were multiplied by $\frac{8/3}{2}$ or 4/3, the result would agree exactly with the unblown rotor. It was assumed that this same factor would apply to both the θ_0 term and δ_0 term for the blown wing and rotor. Hence, in equation (12), the coefficient in front of the θ_0 and δ_0 terms were all increased by the factor of 4/3. Following this procedure for the remaining terms,

$$a_1 = \lambda A_{11} + \theta_0 A_{12} + \theta_T A_{13} + \theta_2 A_{14} + \delta_2 A_{15} + \delta_0 A_{16} \qquad (16)$$

$$b_1 = \beta_0 B_{11} - \theta_1 + \delta_1 B_{13} \qquad (17)$$

$$\beta_0 = \gamma_F \left[\lambda F_1 + \theta_0 F_2 + \theta_T F_3 + \theta_2 F_4 + \delta_0 F_5 + \delta_2 F_6 + a_1 F_7 \right] - \tau \qquad (18)$$

$$C_T = \frac{a\sigma}{2\left(1 + \frac{T_1 a\sigma}{4\mu}\right)} \left[\mu \alpha_s T_1 + \theta_0 T_2 + \theta_T T_3 + \theta_2 T_4 + \delta_0 T_6 + \delta_2 T_6 + a_1 T_7 \right] \qquad (19)$$

The coefficients, A_{11}, B_{11}, T_1, F_1, etc., are defined as:

$$A_{11} = \frac{\mu - \frac{1.8}{2\pi} C_{\mu_R} \left(\mu + \frac{\mu^3}{2}\right)\left(2 - \frac{\mu^2}{2}\right)}{D}$$

$$A_{12} = \frac{8\mu^2}{3D} \qquad A_{13} = \frac{2\mu}{1 - \frac{\mu^2}{2}}$$

$$A_{14} = \frac{1 + 1.8\frac{C_{\mu_R}}{2\pi} + \frac{\mu^2}{2}}{D} \quad \frac{1 + \frac{3\mu^2}{2}}{1 + \frac{\mu^2}{2}}$$

$$A_{15} = \frac{\left[\frac{\sqrt{4\pi C_{\mu_R}}}{2\pi} + \frac{.64 C_{\mu_R}}{2\pi}\right]\left(1 + \frac{3\mu^2}{2}\right)}{D\left(1 + \frac{\mu^2}{2}\right)}$$

$$A_{16} = \frac{\frac{\sqrt{4\pi C_{\mu_R}}}{2\pi}\mu\left(2 - \frac{\mu^2}{2}\right)}{D}$$

$$B_{11} = \frac{4}{3}\frac{\mu + \frac{1.8}{2\pi} C_{\mu_R}\left(\mu + \frac{\mu^2}{2}\right)}{D} \qquad B_{13} = \frac{\frac{\sqrt{4\pi C_{\mu_R}}}{2\pi} + \frac{.64 C_{\mu_R}}{2\pi}}{D\left(1 + \frac{\mu^2}{2}\right)}$$

$$D = 1 + \frac{1.8 C_{\mu_R}}{2\pi}\left(1 + \mu^2 + \frac{\mu^4}{4}\right) - \frac{\mu^2}{2}$$

$$F_1 = \frac{1}{3}\left[1 + \frac{1.8 C_{\mu_R}}{2\pi}\left(1 + \frac{\mu^2}{2}\right)\right]$$

$$F_2 = \frac{1}{4}\left[1 + \mu^2 + \frac{1.8 C_{\mu_R}}{2\pi}\right] \qquad F_3 = \frac{1}{5} + \frac{\mu^2}{6} \qquad F_4 = \frac{\mu}{3}$$

$$F_5 = \frac{1}{6\pi}\left(\sqrt{4\pi C_{\mu_R}} + .64 C_{\mu_R}\right) \qquad F_6 = \frac{\mu}{12\pi}\sqrt{4\pi C_{\mu_R}}$$

$$F_7 = \frac{1.8}{6\pi} C_{\mu_R}\left(\mu + \frac{\mu^2}{4} + \frac{\mu^3}{4}\right)$$

$$T_1 = \left[\frac{1.8\, C_{\mu_R}}{2\pi} \left(1 + \frac{\mu^2}{2} \right) + 1 \right] \frac{1 + \frac{\mu^2}{2}}{2}$$

$$T_2 = \frac{\left[1 + \frac{\mu^2}{2} + \frac{1.3\, C_{\mu_R}}{2\pi} \right] \left(\frac{1}{3} + \frac{\mu^2}{2} \right)}{1 + \frac{\mu^2}{2}}$$

$$T_3 = \frac{+\mu^2}{4} \qquad T_4 = \frac{\mu}{2} \left(1 + \frac{\mu^2}{4} \right)$$

$$T_5 = \frac{\frac{\sqrt{4\pi C_{\mu_R}}}{2\pi} \left(\frac{1}{3} + \frac{\mu^2}{2} \right)}{1 + \frac{\mu^2}{2}}$$

$$T_6 = \frac{\mu \sqrt{4\pi C_{\mu_R}} \left(1 + \frac{\mu^2}{4} \right)}{8\pi}$$

$$T_7 = \frac{1.8\, \mu\, C_{\mu_R}}{2\pi}$$

$$\gamma_F = \frac{c \rho a R^4}{2 I_F}$$

$$\tau = \frac{M_W}{I_F \omega^2}$$

$$\sigma = \frac{B c}{\pi R}$$

where: I_F = blade moment of inertia about its flapping hinge

M_W = blade weight moment about its flapping hinge

a = C_l / rad $\simeq 2\pi$

c = blade chord

$V_T = \omega R$

B = no. of blades

$C_T = T / \rho V_T^2 \pi R^2$

In forward flight, λ is given by

$$\lambda = \mu \alpha_s - \frac{w}{\omega R}$$

Using Glauert's approximation for w,

$$w = \frac{T}{2\rho V \pi R^2} \tag{21}$$

the inflow ratio, λ, becomes:

$$\lambda = \mu \alpha_s - \frac{C_T}{2\mu} \tag{22}$$

Once a_1, b_1, β_o, θ_o, δ_o, δ_1 and δ_2 are known, one can calculate the section angles-of attack from (1) and the jet-flap angles from (7). If V_c is the velocity of sound, then the local Mach number can be calculated from:

$$M = \frac{\omega R}{V_c} \chi + \frac{V}{V_c} \sin \Psi = \frac{V_T}{V_c} \chi + \frac{V}{V_c} \sin \Psi$$

where $V_T = \omega R$

With this information and the airfoil characteristics, it can then be determined whether or not the rotor section is safe from stall or drag divergence.

Tests have been conducted by the NASA in collaboration with the Giravions Dorand Co. of France of a two-bladed jet flapped rotor described in Ref. B-1 and shown in Fig. B-2. Instead of blowing all along the blade, the air is ejected only along the outer 30% of the radius. Hence for such a rotor, by analogy with the jet-flapped wing, the C_{μ_R} to be used in the flapping relationships will be:

$$C_{\mu_R} = \frac{M_J V_J}{B (R - R_J) \frac{1}{2} \rho V_T^2 c} \tag{23}$$

M_J is the total mass flow rate being ejected over the flaps, B is the number of blades, and R_I is the inboard radius where the jet flap begins. Comparing the unblown wing to the unblown rotor, and correcting the blown wing results in proportion, is tantamount to assuming that the jet flap extends all along the blade. Hence, for calculating the flapping only, not all of the C_{μ_R} calculated by (23) should be used. Instead, it is recommended that an effective C_{μ_R} be used by reducing (23) in proportion to the fraction of disc area which is flapped. Hence, the effective C_{μ_R} for evaluating flapping becomes finally:

$$C_{\mu_R} = \frac{M_J V_J (1 + X_I)}{\frac{B}{2} \rho V_T^2 c R} \qquad (24)$$

where $X_I = R_{I/R}$

Power and Mass Flow Rate Requirements

The power required by a helicopter in forward flight is composed of three parts, the parasite power, induced power and profile power.

$$P = P_{par} + P_i + P_p \tag{25}$$

These can be calculated approximately from:

$$P_{par} = 1/2\ \rho\ V^3\ f \tag{26}$$

$$P_i = 1.15\ T\ w \tag{27}$$

$$P_p = \rho\ V_T^3\ \pi\ R^2\ \frac{\sigma \overline{C_d}}{8}\ (1 + 3\mu^2) \tag{28}$$

where:

f = parasite flat plate area of helicopter excluding the rotor.

$\overline{C_d}$ = average profile drag coefficient of rotor blades.

In (27) the induced power obtained from elementary momentum theory has been increased by 15% to allow for tip losses.

For a jet-flapped rotor driven entirely by the jet with no torque being supplied at the shaft, the torque due to the jet must equal the opposing torque produced by the airloads. This latter torque is simply equation (25) divided by the rotor angular velocity, ω.

Consider now the torque produced by a jet-flapped rotor. The thrust produced by a jet-flapped airfoil per unit span is:

$$T = m_J V_J k$$

where k is the thrust recovery factor and lies between zero and one. According to Figure 7-12 of Ref. B-2 , k is given closely by:

$$k = 0.84 \left[1 - \left(\frac{\alpha + \delta}{100}\right)^3\right] \tag{29}$$

with α and δ in degrees. m_J is the mass flow rate per unit span. Applied to the rotor, the average torque of the jet-flapped airfoil would therefore be:

$$\overline{Q}_J = \frac{B}{2\pi} \int_0^{2\pi} \int_0^R m_J V_J r k \, dr \, d\Psi$$

$$= \frac{M_J V_J}{2\pi (R - R_I)} \int_0^{2\pi} \int_{R_I}^R r k \, dr \, d\Psi$$

Substituting for k gives:

$$\overline{Q}_J = \frac{M_J V_J}{R - R_I} \left[\frac{.84 (R^2 - R_I^2)}{2} - \frac{.84 R^2}{2\pi} \int_0^{2\pi} \int_{x_I}^1 \left| \frac{\alpha + \delta}{100} \right|^3 x \, dx \, d\Psi \right] \quad (30)$$

Since the jet mass flow rate is issuing from a rotating blade, a coriolis torque, Q_c, must be subtracted ~ Q_j to give a net torque from the blade. To calculate Q_c, consider Fig. B-3. Here the flow is shown passing through two control stations a distance of dr apart. The flow leaving has a higher angular momentum flux than the flow entering by an amount of dQ.

$$dQ = m \left[\omega (r + dr)^2 - \omega r^2 \right]$$

$$= m \omega 2 r \, dr$$

Where m is the mass rate of flow through the blade at the radius r. Hence, the total reacting torque, Q_c, on the blade to produce dQ over the blades will be:

$$Q_c = B \omega \int_0^R 2 m r \, dr$$

or:

$$Q_c = \frac{\omega R^3 M_J (1 - X_I^3)}{3 (R - R_I)} \quad (31)$$

Defining a power coefficient C_p by:

$$C_p = \frac{P}{\rho V_T^3 \pi R^2}$$

the net C_p produced by the rotor can be written from (30) and (31) as

$$C_{P_{NET}} = \sigma C_{\mu_R} \left[.21(1-X_I^2) - \frac{V_T}{V_J} \frac{(1-X_I^3)}{6} - .0668\,(FCP) \right] \tag{32}$$

where the above C_{μ_R} is calculated from equation (23), and not from (24). FCP is the double integral of the last term in equation (30).

$$FCP = \int_0^{2\pi} \int_{X_I}^{1} \left| \frac{\alpha + \delta}{100} \right|^3 \chi \, d\chi \, d\Psi \tag{33}$$

The mass flow rate is then determined by equating $C_{P_{net}}$ to C_p obtained from (25). (25) in coefficient form can be written in forward flight as:

$$C_p = \frac{f}{2\pi R^2} \mu^3 + \frac{1.15\, C_T^2}{2\mu} + \frac{\sigma \bar{C}_d}{8} (1 + 3\mu^2) \tag{34}$$

In hover where $\mu = 0$,

$$C_p = 1.15 \frac{C_T^{3/2}}{\sqrt{2}} + \frac{\sigma \bar{C}_d}{8} \tag{35}$$

If a fraction, η, of the total mass flow, M_J, is ducted to a nozzle at the tip, then (32) becomes,

$$C_{P_{net}} = \frac{2(1-\eta) V_J}{(1-X_I) V_T} C_{M_J} \left[.21(1-X_I^2) - \frac{V_T}{V_J} \frac{(1-X_I^3)}{6} - 0668(FCP) \right]$$

$$+ \eta C_{M_J} \left(\frac{V_J}{V_T} - 1 \right) \tag{36}$$

In the above C_{μ_R} has been replaced by a more convenient coefficient C_{M_J} defined by:

$$C_{M_J} = \frac{M_J}{\rho V_T \pi R^2}$$

Not all of the coriolis torque actually represents lost power as some is recovered in compressing the flow as it flows toward the rotor tip. From radial equilibrium of an element of flow within the blade, the radial pressure gradient must be:

$$\frac{dp}{dr} = \rho r \omega^2$$

or $\Delta p(r) = p(r) - p\ (r = o) = \dfrac{\rho r^2 \omega^2}{2}$

The total power represented by this compression will be:

$$P = \int_o^R \frac{m \Delta p}{\rho} dr$$

$$= \frac{M_J \omega^2 \left(R^3 - R_I^3\right)}{6\left(R - R_I\right)}$$

The torque corresponding to the above power is P/ω , or:

$$Q = \frac{\omega^2 R^3 M_J \left(1 - X_I^3\right)}{6\left(R - R_I\right)} = \frac{Q_c}{2} \qquad (37)$$

Hence, half of the coriolis torque is recovered in the form of a centrifugal compression of the jet mass flow along the blade.

Gas Flow Relationships

The isentropic flow of a gas from a reservoir having conditions denoted by a sub "0" is governed by:

$$\frac{u^2}{2} + \frac{\gamma}{\gamma-1}\frac{P}{\rho} = \frac{\gamma P_o}{(\gamma-1)\rho_o} \tag{38}$$

If the flow is compressed adiabatically from free-stream conditions of P_∞, ρ_∞ and T_∞ to the reservoir conditions of P_o, ρ_o, and T_o, the work done per unit mass will be:

$$W_g = C_p T_\infty \left[P_r^{\frac{\gamma-1}{\gamma}} - 1 \right] \tag{39}$$

where P_r is the pressure ratio P_o/P_∞

The power will be the product of W_g and the mass flow rate M_j. Hence,

$$P_g = M_J C_p T_\infty \left(P_r^{\frac{\gamma-1}{\gamma}} - 1 \right) \tag{40}$$

For air, $C_p = 6000$

$R = 1720$

$\gamma = 1.4$

Expanding isentropically from p_o to p gives a jet velocity of:

$$V_J = \left[\frac{2\gamma R T_\infty}{\gamma-1} \left(P_r^{\frac{\gamma-1}{\gamma}} - 1 \right) \right]^{\frac{1}{2}} \tag{41}$$

Combining (39) and (40), the expected result is obtained that:

$$P_g = \frac{1}{2} M_J V_J^2 \tag{42}$$

Remember, however, that the compressor need supply only part of the above. The rest is derived from the rotor and from (37) amounts to:

$$P_g \text{ (rotor)} = 1/2\ M_J V_T^2 \left[\frac{1-X_I^3}{3(1-X_I)}\right] \qquad (43)$$

An interesting result is obtained if X_I is allowed to approach one and complete thrust recovery is assumed. In this case the net power produced by the rotor becomes:

$$P_{NET} = M_J V_J (V_J - V_T)$$

The power which the compressor must supply will be:

$$P_g = \frac{1}{2} M_J (V_J^2 - V_T^2)$$

The ideal efficiency therefore becomes:

$$\eta_i = \frac{P_{NET}}{P_g} = \frac{2}{1 + \frac{V_J}{V_T}}$$

Hence, the rotor system behaves as an air-breathing engine. The coriolis torque corresponds to the ram drag while the work of centrifugal compression corresponds to the energy of the flow entering the engine.

Prediction of Mass Flow Required For Jet-Flapped Rotor

In hover, the power coefficient of a rotor can be quickly estimated from:

$$C_p = 1.15 \frac{C_T^{3/2}}{\sqrt{2}} + \frac{\sigma \bar{C}_c}{8} \qquad (44)$$

The first term is the ideal induced power increased by 15% and the second term is the profile power.

The average rotor drag coefficient, $\bar{C}_d$, is related to the average rotor lift coefficient defined by

$$C_L = 6\, C_T / \sigma$$

where σ = is the rotor solidity, $\frac{Bc}{\pi R}$

From the developments given previously, a jet-flapped rotor can develop a C_p given by eq. (36).

C_{J_R} is defined in Ref. B-1 as:

$$C_{J_R} = \frac{M_J V_J}{\rho V_T^2 \pi R^2}$$

Hence, equating eqs. (32) and (44) and solving for C_{J_R} gives:

$$C_{J_R} = \frac{1-X_T}{2} \frac{\frac{1.15\, C_T^{3/2}}{\sqrt{2}} + \frac{\sigma \bar{C}_d}{8}}{.21\left(1-X_T^2\right) - \frac{V_T}{V_J}\frac{\left(1-X_T^3\right)}{6} - .0668\,(FCP)} \qquad (45)$$

FCP is an integral representing a portion of the thrust recovery loss. For most cases, FCP can be neglected in comparison with the other terms resulting in an assumed constant thrust recovery from the jet flap of 84%.

The relationships developed here were programmed in Fortran IV. Three separate programs were developed. The first calculates the rotor lift, propulsive force, flapping angles, and required mass flow given the disc plane angle-of-attack, control angles, tip speed and jet velocity (or pressure ratio). This program is used to compare with wind tunnel test data. The second program calculates the control angles and required mass flow given the tip speed jet velocity and the required rotor lift and propulsive force. This program is used to predict the performance of the rotor when attached to an airframe. Both of these progaams iterate on C_{μ_R} to obtain a final solution. Approximately one second of computing time on an IBM 360/40 RAX system is required for one set of input conditions. The third program neglects flapping and calculates the required mass flow rate and ideal gas power as a function of forward speed from equations (32), (36), (42) and (43) assuming FCP to be a small, constant value. This program has produced results which are close to those from the second program. Since it is considerably faster than the flapping program, requiring no iteration, it is useful for preliminary design purposes.

For comparison with the test results reported in Ref. B-3 the characteristics of the 0012 airfoil were assumed. C_d as a function of C_ℓ was approximated by:

$$C_d = .0085 + .008\,C_\ell^2 \tag{46}$$

$C_{l_{max}}$ as a function of C_μ was calculated from:

$$C_{l_{max}} = 1.4 + C_{l_\alpha}\,\Delta\alpha + C_{\ell_\delta}\,\delta \tag{47}$$

where $\Delta\alpha = \alpha_{MAX} - \alpha_{MAX}\,(C_\mu = 0)$

From Ref.B-2, $\Delta \alpha$ is obtained in degrees as,

$$\Delta \alpha = -9 C_\mu \qquad 0 \leq C_\mu \leq 0.5$$

$$\Delta \alpha = -6\left(1 - \frac{C_\mu}{2}\right) \qquad 0.5 < C_\mu < 2.0$$

$$\Delta \alpha = 6\left(\frac{C_\mu}{5} - \frac{2}{5}\right) \qquad 2.0 \leq C_\mu \leq 7$$

The critical Mach no. as a function of C_l was approximated by:

$$M_{CR} = .74 - .245\, C_l + .0325\, C_l^2 \qquad (48)$$

The above is for a 0012 airfoil at an angle of attack and may be pessimistic with regard to the jet-flapped airfoil. It should be emphasized that $C_{l_{max}}$ and M_{CR} do not enter directly into the calculation of the rotor's performance. However, once the flapping, C_μ and various angles are determined, $C_{l_{max}}$ and M_{CR} are calculated and compared with the section operating values around the azimuth and along the blade.

On the basis of many comparisons with test data, it is concluded that the general method developed here is capable of predicting the performance of a rotor both driven and controlled by a jet flap. Also, it will predict the occurence of blade stall or compressibility effects beyond which the theory would not be expected to hold. It may be possible to modify the method to extend its applicability into this region of operation but even for a shaft-driven rotor, such a procedure is questionable.

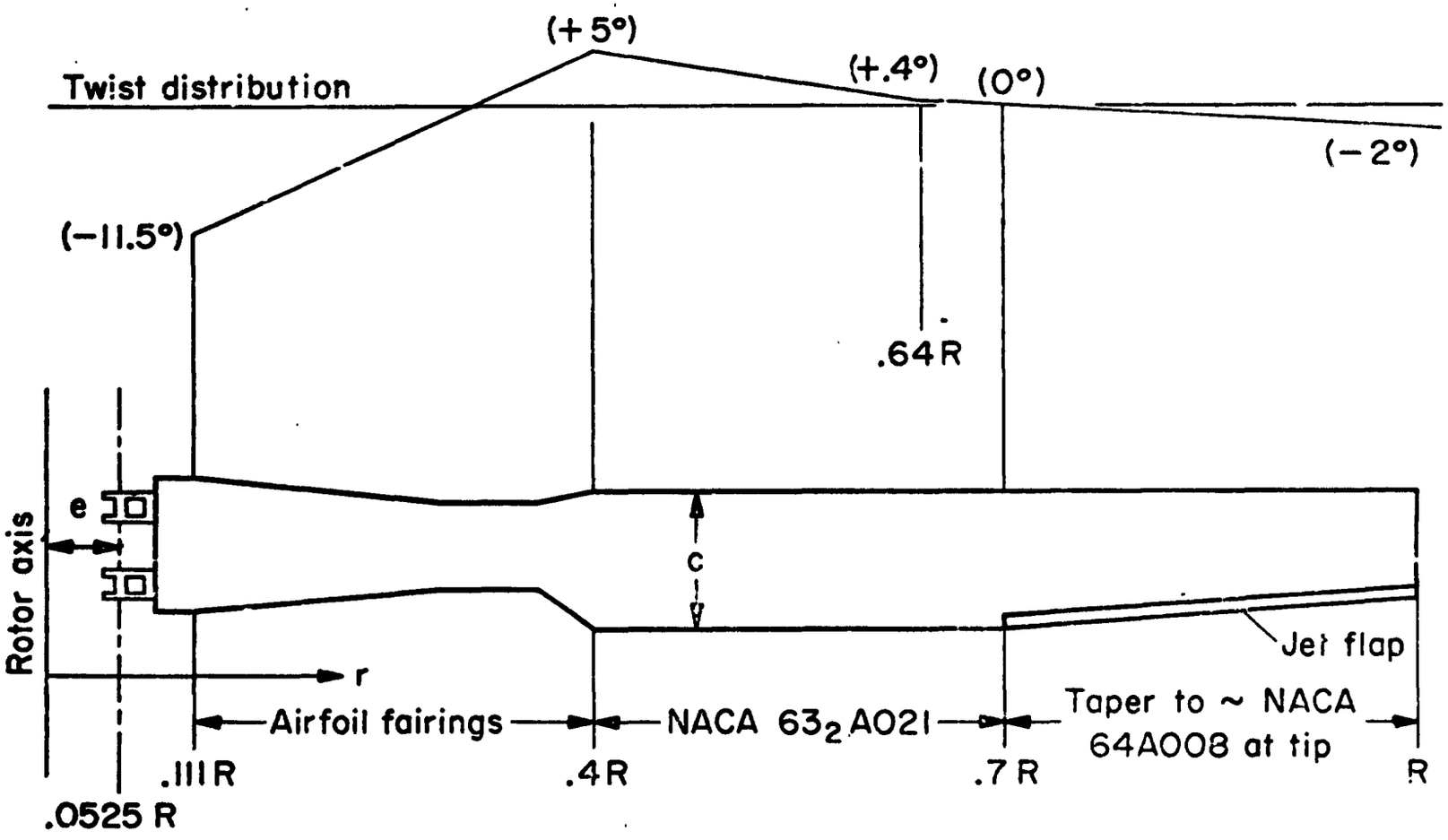

(a) Plan form, section variation, and twist of blade.

Figure B-2 Rotor Details

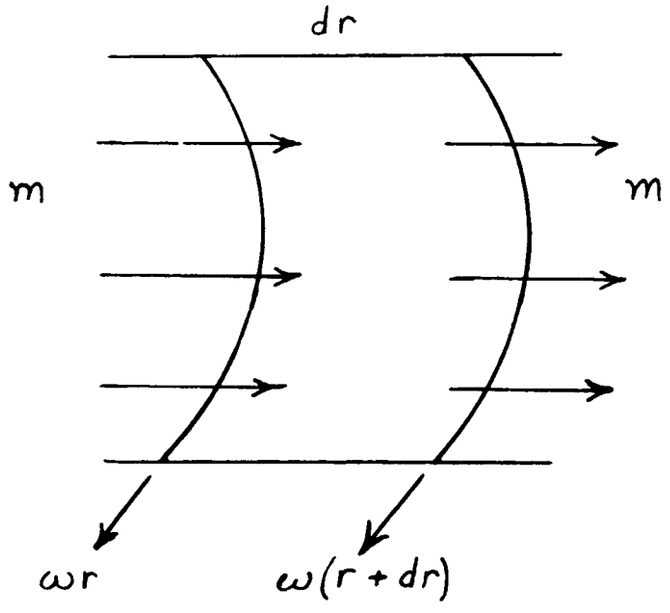

FIGURE B-3

SEGMENT OF FLOW IN BLADE

References

B-1. Evans, W. T. and McCloud, J. L., Analytical Investigation of a Helicopter Rotor Driven and Controlled by a Jet Flap, NASA TND-3028, Sept. 1965.

B-2. McCormick, B. W., Aerodynamics of V/STOL Flight, Academic Press, N.Y., 1967.

B-3. McCloud, J. L. and Evans, W. T., Performance Characteristics of a Jet-Flap Rotor, Conf. on V/STOL Aircraft, NASA Ames Res. Center, April 1966.